Susanne Stefer

Late Pleistocene-Holocene Sedimentary Processes at the Active Margin of South-Central Chile: Marine and Lacustrine Sediment Records as Archives of Tectonics and Climate Variability

Scientific Technical Report STR10/03

Susanne Stefer

Late Pleistocene-Holocene Sedimentary Processes at the Active Margin of South-Central Chile: Marine and Lacustrine Sediment Records as Archives of Tectonics and Climate Variability

Dissertation
zur Erlangung des akademischen Grades
doctor rerum naturalium (Dr. rer. nat.)
in der Wissenschaftsdisziplin Geologie

eingereicht an der Mathematisch-Naturwissenschaftlichen Fakultät
der Universität Potsdam

März 2009

Scientific Technical Report STR10/03

Universität Potsdam, Institut für Geowissenschaften

und

Helmholtz-Zentrum Potsdam Deutsches Geoforschungszentrum (GFZ),
Sektion 5.2 – Klimadynamik und Landschaftsentwicklung

Late Pleistocene-Holocene Sedimentary Processes at the Active Margin of South-Central Chile:

Marine and Lacustrine Sediment Records as Archives of Tectonics and Climate Variability

Dissertation

zur Erlangung des akademischen Grades
"doctor rerum naturalium"
(Dr. rer. nat.)
in der Wissenschaftsdisziplin "Geologie"

eingereicht an der
Mathematisch-Naturwissenschaftlichen Fakultät
der Universität Potsdam

von
Susanne Stefer (geb. Blumberg)

Potsdam, im März 2009

Für BB und den Dude

ABSTRACT

Active continental margins are affected by a complex feedback control between tectonic, climate and surface processes, the intricate relations of which are still a matter of discussion. The Chilean convergent margin, forming the outstanding Andean subduction orogen, constitutes an ideal natural laboratory for the investigation of climate, tectonics and their interactions. In order to study both processes, I examined marine and lacustrine sediments from different depositional environments on- and offshore the south-central Chilean coast (38-40°S). I combined sedimentological, geochemical and isotopical analyses to identify climatic and tectonic signals within the sedimentary records.

The investigation of marine sediments (ODP Site 1232 and SONNE core 50SL) from the margin-parallel trench system focused on frequency changes of turbiditic event layers since the late Pleistocene. In the active margin setting of south-central Chile, these layers were considered to reflect periodically occurring earthquakes and to constitute an archive of the regional paleoseismicity. The new results, however, indicate glacial-interglacial changes in turbidite frequencies during the last 140 kyr: the turbiditic layers have a recurrence time of ~200 years in the glacial parts of the sequences (MIS 2, MIS 3, cold substages of MIS 5, and MIS 6), while their frequency diminishes to approximately one event layer per 1000 years in the interglacial sections (MIS 5 and the Holocene). Hence, on the long-term, the generation of turbidites appears to be strongly influenced by climate and sea level changes. The latter are controlling the amount of sediment delivered to the continental shelf as well as the sediment transport to the shelf edge, thus determining the stability of the continental slope. More stable slope conditions during interglacial periods hence entail lower turbidite frequencies than in glacial periods. Since glacial turbidite recurrence times are congruent with earthquake recurrence times derived from the historical record and other paleoseismic archives of the region, I concluded that only during cold stages the sediment availability and slope instability enabled the complete series of large earthquakes to be recorded.

The sediment transport to the shelf region is, however, not only driven by climate conditions but also influenced by local forearc tectonics. Accelerating uplift rates along major tectonic structures involved drainage anomalies and river flow inversions, which seriously altered (or even blocked) the sediment supply to the Pacific Ocean. Two examples for the tectonic hindrance of fluvial systems along major fault zones are the coastal lakes Lago Lanalhue and Lago Lleu Lleu. Using seismic reflection and sediment analyses, I demonstrated that both lakes developed within former river valleys, which once discharged towards the Pacific. During the Early Holocene, the ancient rivers were dammed by rising sills due to inverse faulting and local tectonic uplift, turning first into marginal-marine lagoonal systems and evolving into lakes thereafter. Both water bodies were ultimately disconnected from the ocean at ~8000 yr BP.

Sedimentological analyses of cores from Lago Lanalhue and Lago Lleu Lleu showed similar successions of marine/brackish sediments at the bottom, covered by lacustrine sediments on top. Dating of the transitions between these different stratigraphic units

i

and comparisons with contemporaneous changes of the global sea level allowed me to calculate local Holocene uplift rates. These rates are up to about twenty times higher for the upraised sills (8.83 ± 2.7 mm/yr for the Lanalhue sill, 11.36 ± 1.77 mm/yr for the Lleu Lleu sill) than for the lake basins (0.42 ± 0.71 mm/yr for the Lanalhue basin, 0.49 ± 0.44 mm/yr for the Lleu Lleu basin). On this account, I considered the sills to be the surface expression of a blind thrust associated with a prominent inverse fault (Morguilla Fault) that is controlling regional uplift and folding.

After the final separation of Lago Lanalhue and Lago Lleu Lleu from the Pacific Ocean at ~8000 years BP, a constant deposition of lacustrine sediments established and continuous records of local environmental changes were preserved. Concerning regional climate changes, sediment sequences from both lakes indicate a multi-millennial trend with a significant shift from more arid conditions during the Mid-Holocene (~8000 – ~4200 cal yr BP) to more humid conditions during the Late Holocene (~4200 cal yr BP – present). Since this trend is consistent with other paleoclimatic data in the surroundings, I interpreted it as reflecting changes in the strength/position of the Southern Westerly Winds.

Late Holocene sediments of Lago Lleu Lleu are characterized by numerous intercalated clastic layers that recur with a mean frequency of ~210 years. This rate is similar to the mean glacial recurrence rate of turbidites that I found in the marine trench sediments and may hence demand a tectonic explanation. However, since the onset of the layer deposition started at ~5000 years BP, coevally with strongest increases found in the frequency and intensity of the El Niño Southern Oscillation (ENSO), and since the periodicity is also in accordance with the ~208-yr cycle of solar variability (Suess-cycle), a climatic explanation seems to be more reasonable. During the last 2000 years, pronounced variations in the terrigenous sediment supply to Lago Lanalhue and Lago Lleu Lleu suggest important hydrological changes on the centennial time-scale as well. A lower input of terrigenous matter points to less humid phases between 200 cal yr B.C. to 150 cal yr A.D., 900 to 1350 cal yr A.D. and 1850 cal yr A.D. to present (corresponding approximately to the Roman, Medieval, and Modern Warm Periods). On the contrary, more humid periods most likely persisted from 150 to 900 cal yr A.D. and 1350 to 1850 cal yr A.D. (corresponding approximately to the Dark Ages and the Little Ice Age).

In conclusion, the combined investigation of marine and lacustrine sediment records is a feasible method for the reconstruction of climatic and tectonic processes on different time scales (10^5-10^2 years). My approach allows exploring both climate and tectonics in one and the same archive, and is largely transferable from south-central Chile to other active margins worldwide.

ZUSAMMENFASSUNG

Aktive Kontinentalränder werden von einem komplexen Rückkopplungssystem zwischen tektonischen, Klima- und Oberflächenprozessen beeinflusst, deren vielschichtige Zusammenhänge bisher nur in Grundzügen verstanden und Gegenstand aktueller Forschung sind. Der chilenische Kontinentalrand – mit den Anden als größtem Subduktionsorogen der Erde – bietet ein ideales natürliches Labor zur Erforschung von Klima und Tektonik sowie deren Wechselbeziehungen. Um beide Prozesse genauer zu verifizieren, habe ich in meiner Arbeit marine und lakustrine Sedimente aus verschiedenen ab- und auflandigen Ablagerungsräumen entlang der südlichen Küste Zentralchiles (38-40°S) untersucht. Die in den Sedimentarchiven enthaltenen klimatischen und tektonischen Signale habe ich dabei mit einer Kombination aus sedimentologischen und geochemischen Messungen sowie Isotopen-Analysen identifiziert.

Die Untersuchung der marinen Sedimente (ODP-Bohrung 1232 und SONNE-Kern 50SL), die im, dem Kontinentalrand vorgelagerten, Tiefseegraben erbohrt wurden, konzentriert sich auf Änderungen in der Ablagerungsfrequenz von turbiditischen Lagen seit dem späten Pleistozän. In der tektonisch aktiven Region süd-zentral Chiles können diese Lagen als grundsätzliche Anzeiger periodisch auftretender Erdbeben und somit als Archiv der lokalen Seismizität gewertet werden. Die gewonnenen Ergebnisse zeigen in den letzten 140 000 Jahren deutliche glazial-interglaziale Änderungen der Turbidit-frequenzen: Während in den Glazialen (MIS 2, MIS 3, kältere Etappen von MIS 5 und MIS 6) durchschnittlich ein Ereignis in 200 Jahren zu verzeichnen ist, treten Turbidite in den Interglazialen (MIS 5 und Holozän) nur etwa alle 1000 Jahre auf. Auf lange Sicht scheint die Auslösung von Turbiditen deshalb nicht nur von der lokalen Seismizität, sondern auch von globalen Klima- und Meeresspiegelschwankungen abhängig zu sein. Beide bestimmen die Sedimentmenge, die den Kontinentalschelf erreicht, sowie den weiteren Sedimenttransport zur Schelfkante, und damit letztendlich die Stabilität des Kontinentalhanges. So führen stabilere Hangverhältnisse während den Interglazialen zu grundsätzlich geringeren Turbiditfrequenzen als in den Glazialen. Da die glazialen Turbidithäufigkeiten gut mit der Häufigkeit von historisch dokumentierten Erdebeben übereinstimmen, interpretiere ich, dass in Abhängigkeit der größeren Sedimentmenge sowie der geringeren Hangstabilität nur in den Kaltzeiten die Gesamtzahl aller großen Erbeben durch Turbidite aufgezeichnet wurde.

Neben den klimatischen Gegebenheiten bestimmt auch die lokale Tektonik im Forearc-Bereich den Sedimenttransport zur Schelfregion. Zunehmende Hebungsraten entlang von tektonischen Strukturen führen zu Veränderungen im Gewässernetz und zu Flussumkehrungen, die die Sedimentzufuhr zum Pazifischen Ozean deutlich modifizieren oder sogar ganz unterbinden. Zwei Beispiele für die tektonische Blockade von Flusssystemen entlang von Störungszonen sind die heutigen Küstenseen Lago Lanalhue und Lago Lleu Lleu. Auf der Grundlage von seismischen Reflexions- und Sedimentkernanalysen konnte ich zeigen, dass sich beide Seen in den Tälern von ehemaligen, zum Pazifik hin entwässernden Flüssen entwickelten. Im frühen Holozän wurden diese Flüsse durch lokale tektonische Hebung entlang einer inversen

Verwerfung abgedämmt; aus den zunächst randlich-marinen Lagunen entwickelten sich vor etwa 8000 Jahren vom Pazifik abgetrennte Seesysteme.

Aus den sedimentologischen Analysen ergab sich für beide Seen eine ähnliche Abfolge von basal marinen und darüber liegenden lakustrinen Sedimenten. Mit Hilfe der genauen Datierung des Übergangs zwischen beiden stratigraphischen Einheiten sowie dem Vergleich mit globalen Meeresspiegelkurven konnte ich lokale holozäne Hebungs-raten errechnen. Für die Schwellen, die Lago Lanalhue und Lago Lleu Lleu eindämmen, sind die errechneten Raten bis zu etwa 20-mal höher (8.83 ± 2.7 mm/Jahr bzw. 11.36 ± 1.77 mm/Jahr) als für die Seebecken selbst (0.42 ± 0.71 mm/Jahr bzw. 0.49 ± 0.44 mm/Jahr). Deshalb interpretiere ich die Schwellen als oberflächiges Anzeichen einer bislang verdeckten Überschiebung, die die Hebung und Verformung in der Region der beiden Seen beeinflusst.

Nachdem Lago Lanalhue und Lago Lleu Lleu vor etwa 8000 Jahren endgültig vom Pazifik abgetrennt wurden, setzte eine beständige Ablagerung lakustriner Sedimente ein; letztere stellen seitdem gut erhaltene Archive der lokalen und regionalen Umwelt- und Klimaänderungen dar. Sedimentsequenzen von beiden Seen zeigen einen eindeutigen Wechsel von relativ ariderem Klima im mittleren Holozän (~8000 bis 4200 Jahre vor heute) zu relativ humideren Bedingungen im späten Holozän (seit ~4200 Jahren). Da dieser Trend mit anderen paläoklimatischen Daten der Umgebung übereinstimmt, interpretiere ich ihn als Anzeiger einer generellen Änderung der Stärke bzw. Breitenlage der südhemisphärischen Westwinde.

Die spätholozänen Sedimente des Lago Lleu Lleu sind durch ein regelmäßiges Auftreten klastischer Lagen – im Mittel etwa alle 210 Jahre – gekennzeichnet. Diese Frequenz ist mit der glazialen Wiederkehrzeit der Turbidite in den marinen Sedimentkernen vergleichbar und verlangt deshalb möglicherweise eine tektonische Erklärung. Weil die klastischen Lagen allerdings erstmals vor 5000 Jahren – etwa gleichzeitig mit stärksten Anstiegen in der Häufigkeit und Intensität der El Niño Southern Oscillation (ENSO) – auftreten, und weil ihre mittlere Periodizität auch mit dem etwa 208-jährigen Zyklus solarer Aktivität (Suess-Zyklus) übereinstimmt, erscheint eine klimatische Erklärung sinnvoller. In den letzten 2000 Jahren weisen Schwankungen im Eintrag terrigener Sedimentanteile in beide Seen auf kurzzeitige hydrologische Änderungen hin. Ein verminderter Eintrag terrigenen Materials lässt auf weniger humide Bedingungen zwischen 200 B.C. und 150 A.D., 900 und 1350 A.D., sowie nach 1850 A.D. (Phasen, die in etwa der römischen, mittelalterlichen und gegenwärtigen Warmzeit entsprechen) schließen. Im Gegensatz dazu waren die Zeiten zwischen 150 und 900 A.D sowie 1350 und 1850 A.D. (die in etwa den ‚Dark-Ages' und der Kleinen Eiszeit entsprechen) von humideren Bedingungen gekennzeichnet.

Abschließend zeigen meine Ergebnisse, dass die verknüpfte Analyse von marinen und lakustrinen Sedimenten ein sinnvoller und praktikabler Ansatz ist, um klimatische und tektonische Prozesse auf verschiedenen Zeitskalen (10^5-10^2 Jahre) zu untersuchen. Dabei ist von besonderem Vorteil, dass die Herangehensweise die Untersuchung von Klima und Tektonik in ein und demselben Archiv erlaubt und die Methode sich weitgehend auch auf andere aktive Kontinentalränder übertragen lässt.

RESUMEN

La investigación de sedimentos marinos desde el sistema de la fosa paralela al margen (ODP Site 1232 y SONNE core 50SL) se enfocó en las variaciones de frecuencia de las capas de eventos turbidíticos desde el Pleistoceno tardío. En el margen activo ubicado en la zona sur-central chilena, se consideraba que estas capas reflejaban la ocurrencia de terremotos periódicos y constituían un archivo paleosísmico regional. Sin embargo, los nuevos resultados indican cambios glacial-interglaciales en las frecuencias de las turbiditas durante los últimos 140 ka: mientras en la parte glacial de las secuencias(MIS 2, MIS 3, subetapas frias de MIS 5 y MIS 6), se registran capas turbidíticas con una frecuencia principal de ~200 años, la frecuencia de las capas disminuye a aproximadamente un evento cada 1000 años en las secciones interglaiales (MIS 5 y el Holoceno). Por lo tanto, en largos períodos la frecuencia de las turbiditas parece estar fuertemente influenciada por cambios climáticos y del nivel del mar. Estos últimos controlan la cantidad de sedimento entregado a la plataforma continental así como también el transporte de sedimento hacia el borde de la plataforma, determinando así la estabilidad de la pendiente continental. Condiciones de mayor estabilidad de la pendiente durante períodos interglaciales suponen por consiguiente menores frecuencias de turbiditas comparado con períodos glaciales.

El transporte de sedimento a la región continental es, sin embargo, no solo conducida por las condiciones sino también influenciada por la tectónica local del antearco. Tasas aceleradas de alzamiento a lo largo de estructuras tectónicas mayores envuelven anomalías de drenaje e inversiones del flujo de ríos, las cuales alteraron seriamente (o incluso bloquearon) el abastecimiento de sedimentos al Océano Pacífico. Dos ejemplos de obstáculo tectónico en un sistema fluvial a lo largo de zonas de fallas mayores son los lagos costeros Lanalhue y Lleu Lleu. Usando reflección sísmica y análisis de sedimentos lacustres, demostré q ambos lagos se formaron dentro de antiguos valles generados por ríos, los cuales alguna vez eran descargados en el Pacífico. Durante el Holoceno temprano, los antiguos ríos fueron embalsados por sills alzados debido a fallamiento inverso y alzamiento tectónico local, generándose primero en sistemas lagunares marinos marginales y transformándose de ahí en adelante en lagos. Ambos cuerpos de agua fueron finalmente desconectados del océano a los ~8000 años BP.

Análisis sedimentológicos de muestras del Lago Lanalhue y del Lago Lleu Lleu muestran sucesiones similares de sedimentos marinos/brackish en el fondo, cubiertos por sedimentos lacustres en el techo. Dataciones de las transiciones entre las distintas unidades estatigráficas y comparaciones con cambios contemporáneos del nivel global del mar me permitieron calcular tasas de alzamientos locales en el Holoceno. Aquellas tasas son cerca de veinte veces mayores para umbrales alzados (8.83 ± 2.7 mm/año para el umbral del Lanalhue, 11.36 ± 1.77 mm/año para el umbral del Lleu Lleu) que para las cuencas de los lagos (0.42 ± 0.71 mm/año para la cuenca del Lanalhue, 0.49 ± 0.44 mm/año para la cuenca del Lleu Lleu). Por este motivo, consideré q los umbrales son la expresión superficial de una falla ciega que está controlando el alzamiento regional y el plegamiento.

Luego de la separación del Lago Lanalhue y del Lago Lleu Lleu desde el Océano Pacífico a los ~8000 años BP, se estableció una constante deposición de sedimentos

lacustres y fueron preservados continuos registros de cambios medioambientales locales. Concerniente a los cambios climáticos regionales, secuencias sedimentarias de ambos lagos indican una tendencia multi-millenial con un cambio significativo desde condiciones más áridas durante el Holoceno Medio (~8000 - ~4000 cal año BP) a condiciones más húmedas en el Holoceno Tradío (~4200 cal año BP – presente) debido a que esta tendencia es consistente con otros datos paleoclimáticos en los alrededores, lo he interpretado como un reflejo en los cambios en la fuerza/posición de los *Southern Westerly Winds*.

Los sedimentos del Holoceno Tardío del Lago Lleu Lleu se caracterizan por numerosas capas clásticas intercaladas que se repiten con una frecuencia promedio de ~210 años. Esta tasa es similar a la tasa de recurrencia media glacial de turbiditas que encontré en los sedimentos de la fosa marina y debería por lo tanto requerir una explicación tectónica. Sin embargo, dado que el comienzo de la deposición de la capa fue a los ~5000 años BP, concomitantemente con un fuerte incremento en la frecuencia e intensidad de la Oscilación Austral de El Niño (ENSO), y dado que la periodicidad está además en concordancia con el ciclo de variabilidad solar de ~208 años (Suesscycle), Una explicación climática parece ser más razonable. Durante los últimos 200 años, variaciones pronunciadas en la provisión de sedimentos terrígenos al Lago Lanalhue y al Lago Lleu Lleu sugieren también importantes cambios hidrológicos en la escala de tiempo centinial. Una menor entrada de puntos de material terrígeno a menos fases húmedas entre 200 cal años B.C. a 150 cal años A.D., 900 a 1350 cal años A.D. y 1850 cal años A.D. al presente (aproximadamente correspondientes a los periodos Romano, Medieval y Moderno) Por el contrario, más periodos húmedos probablemente persistieron desde los 150 a los 900 cal año A.D. y 1350 a 1850 cal año A.D. (correspondiendo aproximadamente a las Eras Obscuras y la Pequeña Edad Glacial).

En conclusión, la investigación combinada de registros de sedimentos marinos y lacustres es un método factible para la reconstrucción de procesos climáticos y tectónicos en diferentes escalas de tiempo (10^5-10^2 años). Mi enfoque permite explorar clima y tectónica en uno y en el mismo archivo, y es en gran medida transferible desde Chile Sur Central a otros márgenes activos alrededor del mundo.

CONTENTS

FIGURES

ix

TABLES

x

ABBREVIATIONS

SCIENTIFIC TERMS

ACC	Antarctic Circumpolar Current
AMS	Accelerator Mass Spectrometry
BBFZ	Bío Bío Fault Zone
BB	Bío Bío Canyon
BC	Bueno Canyon
CVC	Calle Calle/Valdivia Canyon
ENSO	El Niño Southern Oscillation
F.Z.	Fracture Zone
GPS	Global Positioning System
IC	Imperial Canyon
LFZ	Lanalhue Fault Zone
LGM	Last Glacial Maximum
LIA	Little Ice Age
LOFZ	Liquiñe-Ofqui Fault Zone
mbsf	meter below sea floor
mcd	meter composite depth
mccd	meter corrected composite depth
MIS	Marine Isotope Stage
MOWP	Modern Warm Period
MS	Magnetic Susceptibility
MVFZ	Mocha-Villarica Fault Zone
MWP	Medieval Warm Period
OSL	Optically Stimulated Luminescence
pPC	paleo Pellahuén Canyon
RWP	Roman Warm Period
RSL	Relative Sea Level
SEM	Scanning Electron Microscope
STH	SubTropical high pressure cell
SWW	Southern Westerly Winds
TC	Total Carbon (except for Figure 2.2, where TC stands for Toltén Canyon)
TIC	Total Inorganic Carbon
TOC	Total Organic Carbon
VPDB	Vienna PeeDee Belemnite
XRD	X-Ray Diffraction
XRF	X-Ray Fluorescence

INSTITUTIONS AND PROJECTS

AWI	Alfred-Wegener-Institut für Polar- und Meeresforschung
BGR	Bundesanstalt für Geowissenschaften und Rohstoffe
BMBF	Bundesministerium für Bildung und Forschung (German Ministry for Education and Research)
CSAG	Center for System Analysis of Geoprocesses
DFG	Deutsche Forschungsgemeinschaft (German Research Foundation)
GFZ	Helmholtz-Zentrum Potsdam Deutsches GeoFoschungsZentrum
JOI	Joint Oceanographic Institutions
ISSA	Integrated Seismological experiment in the Southern Andes
NSF	National Science Foundation
ODP	Ocean Drilling Program
SPOC	Subduction Processes off Chile
TIPTEQ	from The Incoming Plate to mega-Thrust EarthQuake processes

ACKNOWLEDGMENTS

I would like to thank the many people who supported me during the ups and downs of my PhD-life:

My first and very special thanks go to Gerald Haug – You did not only offer me the possibility of doing my work in the unique field of Paleoclimate, but – what is equally or perhaps even more important – your 'Christmas-' and 'POF-'exercises taught me how to find my way in the world of science and your contagious enthusiasm always reanimated my motivation.

Special thanks also go to Helmut Echtler – You escorted me safely through the vast empire of Chilean tectonics. Without your special sense of humor, something would have been missing.

I gratefully thank Onno Oncken – At the very beginning, you gave me the chance to do a traineeship at GFZ, and, later on, you made possible that I could work on my thesis within the scope of the CSAG virtual institute.

Helge and Frank – Thank you both very much indeed for your constant support, the many discussions, the great field trip to Chile, and so much more… – You two kept me always on the right way!

Many people from GFZ Potsdam, AWI Bremerhaven, BGR Hannover and the Universities of Potsdam, Bremen, Trier and Ghent helped me with the analyses and the interpretation, presentation and publication of my results. Thanks to all colleagues of Sections 5.2 and 3.1 at the GFZ (in particular to Achim Brauer for hosting me in the team, to Jerome Kaiser for discussions and corrections of my manuscripts, and to Christine Gerschke for always solving my administrative problems), to Daniel Melnick, Jasper Moernaut, Marc De Batist, Katrin Rehak, Tim Vietor, Rolf Kilian, Francisca Albert, Carina Lange, Rita Fröhlking, Ulla Röhl, Vera Lukies, Michael Wiedicke and to all those who I forgot to specify here…

I cannot leave Potsdam and Berlin without mentioning Clara, Olga, Iris, Hans, Christian, Tina, Sebastian, Stefan, Gergana, Sascha, Andreas, Steffen and Jan – Thank you so much for the wonderful years, I will always remember our time together!!!

Last but not least I want to thank those people who are all the world to me – My family. I know that you often missed me during the last years; all the more I am proud of you and very glad that the hard times even strengthened the bond between us.

PREFACE

February 20th. -- This day has been memorable in the annals of Valdivia, for the most severe earthquake experienced by the oldest inhabitant. [...] It came on suddenly, and lasted two minutes, but the time appeared much longer. The rocking of the ground was very sensible. [...]

Charles Darwin, 'The Voyage of the Beagle' (1839)

Charles Darwin experienced the strong earthquake that hit the region of Valdivia (south-central Chile) in 1837 and described the observations in his well known travel memoirs 'The Voyage of the Beagle'. This earthquake was only one of numerous seismic events that were and are striking the active Chilean margin at regular intervals (*Figure I*), and that are induced by the subduction of the oceanic Nazca Plate beneath the South American continent.
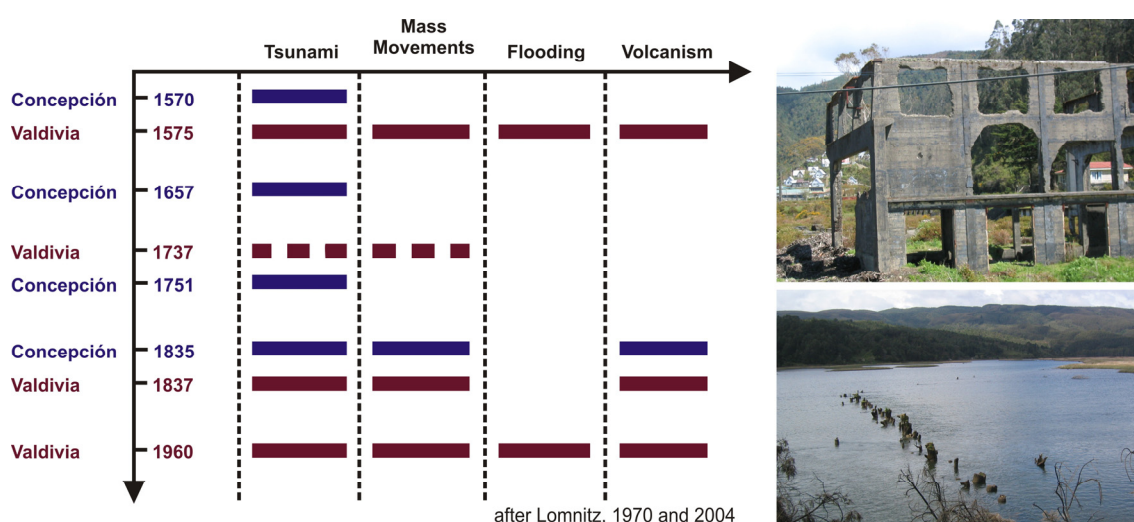
Figure I: Frequency and consequences of mega-earthquakes in south-central Chile. Left: Historical record of seismic events and their secondary effects (compiled after Lomnitz 1970 and 2004). Blue bars indicate events that hit the area of Concepción; red bars indicate events that hit the area of Valdivia. Displayed are all the events with M>8. Right: Destroyed factory building near Valdivia and drowned alley trees as consequences of the tsunami associated with the 1960 'Great Chilean Earthquake' (photographs by courtesy of Dr. T. Vietor).

High seismicity, like it is observed at the Chilean convergent margin, is typical for active subduction zones worldwide and turns them into the most dynamic, energetic, and hazardous regions of the globe (e.g. Ruff and Kanamori, 1980; Stern, 2002; Bird, 2003; McCaffrey, 2008). Nevertheless, since they also entail scores of natural resources, as for instance ore deposits (e.g. copper, silver, lead, zinc) and geothermal heat, the circumjacent regions of subduction zones are often densely populated. The timely prediction of natural hazards is hence indispensable and requires best knowledge of the subduction system as a whole. Considerable effort on understanding natural processes concurring at the convergent margins is hence essential.

1.   INTRODUCTION

Given the high risk of natural catastrophes paired with the high potential for exploitation of natural resources, convergent continental margins are intensively studied ever since the theory of plate tectonics evolved in the 1960s. Complex interactions between tectonic, climatic and surface processes are working in these highly active regions, constituting a multifaceted object of research. A dynamic feedback exists between tectonically-driven surface deformation and climatically-driven surface erosion that has likely a first-order control on the development and style of the convergent margins (*Figure 1.1*). However, the puzzling interrelations between these processes are still not fully understood.

It has been known for a long time that tectonics are capable of affecting climate through, for instance, the uplift of orographic barriers and the opening and closure of oceanic gateways, since these influence atmospheric and oceanic circulation patterns. Only recently, it has become evident that the climate is able to greatly modify crustal deformation processes as well, for instance via the amount of surface-eroded material that is redistributed into the subduction system. As a consequence, the formation and evolution of orogens, the rate and frequency of precipitation, and the resultant rate of surface erosion should be perceived in combination rather than isolated in order to understand the complex background mechanisms working at convergent plate margins.

Tectonics (surface deformation) → *topography* → **Climate** (precipitation & temperature)

e.g. reduction of orogen mass   *e.g. enhanced relief*

e.g. enhanced precipitation

Erosion (fluvial, glacial & mass wasting processes)
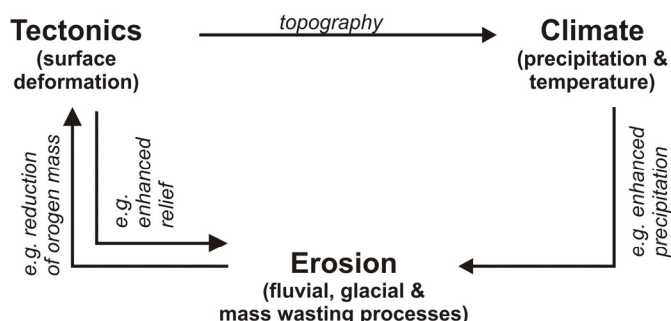
Figure 1.1 *Schematic diagram of processes and their feedbacks working at convergent plate margins (modified after Willet et al., 2006)*

The Chilean convergent margin comprises the longest – and probably best studied – subduction orogen of the world: the Andes. Due to their exceptional large N-S-extension of more than 7500 km, the Andes are the only mountain chain on Earth that crosses several zones of different climate character (Ziegler et al., 1981), subduction geometries and subduction rates (Cahill and Isacks, 1992). The orogen hence constitutes an ideal natural laboratory for investigating interactions between climate and tectonics at active continental margins, and increasing effort has been made during recent years to better understand feedbacks between both processes.

General consensus is that the continuous uplift of the Andes during the Neogene created an effective barrier that is blocking the southern hemisphere westerly winds and leads to enhanced precipitation at the western side of the southern orogen. An important finding

1

of the last decades is that the rate and style of subduction is also inversely influenced by the amount of sediments deposited in the margin-parallel trench, which is ultimately a function of climate (particularly of precipitation). Unconsolidated trench-sediments are thought to have a lubricating effect on the plate interface. In that they do not only control if subduction runs erosive or accretionary (e.g. von Huene and Scholl, 1991; Bangs and Cande, 1997; Clift and Vannucchi, 2004), but also directly determine the propagation and extent of seismic rupture (Ruff, 1989; Lamb and Davis, 2003). Lamb and Davis (2003) also suggest that the height of the Andean orogen is depending on shear stresses along the plate interface. They hence consider the Cenozoic climate change and related intensification of climate-induced erosion to be responsible for the ultimate uplift of the Andes.

1.1 Research motivation

In logical consequence of the above, sedimentation at the Chilean active margin is highly affected by both climatic and tectonic processes. As final products of surface erosion, the local sedimentary sequences often preserve complex archives of past environmental changes, instead of reflecting clear records of previous climate or tectonics. These combined signals bear the advantage of studying local climate and tectonics in one and the same archive. However, the interpretation of sedimentary records from tectonically active regions is often difficult and requires accurate unraveling of the merged patterns before drawing conclusions on past climate changes and/or tectonic developments.

Figure 1.2 Sketch of different sedimentary environments at the south-central Chilean margin (not to scale): Trench, slope and shelf basins, as well as onshore lake systems
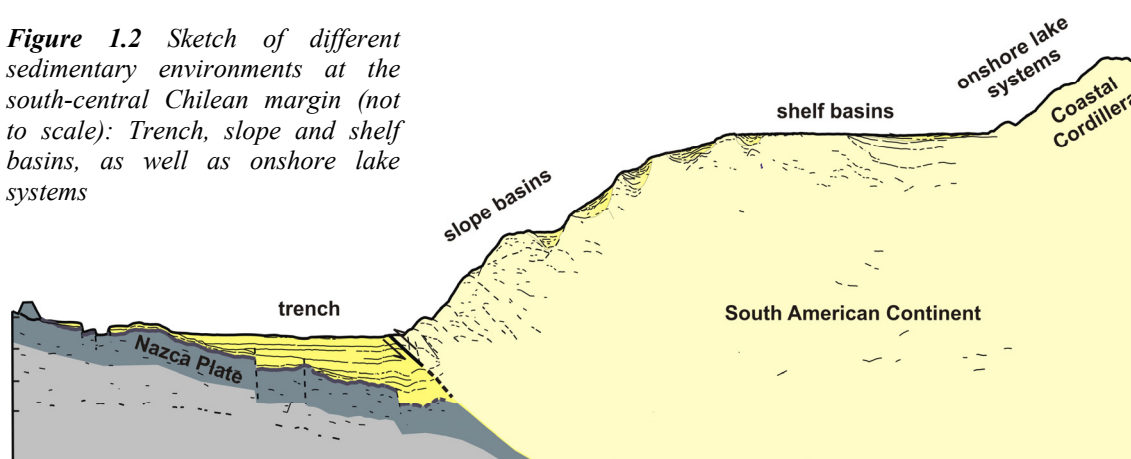
In my thesis, I studied marine and lacustrine sediment cores from different depositional provinces along the south-central Chilean margin with the overall objective to identify their records of paleoclimate and paleotectonics. First of all, I investigated sedimentary sequences that were recovered within the margin-parallel trench system (cp. *Figure 1.2*) and hence constitute long-term recorders (10^4-10^5 years) of the sediment transport between the continent and the abyssal zone of the lower plate. These sedimentary deposits document periodically occurring depositional events and constitute excellent recorders of past turbidity currents. In addition, I studied lacustrine sediment records from onshore lake systems near the coast. On shorter time-scales (10^2-10^3 years), these

deposits document the (intermediate) storage of eroded material at the continental upper plate margin on its way down from the orogen towards the trench.

I exploited the different nature, time-scales and temporal resolution of the investigated records to address a number of important questions concerning the climate and environmental history of the south-central Chilean margin. Overall points to be discussed in this context are:

· the identification of the climatic and tectonic signals within the sedimentary records,

· the reconstruction of tectonic events/features in consideration of the large-scale tectonic framework at the Chilean margin,

· the reconstruction of local and regional-scale climate changes with regard to the south-American climatic evolution,

· the identification of potential interactions between climatic and tectonic processes.

Additionally, I raised specific issues from each of the distinct sedimentary archives. In case of the marine trench sediments, my main objectives were:

· to examine earthquakes as ultimate trigger mechanism for the documented mass flow events and to assure the importance of the sediment records as archives of paleoseismicity,

· to understand which factors are controlling prominent frequency changes of the recorded turbidity currents (variations in the seismic cycle vs. long-term climate changes),

· to evaluate if the sediment records may be helpful for the prediction of probable earthquake events in the near future.

The particular intentions of investigating sediment sequences from the near-coast lake systems were

· to gain new knowledge about local forearc tectonics, which likely induced the lakes formation (and that way to ascertain the timing and mode of origin of the lake basins as well as their subsequent evolution)

· to detect possible indications for local mass flow events that could be correlated with the marine turbiditic records,

· to derive information about climate changes in south-central Chile, which likely left their marks in the sediments ever since the lakes formed.

1.2   The study area: south-central Chile

1.2.1   Tectonics

The active margin of western South-America is a high-strain convergent plate margin formed by the oblique subduction of the oceanic Nazca Plate beneath the South American continent. This active margin setting sustained since the Late Palaeozoic/Early Mesozoic and led to the formation of the outstanding Andean mountain chain (e.g. Mpodozis and Ramos, 1989), which nowadays ranges over more than 7500 km in N-S direction, nearly 7 km in height, and more than 800 km in W-E direction (*Figure 1.3*). Global Positioning System (GPS) data indicate that present-day plate convergence is taking place with a horizontal velocity magnitude of ~47-80 mm/yr and a velocity azimuth of 76-82 °NE (Angermann et al., 1999; Kendrick et al., 2003).

The Andean margin is characterized by conspicuous along-strike segmentation that becomes obvious by variations in several aspects such as topography, crustal thickness, subduction geometry, volcanism, morphology, seismicity, and/or rate and style of deformation (e.g. Lomnitz, 1970; Kley et al., 1999; Montgomery et al., 2001; Lomnitz, 2004; Stern, 2004; Tassara, 2005; Melnick, 2007; Rehak et al., 2008). Roughly subdivided, these segments are the northern Andean segment (north of 15°S), the central Andean segment (15-34°S), the southern Andean segment (34-47°S), and the austral Andean segments (south of 47°S) (according to Tassara, 2005) (*Figure 1.3*). Ultimate causes for the margin segmentation are in the focus of research since several decades, but still remain a matter of debate. According to different authors, the division is due on bathymetrical irregularities of the subducted oceanic Nazca Plate (Jordan, et al., 1983; Yañez and Cembrano, 2004), to peculiarities of the pre-Andean continental basement (Mpodozis and Ramos, 1989; Ramos, 1999), and/or to zonal gradients in climate-related erosion potential (Montgomery et al., 2001; Melnick and Echtler, 2006a).

Onshore south-central Chile, the margin-parallel Liquiñe-Ofqui Fault Zone (LOFZ; *Figure 1.4*) represents a first order discontinuity of the overriding continental plate. Intra-arc decoupling along this major dextral strike-slip discontinuity is suggested to turn the forearc into a northward gliding sliver (Cembrano et al., 2002; Rosenau et al., 2006). Margin-oblique NW-SE trending fault zones that are further subdividing the region are interpreted to implement the morphotectonic segmentation of the margin (Echtler et al., 2003; Rehak et al., 2008; Melnick et al., 2009). Most prominent structures are − from north to south − the Bío Bío Fault Zone (BBFZ), the Lanalhue Fault Zone (LFZ; Glodny et al., 2008) and the Mocha-Villarica Fault Zone (MVFZ, Melnick and Echtler 2006b) (*Figure 1.4*). Different segments of the margin, defined by these fracture zones, are characterized by differential coastal deformation and uplift (Hackney et al., 2003; Rehak et al., 2008).

Morphotectonically, the upper plate is divided into four main margin-parallel units (Melnick and Echtler, 2006a) (*Figure 1.4*): (I) the Coastal Platform in the west, which is constituted by uplifted Cenozoic marine and coastal sediments, focus of a part of my study; (II) the Coastal Cordillera (Cordillera del Nahuelbuta), which is build up by a Permo-triassic accretionary complex (Glodny et al., 2005) and a late Palaeozoic

magmatic arc (Hervé, 1988); (III) the Central Depression, which is formed by Oligocene-Miocene volcanic rocks and sediments covered by Pliocene-Quaternary fluvial-alluvial sediments; and (IV) the Main Cordillera in the east, which is composed of a Mesozoic-Cenozoic magmatic arc and intra-sedimentary basins.
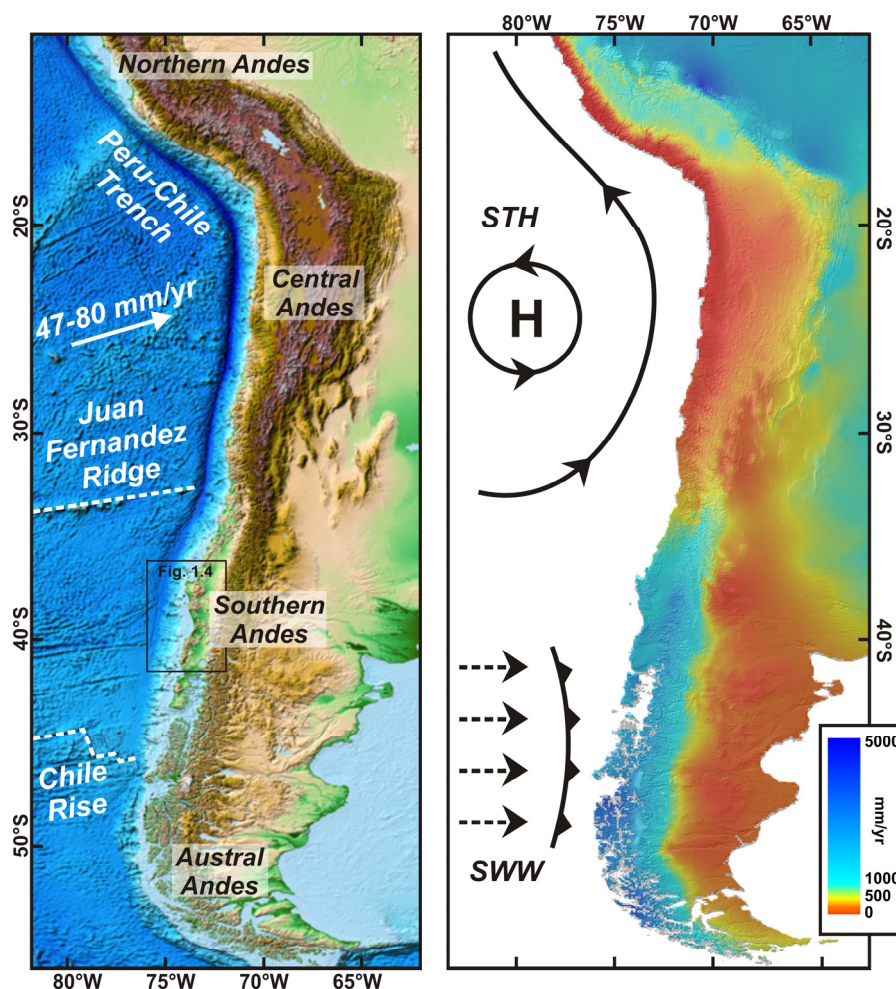
Figure 1.3 *Climatic and tectonic setting at the Andean margin of South America. Left: Bathymetry and topography along the Chilean convergent margin (map source: ETOPO1 Global Relief Model; Amante and Eakins, 2008); major tectonic structures of the oceanic plate and the trench system are highlighted in white; plate convergence rate after Angermann et al., 1999 and Kendrick et al., 2003. Right: Mean annual precipitation (data from New et al., 2002); the present-day positions of the Subtropical High Pressure Cell (STH) and the Southern Westerly Winds (SWW) are indicated.*

1.2.2   (Paleo-) Climate

At present, the climate of the coastal region of western South America is controlled by two prevalent atmospheric circulation structures: I) the Subtropical High Pressure Cell (STH) over the South Pacific Ocean, and (II) prevailing westerly winds in the higher latitudes (e.g. Cerveny, 1998; Markgraf, 1998) (*Figure 1.3*). The quasi-stationary South Pacific Anticyclone in the north induces strong subsidence of air masses, which in combination with cold waters of the northwards flowing Peru-Chile-Current result in extremely dry climate conditions. Aridity is culminating in the Atacama Desert (~22°S latitude), where mean annual precipitation is virtually zero (e.g. Miller, 1976;

5

Schwerdtfeger, 1976; New et al., 2002). Rainfall amounts are strongly increasing southwards, where the westerly winds are gaining more and more influence, until they are dominating the climate south of ~40°S. These strong zonal winds result from a large thermal and pressure gradient between cold Antarctic air masses and relatively warmer waters and landmasses in the tropical latitudes (Cerveny, 1998). Due to the lack of large continents in the high latitudes of the southern hemisphere, the westerly wind belt is more persistent and stronger than its northern hemisphere counterpart. The associated cyclonic storms are bringing heavy rainfalls to Southern Chile, for which reason precipitation is highest in the core zone of the Westerlies (>5000 mm/yr) (New et al., 2002; *Figure 1.3*). At present, this zone is centred around 49-50°S in austral summer; during austral winters, it is ranging over a broader area and located ~2° poleward compared to its summer-position (Trenberth,1991).

It follows from the above that the area between 38-40°S − focus of my study − is presently characterized by an extreme north-south gradient in precipitation since it is located in the sensitive transition zone amongst summer-dry Mediterranean-like climate conditions north of ~37°S and all-season humid conditions south of 42°S (*Figure 1.3*).

Superimposed on the two main climatic regimes are inter-annual variations in precipitation, induced by the ENSO (El Niño Southern Oscillation) anomaly (e.g. Markgraf, 1998; Montecinos and Aceituno, 2003). Most of the apparent climatic irregularities are explained by associated changes in the strength of the Subtropical Anticyclone over the South-eastern Pacific (Cerveny, 1998). During La Niña phases, the pressure cell is consistently strong all-year-round, forcing the westerly wind belt to remain south of 45°S. During El Niño years on the other hand, the anticyclone is weakened, permitting a northward advance of the storm tracks and hence inducing increased rainfall in the Chilean mid-latitudes.

Paleoclimatic data from marine and lacustrine sediment cores indicate that the present zonation of the Chilean climatic conditions shifted during the Late Quaternary. Latitudinal displacements of the Southern Westerlies, caused by changes in the meridional pressure and thermal gradients, are regarded to be the main driver for these climatic variations (Denton et al., 1999; Moreno et al., 2001; Lamy et al., 2004). During the last glacial, southernmost Chile was covered by the Patagonian Ice Sheet, which dispersed ~1800 km along the Andes between ~38°S to ~56°S at the time of the Last Glacial Maximum (LGM). At that time, climatic conditions were wetter and colder compared to today probably up to the southern margin of the Atacama Desert at ca. 27°S (e.g. Lamy et al., 1998; Amman et al., 2001), while snowfall in the very south (50-55°S) was reduced in the same period (Hulton et al., 1994). According to Denton et al. (1999), this situation is at best explained by a northward shift of the Southern Westerlies by ~5° latitude. During the last deglaciation, the Westerlies moved southwards again until they reached, at ~14.3 kyr BP, a position similar to the present-day situation (McCulloch et al., 2000). The wind belt appeared to be located even further poleward during the early to middle Holocene, as it is inferred from drier and warmer climatic conditions compared to today (e.g. Veit, 1996; Lamy et al., 2001; Jenny et al., 2002b; Abarzúa, et al., 2004; Bertrand et al. 2008). On the contrary, climate conditions were once more getting colder and wetter during the Late Holocene, indicating a northward shift of the Westerlies again (e.g. Lamy et al., 2001; Maldonado and Villagran, 2006). Superimposed on the long-term millennial-scale climate changes, Lamy et al. (2001)

and Kaiser et al. (2007) found centennial-scale variations with dominating frequencies of ca. 900 and 1500 years during the Holocene and the last glacial period; these are interpreted to display significant changes in rainfall variability caused by latitudinal shifts of the Southern Westerlies also on the short-term scale (Lamy et al., 2001; Kaiser et al., 2007).

1.3   Material, methods and structure of this work

1.3.1   Material

My work is based on marine and lacustrine sediment records from different sedimentary environments at the south-central Chilean margin. The coring positions are distributed between 38°S and 40°S. Two of the investigated cores are of marine origin and situated within the margin-parallel Perú-Chile Trench. Two additional studied records are of lacustrine type and originate from onshore coastal lakes of the southern Arauco Peninsula (*Table 1.1* and *Figure 1.4*).

Table 1.1 *Sediment cores used for this study*

CORE	TYPE	LATITUDE	LONGITUDE	WATER DEPTH	CORE LENGTH
ODP Site 1232	marine	39°53,45'S	75°54.08'W	4072 m	381.7 mcd* (uppermost 100 mcd investigated)
SONNE 50SL	marine	38°18.75'S	74°41.85'W	4380 m	7.32 m
LA-KL013	lacustrine	37°53.38'S	73°22.65'W	18 m	13.25 mcd*
LL-KL009	lacustrine	38°09.01'S	73°19.10'W	40 m	12.22 mcd*

*mcd = meter composite depth

The first investigated marine record was drilled during Leg 202 of the Ocean Drilling Program (ODP) at Site 1232 (39°53.45'S, 75°54.08'W) (Mix et al., 2003), which is located in the Chile Basin between the Mocha and Valdivia Fracture Zones (*Figure 1.4* and *Table 1.1*). The drilling position is situated at the outer rim of the Perú-Chile Trench, ~85 km west of the continental margin, where water depth reaches more than 4000 m. The composite profile of the recovered sedimentary sequence adds up to 381.7 mcd (meter composite depth). As it is ascertained by paleomagnetic and biostratigraphic age constraints, the whole record reaches back into the Late Pleistocene (<0.8 Myr) (Mix et al., 2003). Given that the lower part of the sequence is strongly affected by coring disturbances, my analyses concentrate on the uppermost 100 mcd. The main lithology of the sediment core is composed of hemipelagic silty clay. At regular intervals, the hemipelagic deposits are interrupted by coarser layers that are interpreted as basal parts of distal turbidites.

The frequent intercalation of turbiditic layers and hemipelagic sediments is also typical for the second investigated marine record: gravity core 50SL that was drilled during

7

SONNE cruise 161-5, on top of an unnamed seamount (38°18.75'S, 74°41.85'W). The recovered sedimentary sequence is 7.32 m long and covers the last ~25 kyr. Similar to ODP Site 1232, SONNE core 50SL is located within the Perú-Chile Trench in a water depth of 4380 m (Wiedicke-Hombach et al., 2002) (*Figures 1.4* and *1.5*).
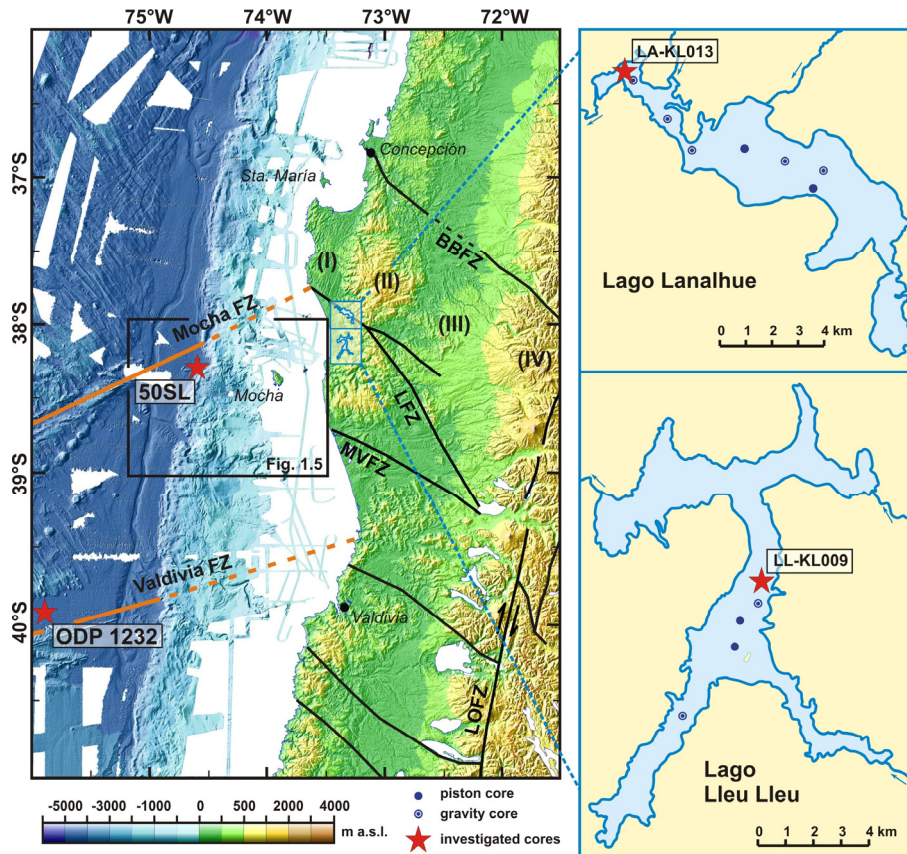
Figure 1.4 *Regional setting of the south-central Chilean forearc and location of the investigated sediment records. Left: Local bathymetry (modified after Grevemeyer et al., 2005; Völker et al., 2006), topography, major faults (modified after Melnick and Echtler, 2006b). Continental plate structures (black): BBFZ = Bío Bío Fault Zone, LFZ = Lanalhue Fault Zone, MVFZ = Mocha-Villarica Fault Zone, LOFZ = Liquiñe-Ofqui Fault Zone). (I) Coastal Platform (Arauco Península), (II) Coastal Cordillera, (III) Central Depression, (IV) Main Cordillera. Oceanic plate structures (orange lines): F.Z. = Fracture Zone. Right: Contours, bathymetry and tributaries of the lakes Lanalhue and Lleu Lleu. Bathymetric contour interval for Lago Lanalhue = 1m, for Lago Lleu Lleu = 10 m.*
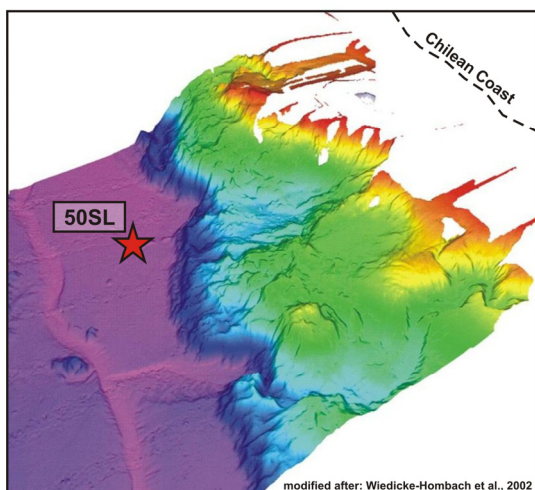
Figure 1.5 *Bathymetry of the continental slope and the margin-parallel trench system (modified after Wiedicke-Hombach et al., 2002). The location of SONNE core 50SL within the trench is indicated by the red star. The dashed line is indicating the Chilean coastline.*

The investigated lacustrine sediment cores – LA-KL013 (37°53.38'S, 73°22.65'W) and LL-KL009 (38°09.01'S, 73°19.10'W) – were drilled in the coastal lakes Lanalhue and Lleu Lleu during an expedition in November/December 2005. Lago Lanalhue and Lago Lleu Lleu are located close to each other on the western slopes of the Coastal Cordillera at ~38°S (*Figure 1.4*). From both lakes several gravity and piston cores were drilled, of which LA-KL013 (Lago Lanalhue) and LL-KL009 (Lago Lleu Lleu) had the best recovery and were hence defined as master cores (*Figure 1.4* and *Table 1.1*). The composite profile of core LA-KL013 is 13.25 mcd long, water depth at the coring site was 18 m. Core LL-KL009 has a composited length of 12.22 mcd and was drilled in a water depth of 40 m. Both cores are composed of brackish/marine sediments at their bottoms, overlain by lacustrine sediments on top.

1.3.2   Methods

Dependent on the sediment character (marine/lacustrine), the roughly estimated age of the sequence (Pleistocene/Holocene), and the priority objective of the investigation, different sedimentological analyses were carried out on the different cores. *Figure 1.6* gives an overview over the basic sampling strategy and the methods that were applied on the marine sediment cores; *Figure 1.7* shows the operation chart for the lacustrine sequences. The most important methods are briefly described below (more detailed descriptions on single methods can be found in *Chapters 2* to *4*).
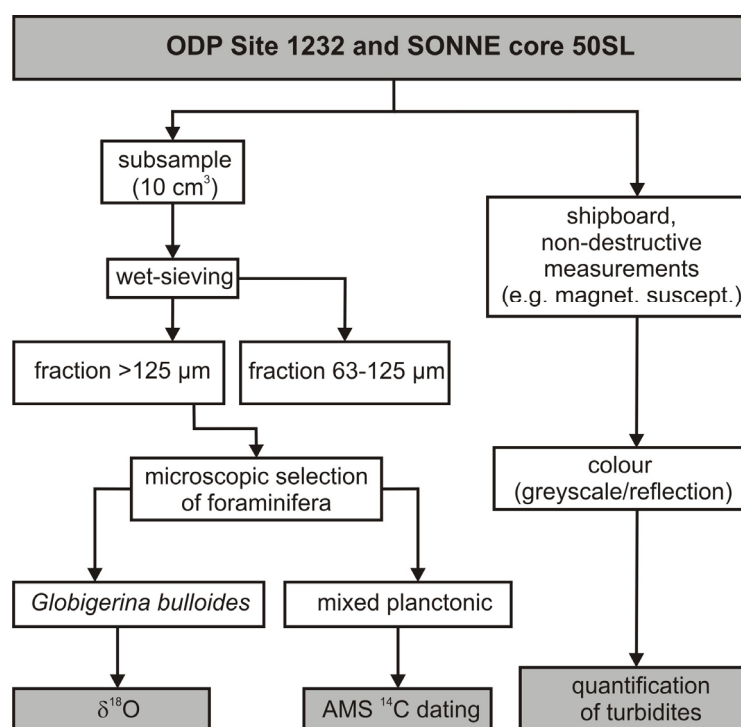
Figure 1.6 Operation chart for the marine sediment records ODP Site 1232 and SONNE core 50SL

```
┌─────────────────────────────────────────────────────────────────┐
│                   Lanalhue and Lleu Lleu cores                    │
└─────────────────────────────────────────────────────────────────┘
                                 │
                                 ▼
        ┌──────────────────────────────────────────────────┐
        │ coring, core opening, facies description, digital imaging │
        └──────────────────────────────────────────────────┘
                                 │
                                 ▼
    ┌──────────────────────────────────────────────────────────┐
    │ magnet. suscept., splice construction & definition of 'master core' │
    └──────────────────────────────────────────────────────────┘
```

Figure chart with boxes: subsampling (working halves); organic matter sampling; SEM micrographs; freeze-drying, weighing, homogenizing; X-ray fluorescence; AMS ¹⁴C dating; TC, TOC & N analyses; X-ray diffraction
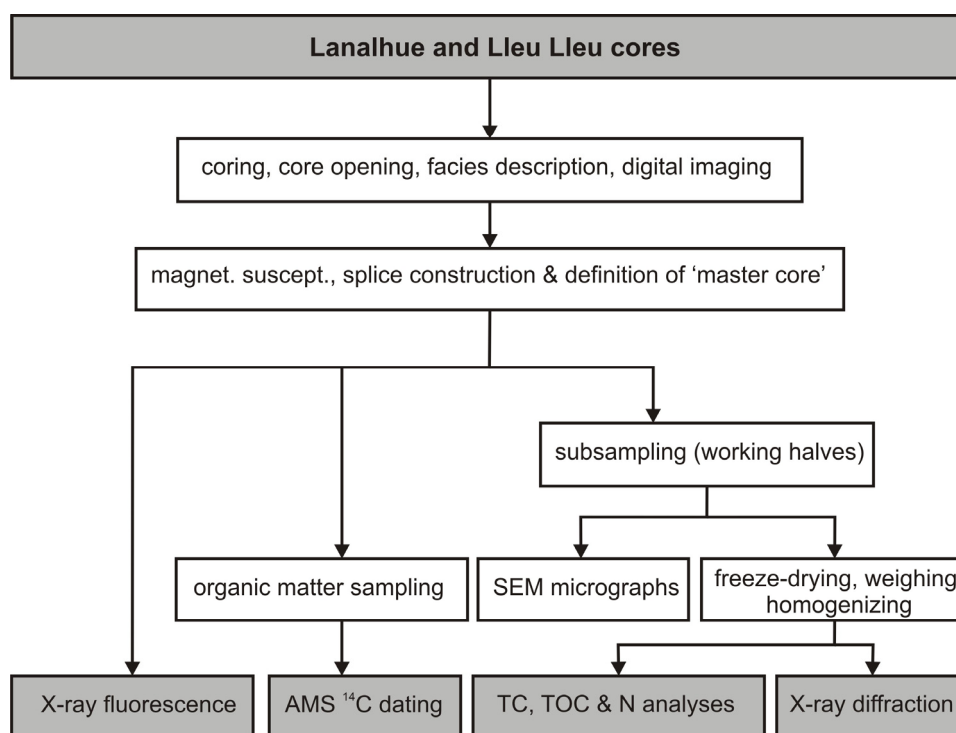
Figure 1.7 *Operation chart for the lacustrine sediment records of Lago Lanalhue and Lago Lleu Lleu*

Magnetic susceptibility measurements

The magnetic susceptibility of sediments is the degree to which the studied material can be magnetized in an external magnetic field. It is largely a function of ferrimagnetic minerals contained in a sample like, for example, magnetite (Oldfield et al., 1978). Since magnetic susceptibility measurements have the advantage of being simple, rapid and low cost analyses, they were initially performed on all studied sediment cores. Whole-core measurements were done shipboard for the core of ODP Site 1232 (ODP Multisensor track, 5-cm resolution, Mix et al., 2003) and the SONNE core 50SL (GEOTEK Multisensor system, 2-cm resolution, Wiedicke-Hombach et al., 2002). On the Lanalhue and Lleu Lleu sequences, magnetic susceptibility was measured at 1-mm resolution with an automatic logging system, developed at the GFZ Potsdam, in combination with a Bartington MS2E/1 spot-reading sensor directly after opening, description, and digital imaging of the cores.

Magnetic susceptibility results were used for constructing composite profiles of the ODP core and the lacustrine records of the lakes Lanalhue and Lleu Lleu. Three holes were drilled at ODP Site 1232 from which a composite sequence and splice was build for the uppermost 100 mcd (Mix et al., 2003). In Lago Lanalhue and Lago Lleu Lleu, two to three overlapping core-sections were recovered at each drilling site, ensuring the completeness of the sedimentary sequences. Magnetic susceptibility values were further used for a first rough quantitative estimate of turbiditic layers in the ODP record.

10

Dating methods

Basis for the following measurements is the accurate and reliable dating of the sediments investigated. For absolute age determination, Accelerator Mass Spectrometry (AMS) ^{14}C dating was done on foraminifera (ODP Site 1232 and SONNE core 50SL) and plant remains (LA-KL013 and LL-KL009) at the Leibniz-Laboratory for Radiometric Dating and Stable Isotope Research in Kiel (Germany) and at the ETH Zürich (Switzerland).

From the marine sediments of ODP Site 1232 and SONNE core 50SL, mixed planktonic foraminifera were extracted out of the hemipelagic intervals just beneath the turbiditic layers. Six AMS ^{14}C dates provide the age control for the ODP sediments between 0.8 to 34.14 mcd (18.04 ± 0.33 to 44.24 ± 1.29 cal kyr BP), four dates were measured for core 50SL between 1.05 to 6.15 mcd (2.21 ± 0.08 to 22.08 ± 0.45 cal kyr BP). All ages were calibrated with the CALPAL software, using the 2004 January calibration curve (Stuiver et al., 1998; Hughen et al., 2004). For the lacustrine records, measurements were done on organic material (plant fragments, bivalves or foraminifera) or, alternatively, on bulk sediments. The age models are based on 17 datings for LA-KL013 and 10 datings for LL-KL009; radiocarbon ages were calibrated with the CALIB 5.0 software (Stuiver et al., 2005), using the Southern Hemisphere Calibration Curve (SHCal04; McCormac et al., 2004) and the marine calibration curve (marine 04; Hughen et al., 2004).

The radiocarbon dating method is based on the exponential decay of radioactive ^{14}C implemented by living organisms during their lifespan. After the death of an organism, radioactive ^{14}C is decaying to ^{12}C with a half-life of 5730 years (e.g. Meyers and Ishiwatari, 1995). AMS ^{14}C dating is hence applicable for organic material younger than ~50 kyr (Walker, 2005). Sediments of the ODP sequence below 34.14 mcd (44.24 ± 1.29 cal kyr BP) were thus dated by the establishment of an oxygen isotope curve (δ^{18}O) and its correlation to a well-dated oxygen isotope record from the south-western Pacific (MD 97-2120; Pahnke et al., 2003). The oxygen isotope chronostratigraphy is based on the assumption that foraminiferal δ^{18}O is dependent on the temperature and the δ^{18}O of the seawater in which the species formed; the δ^{18}O of the seawater is in turn a function of global ice volume and water salinity (e.g. Lisiecki and Raymo, 2005). Since the signals of most globally distributed marine δ^{18}O records are largely consistent, oxygen isotope ratios of calcareous microfossils are widely used in correlating Quaternary marine sediments (e.g. Walker, 2005).

Oxygen isotope analyses of the ODP sediments were done on planktonic foraminifera of the species *Globigerina bulloides* at the GFZ Potsdam with a Finnigan MAT 253 mass spectrometer coupled with an automatic carbonate preparation system (Kiel IV device). For each measurement, ten foraminifera with a diameter of 250-350 μm were carefully selected under a binocular microscope in order to avoid size-depending δ^{18}O effects. Sample spacing was about 30 cm; however, since several samples did not contain enough material for reliable analyses, the final resolution of the oxygen isotope record is partly lower.

X-ray fluorescence (XRF) scanning

X-ray fluorescence (XRF) scanning is a non-destructive analytical technique for the semi-quantitative detection of major chemical elements (e.g. Al, Si, S, K, Ca, Ti, Mn and Fe) in the sediment, directly at the surface of split cores (e.g. Jansen et al., 1998; Croudace et al. 2006; Haschke 2006; Richter et al., 2006). While standard geochemical analyses of individual samples are destructive, time-consuming and expensive, XRF-scanning allows fast whole-core measurements of the geochemical composition of sediments and results in high resolution data sets.

The principle of the XRF method is based on the excitation of electrons by the incidence of X-radiation (e.g. Richter et al., 2006). Ejected electrons from the inner shell of an atom are substituted by electrons falling back from the outer shells. Occurring energy differences are emitted as electromagnetic radiation, whose wavelength spectra are characteristic for the atoms of specific elements and allows an estimation of their relative abundance. Admittedly, the conversion of the measured element intensities into quantitative element concentrations is still problematic (e.g. Weltje and Tjallingii, 2008). Results are hence given as element intensities, count rates (counts per unit time per unit area), or ratios of counts (e.g. Richter et al., 2006, Thomson et al., 2006). In recent years, XRF-analyses of sediment cores are used for paleoenvironmental reconstructions on various time scales, high-resolution time-series studies and stratigraphic correlations (e.g. Arz et al., 2001; Haug et al., 2001; Lamy et al., 2001; Jaccard et al., 2005).

For the present study, XRF-measurements were performed on the sediment cores of Lago Lanalhue and Lago Lleu Lleu (LA-KL103 and LL-KL009) with the AVAATECH XRF-scanner at the Alfred-Wegener-Institut (AWI) in Bremerhaven, Germany. Values are given in total counts (tc). The scanning-resolution for both cores was 1 cm (tube voltage: 10kV; X-ray current: 350 mA; counting time: 30s). The uppermost ~5 mcd of the Lanalhue sequence were additionally scanned at 2-mm resolution (tube voltage: 10kV; X-ray current: 1000 mA; counting time: 60s).

Carbon and nitrogen measurements

The total carbon (TC), total organic carbon (TOC) and organic nitrogen (N) contents of the lacustrine sediments (LA-KL013 and LL-KL009) were measured with an elemental analyzer (Eurovector) at the GFZ Potsdam, Germany. The amount of total inorganic carbon (TIC) was subsequently calculated as the difference between TC and TOC (TC-TOC = TIC). Resolution of the measurements was 5 cm for core LA-KL013, 2 cm for the uppermost part of LL-KL009 (0-3.72 mcd) and 20 cm for the lower part of the Lleu Lleu core (3.72-12.22 mcd). Values are given in weight-%.

The measurement of the total organic carbon concentration in sediments is one of the most common geochemical analyses in paleolimnology (Cohen, 2003). TOC reflects the bulk of allochthonous and autochthonous organic matter that was not affected by remineralization during the process of sedimentation (Meyers, 2003). The principal origin of the organic material (aquatic or terrestrial) can be distinguished using the amount of carbon relative to the amount of nitrogen (C/N ratio). Aquatic organic matter is richer in N and has lower C/N ratios (between 4 and 10) than terrestrial organic

12

matter from vascular land plants (C/N ratios higher than 20) (e.g. Meyers, 1994; Meyers and Teranes, 2001; Cohen, 2003). Determination of the C/N ratio is hence a useful tool for reconstructing temporal changes in the source of organic material (Meyers and Ishiwatari, 1995). The TIC content of lake sediments reflects the sum of carbonate minerals, including both inorganic and biogenic components (e.g. Ito, 2001). Inorganic carbonate may be of autochthonous and/or allochthonous origin and hence provide information about the lake system and/or the lake catchment. Biogenic carbonate is present in the form of calcareous microfossils.

1.3.3   Structure of this work

In the following chapters, I present the results of my research in the form of three individual manuscripts (*Chapters 2 to 4*), which are already published or submitted to peer-reviewed journals.

In the first manuscript, entitled '*Turbiditic Trench Deposits at the South-Chilean Active Margin: A Pleistocene-Holocene Record of Climate and Tectonics*' (*Chapter 2*), I focussed on the changes in turbidite frequencies found in the marine sediment records of ODP Site 1232 and in SONNE core 50SL. Assuming that turbiditic layers in the marine sediments at the highly active margin of Southern Chile are mainly seismically triggered, frequency changes might indicate temporal variations in the earthquake cyclicity. The main outcome is the detection of high turbidite frequencies during glacial and low turbidite frequencies during interglacial periods, indicating a climatic rather than a seismic control on the event layer deposition.

In the second manuscript '*Forearc uplift rates deduced from sediment cores of two coastal lakes in south-central Chile*' (*Chapter 3*), I interpret the sedimentary records of Lago Lanalhue and Lago Lleu Lleu with regard to local tectonics. Both lake basins are at present impounded behind an uplifted sill, whereas in former times they were in connection with the Pacific Ocean. Dating of the transition from marginal-marine to lacustrine conditions allowed reconstructing the time of lake formation and calculating local uplift rates. Based on these findings, I subsequently discussed the alignment of major local fault systems.

Ever since the formation of Lago Lanalhue and Lago Lleu Lleu, lacustrine sediments accumulated in their basins and preserved continuous records of climate variability. Given these premises, I discuss the sedimentary sequences of both lakes in terms of climate in the third manuscript '*Holocene climate and environmental changes documented in the sedimentary records of two coastal lakes in south-central Chile (38°S)*' (*Chapter 4*). Although the sedimentation in both lakes reacted individually to changes in the local climate, the records show a similar long-term trend of increasing aridity from the Mid- to Late Holocene. During the last 2000 years, pronounced variations in the lake sedimentation suggest important hydrological changes also on the centennial time-scale.

In the last chapter of my thesis (*Chapter 5*), I combine and summarize the main results of all three articles, before drawing the final conclusions.

2. TURBIDITIC TRENCH DEPOSITS AT THE SOUTH-CHILEAN ACTIVE MARGIN: A PLEISTOCENE - HOLOCENE RECORD OF CLIMATE AND TECTONICS

S. Blumberg, F. Lamy, H.W. Arz, H.P. Echtler, M. Wiedicke, G.H. Haug, O. Oncken

Abstract: The active plate margin of South America is characterized by a frequent occurrence of large and devastating subduction earthquakes. Here we focus on marine sedimentary records off Southern Chile that are archiving the regional paleoseismic history over the Holocene and Late Pleistocene. The investigated records – Ocean Drilling Program (ODP) Site 1232 and SONNE core 50SL – are located at ~ 40°S and ~ 38°S, within the Perú-Chile trench, and are characterized by frequent interbedded strata of turbiditic and hemipelagic origin. On the basis of the sedimentological characteristics and the association with the active margin of Southern Chile, we assume that the turbidites are mainly seismically triggered, and may be considered as paleo-megaearthquake indicators. However, the long-term changes in turbidite recurrence times appear to be strongly influenced by climate and sea level changes as well. During sea level highstands in the Holocene and Marine Isotope Stage (MIS) 5, recurrence times of turbiditic layers are substantially higher, primarily reflecting a climate-induced reduction of sediment availability and enhanced slope stability. In addition, segmented tectonic uplift changes and related drainage inversions likely influenced the postglacial decrease in turbidite frequencies. Glacial turbidite recurrence times (including MIS 2, MIS 3, cold substages of MIS 5, and MIS 6), on the other hand, are within the same order of magnitude as earthquake recurrence times derived from the historical record and other terrestrial paleoseismic archives of the region. Only during these cold stages sediment availability and slope instability were high enough to enable recording of the complete sequence of large earthquakes in Southern Chile. Our data thus suggest that earthquake recurrence times on the order of 100 to 200 years are a persistent feature at least during the last glacial period.

2.1   Introduction

Submarine slopes at active convergent plate margins are preferential regions for the generation of large-scale turbidity currents. In the trench sediment records the deposits of these underwater mass movements are interbedded as clearly identifiable turbiditic layers within the otherwise (hemi-)pelagic sediments. Assuming that the turbidity currents within seismically active regions are predominantly earthquake-triggered, the appropriate turbidite records can be used for paleoseismic investigations. Recently, this approach has been successfully applied for instance in Cascadia (Adams, 1996; Goldfinger et al., 2003; Goldfinger et al., 2007), Saanich Inlet in British Columbia (Blais-Stevens and Clague, 2001), California (Gorsline et al., 2000), Northern Chile (Vargas et al., 2005), Taiwan (Huh et al., 2004) and Japan (Inouchi et al., 1996; Nakajima and Kanai, 2000).

In this study, we applied the approach to the area of Southern Chile by using turbiditic sequences as paleoseismic records. The tectonically active region of Southern Chile along the convergent continental margin is characterised by high deformation rates, uplift and subsidence, and severe earthquakes, including the strongest event ever recorded from 1960 with a magnitude of 9.5 (Plafker and Savage, 1970). Paleoseismic studies in Southern Chile so far focus on coseismically uplifted beach berms (Nelson and Manley, 1992; Bookhagen et al., 2006), their active and longer term tectonic context (Melnick et al., 2006), sedimentary tsunami horizons (Cisternas et al., 2005) as well as on historical evidence of earthquakes and their secondary effects (Lomnitz, 1970; Lomnitz, 2004). Based on these different archives, the earthquake recurrence intervals in south-central Chile are fairly discussed for the mid to Late Holocene but, as elsewhere, are hardly investigated for older periods, e.g. the Pleistocene. Here, we present the first paleoseismic study covering a complete glacial to interglacial cycle. Due to its position in front of the active continental margin of Southern Chile the marine sedimentary record of ODP Site 1232 is well suited for a paleoseismicity study. Late Pleistocene in age, the succession is characterised by hemipelagic sediments with frequently interbedded turbiditic deposits.

Climatic and hydrologic conditions of Southern Chile have influenced sedimentation since the onset of the glaciation in the Patagonian Andes six million years ago. Since then, the sediment influx to the Chile Trench south of the Juan-Fernández Ridge has increased tremendously and induced persistent accretion and subduction of terrigenous material (Bangs and Cande, 1997; Melnick and Echtler, 2006a). In particular, the climate variations during the Pleistocene period affected the sedimentation rate and pattern on- and offshore (Lamy et al., 2001; Lamy et al., 2002; Lamy et al., 2004; Hebbeln et al., 2007). Our study suggests that these climate changes and related sea level variations over the last glacial to interglacial cycle impacted particularly the long-term pattern of earthquake recurrence as recorded in the submarine sediment sequence: Only during cold stages of the past 140 kyr, sediment availability and slope instability were high enough to allow recording of the complete sequence of large earthquakes in Southern Chile.

2.2   Investigation area

2.2.1   Tectonics and bathymetry

The active margin of Southern Chile is part of the convergence zone between the oceanic Nazca Plate and the South American continent. The oblique subduction of the Nazca Plate is taking place at a rate of 66 mm/yr (Angermann et al., 1999) forming the long range of the Andes as well as the outstanding depression of the Perú-Chile trench. Between the Juan Fernández Ridge in the north (34°S) and the Chile Rise in the south (46°S), the trench is filled by sediments of partly more than 2 km thickness (*Figure 2.1*) locally appearing rather as a flat plain than as a bathymetric depression (Miller, 1976; Schweller et al., 1981; Bangs and Cande, 1997).
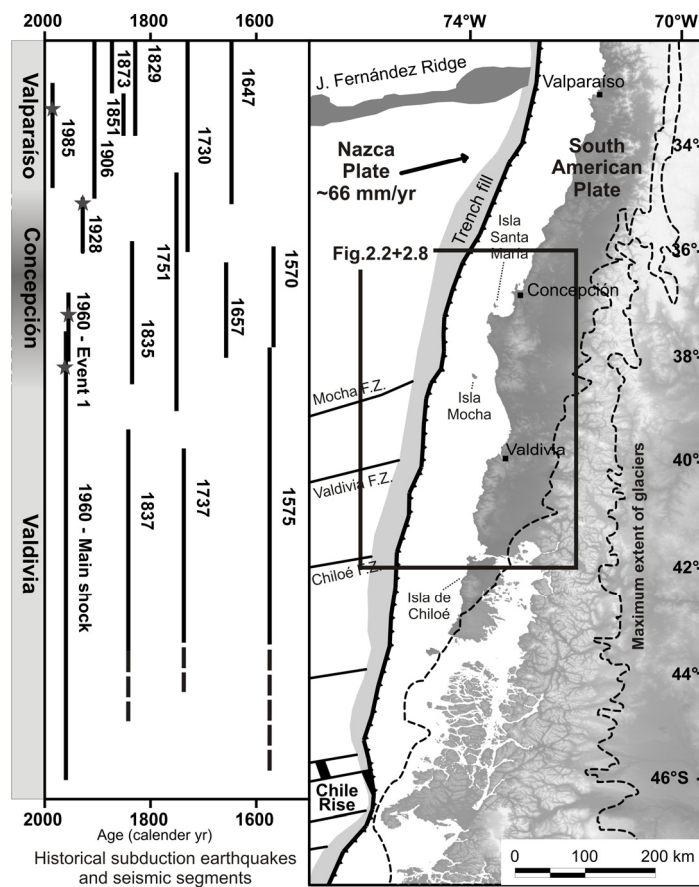

Figure 2.1: Survey map of the on- and offshore study area including the historical earthquake record and geographical extent of the stated events; the particular seismic segments are indicated on the left, main tectonic features of the South-Chilean active margin on the right (modified after Melnick et al., 2006). Compilation of earthquakes according to Lomnitz (1970, 2004), Kelleher (1972), Comte et al. (1986), Cifuentes (1989), Beck et al. (1998) and Campos et al. (2002). Tectonic features and trench fill were taken from Bangs and Cande (1997) and Tebbens and Cande (1997). The white shaded area indicates the maximal extension of the Patagonian Ice Sheet during the Last Glacial (after Rabassa and Clapperton, 1990). F.Z. = fracture zone.

The trench infill is composed of interbedded turbiditic and hemipelagic strata which show certain cyclicity in their overall seismic reflection pattern interpreted to express the influence of global climate cycles on sedimentation (Rauch, 2005; Völker et. al.,

17

2006). Since the onset of glacial erosion and denudation in the Andes about six million years ago the trench fill sediments controlled the subduction dynamics, changing the formerly erosive to an accretionary margin (Melnick and Echtler, 2006a). The excess trench sediments moreover smoothed out the surface of the subducting plate with a lubricating effect on the plate interface. That way, the trench fill sediments and the consequent subduction channel enhance the occurrence of great subduction earthquakes since it is allowing the rupture to disperse over a wider zone (Lamb and Davis, 2003; Ruff, 1989). On this account, the Southern Chilean margin is periodically affected by devastating earthquakes of M>8 (Lomnitz, 1970; Lomnitz, 2004), including the prominent M_W 9.5 Valdivia event in 1960 which ruptured about 1000 km of the Chilean forearc between ~ 37° and 46°S (Plafker and Savage, 1970) (*Figure 2.1*). Even though this widespread rupture zone indicates a rather homogenous plate interface, the long-term morphotectonic evolution of the Chilean forearc appears to be highly complex (Rehak et al., 2008). Between 36° and 42°S, the Chilean forearc is characterized by a distinct morphotectonic segmentation that follows the main NW-SE orientated fault zone (Hackney et al., 2006). The individual segments are showing a differentiated structural and geomorphological evolution (Rehak et al., 2008).

The continental hinterland is characterized by three principal physiographic and morphotectonic units: the Coastal Cordillera, the Longitudinal Valley (Munoz et al., 2000), and the Main Cordillera (Thornburg and Kulm, 1987). The Coastal Cordillera exposes moderate elevations generally below 500 m a.s.l. while the Main Cordillera reaches up to 2000-3000 m a.s.l. The Longitudinal Valley between both mountain ranges is filled with up to 4000 m thick Neogene to recent mainly alluvial sediments (Melnick and Echtler 2006b). In the investigated area, the intermediate width of the Chilean continental shelf averages 20-30 km, with the shelf edge lying in a water depth of maximal 150-250 m (Zapata, 2001). Large submarine canyon systems are crossing the westwards sloping margin in prolongation of major onshore river systems. These canyons are acting as natural sediment traps and channels for terrestrial sediments that are transported down the continental slope filling the Perú-Chile trench at about 4000 m water depth (Völker et al., 2006).

Several canyon systems can be distinguished within the study area; from south to north they are associated with the Valdivia, Toltén, Imperial, and Bío Bío River systems (*Figure 2.2*). Most of these canyons are building up submarine fans where they enter the trench. The outer limit of these fans is marked by a slightly winding axial channel of 1 to 5 km width and 50 to 200 m depth (Völker et al. 2006), which takes course northwards within the trench for more than 1000 km. The channel is part of the collective depositional trench system in which the sediments are generally transported equatorwards due to a slightly northward tilting of the northward older and in consequence colder and less buoyant oceanic plate (Thornburg et al., 1990; Thornburg and Kulm, 1987). The Juan-Fernández ridge (33°S) forms a natural barrier to these mass flows (Melnick and Echtler, 2006a).
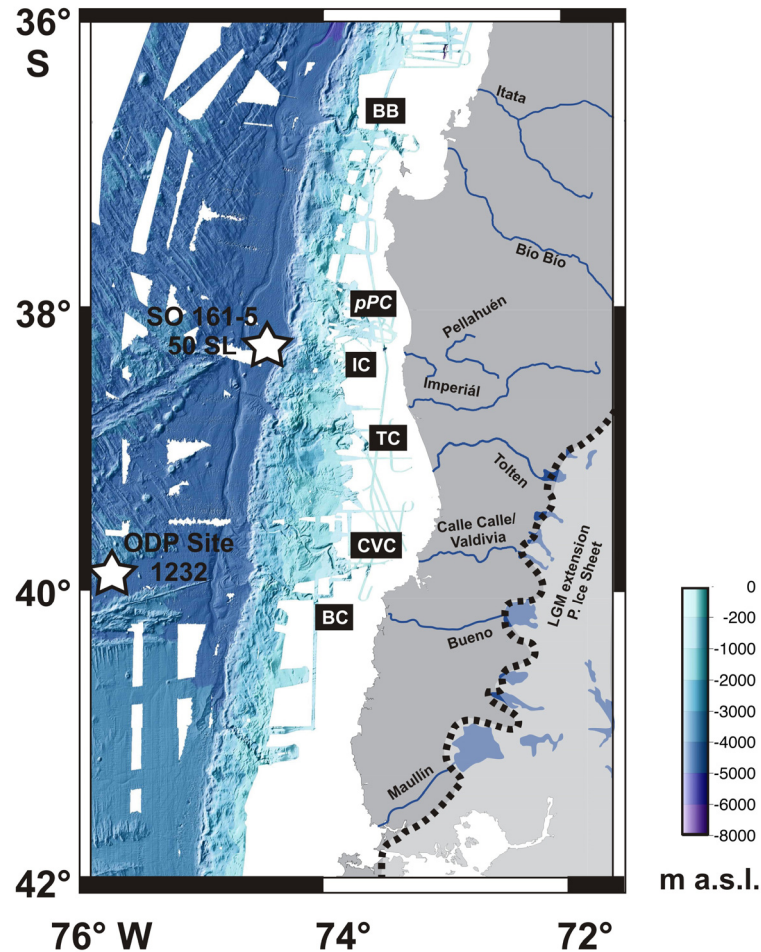
Figure 2.2: *Local bathymetry (modified after Grevemeyer et al., 2005 and Völker et al., 2006), courses of rivers and corresponding canyon systems (canyon systems after Thornburg et al., 1990). BB = Bío Bío Canyon, pPC = paleo Pellahuén Canyon, IC = Imperial Canyon, TC = Toltén Canyon, CVC = Calle Calle/Valdivia Canyon, BC = Bueno Canyon. Core locations of both investigated sediment cores are plotted.*

2.2.2 Present and past climate

Today, the study area is located within the transition zone between a summer dry Mediterranean climate north of 37°S and year-round humid conditions south of 42°S. The local climate is characterized by humid temperate conditions with all-season precipitation peaking in austral winter (Miller, 1976). Prevalent cyclonic storms originating from the Southern Westerlies are bringing heavy rainfalls to the coastal mountains and the Andes (~ 2500 mm/yr at 40°S). As a consequence, local erosion rates are high and induce enormous fluvial sediment fluxes to the ocean (Lamy et al., 2001). The track and intensity of the prevailing storms is generally regulated by the strength and position of the subtropical anticyclone in the Southeast Pacific and by the circum-Antarctic low pressure belt (Markgraf, 1998). The persistent blowing westerly winds prevent coastal upwelling south of 39°S (Mohtadi et al., 2005).

Studies of terrestrial and marine paleoclimatic records demonstrate that the overall rainfall pattern and oceanographic regime shifted by ~ 5° of latitude between glacials

19

and interglacials (Veit, 1996; Lamy et al., 2001). Apparently, this shift is due to a northward displacement of the Antarctic Circumpolar Current and the associated Southern Westerlies under glacial conditions (Lamy et al., 2004). Compared to the Holocene, the local continental precipitation was remarkably high during the last glacial period. At the same time, southern Chile was covered by the Patagonian Ice Sheet, which stretched out ~ 1800 km along the axis of the Andes (between ~ 38° and 56°S) during the Last Glacial Maximum (*Figure 2.1*).

2.3   Materials and methods

The present study is based on marine sediments that were recovered in the Chile Basin at ODP Site 1232 during Leg 202 (Mix et al., 2003). The Site is located at the outer rim of the Perú-Chile trench, ~85 km west of the continental slope (39°53.45′S, 75°54.08′W) in a water depth of 4072 m (*Figure 2.2*). Three Advanced Piston Corer holes were drilled to ensure a complete stratigraphic record. The recovered sediments extended to 362.1 m below sea floor (mbsf), and a composite section of 381.7 mcd (meter composite depth) was constructed.

The dominant lithology of the sequence is composed of greenish-gray to light-gray hemipelagic silty clay, displaying little visual variability and showing very few sedimentary structures (Mix et al., 2003). Some mottling, light brown nodules and thin silt layers are occurring sporadically. The sand content is negligible; the silt content is varying between ~ 10% and 40%. Clay minerals and feldspars are abundant whereas amphiboles, pyroxenes, and quartz are present in minor amounts. Biogenic components are generally sparse.

A second lithology is intercalated with the dominant hemipelagic silty clay on decimeter scale (Mix et al., 2003). It consists of coarser and much darker material – typically silty sand or sandy silt – that strongly differs from the hemipelagic sediments in texture and physical properties, although not in mineralogy. In general, the coarser layers are overlying sharp, partly erosional basal contacts and grading upward over several centimeters to silty clay. They are interpreted as basal parts of distal turbidite deposits.

In the present study, we focus on the uppermost 100 mcd of the sedimentary sequence because the deeper part of the core is strongly influenced by coring disturbance (Mix et al., 2003). The alternation of hemipelagic clays and coarser turbiditic deposits is also typical for gravity core 50SL that was recovered during SONNE cruise 161-5 on top of an unnamed seamount that rises 200 m from the surrounding flat, sediment-filled floor of the Perú-Chile trench (Wiedicke-Hombach et al., 2002). The 732 cm long core is located north of ODP Site 1232 at 38°18.75′S, 74°41.85′W in a water depth of 4380 m, 15 km west of the Chilean continental slope (*Figure 2.2*).

2.3.1 Turbidite identification

Turbiditic layers of ODP Site 1232 were identified by means of their physical properties like magnetic susceptibility and color, as these proxies show characteristic differences between the turbidites and hemipelagic background sediments (*Figure 2.3*).
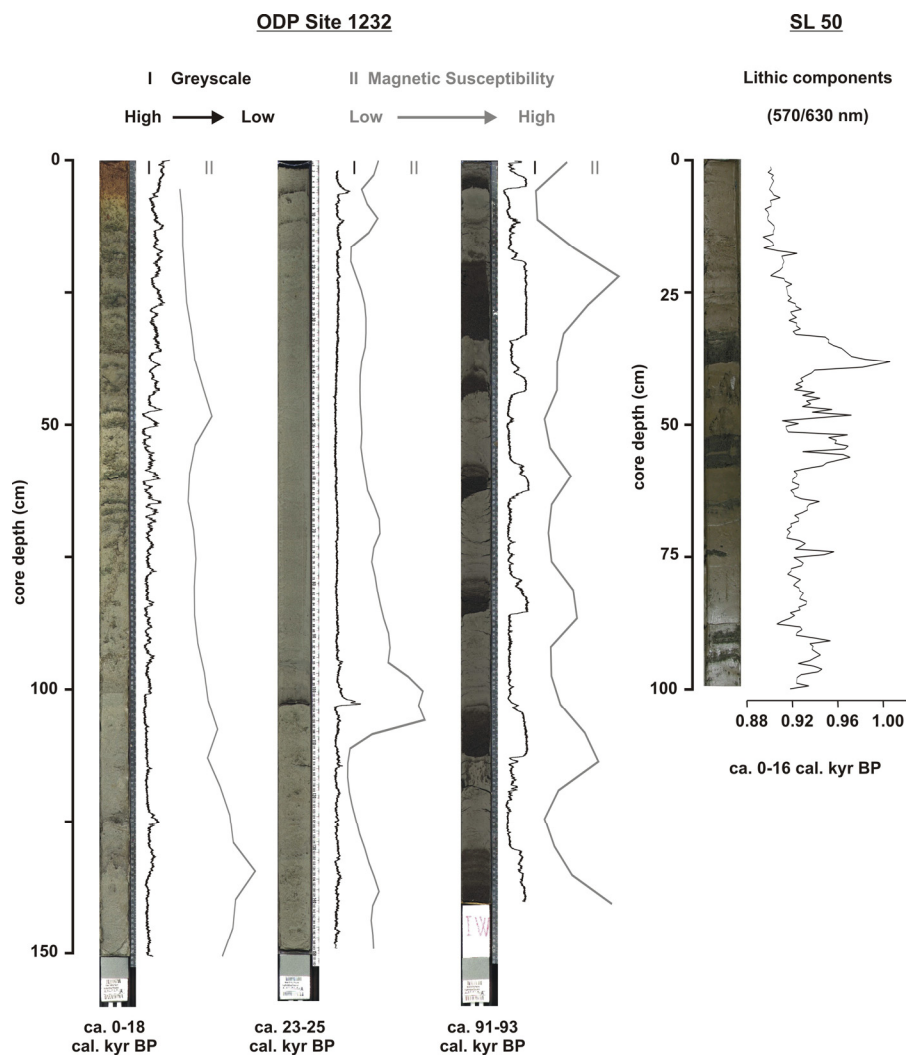

Figure 2.3: *High-resolution greyscale data profile of ODP core 1232 derived from core photography and magnetic susceptibility data measured onboard with a Multisensor Core-Logger at 5-cm intervals (Mix et al., 2003). Both parameters display distinctly different values for the turbiditic layers and for the hemipelagic layers and are, thus, used for the quantification of the turbidites. Turbidites of core SL 50 were identified by means of colour scanning with a Spectrolino scanner; the ratio of the reflectance at 570 nm over that of 630 nm provides a proxy for lithic sediment components (Rein and Sirocko, 2001; Rein, 2003).*

Whole core magnetic susceptibility measurements were collected on board the drilling vessel *JOIDES Resolution* at 5-cm increments with the ODP multisensor track (Mix et al., 2003). This relatively low resolution did not allow the detection of each single turbidite layer. A more precise identification of turbidites was attained by a detailed description of the split core and by high resolution greyscale processing of digital core pictures. In this way, the core depth and the thickness of each turbiditic layer could be clearly identified. Afterwards, all turbidites were subtracted from the record, in order to

correct the depth for stratigraphic purposes, considering only the undisturbed hemipelagic sediments. In the following, all corrected depth information of ODP Site 1232 is given in meter corrected composite depth (mccd).

Turbidites in RV SONNE core 50SL (SO161) were initially identified by core logging with a GEOTEK core logger using a gamma attenuation probe; logging interval was 2 cm. A refinement of the result was achieved by core description of the split and opened core and subsequent high-resolution colour scanning with the Spectrolino scanner of GRETAG; scanning interval was 5 mm. This instrument acquires reflectance spectra of visible light in 36 discrete wavelength intervals between 380-730 nm. According to Rein and Sirocko (2001) and Rein (2003) a simple ratio of the reflectance at 570 nm over that of 630 nm provides a proxy for lithic sediment components (*Figure 2.3*). Consistent with ODP Site 1232, the identified turbidites of core 50SL were subtracted from the original record for depth correction.

2.3.2   Stratigraphy

A preliminary age model for ODP Site 1232 was created on board the vessel, based on biostratigraphic and paleomagnetic data (Mix et al., 2003). We updated and improved this model by using ^{14}C accelerator mass spectrometry (AMS) dating and stable oxygen isotope measurements on planktonic foraminifera (*Globigerina bulloides*). Samples for dating and stable isotope measurements were extracted from the hemipelagic sediments just beneath the turbiditic sequences. Sample spacing was about 30 cm. The resolution of our isotope record is lower for the MIS 5, as carbonate content is very low and many samples did not contain sufficient foraminifera.

Table 2.1: *AMS ^{14}C ages of ODP Site 1232 and correlation points to oxygen isotope data of core MD 97-2120 from the south-western Pacific (Pahnke et al., 2003).*

Orig. Depth (mcd)	Corr. Depth (mccd)	^{14}C AMS Age (kyr)	Calibrated Age (kyr cal. B.P.)	Dating Method	Dated Material
0.6	0.35	-	12.47	correlation to MD 97-210	*G. bulloides*
0.8	0.48	15.31 ± 0.07	18.04 ± 0.33	^{14}C AMS (KIA 27368)	Mixed planktonic
3.69	2.99	17.83 ± 0.09	20.53 ± 0.34	^{14}C AMS (KIA 27369)	Mixed planktonic
6	4.76	20.14 ± 0.11	23.03 ± 0.18	^{14}C AMS (KIA 27370)	Mixed planktonic
14.64	11.66	25.25 ± 0.21	28.82 ± 0.29	^{14}C AMS (KIA 27371)	Mixed planktonic
23.74	17.55	30.47 ± 0.37	34.34 ± 0.43	^{14}C AMS (KIA 27372)	Mixed planktonic
34.14	23.18	43.09 ± 1.7	44.24 ± 1.29	^{14}C AMS (KIA 27373)	Mixed planktonic
48.36	32.07	-	66.09	correlation to MD 97-2120	*G. bulloides*
81.68	53.98	-	113.58	correlation to MD 97-2120	*G. bulloides*
91.93	60.23	-	120.21	correlation to MD 97-2120	*G. bulloides*
92.64	60.69	-	129.25	correlation to MD 97-2120	*G. bulloides*
96.8	64.26	-	138.16	correlation to MD 97-2120	*G. bulloides*

Absolute age control for the interval between 0.8 and 34.14 mccd is provided by six AMS ^{14}C-dates on mixed planktonic foraminifera samples, which were analysed at the Leibniz Laboratory in Kiel (*Table 2.1*). We calibrated the ages with the CALPAL software, using the CALPAL 2004 January calibration curve (Stuiver et al., 1998; Hughen et al., 2004b). We presume no regional variation from the global reservoir effect of 400 years because the site is situated distinctly south of the Chilean upwelling zone and well north of the southern polar front. This corresponds to the mean reservoir effect for the Pacific Ocean of 400 years (Lamy et al., 2004).

Age control below 34.14 mccd is provided by the correlation of the oxygen isotope data of ODP Site 1232 and the well dated oxygen isotope record of core MD 97-2120 from the south-western Pacific (Pahnke et al., 2003) (*Table 2.1*). Stable oxygen isotope measurements of both records are based on the planktonic foraminifera *Globigerina bulloides*. The oxygen isotopes of ODP Site 1232 were analysed at the GFZ Potsdam, using a Finnigan MAT 253 mass spectrometer coupled with an automatic carbonate preparation system (Kiel IV device). To prevent a size-dependent effect on the $\delta^{18}O$ values and to reduce a possible intrasample noise, ten foraminifera with a diameter of 250-350 μm were hand-picked per sample and used for the measurements. The $^{18}O/^{16}O$ ratio is given in delta notation and per mil (‰) relative to the VPDB standard calibrated with NBS-19. Analytical standard deviation for $\delta^{18}O$ is less than 0.06‰.

Table 2.2: *AMS ^{14}C ages of SONNE core 50SL and correlation points to oxygen isotope data of core MD 97-2120 from the south-western Pacific (Pahnke et al., 2003).*

Orig. Depth (m)	Corr. Depth (m)	[14]C AMS Age (kyr)	Calibrated Age (kyr cal. B.P.)	Dating Method	Dated Material
0.1 - 0.25	0.1 - 0.25	2.58 ± 0.035	2.21 ± 0.08	[14]C AMS (KIA 21757)	Mixed planktonic
1.05	0.82	-	15.24	correlation to MD 97-120	*G. bulloides*
1.26	1.01	-	17.54	correlation to MD 97-120	*G. bulloides*
1.45 – 1.60	1.18 – 1.33	15.25 ± 0.09	18.0 ± 0.35	[14]C AMS (KIA 21758)	Mixed planktonic
4.0 – 4.15	3.06 – 3.21	17.38 ± 0.1	19.9 ± 0.18	[14]C AMS (KIA 25258)	Mixed planktonic
6.10 – 6.20	4.41 – 4.51	19.16 ± 0.12	22.08 ± 0.45	[14]C AMS (KIA 25259)	Mixed planktonic
7.26	5.42	-	23.25	correlation to MD 97-120	*G. bulloides*

Similarly, stable oxygen isotope analyses of SONNE core 50SL were established using the planktonic foraminifera *Globigerina bulloides*; a general stratigraphy is presented in Völker et al. (2006). In accordance with the age model generation of ODP Site 1232, we also correlated the oxygen isotope data of core 50SL to the oxygen isotope record of core MD 97-2120 (*Table 2.2*). For absolute age control of core 50SL four AMS ^{14}C mixed planktonic foraminiferal samples were extracted from 15 cm depth-sections of the core (*Table 2.2*). Analyses were done at the Leibniz Laboratory in Kiel. All ages were calibrated as described above.

2.4   Results

2.4.1   Turbidites

In total, more than 600 turbiditic layers were identified within the uppermost 100 mcd of the Site 1232 sedimentary sequence using the combined macroscopic and colour scan identification. All of them show a characteristic sharp, although rarely planar, basal contact. Many of the contacts have a potential erosional surface and/or are deformed and inclined from parallel to nearly perpendicular to the overall layering, perhaps as a result of drilling disturbances (Mix et al., 2003). Internally, the turbiditic layers show the typical grading upward. In many cases the upper limit of the layers is blurred and poorly defined; it is then difficult to exactly determine the boundary between the turbiditic layers and the new start of the hemipelagic sedimentation. However, measured from the basal contact to the first clear shift in colour and magnetic susceptibility, the turbidite thicknesses vary between few millimeters and several decimeters, with an average of ~ 5 cm (*Figure 2.3*). The total thickness of all turbiditic layers adds up to more than 30 meters (~ 30% of the whole section), which leaves 70 meters of undisturbed hemipelagic sediments (~ 70% of the whole section).

A total of 47 turbiditic layers were identified in SONNE core 50SL. Turbidites vary in thickness between about 5 mm and ~ 11 cm with an average of ~ 3.9 cm. The layers display sharp to diffuse (bioturbation) lower boundaries and commonly well developed upward fining (Wiedicke-Hombach et al., 2002). Several turbidites show multiple sedimentation pulses, which in some cases complicate proper turbidite counting. As it is furthermore difficult to accurately identify the upper boundary of the turbiditic layers, a potential underestimation of their thicknesses should be considered. The cumulative thickness of the turbiditic layers is 184 cm, which is 25% of the considered core interval.

2.4.2   Stratigraphy and sedimentation rates

According to our stratigraphy, the investigated section of ODP Site 1232 has a basal age of ~ 140 kyr BP and is covering one complete glacial/interglacial cycle (*Figure 2.4A*). Unfortunately, no ^{14}C-datings were possible for the Holocene and very few correlation points were available for MIS 5, because only few foraminifera were recovered in these stratigraphic intervals.

Over the entire 140 kyr, the mean sedimentation rate of the hemipelagic background sediments, excluding the turbidites, accounts for ~ 0.5 m/kyr (*Figure 2.4A*). During Termination I and the Holocene, as well as during Termination II and the early MIS 5.5, the sedimentation rate is distinctly reduced, down to values of less than 0.1 m/kyr. That way, the complete Holocene unit, for example, is less than 80 cm. Values of 1 m/kyr or more are found during the Last Glacial and the late MIS 5.5. The most pronounced reduction of the sedimentation rate is taking place at approximately 18 kyr BP. The uncorrected sedimentation rate, including also the turbiditic layers, is close to the hemipelagic sedimentation rate during the Holocene and early MIS 5.5, and about 40% higher for the remaining parts of the record.

SONNE gravity core 50SL reaches back into the Last Glacial (*Figure 2.4B*). The Holocene sedimentation rate is less than 0.1 m/kyr which is one order of magnitude lower than the rate during the Pleistocene (~ 1 m/kyr). Similar to ODP Site 1232, the most striking change in sedimentation rate takes place at approximately 18 kyr BP.
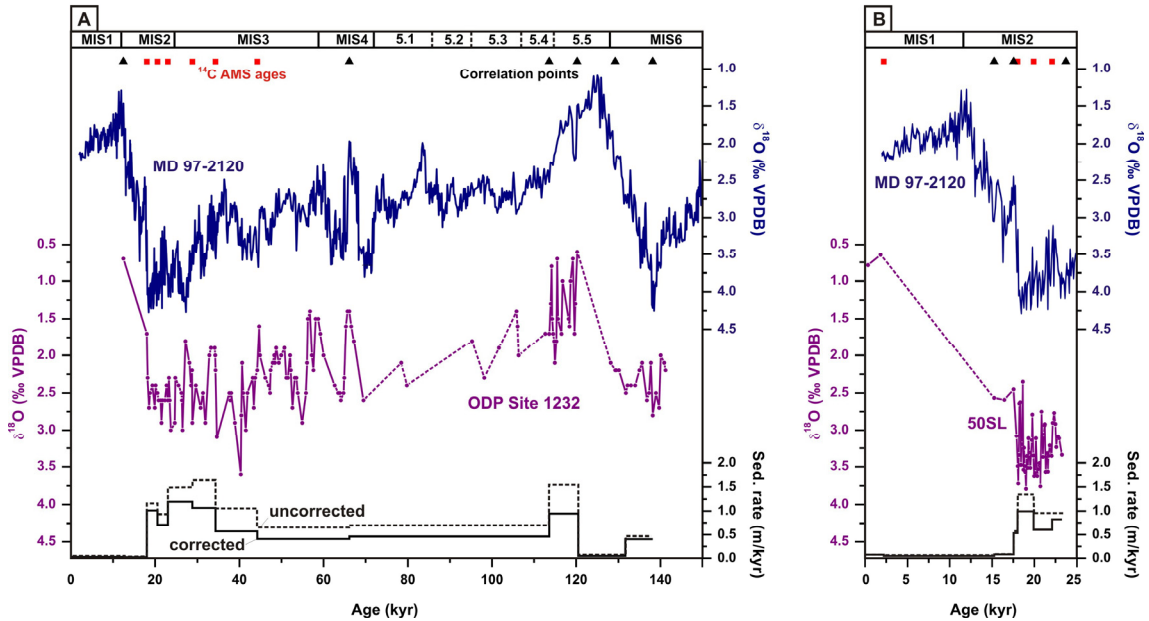

Figure 2.4: Correlation of the ODP Site 1232 (A) and SONNE core 50SL (B) oxygen isotope records with the oxygen isotope record of core MD 97-2120 (Pahnke et al., 2003). All data sets are based on planktonic foraminifera (Globigerina bulloides). Red quadrates are indicating AMS ^{14}C dating points; black triangles are indicating oxygen isotope correlation points. Dashed parts of the ODP and SONNE graphs correspond to sections with insufficient amounts of foraminifera. The sedimentation rate was calculated for the whole sedimentary sections including turbiditic layers (uncorrected – dashed line) as well for the hemipelagic sections excluding the turbidites (corrected – solid line).

2.4.3   Turbidite recurrence rate

We calculated the recurrence times of the turbiditic layers on the base of the developed stratigraphy and compared their variations to changes of the global sea level curve for the investigated period. The time intervals between successive turbidite layers are distinctly longer for periods of high sea level than for those of low sea level.

In ODP Site 1232, the recurrence times of turbidites are consistently ≥ 1 kyr for the Holocene, MIS 5.1, MIS 5.3, and MIS 5.5 (*Figure 2.5A*). In contrast, during MIS 2, MIS 3, the cold substages of MIS 5, and MIS 6, the average recurrence times are between 0.1-0.2 kyr. Recurrence times of turbidites in SONNE core 50SL are likewise ≥ 1 kyr during the Holocene and fluctuating around 0.2 kyr for the Last Glacial (*Figure 2.5B*).

In addition, periods of high recurrence rates tend to display slightly thicker turbidites (*Figure 2.6*): almost all turbiditic layers that were deposited during the interglacial periods are less than 5 cm thick, while numerous glacial turbidites reach a thickness of ≥ 20 cm. Especially in the Holocene section, the turbidites are remarkably thin and difficult to identify.
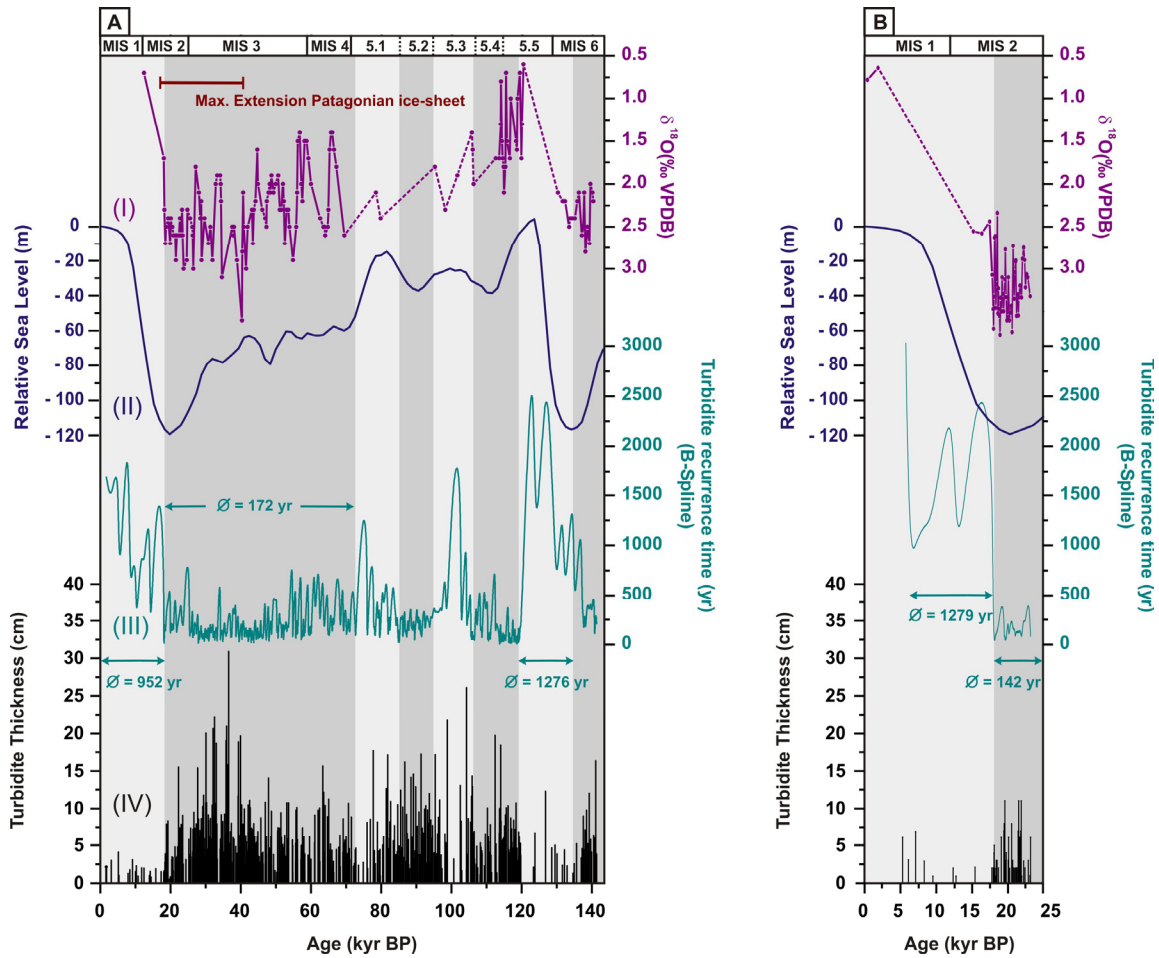
Figure 2.5: *Turbidite and oxygen isotope records of ODP Site 1232 (A) and SONNE core 50SL (B) compared to the global sea level record for the past 140 kyr. (I) Oxygen isotope record (‰VPDB), (II) global sea level record (after Waelbroeck et al., 2002), (III) calculated turbidite recurrence time (kyr) displayed as B-Spline, (IV) thickness of turbiditic layers (cm). Light gray bars highlight episodes of long turbidite recurrence times during periods of sea level highstand and during terminations; darker gray bars highlight episodes of short turbidite recurrence times during periods of low sea level. The period of maximal Patagonian ice sheet extension is indicated by the brown bar at the top of the graph.*
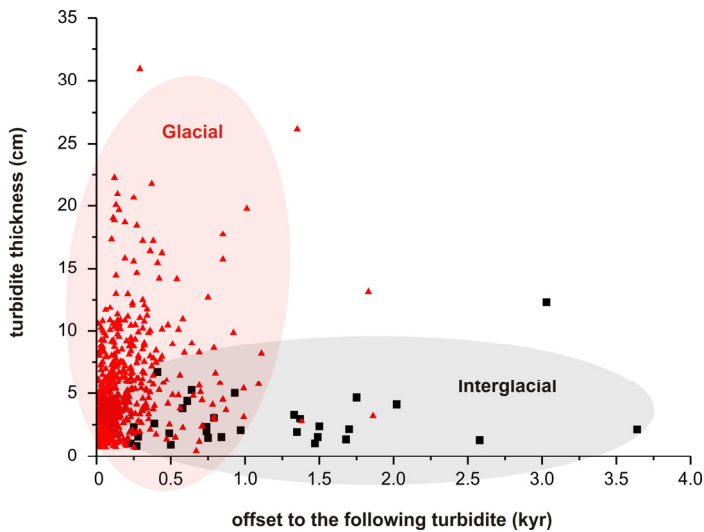
Figure 2.6: *Relation between the thickness of ODP Site 1232 turbidites (cm) and the offset to the following turbiditic layer (kyr). Glacial periods are generally characterized by slightly thicker turbidites and shorter offsets than interglacial periods.*

26

All turbidite data (original and corrected depth, thickness, age and recurrence time) as well as the oxygen isotope data are available in an electronic Appendix A of this paper and under the name of the corresponding author through the PANGAEA server (www.pangaea.de).

2.5 Discussion

2.5.1 Turbidite generation

Einsele et al. (1996) showed that the generation of event deposits such as turbidites takes place in several phases and stressed the need for a pre-event phase of sufficient sediment accumulation. Thus, the composition and accumulation of the sediment in the source area − in our case the amount of sediments stored on the South-Chilean upper continental slope − is an important precondition for the generation of turbidites. Due to the humid climatic conditions and pronounced topographic gradients in the hinterland of the study area, the terrigenous sediment delivery to the continental shelf is at present mainly fluvial (Lamy et al., 2001). The sediments are mostly originating from the Main Cordillera and the western foreland as the high precipitation along the Andean barrier allows the rivers to cut through the Coastal Ranges and to transport their sediment load towards the continental slope (Stuut et al., 2007). The main regional sediment supply to ODP Site 1232 comes from the Calle Calle/Valdivia and Bueno Rivers, which originate at ~ 40°S in the Chilean Lake district, and which channel the sediments through large hydrographical systems across the continental shelf into the deep sea trench (*Figure 2.2*). Similarly, Rio Imperial and Rio Toltén are the main river agents that supply sedimentary material to the locality of SONNE core 50SL.

Ultimate trigger mechanisms for the periodically occurring depositional events could be great earthquakes, tsunamis, storm wave loading, or simply the dimension of the sediment loading (Mutti et al., 1984; Adams, 1990; Einsele et al., 1996). Depending amongst others on the trigger mechanism, the resulting turbidites will be varying in size. Due to their specific locations far from the continental slope and high above the trench surface, ODP core 1232 and SONNE core SL50 are likely non-ideal archives in regard to the registration of all occurring turbidites. Many events may be missing in the sedimentary record as their extent has been simply too small to reach the site positions. On this account, a) the long distance between ODP Site 1232 and the potential source area of turbidites, b) the elevated position of SONNE core SL50 high above the trench surface, and c) the none the less remarkable thicknesses of individual turbiditic layers, account for exceptionally large and geographically extended depositional events. As giant turbidites are rather triggered by earthquakes than by storms or other local mechanisms (Gorsline et al., 2000), and in view of the seismic activity in Southern Chile, it is thus very likely that the turbidites of ODP Site 1232 and SONNE core 50SL are, in general, earthquake-triggered. This interpretation is supported also by sedimentological observations: many of the identified turbiditic layers consist of multiple pulses rather than a single one; this is thought to be a distinct feature of seismically induced turbidites (Nakajima and Kanai, 2000; Shiki et al., 2000). However, sedimentological arguments are not considered to be definite reliable evidence for

27

seismically triggered turbidites. A more plausible and indicator would be the synchrony of turbiditic flows in several submarine drainage systems (Goldfinger et al., 2003). Due to a lack of neighbouring records in the study area with individually dated turbidites, we cannot prove synchrony of event layers off Southern Chile. However, the generally similar variations in turbidite recurrence times of ODP Site 1232 and core 50SL corroborate our approach, even though a precise age control of single events is not possible.

According to the previous points, the cyclicity in turbidite recurrence and thickness that is observed for both investigated records may be either due to changes in the accumulation of sediments in the source area or to changes in the turbidite trigger mechanism. The sediment supply to the source are of turbidites is likely affected by variations in climate. For instance, during the Late Pleistocene, glaciers covered part of the continental shelf south of 42°S (*Figure 2.1*) and delivered large amounts of sediments to the Pacific Ocean. We suggest that this extraordinary sediment supply explains the particularly thick turbidite beds of the Pleistocene trench fill.

2.5.2 *Turbidite deposition and climate changes*

According to our stratigraphy, the sedimentary record of ODP Site 1232 contains one complete glacial cycle, while the shorter core 50SL reaches back into the Last Glacial (*Figure 2.4*). This allows us to compare glacial and interglacial turbidite recurrence times and to detect possible variations in relation to climate changes. In general, the pattern of the turbidite recurrence time follows the pattern of the glacio-eustatic sea level change. Average time spacing between turbidites is low during sea level lowstands and distinctly higher during interglacials. This glacial/interglacial contrast is not unique to Southern Chile but seems to follow a global-scale pattern. A Holocene decline in the recurrence time of turbidites is, for example, described for the Cap Timiris Canyon off Mauritania (Wien et al., 2006), the Ulleung Basin in the Japan Sea (Lee et al., 1996) and in the Mediterranean Sea (Baraza et al., 1990). We therefore interpret the long-term glacial-interglacial pattern in our turbidite recurrence rates to be primarily modulated by global climate and associated eustatic sea level changes.

The extensive glaciation of the continental hinterland and enhanced precipitation result in increased terrestrial erosion and sediment supply to the Pacific Ocean. Coevally, the global sea level is at a minimum under glacial conditions and shelf areas are exposed to erosion during these periods (*Figure 2.7a*). This is not only enhancing the anyway high terrestrial sedimentation rate but also reducing the sediment accumulation space on the shelf. As a result, the sediment transport to the shelf edge and to the slope basins is pronounced, leading to unstable slope conditions. The sea level drop may also reduce the hydrostatic pressure on the near-surface slope sediments, leading to the build-up of excess pore pressure within the sediment further lowering the slope stability (Lee et al., 1996). The risk of a slope failure is, therefore, highest during phases of sea level lowstand (Einsele, 1996). Although ODP Site 1232 is located ~ 85 km west of the lowermost slope far from the terrestrial sediment source, the sedimentation rate is high during cold stages and, in particular, during the Last Glacial (*Figure 2.4A*); these findings are also consistent with the SONNE core 50SL record (*Figure 2.4B*) and previous local studies (Lamy et al., 1999; Hebbeln et al., 2007).

During periods of falling sea level, storm waves should also be considered as trigger for turbidity currents. As the maximum water depth of wave-induced effects is estimated to be 80-120 m (Lee and Edwards, 1986), no significant effects can be expected for the Holocene high stand. However, during the Last Glacial, with a maximum sea level drop of ~120 m, the shelf edge and upper slope were within the reach of storm waves and potentially vulnerable to storm-induced turbidites.
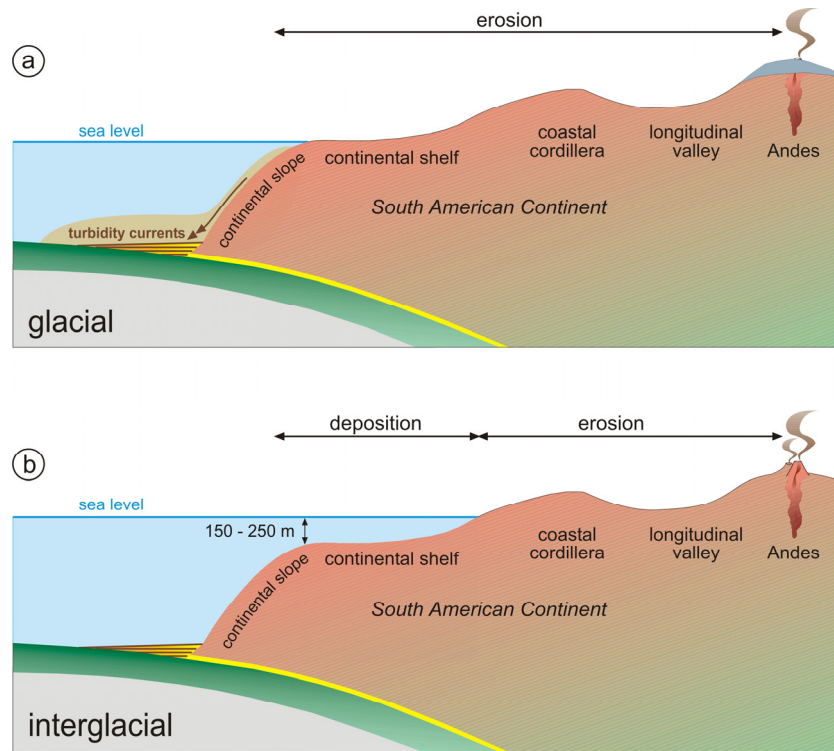

Figure 2.7: *Schematic representation of a glacial and an interglacial scenario (not to scale). (a) Glacial period with lowered sea level and exposed continental shelf. The shelf is being eroded and the accumulation space for sediments is reduced; that way, sediment is bypassing the shelf area. Turbidity currents occur frequently. (b) Interglacial period with a high sea level and drowned continental shelf. The shelf region acts as depositional center for terrestrial sediments. Turbidity currents are occurring sporadically.*

The interglacial scenario is characterized by a very limited Patagonian Ice Sheet and by lower precipitation (e.g. Lamy et al., 2004; Hebbeln et al., 2007). Consequently, the continental erosion, the sediment supply to the Pacific Ocean, and the sediment accumulation on the continental shelf are reduced. As a result of the high sea level, the trench becomes more distal to the shoreline and the source areas of sediments. The shelf is spaciously drowned and acts as a first order depositional centre for the fluvially delivered sediments (*Figure 2.7b*). Furthermore, the higher water column above the sediments may exert a stabilizing effect. While the basins of the Finger Lakes in the Chilean Lake District and the Chilean Fjords to the south were being occupied by glaciers during the Last Glacial, they may represent additional onshore depocenters during the interglacial. South of ~ 42°S, glaciers reached the continental shelf during the LGM and likely supplied large amount of sediment that has been transported northwards along the trench. Today, and most likely also during previous interglacials, the shelf is ice free, acting as large sediment trap for eroded continental material. That

29

way, less sediment reaches the outer continental shelf and the generation of turbidites is less likely.

Recapitulatory, slope conditions are more stable under a high sea level regime and many of the occurring earthquakes not succeed to cause a slope failure. In contrast, slope conditions at a low sea level period with high sedimentation rates are less stable and earthquakes are able to continuously generate submarine mass movements. We therefore consider the turbidite recurrence times of glacial periods to mainly reflect the recurrence times of earthquakes in the area.

2.5.3   *Turbidite deposition and earthquake recurrence times*

To evaluate whether the turbidite recurrence time can be considered as a useful proxy for the regional earthquake recurrence time, we compared our results with data of known paleoseismological archives in Southern Chile. The historical earthquake record for the Valdivia rupture zone contains mega-earthquakes (M≥8) and secondary effects in the years 1575, 1737, 1837 and 1960, resulting in an average recurrence interval of 128 years (Lomnitz, 1970; Lomnitz, 2004) (*Figure 2.1*). More recent interpretations of written historical documents closer differentiate between these single events, i.e. the1575 and 1960 earthquakes were evidently greater than the effects of the 1737 and 1837 events (Cisternas et al., 2005; supplementary information). Based on these interpretations, the temporal distance between the two megaquakes of a similar strength in 1575 and 1960 is 385 years.

South of Valdivia, in the estuary of the river Maullín, Cisternas et al. (2005) investigated buried soils and sand layers as records of coseismic subsidence and tsunami flooding. These authors came up with an earthquake recurrence time of ~ 285 years for the last two millennia. Since not all earthquakes generate sufficient subsidence and/or tsunamis, these recurrence times may be somewhat long.

A study of coseismically uplifted beach berms on the Isla Santa María resulted in a much higher earthquake frequency of 180 ± 65 years for the last 3 kyr (Bookhagen et al., 2006). However, the island is located on the Concepcion segment, neighbouring the Valdivia segment in the north. This indicates a difficulty in exactly correlating records of neighbouring segments and rupture zones that generated historic megaquakes do not necessarily correspond to single segments of the Chilean forearc but propagate well across segment boundaries (Melnick et al. 2006). The 1960 earthquake is a prominent example, as it originated close to the northern edge of the Valdivia rupture zone (Krawczyk and SPOC-Team, 2003) in the Nahuelbuta segment and propagated about 1000 km southward across the Toltén and Bueno segments.

When comparing our turbidite recurrence times with the values derived from the above cited Late Holocene earthquake records, two aspects should be considered: (a) our data cover a distinctly longer time period and (b) are considerably influenced by global climate changes. As a matter of fact, the Holocene turbidite recurrence times at ODP Site 1232 and SONNE core 50SL (> 1000 yr) seem to be inconsistent with the earthquake recurrence periods of the onshore paleoseismic archives (180-385 yr). However, during the glacial periods of sea level lowstands, the turbidite recurrence times (~ 100-290 yr) are fairly consistent with the onshore data. We therefore suggest

that only during glacial periods, when the sediment availability and slope instability were high enough, all occurring earthquakes triggered turbidites and left their marks in the sedimentary records. As during these periods other trigger mechanisms came into operation as well, the glacial earthquake recurrence times may be even overestimated.

2.5.4   *Turbidite deposition and forearc tectonics*

Along the active continental margin of Southern Chile, changes in turbidite thickness and frequency may not only be related to glacial-interglacial climate changes but also to particularities in the segmented forearc tectonics. In both records ODP Site 1232 and SONNE core 50SL, the most obvious decline in the turbidite recurrence time and thickness is taking place at the end of the Last Glacial, at ~ 18 kyr BP (*Figure 2.5*). This frequency decline is certainly mainly controlled by climate changes, but we postulate a likely additional indirect influence of tectonic uplift via influence on the on- and offshore sedimentation pattern.
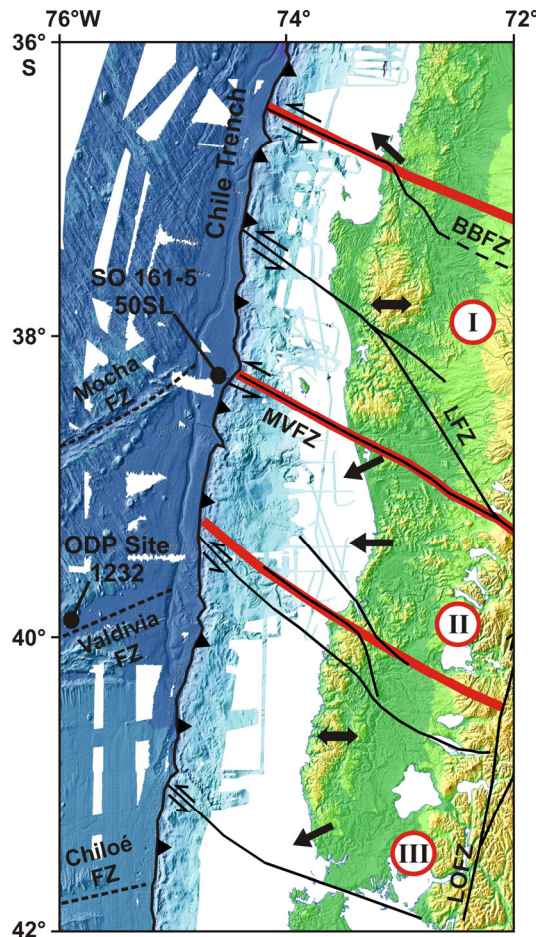
Figure 2.8: *Structural features and morphotectonic units of the study area (modified after Hackney et al. 2006; Rehak et al., 2008). Thick red lines separate the individual morphotectonic segments (I = Nahuelbuta Segment, II = Toltén Segment, III = Bueno Segment). Thick black arrows indicate the present-day drainage pattern of the region with river flow inversions in the northern and southern segments and with a culmination of basin outlets in the low-relief Toltén Segment. Local topography and bathymetry modified after Grevemeyer et al. (2005) and Völker et al. (2006). F.Z. = Fracture Zone, BBFZ = Bío Bío Fault Zone, LFZ = Lanalhue Fault Zone (Glodny et al., 2008), MVZ = Mocha-Villarica Fault Zone, LOFZ = Liquiñe-Ofqui Fault Zone.*

31

Between 37° and 41°S, the Chilean forearc is divided into three morphotectonic segments that have undergone different subduction-related deformation during the Neogene (Hackney et al., 2006; Melnick and Echtler, 2006b) and Quaternary (Rehak et al., 2008) (*Figure 2.8*). The central Toltén segment appears to be tectonically stable. The northern Nahuelbuta and the southern Bueno segment, however, are characterized by tectonically controlled drainage anomalies and rerouting of sediments by river flow inversions, indicating a steady uplift of both coastal regions (Rehak et al., 2008). Today, the most striking paleodrainage feature of the northern Nahuelbuta segment is the wind gap between the Pellahuén and Tirúa basin (Rehak et al., 2008, *Figure 2.2*). While Río Pellahuén formerly drained directly to the Pacific Ocean, it is at present crossing the Coastal Cordillera to the east. Its corresponding and previous active submarine canyon system is nowadays completely inactive due to the drainage inversion. That way the sediment supply to the deeper Ocean starved and, as a consequence, the generation of turbidites potentially diminished. In general, the drainage system of the southern Bueno segment indicates the same reorganization as the northern Nahuelbuta segment. The flow reversals are not precisely dated yet but would provide an explanation for the sudden drop in both the sedimentation rate and the turbidite frequency at ~18 kyr BP.

2.6   Conclusions

In this study, we analyse the recurrence time of turbidite layers in the marine sedimentary sequence of ODP Site 1232 and SONNE core 50SL off Southern Chile. In this active margin setting, we investigate the significance of trench deposits as paleoseismic archives. For the first time we examine a proxy record of 140 kyr length, while previous similar studies focused merely on the Late Holocene. The new long-time record reveals a glacial-interglacial change of turbidite recurrence times which seems to be related to global climate and sea level changes. The comparison of our record with different shorter onshore paleoseismic proxy records indicates that the turbidite recurrence times during glacial periods of low sea level are very similar to earthquake recurrence intervals found for the last three millennia (Cisternas et al., 2005; Bookhagen et al., 2006).

There is much evidence that the climate is the driving factor of the long-term differences in the turbidite recurrence rates off Southern Chile by changing the sediment availability in the source area affecting the slope stability. Nevertheless, the change could be also more than a simple problem of sediment flux from the continent. It could be driven by a 'real' variation in the local earthquake recurrence rates, possibly induced by glacial load or post-glacial isostatic rebound in the southern realm (ODP Site 1232), that could have influenced the coupling at the plate interface. More frequent mega-earthquakes during the glacial period could well explain the Holocene decline of turbidites in our record. However, as we do not know enough about the control and nature of turbidites triggered by differential mechanisms (e.g. seismic, sea-level, sediment flux), we have to leave this discussion open.

Turbiditic layers in sedimentary sequences are indirect records of paleoseismicity. Turbidite generation is highly depending on the amount and availability of sediment material and, in consequence, potentially affected by external factors such as climate

and tectonics. Therefore, besides the need to verify earthquakes as trigger mechanism, it is also necessary to identify potential external factors which may obscure the use of turbidites as proxy for paleoseismicity, at least on glacial-interglacial time scales. Nevertheless, if these aspects are properly considered, our data emphasize that turbidite records of trench sequences at active margins with high sediment supply are valid archives of paleoseismology.

# 3.	FOREARC UPLIFT RATES DEDUCED FROM SEDIMENT CORES OF TWO COASTAL LAKES IN SOUTH-CENTRAL CHILE

S. Stefer, J. Moernaut, D. Melnick, H.P. Echtler, H.W. Arz, F. Lamy, M. De Batist, O. Oncken, G.H. Haug

Abstract: The present paper introduces a new approach for deriving information about local forearc tectonics and related uplift rates based on the study of lake sediments. We investigated two coastal lakes at the south-central Chile margin, Lakes Lanalhue and Lleu Lleu, located south of the Arauco Peninsula (38°S). Both lakes developed within the valleys of ancient rivers that once drained to the Pacific Ocean, being subsequently dammed by rising sills in the Late Pleistocene/Early Holocene. Seismic profiling and sedimentological analyses of cores from both lakes revealed similar successions consisting of marine to brackish sediments covered by lacustrine deposits. Radiocarbon dating indicates that the marine-lacustrine transition occurred at 8000 cal yr BP and 8150 cal yr BP, respectively. The correlation of this transition with global sea-level curves allowed the calculation of local uplift rates for the Holocene. Uplift rates for the lake basins amount to 0.42 ± 0.71 mm/yr and 0.49 ± 0.44 mm/yr, respectively, which are consistent with rates determined from a Late Pleistocene marine terrace in the area. However, conspicuously higher, though likely transient, vertical movements at 8.83 ± 2.7 mm/yr and 11.36 ± 1.77 mm/yr, respectively, were calculated for the sills that block both lakes nowadays. These barriers are interpreted to be the surface expression of a blind reverse fault associated to the Morguilla fault system, a seismically-active structure that controls uplift and folding along the adjacent Arauco Peninsula.

Keywords: forearc tectonics, uplift rates, Lago Lanalhue, Lago Lleu Lleu, Arauco Peninsula, sea-level change

3.1. Introduction

Uplift and subsidence are common phenomena in tectonically active coasts worldwide (e.g. Antonioli, et al., 2006; Chen and Liu, 2000; Hsu, 1992; Lajoie, 1986; Rajendran, et al., 2008). The analysis and measurement of vertical deformation can provide insight into fundamental tectonic mechanisms and associated crustal responses (e.g. Abbott, 1997). The most conventional approach for calculating surface uplift rates at tectonically active margins is the analysis and dating of deformed marine terraces that emerged from the ocean and are nowadays situated above sea-level (e.g. Antonioli, et al., 2006; Burbank and Anderson, 2001; Keller and Pinter, 2002; Rajendran, et al., 2008). These relict shorelines bear evidence of both past sea-level highstands during interglacial/ interstadial periods and of subsequent tectonic uplift. Therefore, if the age and elevation of the marine terrace surfaces and of the paleo-sea level highstands are known, an averaged uplift rate of each marine terrace can be calculated for the period since its formation. However, marine terrace surfaces are ephemeral geomorphic entities whose capacity to record changes in the landscape caused by surface uplift, folding, or faulting, basically depends on the local rate of erosion and deformation, as well as on the local bedrock erodibility (e.g. Anderson et al., 1999). In regions where weak bedrock, high precipitation and low deformation rates coexist, the tectonic record provided by marine terrace surfaces will probably not exceed the past 10^4 to 10^5 years.

In this study, we attempt to use an alternative, novel approach for calculating surface uplift rates using the sediment archives of two coastal lakes from the south-central Chile subduction margin (*Figure 3.1*). We focus on Lago Lanalhue and Lago Lleu-LLeu, located south of the Arauco peninsula (38°S), and combine seismic-reflection profiles, dated sediment cores, and geomorphic field observations to decipher landscape evolution and explore the capacity of these lakes to record coastal tectonic processes.

3.2   Tectonic framework

3.2.1   Regional tectonic and geologic setting

The Chile margin is formed by oblique convergence between the oceanic Nazca Plate and the South American continent at ~66 mm/yr (Angermann et al., 1999; Kendrick et al., 2003). Adjacent to the study area, the subducting Nazca Plate is ~32 Myr old and the Perú-Chile trench is filled by 1.5-2.0 km of sediments (e.g. Bangs and Cande, 1997). Sediments have filled the trench since the onset of glaciation in the Patagonian Andes ca. 6-5 Myr ago, leading to a change from erosive to accretionary conditions during the Pliocene, and resulting in the inversion of forearc basins (Bangs and Cande, 1997; Melnick and Echtler, 2006b).

Onshore, this sector of the margin is characterized by four main morphotectonic units (e.g. Melnick and Echtler, 2006b): (1) the Coastal Platform, which is composed of uplifted Cenozoic marine and coastal sedimentary sequences, and where our study region locates, (2) the Coastal Cordillera, which is formed by a Permo-Triassic accretionary complex south of ~38°S and a Late Paleozoic magmatic arc to the north (Hervé, 1988; Glodny et al., 2005; Glodny et al., 2008 and references therin), (3) the

Central Depression, which is made up by Oligocene-Miocene volcanic and sedimentary rocks, overlain by Pliocene-Quaternary fluvial-alluvial sediments (Muñoz et al., 2000; Jordan et al., 2001), and (4) the Main Cordillera, which constitutes a Mesozoic-Cenozoic magmatic arc with intra-arc sedimentary basins (Mpodozis and Ramos, 1989).
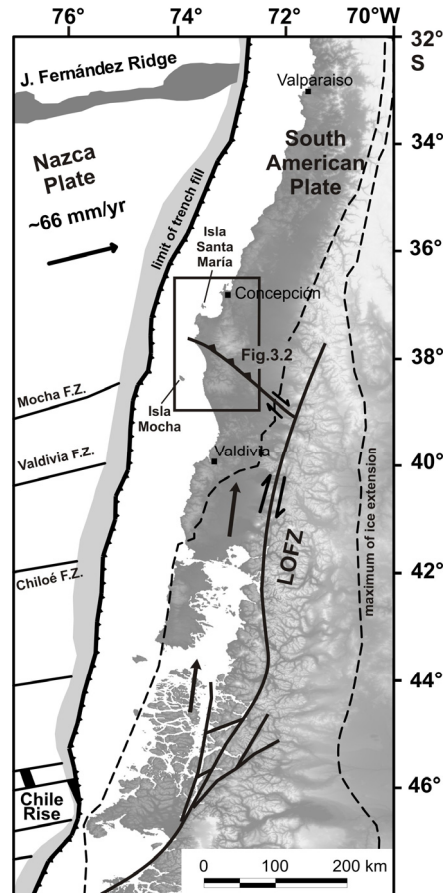
Figure 3.1: *Tectonic conditions at the south-central Chilean margin. Major Fracture Zones (F.Z.) of the subducting Nazca Plate are labeled and the limit of trench filling sediments is indicated (after Bangs and Cande, 1997; Tebbens and Cande, 1997). Major Quaternary faults of the South American Plate after a compilation of Melnick et al. (2009). LOFZ = Liquiñe-Ofqui Fault Zone. Black arrows are indicating the northward gliding Chiloé block. The dashed line marks the maximum extent of the Patagonian Ice Sheet during the Last Glacial Maximum (after Rabassa and Clapperton, 1990).*

A first-order discontinuity of the Main Cordillera is the N-S trending Liquiñe-Ofqui Fault Zone (LOFZ). This dextral strike-slip discontinuity is mainly a result of oblique plate convergence (Hervé, 1994) and collision of the Chile Rise at its southern end (Nelson et al., 1994). The LOFZ decouples the south-central Chilean forearc, which is suggested to behave as a northward gliding sliver (so-called 'Chiloé block', *Figure 3.1*) by several authors (e.g. Cembrano et al., 2002; Rosenau et al., 2006). At its northern edge, this block is bounded by the NW-striking Lanalhue fault system (Glodny et al., 2008), which splays out from the LOFZ at ~39°S. Along this fault system, the Chiloé block collides against a buttress formed by the Arauco-Nahuelbuta block resulting in ~6 mm/yr of margin-parallel shortening (Melnick et al., 2009). Global Positioning System (GPS) data indicate vertical axis counter-clockwise rotations along the northern edge of

the Chiloé block, supporting ongoing collision and decoupling of crustal blocks across the Lanalhue fault system (Moreno et al., 2008).

The Lanalhue fault, running along Lanalhue Lake, juxtaposes two distinct units in the metamorphic basement of the Coastal Cordillera (*Figure 3.2*). It separates high-pressure metasedimentary rocks and ophiolitic components of the Western Series from high-temperature contact metasedimentary rocks of the Eastern Series (Hervé, 1988). The Morguilla fault runs along the southern flank of the Arauco Peninsula, forming a pronounced, up to 150-m-high scarp. The height of this scarp decreases toward the southeast where it becomes blanketed by active dunes (*Figure 3.3*). The fault cuts through the western side of Lago Lleu Lleu, juxtaposing metamorphic rocks with Pleistocene sediments of the Cañete surface. The Morguilla and Lanalhue faults appear to be connected west of Lago Lanalhue, where several small ponds are aligned along the fault trace (*Figure 3.3*) (Melnick and Echtler, 2006b).

3.2.2   Seismicity, neotectonics and deformation at the Arauco Peninsula and its vicinity

The most striking structural feature of the fairly straight south-central Chile margin is the protruding Arauco Peninsula (~38°S, *Figure 3.2*). Morphologically, it is defined by the Cordillera de Nahuelbuta in the east, the coastal plain in the west, and the Bío Bío and Imperial Rivers to the north and south (36-38°S). The peninsula is considered to be an uplifted part of the continental shelf (Kaizuka et al., 1973) that underwent a temporally and spatially discontinuous forearc-basin formation since the Late Cretaceous (Melnick and Echtler, 2006a). Since the Late Pliocene, Arauco is characterized by constant coastal uplift (Melnick et al., 2009).

The Arauco-Nahuelbuta forearc is located within the overlapping rupture zone of the 1960 Valdivia (M_W 9.5) and the 1835 Concepción (M ~8.5) megathrust earthquakes (Lomnitz, 1970; Lomnitz, 2004). Temporary seismological networks of the ISSA (Integrated Seismological experiment in the Southern Andes) and TIPTEQ (from The Incoming Plate to mega-Thrust EarthQuake processes) projects observed seismic events in the region during 2000 and 2004/2005, respectively (Bohm et al., 2002; Bruhn, 2003; Haberland et al., 2006). These data demonstrate that shallow earthquakes (M $\leq$ 5) are concentrating north and south of the Arauco Peninsula; they are related to a northeast-striking reverse fault adjacent to the Isla Santa María (Melnick et al., 2006) and to the northwest-striking Morguilla and Lanalhue faults, respectively.

Quaternary and recent forearc deformation on the Arauco peninsula is mostly expressed by emerged and warped coastal landforms. Several marine surfaces bear evidence of the complex interplay between local tectonic uplift and glacio-eustatic sea-level changes (e.g. Kaizuka et al., 1973; Melnick et al., 2009). The largest and best preserved surface is the Cañete terrace that developed during MIS 5e (~125 kyr ago). Two less preserved marine surfaces, named Buena Esperanza and Las Nochas, are found above the Cañete terrace and attributed to the interglacial periods of MIS 7 and MIS 9 (Kaizuka et. al., 1973). The shoreline angle elevation of these three surfaces increases towards the center of Arauco, where they reach 232 m (Cañete), 360 m (Buena Esperanza), and 471 m a.s.l. (Las Nochas), respectively. Uplift rates are hence highest at the center of the

peninsula (1.8 ± 0.2 mm/yr) and lowest in its northern sector (0.36 ± 0.07 mm/yr) (Melnick et al., 2009). The uplift rate deduced from shoreline-angle elevations of the Cañete surface adjacent to Lanalhue and Lleu-Lleu lakes is 0.51 ± 0.1 mm/yr. These variations in uplift rate and shoreline-angle elevations have been attributed to a major WNW-ESE oriented anticline running along the center of the peninsula, which is ultimately responsible for its emergence. However, this fold has a complex geometry leading to a slight eastward tilt of the Cañete terrace, evident in the surroundings of the Lanalhue Lake. The fold is bounded at its northern and southern flanks by deep-seated reverse faults that are likely rooted in the plate interface, as suggested from the continuous alignment of microseismicity.
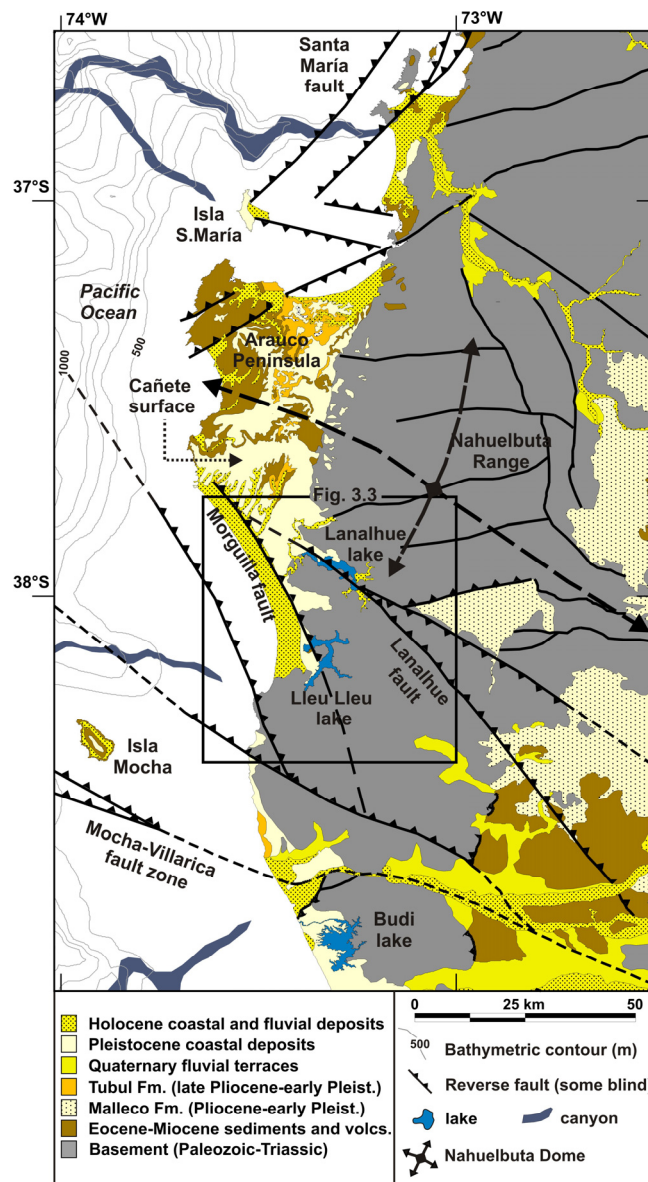
Figure 3.2: *Simplified geologic map of the Arauco-Nahuelbuta region (modified after Melnick et al., 2009). The Arauco Peninsula as an uplifted part of the continental shelf is well distinguishable from the Paleozoic-Triassic basement of the Nahuelbuta Range.*

39

Further studies on local deformation have been conducted on two islands adjacent to the Arauco peninsula (*Table 3.1*). In their pioneer work, Kaizuka et al. (1973) studied marine terraces on the Isla Santa María, north of Arauco (37°S), and correlated the uppermost surface to the Cañete terrace. Recently, Melnick et al. (2006) used radiocarbon dating of shoreline markers deriving a mean uplift of 1.8 ± 0.4 mm/yr during the last 40 kyr, and showing that the upper surface is only ~27 kyr old. Bookhagen et al. (2006) studied uplifted Holocene beach berms of the island and derived a mean uplift rate of 2.3 ± 0.2 mm/yr over the last ~3 kyr. On Mocha Island, south of Arauco (38.5°S), Radtke (1989) found uplift rates of 4.9 ± 1.1 mm/yr during the last ~6 kyr, based on radiocarbon dating of elevated marine terraces. This is concordant with the results of Nelson and Manley (1992), who derived an uplift rate of 5.4 ± 1.2 mm/yr for the same period of time. However, the authors provide a more complex study of strandlines on Isla Mocha in which they reveal that uplift of the island increased steadily over the past millennia (Nelson and Manley, 1992). In contrast to the Arauco peninsula and the Cañete surface, the marine terraces at Isla Mocha and Santa Maria are steeply tilted. This tilt has been related to their positions in the limbs of tight reverse-fault cored anticlines (Melnick et al., 2006). Thus, changes in uplift rates at these islands might reflect transient periods of enhanced crustal faulting and folding.

Table 3.1: *Hitherto existing studies of uplift-rates in the vicinity of the studied lakes.*

Location	Latitude	Time-period	Uplift (mm/yr)	Study based on	Author(s)
Sta. María Island	37°S	last 40,000 yr	1.8 ± 0.4	Paleosols, peat, clay layers (^{14}C AMS dating)	Melnick et al. (2006)
		last 3000 yr	2.3	Elevated strandlines (OSL dating)	Bookhagen et al. (2006)
Arauco Peninsula	37-38.5°S	last 125,000 yr	0.8-2.0	Eemian terrace (geomorphic observation)	Kaizuka et al. (1973)
		last 125,000 yr	max. 1.8 ± 0.2 min. 0.36 ± 0.07	Eemian terrace (cosmogenic nuclide dating)	Melnick et al. (2009)
Mocha Island	38°S	last 6000 yr	4.9 ± 1.1	Terraces (dated shell fragments)	Radtke et al. (1989)
		last 6000 yr	5.4 ± 1.2*	Strandlines (radiocarbon dated shells)	Nelson and Manley (1992)

* Before calculating the uplift rate we recalibrated the radiocarbon age (^{14}C BP) given by Nelson and Manley (1992) with the online version of the CALIB Radiocarbon Calibration program (Execute Version 5.0.2html; Stuiver et al., 2005)

3.3   *Morphometry and characteristics of the Lanalhue and Lleu Lleu lakes*

A peculiarity of the south-central Chile margin is the occurrence of several coastal lagoons which are found north of the maximum extent of Patagonian glaciations precluding a glacial origin and the influence of local post-glacial isostatic rebound. They are located, for example, south of the Bío Bío river mouth (~37°S), in the coastal plain of southern Arauco (~38°S) where our study focuses on, south of the Imperial River (~39°S), and south of Valdivia (40°S) (Endlicher and Mäckel, 1985). Today, these lagoons are mostly disconnected from the Pacific Ocean, hence forming lake basins. It has been hypothesized that the lagoons on the southern Arauco Peninsula, Lago Lanalhue and Lago Lleu Lleu (*Figure 3.3*), developed in former river valleys at the western slope of the coastal Cordillera de Nahuelbuta (Mardones and Reuther, 1999). In their western sectors, both lakes are bordered by a coastal plain, which is composed of marine and aeolian sands as well as locally active dune belts (Mardones and Reuther, 1999). The transition area between the coastal plain and the cordillera features the Late Pleistocene Cañete terrace.
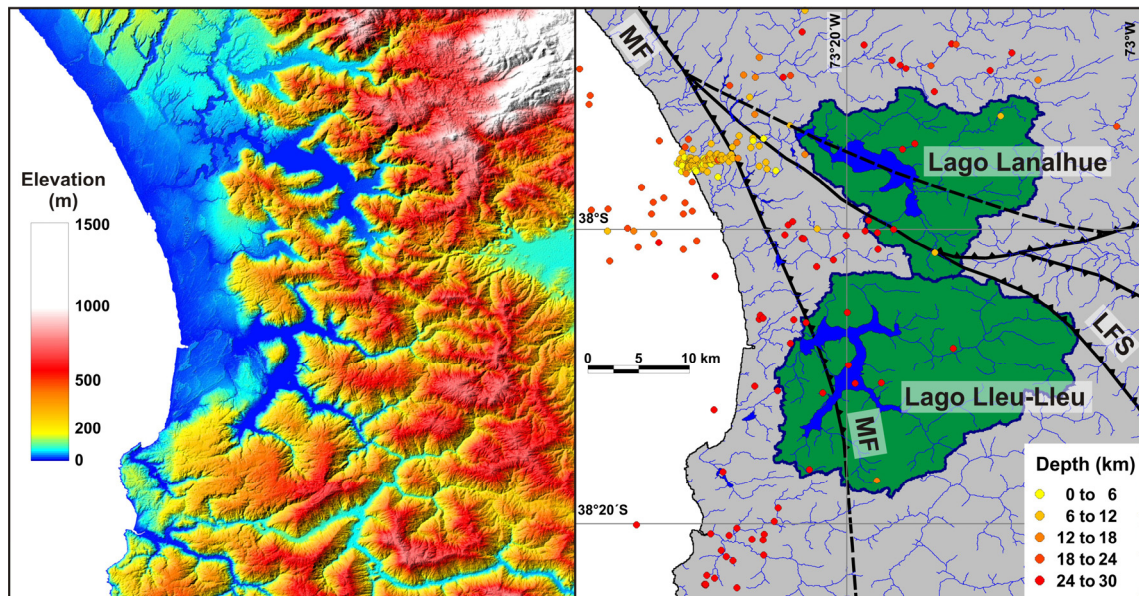
Figure 3.3: *Topography, seismicity and local river network in the direct vicinity of Lago Lanalhue and Lago Lleu Lleu. Left: Shaded topography (SRTM, NASA). The black arrow marks the tectonically induced flow reversion of the Pellahuén River (according to Rehak et al., submitted). Right: Depth-colored seismicity according to the ISSA (Bohm et al., 2002; Bruhn, 2003; Bohm, 2004) and TIPTEQ (Haberland, 2006) networks. Green-shaded areas mark the drainage basins of the lakes. MF = Morguilla Fault (blind thrust, not outcropping; northern part after Melnick et al., 2009), LFS = Lanalhue Fault System (Glodny et al., 2008).*

The formation of Lago Lanalhue and Lago Lleu Lleu has been the matter of debate, with interpretations reaching from tectonic downwarping of the lake basins (Börgel, 1953) to an impounding of coastal rivers by eastward moving dunes (Endlicher and Mäckel, 1985). In the most recent study, Mardones and Reuther (1999) suggested a formation caused by uplifted barriers forming natural dams.

3.3.1   *Lago Lanalhue*

Lago Lanalhue is located in a SE-NW oriented, elongated depression, which can be divided into three morphologically and bathymetrically distinct segments (*Figure 3.4a*) (Mardones and Reuther, 1999). The southern sector trends N-S, has a shallow depth of ~4 m and subdued slopes, whereas the central part is SE-NW oriented and up to 22 m deep. The western T-shaped segment holds the deepest part of the lake, which is reaching a water depth of 24 m in the center of the former fluvial valley. In front of Lago Lanalhue, the Cañete-terrace is tilted eastward about a NNW-SSE oriented axis and currently dams the catchment, thereby impounding the lake.
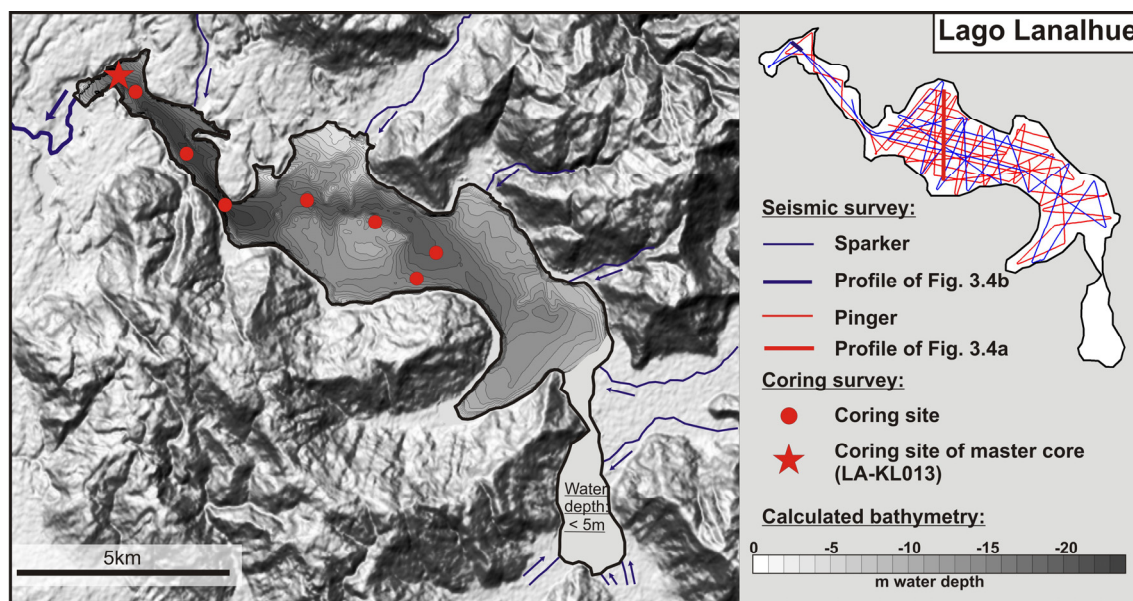
Figure 3.4a: *Bathymetry, coring positions, and seismic survey lines of Lago Lanalhue. Bathymetry calculated using seismic profiles; isobath every 1 m.*

The present drainage area of Lago Lanalhue covers ~ 360 km^2 with a water surface area of 32.05 km^2. At present, its water level is at 8.0 ± 1.44 m a.s.l. (elevation deduced from the SRTM waterbody dataset with a mean local instrumental error of 1.44 m according to Becek, 2008). Several small streams running down the western slope of the Cordillera de Nahuelbuta are discharging into the lake. The outlet of Lago Lanalhue – a small stream named Río Paicaví – is located at the western end of the lake, from where it flows out to the Pacific Ocean through an oversized fluvial valley incised in the Cañete surface (*Figure 3.3*). Along the course of the stream, the entire sequence of the Cañete deposits has been incised and the Río Paicaví is currently flowing on the local metamorphic bedrock.

3.3.2   *Lago Lleu Lleu*

Lago Lleu Lleu is located ~15 km south of Lago Lanalhue and has a characteristic branched shape (*Figure 3.4b*). Its main water body extends about 17 km in NNE-SSW direction as well as 0.5 – 3 km in W-E direction. The frontal (northwestern) part of the

lake is very shallow with a depth of ~10 m, whereas water depth reaches more than 40 m in the central and deepest part.
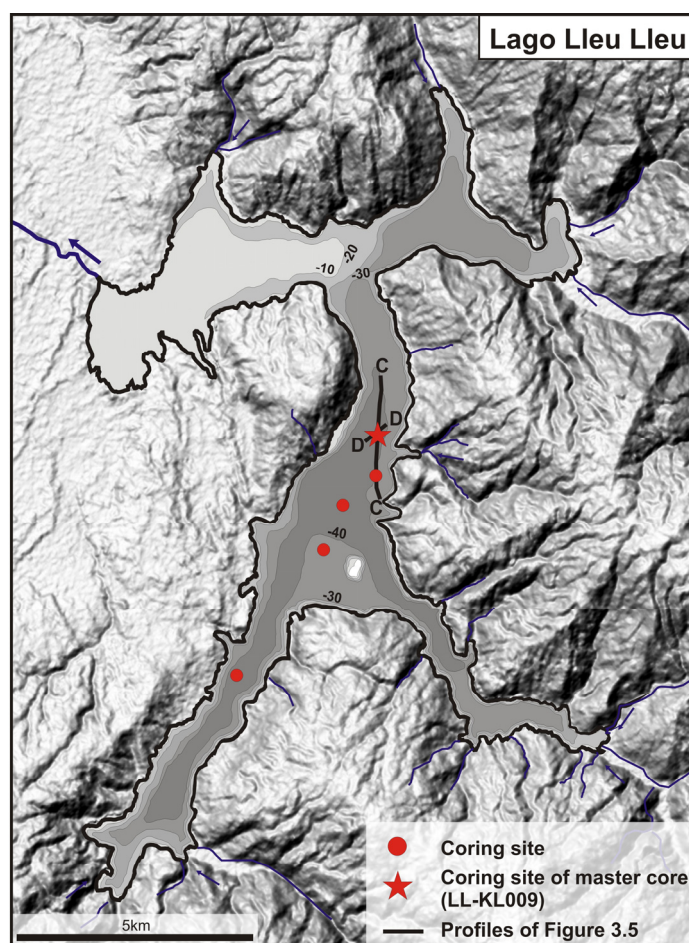
Figure 3.4b: *Bathymetry and coring positions of Lago Lleu Lleu. Bathymetry derived from Urrutia et al. (2000); isobath every 10 m.*

The present drainage area of the lake amounts to ~580 km^2 with an area of the water surface of 37 km^2. The present water level of Lago Lleu Lleu is situated at 5.0 ± 1.44 m a.s.l. Small tributaries are draining into the lake mainly from the Cordillera de Nahuelbuta in the east. The small outlet that drains the lake to the Pacific Ocean – Río Lleu Lleu – is located in the outmost northwest and is only ~6.3 km long (*Figure 3.3*).

3.4   *Material and Methods*

3.4.1   *Seismic survey*

Reflection seismic surveys were executed on Lago Lleu Lleu in January 2002 and on Lago Lanalhue in November 2005 with a high-resolution *CENTIPEDE* sparker and a very-high resolution *GEOPULSE* subbottom profiler ('pinger'). The small scientific vessel "Huala II" from the Universidad Austral de Chile towed the *CENTIPEDE* multi-electrode sparker (300 J, main frequency: 400-1500 Hz) as seismic source and a single-

43

channel high-resolution streamer as receiver. For a more detailed image of the subsurface, we used the "pinger" source/receiver (3.5 kHz), which was mounted on a Cataraft system. Navigation and positioning was done by GPS (Global Positioning System). All data were recorded digitally on a *TRITON-ELICS* Delph-2 acquisition system. Seismic stratigraphic interpretation was done using SMT's Kingdom Suite package. Water and subsurface depths were calculated using a mean acoustic velocity of 1500 m/s. Acoustic penetration in the deeper parts of Lago Lanalhue was rather limited due to gas blanking.

3.4.2   Coring and core processing

Several sediment cores of 6.6 cm inner diameter were retrieved from both lakes in November/December 2005, using a gravity corer as well as a 5-m-long piston-corer system from an anchored raft. With the piston-corer, two or three overlapping core pieces were taken at one and the same position, assuring a complete recovery of up to ~13 m. All coring positions were defined on the basis of seismic reflection profiles before drilling; navigation and positioning was again done by GPS. Due to strong winds and lake currents, positioning and anchoring of the raft hit the defined locations within a tolerance of ± 30 m. A summary of the retrieved cores and an overview of their locations are given in *Table 3.2* and *Figures 3.4a+b*.

Table 3.2: *List of gravity and psiton cores from Lago Lanalhue (LA) and Lago Lleu Lleu (LL).*

Core name	Core type	Original core length (cm)	Site position (UTM coordinates) Easting (18H)	Northing
LA-SL001	gravity core	172	646857	5802276
LA-SL002	gravity core	42	648275	5801860
LA-SL003	gravity core	172	649571	5801279
LA-SL004	gravity core	168	649206	5800683
LA-KL005	piston core	895	649206	5800683
LA-KL006-008	piston core	232-1280	646857	5802276
LA-KL009	gravity core	222	644990	5802300
LA-KL010	gravity core	205	644206	5803390
LA-KL011	gravity core	188	642984	5804850
LA-SL012	gravity core	185	642668	5805180
LA-KL013-014	piston core	1248-1308	642668	5805180
LL-SL001	gravity core	106	644421	5771320
LL-SL002	gravity core	124	646234	5773892
LL-SL003	gravity core	147	646648	5774903
LL-SL004	gravity core	132	647301	5775339
LL-KL005-006	piston core	893-942	646648	5774903
LL-KL007	piston core	454	646234	5773892
LL-SL008	gravity core	129	647347	5776185
LL-KL009	piston core	1260	647347	5776185

All cores were opened, photographed and lithologically described concerning their colour, grain size, structure and the occurrence of microfossils. Subsequently, magnetic susceptibility was measured with a *BARTINGTON* MS2E sensor in 1-mm-steps. The overlapping 5 m-long sections at each coring position were combined, using the magnetic susceptibility results and the detailed core description. Using this method a composite depth was developed for every single core. For each lake, the core with the best and longest recovery was defined as the respective 'master-core', on which the further measurements, e.g. radiocarbon dating, were carried out. The Lago Lanalhue master core has a composite depth of 13.25 mcd (meter composite depth); it is constructed by using part of the corresponding gravity core LA-SL012 for the uppermost meter and the piston core LA-KL013 (1.0-13.25 mcd) below. The master core of Lago Lleu Lleu is 12.22 mcd long; it is composed of gravity core LL-SL008 in the topmost 0.55 mcd and the corresponding piston core LL-KL009 below (0.55-12.22 mcd). For simplification, we refer to them as LA-KL013 and LL-KL009 for the composited sequences in the following.

3.4.3 *Radiocarbon dating*

The chronology for both lakes is based on radiocarbon dating of their respective master cores. The radiocarbon measurements were done at the Leibniz Laboratory in Kiel and at the ETH (Swiss Federal Institute of Technology) Zurich. If procurable, dating was done on plant fragments, bivalve shells or foraminifera. The latter were sampled using wet-sieving (mesh-width: 125 μm) and identifies as well as hand-picked under a binocular microscope. In those parts of the cores that were lacking datable material, we used bulk sediments. Absolute age control is provided by 13 AMS radiocarbon dates for Lago Lanalhue. Eight datings were done on material of the piston-core LA-KL013 (*Table 3.3a*); the remaining dates were measured on material of gravity cores LL-SL010+SL012 and correlated by means of magnetic susceptibility. Age control for the Lleu Lleu sequence is provided by ten AMS radiocarbon dates of which nine were done on piston-core LL-KL009 (*Table 3.3b*). One age was determined on material of gravity core LL-SL008 and correlated by magnetic susceptibility as well.

To calibrate the radiocarbon ages to calendar years we used the online version of the *CALIB* Radiocarbon Calibration (Execute Version 5.0.2html) of Stuiver et al. (2005) with the Southern Hemisphere Calibration curve (SHCal04) of McCormac et al. (2004) and the marine calibration curve (marine04) of Hughen et al. (2004a) for the lowermost marine sections of both cores. All ages are reported in years BP (before present). For those datings done on marine samples, a regional deviation of the global reservoir effect ($\Delta R = 61 \pm 50$ years) was considered according to the embedded Marine Reservoir Correction Database (http://intcal.qub.ac.uk/marine/). To generate point estimates, we calculated the weighted average of the obtained 2σ ranges, using the range mid-points (cf. e.g. Telford et al., 2004). For the subsequent construction of the age models we used linear interpolation between these point data, as well as linear extrapolation to the cores top and base.

Table 3.3a: *AMS ^{14}C ages of the Lanalhue master core (LA-KL013).*

Orig. Depth (m)	Core nr. (LA-)	Comp. Depth (mcd)	^{14}C AMS Age (yr)	Calibrated Age (yr cal. B.P.)	Laboratory number	Dated Material
0.63	SL012	0.63	210 ± 25	198	KIA31962	Plant fragments
0.67	SL010	0.70	215 ± 25	204	KIA31957	Degr. leaves
1.33	SL010	1.42	1040 ± 30	888	KIA31960	Plant fragment
1.83	SL012	2.17	1750 ± 30	1606	KIA31963	Degr. leaves
2.59	KL013	2.88	3915 ± 25	4297	KIA31964	Bulk sediments
4.60	KL013	4.76	3555 ± 30	3779	KIA29621	Plant leaf
5.80	KL013	5.96	3855 ± 31	4192	KIA31965	Plant fragments
7.27	KL013	7.43	4175 ± 30	4751	KIA29622	Wood fragment
8.71	KL013	8.85	5860 ± 35	6593	KIA29422	Shell fragments
9.39	KL013	9.53	6150 ± 35	6972	KIA31966	Bulk sediments
10.68	KL013	10.82	7240 ± 35	7662	KIA29623	Bivalve shell
12.19	KL013	12.33	7280 ±	8053	KIA29624	Wood fragment
12.29	KL013	12.43	7790 ± 40	8186	KIA29625	Bivalve shell

Table 3.3b: *AMS ^{14}C ages of the Lleu Lleu master core (LL-KL009).*

Orig. Depth (m)	Core nr. (LL-)	Comp. Depth (mcd)	^{14}C AMS Age (yr)	Calibr. Age (yr cal. B.P.)	Laboratory number	Dated Material
0.09	KL009	0.03	550 ± 45	533	ETH-35361	Degr. leaves, wood
0.20	SL008	0.20	770 ± 25	681	KIA31982	Plant leave
107.5	KL009	1.02	2325 ± 45	2256	ETH-35362	Degr. leaves, wood
1.29	KL009	1.23	2635 ± 45	2656	ETH-35363	Degr. leaves, wood
2.57	KL009	2.51	5210 ± 55	5883	ETH-35364	Degr. leaves, wood
4.30	KL009	3.93	7675 ± 40	8076	KIA29626	Shell fragments
4.68	KL009	4.31	8075 ± 45	8481	KIA29627	Shell fragments
9.10	KL009	8.73	9310 ± 50	10,033	KIA31979	*Ammonia tepida*
11.65*	KL009	11.28	9230 ± 55	10,366	KIA31980	Degr. leaves
12.40*	KL009	12.03	10,170 ± 55	11,056	KIA31981	*Ammonia tepida*

3.5   Results

3.5.1   Seismic interpretation

Seismic-stratigraphic analyses reveal a major unconformity in the sedimentary infill of both basins. It forms an irregular morphology with pre-lake incisions up to 20 m and 30 m deep in the underlying basement of Lago Lanalhue and Lago Lleu Lleu, respectively; slope angles of the incision reach values of more than 20° (*Figure 3.5*). These erosional

features developed into thick pre-Holocene sedimentary sequences. The dense survey spacing in Lago Lanalhue allowed the detailed mapping of the major unconformity, which has the morphology of a main valley and several smaller lateral gullies. Some of these channels and the overall morphology of the former fluvial drainage system are still visible in the bathymetric map (*Figure 3.4a*). The incisions originate at the main tributaries discharging into the lake and generally deepen in westward direction, emphasizing pre-lake fluviatile morphology.
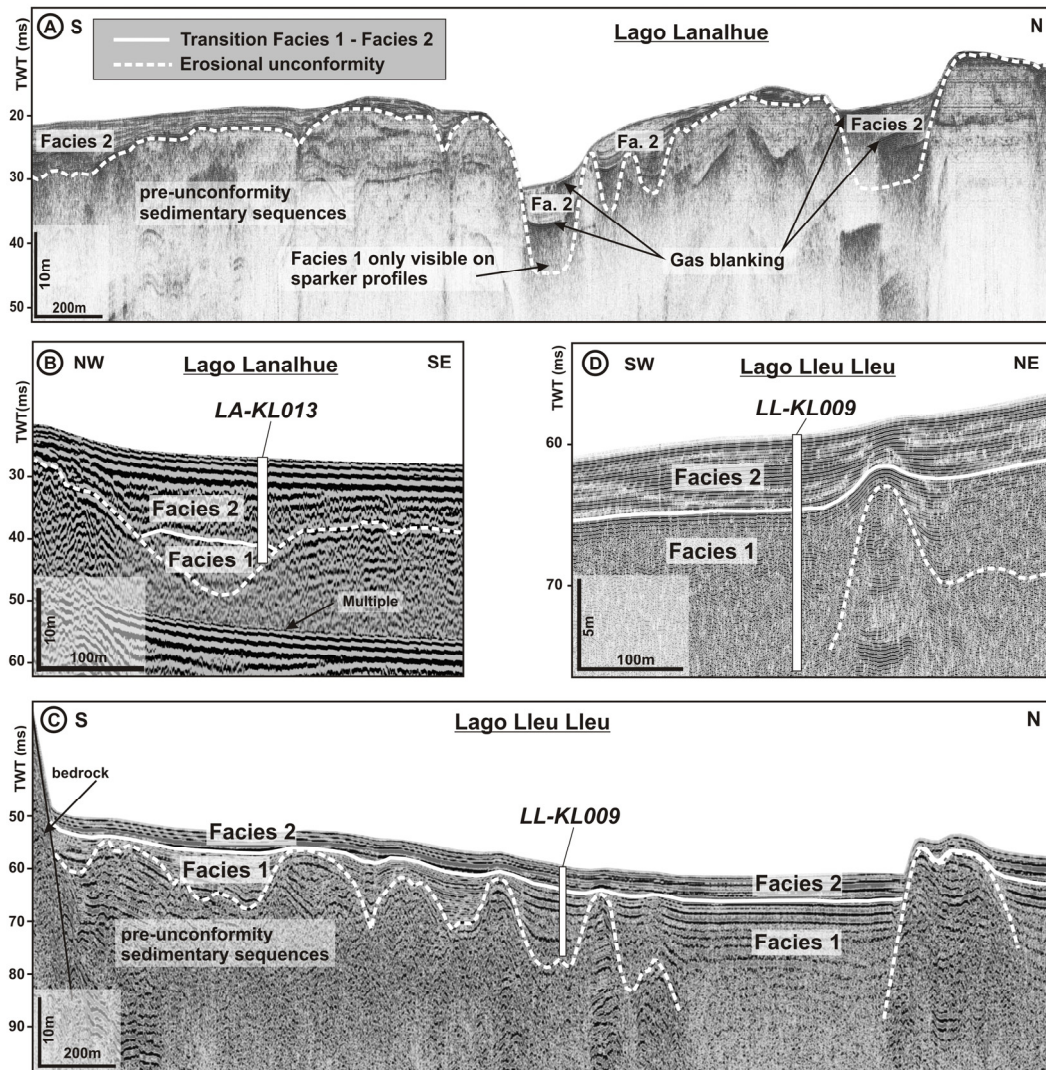
Figure 3.5: *Seismic profiles of Lago Lanalhue and Lago Lleu Lleu. The position of the respective seismic lines is indicated in Figure 3.4 (a+b). The unconformity, stratigraphic boundary, and core-to-seismic correlation are shown. A: S-N pinger profile in the central part of Lago Lanalhue. B: NW-SE sparker profile with projection of LA-KL013. C: S-N sparker profile in the central part of Lago Lleu Lleu with projection of LL-KL009. D: Pinger profile with projection of LL-KL009.*

Seismic reflection profiles also indicate a major stratigraphic boundary in the lake filling sediments, which is clearly pronounced in Lago Lleu Lleu but less distinct in Lago Lanalhue (*Figure 3.5*). On pinger sections from Lago Lleu Lleu this transition is marked by the lower limit of the clear acoustic penetration, while sparker sections of both lakes indicate a subtle change in depositional conditions. The apparent transition

delimits a lower sedimentary unit (Facies 1, see *Figure 3.5*), which is restricted to the topographic lows of the ancient fluvial drainage system, and an upper sedimentary unit (Facies 2) that fills these former depressions but also drapes the shallower areas (being condensed in those parts). Generally no sedimentation occurred in regions of the lake where water depth is less than 14 m. This sediment focussing process generally smoothes the irregular lake bottom morphology, but still the contours of the former fluvial valleys are clearly visible in the present-day bathymetry. Core-to-seismic correlation further suggests that drilling operations reached the former river bed in Lago Lanalhue, although no fluvial material could be recovered (probably due to its higher resistance and coarser grain size), whereas in Lago Lleu Lleu coring stopped some decimeters above this discontinuity (*Figure 3.5*).

3.5.2   *Sediment lithology*

Similar to the seismic analyses, two main stratigraphic units have been identified from the lithological description of the cores (Facies 1 and Facies 2), both in Lago Lanalhue and Lago Lleu Lleu (*Figures 3.6a+b*).

Lago Lanalhue
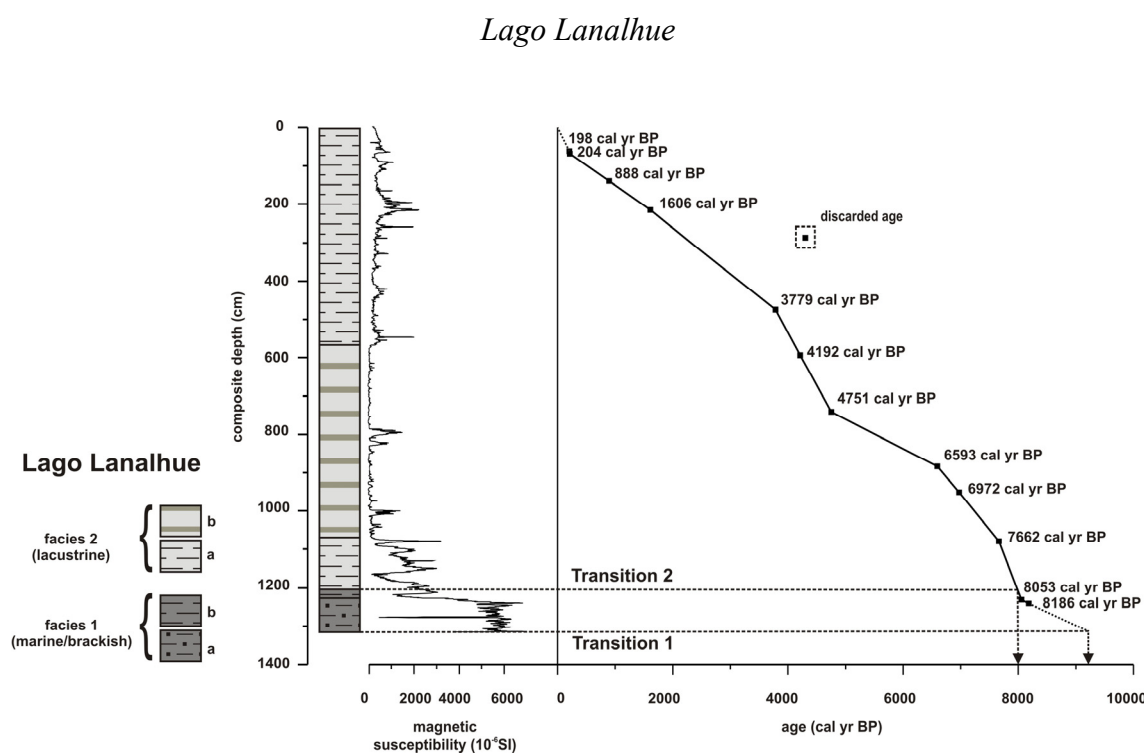
Figure 3.6a*: Lithological units, magnetic susceptibility values and age model of the Lanalhue master core LA-KL013. Facies 1 (dark-grey) is of marine/brackish, facies 2 (light-grey) of lacustrine origin. The facies transitions are indicated with dashed lines/arrows. All dating results, except one age, are in stratigraphic order; the non-fitting age is marked by the dashed square and ignored for the age model.*

The lowermost facies of the Lanalhue sediments (Facies 1a, 13.25-12.44 mcd) unconformably overlies the ancient riverbed, as revealed by seismic data. It consists of dark-grey clayey sand with sporadically embedded, non-destructed bivalve shells (*Mulinia edulis* King and Broderip, 1832) and foraminifera of the benthic species

Ammonia tepida (Cushman). Magnetic susceptibility is higher-than-average for this part of the section, reaching values around 6000*10^{-6}SI (*Figure 3.6a*). Upwards, the clayey sand grades to homogeneous silty clay (Facies 1b, 12.44-12.09 mcd) that still contains benthic foraminifera but has lower values of magnetic susceptibility (~2000*10^{-6}SI).

Facies 2 of the Lanalhue sequence is lying on top of Facies 1 and composed of organic-rich silty clay. Calcareous microfossils are completely absent. The mean values of magnetic susceptibility are 1000*10^{-6}SI, just a fractional amount of the values that were measured for Facies 1. Large parts of Facies 2 appear to be very homogenous and just slightly laminated (Facies 2a, 12.09-10.80 mcd and 5.81-0 mcd); a smaller part is, however, characterized by a regular occurrence of diatom-rich layers (Facies 2b, 10.80-5.81 mcd). A more detailed description of the diatoms as well as geochemical analyses of the sediments can be found in Stefer et al. (submitted).
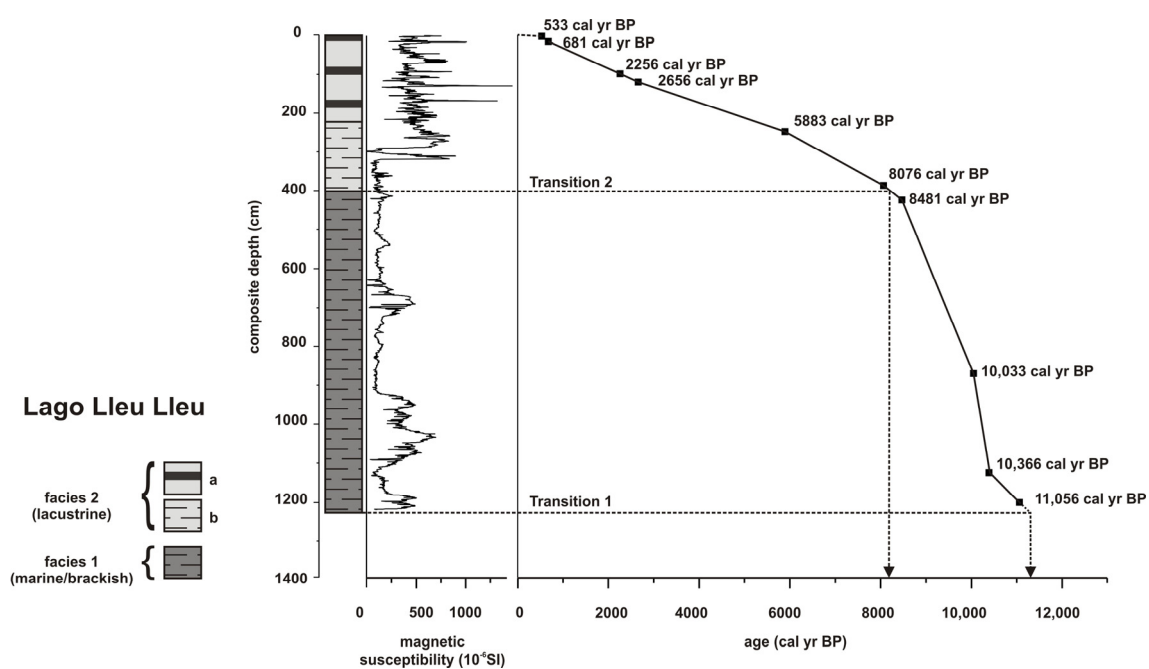
Figure 3.6b: *Lithological units, magnetic susceptibility values and age model of the Lleu Lleu master core LL-KL009. Facies 1 (dark-grey) is of marine/brackish, facies 2 (light-grey) of lacustrine origin. The facies transitions are indicated with dashed lines/arrows. In the case of Lleu Lleu, all dating results are in constant stratigraphic order.*

The lowermost facies of the Lleu Lleu sediments (Facies 1) is composed of homogenous silty clay and also containing foraminifera of the benthic species *Ammonia tepida* (Cushmann); non-destructed marine bivalves (*Thyasira cf. magellanica* Dall 1901, *Tindaria striata* King and Broderip, 1832) are sporadically occurring. Magnetic susceptibility values average ~500*10^{-6}SI (*Figure 3.6b*) and are hence distinctly lower than those of the analogue facies in Lago Lanalhue. With a thickness of nearly eight meters (12.22-4.01 mcd) Facies 1 of Lago Lleu Lleu is also a fivefold thicker than its counterpart at Lago Lanalhue.

Facies 2 of the Lleu Lleu sequence is situated above Facies 1 and consists of dark laminated, organic-rich, silty clay devoid of foraminifera. In its lowermost part (Facies 2a, 4.01-2.12 mcd), the sediments are very homogeneous, but, nevertheless, showing a sudden increase of magnetic susceptibility values from $\sim 250*10^{-6}$SI to $\sim 1000*10^{-6}$ SI (*Figure 3.6b*). In its upper part, Facies 2 is characterized by frequent interbedded layers of homogenous clay, organic matter and mica (Facies 2b, 2.12-0 mcd). Magnetic susceptibility values remain high ($\sim 1000*10^{-6}$SI).

3.5.3   *Stratigraphy and timing of the transition between the main facies*

According to the radiocarbon dating and the developed age model, the base of the Lanalhue master core (LA-KL013) has an age of $\sim$9200 calibrated years (cal yr) BP (*Figure 3.6a*). Age control is provided by 13 dating points, which are, except for one outlier, in stratigraphic order. The non-fitting age, however, was measured on bulk sediments and may have been contaminated by reworked material. As a matter of course, the erroneous age was neglected for the age model. The master core of Lago Lleu Lleu (LL-KL009) has a basal age of $\sim$11,250 cal yr BP. Age control of the Lleu Lleu sequence is provided by ten dating points in stratigraphic order (*Figure 3.6b*).

Based on the developed age models, we calculated the timing of transition between the two main facies for each of the lakes. We defined the transition point of the respective core as the point at which foraminifera start to be absent. According to this approach, the transition took place first in Lago Lleu Lleu, at approximately 8150 cal yr BP, and then in Lago Lanalhue, at about 8000 cal yr BP (*Figures 3.6a+b*).

3.6   *Discussion*

Sedimentary records are regularly used for the reconstruction of past natural environments since their depositional processes are highly susceptible to changes in the environmental conditions. Accordingly, in terms of tectonics in active regions like south-central Chile, sedimentary sequences may provide insight into local deformation processes (e.g. Encinas et al., 2006), recurrent seismicity (e.g. Bertrand et al., 2008; Moernaut et al., 2007), and secondary implications (e.g. tsunamis; Cisternas et al., 2005). In this study, we focus on the first mentioned aspect and evaluate the sediments of Lago Lanalhue and Lago Lleu Lleu concerning their potential of recording local forearc deformation. The most relevant observations obtained from our seismic and sedimentary analyses of both lakes are 1) the existence of ancient fluvial drainage systems where the lakes developed and that predetermined the shape and depth of the present-day lakes, and 2) the occurrence of a marked marine-to-lacustrine transitional layer in the lake sediments, which enabled us to calculate the attendant local uplift rates. Based on those major findings, we interpret the different stages of the lakes development and interpret the lake-forming deformation processes.

3.6.1   Geomorphic and stratigraphic evolution of the lakes

In the most recent study about Lago Lanalhue and Lago Lleu Lleu, Mardones and Reuther (1999) speculated that the lakes developed in estuary systems of pre-existing river valleys that were once connected with the Pacific Ocean. The formation time of the ancient valleys is not known, but it is most likely that they were at least deepened during the last glaciation when the sea-level was ~120 m lower, leading to an inferior local base level and probably to a higher stream power, which thus likely enhanced erosion rates. It has been previously suggested that the lakes are separated from the ocean by uplifted barriers forming natural dams and impounding the water bodies behind them (Mardones and Reuther, 1999); as shown in the following, our data support this hypothesis. However, the time at which the fluvial system was blocked and the lakes fully developed has remained unclear so far. By analyzing the sedimentary sequences deposited on top of the former river beds, we are able to reconstruct the lakes history circumstantially (cf. *Figure 3.7*).

Sediment deposition above the former river valley started at 9200 cal yr BP in Lanalhue and 11,250 cal yr BP in Lleu Lleu. Since drilling operations stopped little above the ancient valley floor in Lago Lleu Lleu, it is important to regard the given age as a minimal value. In both lakes, the sedimentary unit directly above the former river bed is containing marine bivalves and foraminifera of the benthic species *Ammonia tepida* (Cushman). As the genus *Ammonia* (Bruenich) generally typifies a marginal marine, saline to brackish environment (e.g. Murray, 1991), its occurrence clearly manifests the development of lagoon-like conditions. Furthermore, a restricted abundance of microfossil species is another argument in favor of a restricted environment (brackish in this case). We hence interpret that the former river valleys were flooded - at least marginally - by the marine transgression at the end of the last deglaciation/beginning of the Holocene (*Figure 3.7A*). The temporal mismatch of ~2000 years between the marine flooding of the two river valleys is most likely due to differences in their height above sea level at the respective times, originating from the very different morphometric and geologic (e.g. bedrock erodibility) character of the river catchments. Moreover, the differences in thickness and characteristic of the marine parts in Lago Lanalhue (> 1 m thick, mainly sandy material) and Lago Lleu Lleu (nearly 8 m thick, clayey material; cp. paragraph 3.5.2) are in all likelihood a consequence of different depositional conditions during the time when both systems were in connection with the Pacific Ocean.

In contrast to the marine facies, the upper sedimentary facies is completely devoid of any foraminifera in both of the lakes. The absence of foraminifera indicates the transition from the lagoonal-like to a lacustrine environment, and hence points to the ultimate separation of the lakes from the Pacific Ocean. We therefore suppose that the timing of the marine/brackish – lacustrine transition is also the timing of the final lake formation, which is dated to 8000 cal yr BP for Lago Lanalhue and to 8150 cal yr BP for Lago Lleu Lleu. Thus at those times the barriers that are nowadays impounding the lakes must have been uplifted and emerged above sea level, consequently separating the water bodies from the Pacific Ocean (*Figure 3.7B*).
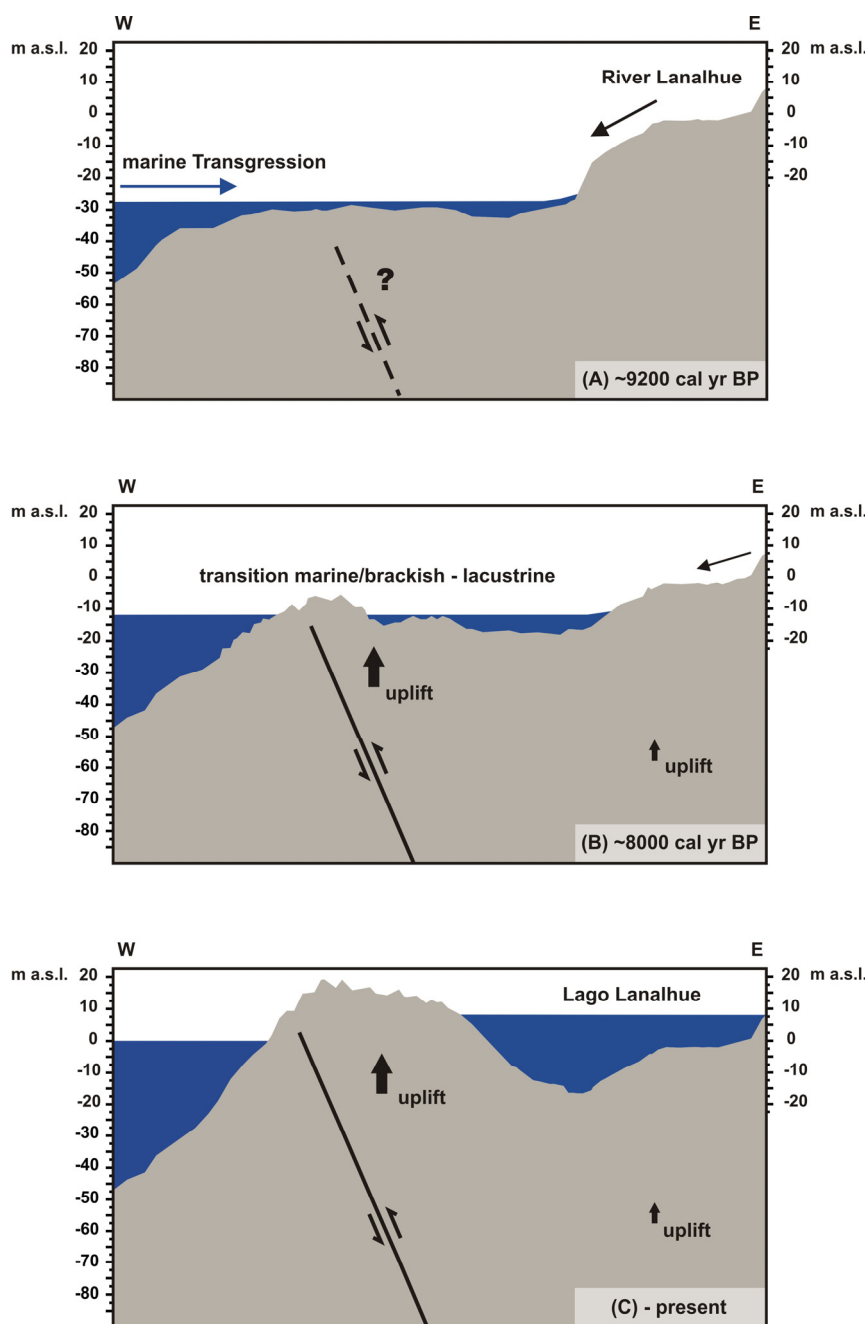
Figure 3.7: *Model of the lake development, exemplary shown for Lago Lanalhue (not to scale). Elevation (m a.s.l.) relative to present sea level. (A) At 9200 cal yr BP, the valley of the former River Lanalhue was drowned by the marine transgression for the first time; depositional conditions were marginal marine to brackish. (B) At 8000 cal yr BP, the swell was uplifted above the global sea level; the marginal marine/brackish conditions changed into lacustrine ones. (C) At present, Lago Lanalhue is impounded behind the uplifted swell.*

The surface topography of the barrier that blocks Lago Lanalhue shows a deep incision by the formerly westward flowing 'river Lanalhue', which left a rather oversized valley when compared with the small stream that is nowadays draining the lake (*Figure 3.3*). Currently, this small stream is flowing on resistant crystalline basement (visible, for instance, where the highway P-70 is crossing the Lanalhue outlet; coordinates: 37°54'12''S, 73°23'57''W), which let us hypothesize that a change in the erodability of the swell-building material could have been jointly causative for the final lake

formation as well. As long as the ancient river was flowing on the less resistant, poorly consolidated Pleistocene deposits of the Cañete terrace, it was incising the slowly uplifting swell and consequently maintaining a connection with the Pacific Ocean. When the river incised through the entire Cañete sequence reaching the underlying resistant basement, it was barely capable to further incise the uplifting barrier. As a result, the river was finally defeated and the lake impounded.

The sediments of both lakes remained of lacustrine character ever since the first blockage, indicating that both water bodies never had mixing contact with the ocean again. However, other environmental changes, as for instance variations in the regional climate, took place in the catchments areas and left their mark in the sedimentary records. These youngest stages of the lakes history and the inferable climate signals are circumstantially discussed in a companion paper (Stefer et al., submitted). Considering a modeling study of the long-term evolution of tectonic lakes proposed by Garcia-Castellanos (2006), Lago Lanalhue and Lago Lleu Lleu will most probably persist in the future as long as tectonic uplift of the barriers is holding up. Potentially, the lakes could even become full endorheic if either the uplift rate accelerates to completely defeat fluvial erosion of the swells, or if evaporation in the drainage basins becomes strong enough to completely outpace the erosive capacity of their fluvial outlets. If, however, the tectonic forcing tapers off at any time, an extinction of the lakes by sediment overfills and/or outlet erosion is predetermined.

3.6.2   Calculation of local uplift rates

The transitional layers, determined by both seismic and sedimentary analyses, mark the beginning (Transition 1) and the end (Transition 2) of the marine influence on the sedimentary deposition in the Lanalhue and Lleu Lleu systems. The comparison with the Holocene evolution of the global sea level hence allows for the calculation of local surface uplift rates. Therefore it is first necessary to assess the following parameters: I) the timing of the transitions, II) the present elevation (m a.s.l.) of the transitional layers, and III) the global sea-level at the time of the transitions.

Table 3.4: *Parameters used for the calculation of uplift rates.*

	Lago Lanalhue (LA)	Lago Lleu Lleu (LL)
Timing of Transition 1 (t_1)	9200 ± 70 cal yr BP	$11{,}250 \pm 55$ cal yr BP
Present-day elevation of layer (h_1)[*1]	-23.25 ± 1.44 m a.s.l.	-47.22 ± 1.44 m a.s.l.
Relative Sea Level (RSL) at t_1[*2]	-27.17 ± 6.40 m a.s.l.	-52.74 ± 4.5 m a.s.l.
Timing of Transition 2 (t_2)	8000 ± 50 cal yr BP	8500 ± 64 cal yr BP
Relative Sea Level (RSL) difference ($t_1 - t_2$)[*2]	10.59 ± 3.1 m	35.23 ± 1.43 m

[*1] *calculated as*: present-day elevation of lake level (LA: 8.0 ± 1.44 m a.s.l.; LL: 5.0 ± 1.44 m a.s.l) *minus* present-day water depth (LA: 18 m; LL: 40 m) *minus* thickness of the sedimentary sequence above the transitional layer (LA: 13.25 m; LL: 12.22 m)
[*2] *calculated as*: mean difference $\pm$ standard deviation between the sea level at the time of transition 1 (t_1) and the sea level at the time of transition 2 (t_2), deduced from: Global stack (Fleming et al., 1998), Barbados (Bard et al., 1990), Tahiti (Bard et al., 1996)

The first two parameters (timing of the transitions and present-day elevation of the transitional layers) can be derived from the age model and the combination of water depth, actual elevation of the lake level, and thickness of the sedimentary sequence (assuming that there has not been sediment compaction). We calculated them for the master core sites, at which the depths of the transitional layers have an averaged, representative depth for the entire lake; resulting data are listed in *Table 3.4*. The third parameter (relative sea-level, RSL), however, has to be necessarily taken from literature. This poses the problem that, especially when considering the Holocene time period, RSL curves are scarce and conspicuous differences between individual curves are apparent (e.g. Bassett, et al., 2005; Caputo, 2007; Milne et al., 2005). Accordingly, even though the exact present-day altitude and the exact timing of the transition from marginal-marine to lacustrine conditions are known, the height of the past sea level is a relative uncertain factor. Hence the use of only one global sea level curve makes the calculated uplift rates tenuous. To reduce this uncertainty and to avoid any bias introduced by selecting a particular curve, we compiled several sea-level curves and calculated a range in the uplift rates according to the resulting values. In this regard, we implemented the sea-level records from Barbados (Bard et al., 1990; Fairbanks, 1989) and Tahiti (Bard et al., 1996), both based on fossil coral samples, as well as the global stack of sea-level curves of Fleming et al. (1998) (*Figure 3.8*).
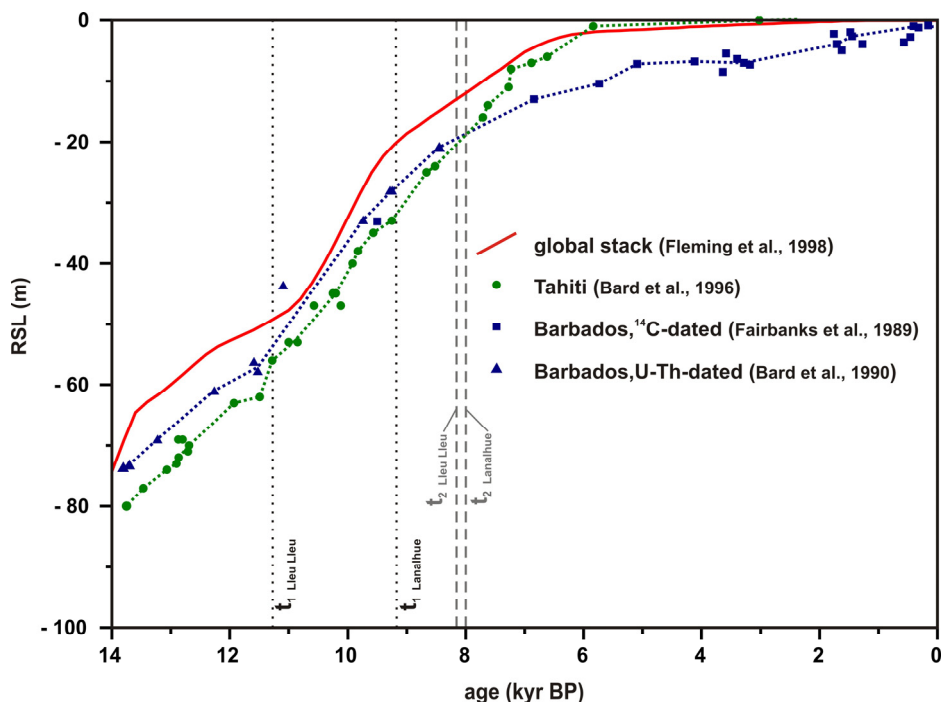
Figure 3.8: *Comparison of the different Holocene sea-level curves used for the calculation of uplift rates: the global stack of Fleming et al. (1998) (red line), the Tahiti coral record of Bard et al. (1996) (green dotted line + dots), the ^{14}C-dated Barbados coral record of Fairbanks et al.(1989) (blue dotted line + squares), and the U-Th-dated Barbados coral record of Bard et al. (1990) (blue dotted line + triangles). The timing of Transition 1 (t_1, black dotted line) and Transition 2 (t_2, grey dashed line) is indicated for Lago Lanalhue and Lago Lleu Lleu, respectively.*

Based on these parameters, we calculate two different uplift rates: (I) a rate for the overall lake basins and (II) a rate for the barriers that are impounding the lakes and which must hence have experienced a stronger vertical deformation:

(I) When the valleys of the former rivers Lanalhue and Lleu Lleu were first flooded by the marine transgression at 9200 cal yr BP and 11,250 cal yr BP, respectively, they must have been at the height of the global sea level. By means of known sea-level reconstructions, we can hence deduce the elevation of the river valleys at the time of Transition 1 and compare it to the present-day one. Accordingly, the uplift of the lake basins since the time of the first flooding can be calculated as follows:

$$uplift \geq (h_{Transition\ 1} - sea\ level_{Transition\ 1}) / t_{Transition\ 1}$$

with $h_{Transition\ 1}$ = present elevation of the transitional layer (m a.s.l.), sea level$_{Transition\ 1}$ = RSL at the time of Transition 1, and $t_{Transition\ 1}$ = timing of Transition 1. In the case of Lago Lanalhue, the uplift rate is 0.42 ± 0.71 mm/yr, whereas for Lago Lleu Lleu the rate is 0.49 ± 0.44 mm/yr (inserted values listed in *Table 3.4*).

We have to admit an uncertainty concerning the water depth in which the lagoon sediments were deposited. To simplify matters, we assumed a deposition at mean sea level for the calculation above. However, since the sediments may have been deposited in some meters of water depth, it is to be considered that the calculated rates are only minimum estimates of uplift.

(II) For allowing the marine transgression to flood the former river valleys, the barriers that are nowadays impounding the lakes must have been at the height of, or slightly lower than the sea level. However, when the conditions changed from marginal marine to lacustrine, the barriers must have been elevated above sea level to truncate the systems from the Pacific Ocean and to let the lakes finally develop. As a result, the uplift of the barriers in the period between Transition 1 and Transition 2 must have been of a similar dimension as the increase of the global sea level. Therefore, their vertical deformation can be calculated as:

$$uplift \geq (sea\ level_{Transition\ 1} - sea\ level_{Transition\ 2}) / (t_{Transition\ 1} - t_{Transition\ 2})$$

with sea level$_{Transition\ 1}$ = sea level at the time of Transition 1, and $t_{Transition\ 2}$ = timing of Transition 2. For this calculation it is to keep in mind, that the barriers are also exposed to erosional processes, acting contrary to the local surface uplift. An additional element of uncertainty is that the barriers could have been located several meters below sea level at Transition 1 and several meters above sea level at Transition 2. Therefore, the calculated uplift rates can only be minimum estimates. For the barrier impounding Lago Lanalhue we obtained an uplift rate of 8.83 ± 2.7 mm/yr, whereas for the barrier impounding Lago Lleu Lleu a rate of 11.36 ± 1.77 mm/yr was calculated (inserted values listed in *Table 3.4*).

3.6.3 Uplift rates in the regional context

A comparison of our data with independent uplift rates derived from emerged marine terraces and incision of fluvial terraces in the Arauco Peninsula region and the adjacent Coastal Cordillera allows appraising the actual relevance of uplift rates derived from our novel approach. In general, differential uplift rates arose for the swells that are impounding the lakes and for the lake basins themselves. The calculated uplift rates for

the lake basins of Lago Lanalhue (0.42 ± 0.71 mm/yr) and Lago Lleu Lleu (0.49 ± 0.44 mm/yr) during the Holocene indeed have a large range. Nevertheless, they are basically coincident for both lakes and, furthermore, in good agreement with uplift rates calculated for the southern Arauco Peninsula. Melnick et al. (2009), for instance, determined uplift rates of 0.51 ± 0.1 mm/yr since ~125 kyr, based on emerged marine terraces. Rehak et al. (2008) and Rehak et al. (submitted) used incised fluvial terraces to calculate uplift rates ranging between 0.27 and 0.88 mm/yr since ~80 kyr. We hence believe our results to be reliable and conclude that in general uplift of the Arauco peninsula has not changed substantially during the Late Pleistocene and Holocene.

However, with rates of 8.83 ± 2.7 mm/yr (Lago Lanalhue) and 11.36 ± 1.77 mm/yr (Lago Lleu Lleu), uplift of the swells that are impounding the lakes is approximately 20 times higher than for the lake basins themselves. Unfortunately, it is not inferable from our data if these high rates of vertical deformation are temporally constricted to the time periods between 9200 to 8000 cal yr BP (Lago Lanalhue) and 11,250 to 8150 cal yr BP (Lago Lleu Lleu), or if they have been sustained since. Disregarding erosional processes and assuming that these uplift rates have been constant through the entire Holocene, the barriers would be at an altitude of ~ 54 m a.s.l. (Lago Lanalhue) and ~ 77 m a.s.l. (Lago Lleu Lleu) nowadays. Since they are situated distinctly lower, at ~ 30 m a.s.l. for Lanalhue and at ~25 m a.s.l. for Lleu Lleu, it is likely that their apparent extreme high uplift rates were transient. Taking the present barrier elevation as an opportunity to calculate the uplift of the barriers for the time period since ~8000 cal yr BP, we obtained rates of 3.75 mm/yr (for the Lanalhue barrier) and 3.07 mm/yr (for the Lleu Lleu barrier). Although these rates represent minimal amounts by which the swells must have been uplifted, they are still around 7 times higher than the rates calculated for the lake basins.

The large vertical motion of the lake barriers may be a result of the eastward tilt of the Cañete terrace, which is affected by the Morguilla Fault. Despite the lack of clear field evidence for this fault, Melnick et al. (2009) interpret it as an active reverse fault based on seismological data (focal mechanisms), age determinations of deformed marine terraces and offshore reflection seismic lines. It is thought to be one of several active deep-reaching faults that are controlling uplift at the Arauco Peninsula with an associated cluster of crustal seismicity (Melnick et al., 2009). In its northwestern part, the fault is expressed as a pronounced escarpment of up to 150 m height, which decreases toward the southeast where it is hidden due to progressive blanketing by active dunes (cp. *Figure 3.3*). We suggest that the strong uplift of the Lanalhue and Lleu Lleu swells provides evidence for enhanced vertical deformation along the Morguilla Fault, and hence constitutes an indication of incipient exposure in its southern part as well. Topographic swath profiles spanning from the Pacific to the lake outlets exhibit cross-sections of the uplifted swells and allow identifying the approximate course of the fault (*Figure 3.9*). Our interpretation is in line with a study of Rehak et al. (submitted), who found a tectonically induced flow reversal of the formerly westward flowing Pellahuén River that is located directly south of Lago Lleu Lleu (*Figure 3.3*). The authors suggest that the defeat of the river is controlled by local uplift above a blind reverse fault (Rehak et al., submitted). According to our results, this is another indication for the southern prolongation of the Morguilla Fault also controlling the formation of the two coastal lakes.
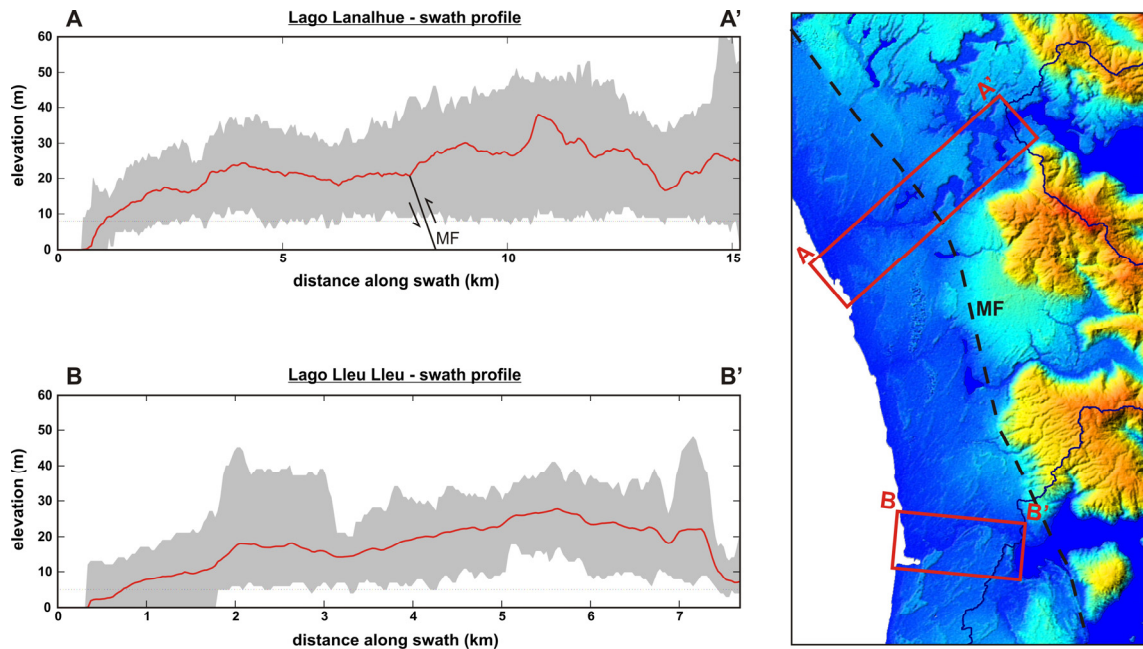
Figure 3.9: *Topographic swath profiles across the Lanalhue and Lleu Lleu swells. Right: Areas of the profiles (A-A': Lanalhue swell. B-B': Lleu Lleu swell). Left: Lanalhue profile (A-A') and Lleu Lleu profile (B-B'). Each profile shows maximum, minimum (shading), and mean elevations (red solid line) of topography. MF = Morguilla Fault.*

3.7   *Conclusions*

The sediments of Lago Lanalhue and Lago Lleu Lleu are excellent recorders of environmental changes. In the present study, we investigated the lake sediments with special emphasize on their capacity of giving information on local tectonics, in particular about surface uplift rates. We demonstrated that both lakes developed in former fluvial valleys, which became first lagoonal systems with a close connection to the Pacific Ocean, being subsequently separated from the ocean by tectonically upraised sills. The differing character of the sediments deposited during each of these phases, the dating of the transitions between the varying facies, and the overall comparison with the global seal level evolution, allowed calculating local uplift rates during the Holocene of ~0.4 mm/yr for both lake basins.

So far, uplift rates of the Arauco Peninsula have been calculated on the base of emerged marine terraces that formed during the different interglacial stages of the Pleistocene. These rates hence constitute average long-term values over 10^5-10^6 years. Our novel approach is the first attempt to achieve local deformation rates on shorter time scales of 10^3-10^4 years. The good agreement between the uplift rates calculated for the basins of Lago Lanalhue and Lago Lleu Lleu emphasizes the reliability of our approach. The comparison of our results with inferred tectonic structures in the Arauco region revealed new and detailed information about local forearc tectonics and distribution of active fault systems. On that account, we highlight the potential of sedimentary archives for the reconstruction of local tectonics.

4. HOLOCENE CLIMATE AND ENVIRONMENTAL CHANGES DOCUMENTED IN THE SEDIMENTARY RECORDS OF TWO COASTAL LAKES IN SOUTH-CENTRAL CHILE (38°S)

S. Stefer, H.W. Arz, F. Lamy, J. Kaiser, R. Kilian, G.H. Haug

Submitted manuscript

Abstract: *This paper presents a reconstruction of regional Mid- to Late Holocene environmental changes in south-central Chile (38°S) based on multi-proxy analyses of sediment cores from two coastal lakes. The investigated lakes, Lago Lanalhue and Lago Lleu Lleu, developed in former river valleys that once discharged to the Pacific Ocean. Both valleys were flooded by the Late Pleistocene/Early Holocene marine transgression, but were subsequently dammed by tectonically uplifted barriers. Radiocarbon dating indicates that a continuous lacustrine sedimentation started at 8000 cal yr BP in Lago Lanalhue and at 8150 cal yr BP in Lago Lleu Lleu, respectively. The lacustrine sediment records of both lakes show a multimillennial long-term trend with a significant shift from more arid conditions during the Mid-Holocene (lasting from 8000-4200 cal yr BP in Lago Lanalhue and 8150-4800 cal yr BP in Lago Lleu Lleu, respectively) to more humid conditions during the Late Holocene. This shift is in accordance with other paleoclimatic findings in the region and attributed to changes in the position/strength of the Southern Westerly Winds. In Lago Lleu Lleu, the transition out of the Mid-Holocene is characterized by the onset of frequent detrital layers that appears synchronously with the strongest increase in intensity and frequency of the El Niño Southern Oscillation (ENSO). In the sediments of Lago Lanalhue, distinct centennial-scale climate changes are particularly present during the last 2000 years. Relatively less humid phases are corresponding to the Roman, Medieval, and Modern Warm Periods (200 cal yr B.C.-150 cal yr A.D., 900-1350 cal yr A.D., and 1850 cal yr A.D.-present); more humid phases are congruous with the Dark Ages and the Little Ice Age (150-900 cal yr A.D and 1350-1850 cal yr A.D.). This pattern of findings suggests that the prominent climate events of the Late Holocene were rather global than local phenomena.*

Keywords: Holocene, lake sediments, X-ray fluorescence, south-central Chile, Paleoclimate

4.1   Introduction

Compared to the extreme climate fluctuations of the Last Glacial and deglaciation, the Holocene climatic conditions may appear to be of an exceptional consistency (e.g. Dansgaard et al., 1993). However, scores of globally distributed studies demonstrate that the Holocene climate was essentially variable (see reviews of Mayewski et al., 2004 and Wanner et al., 2008, for instance). Most of the knowledge about Holocene climate changes is gained from studies in the Northern Hemisphere, where cyclic variations on millennial and (multi-)centennial time-scales seem to be temporally consistent at high and low latitudes (deMenocal et al., 2000). Millennial-scale 'long-term' changes even appear to correlate in different archives all over the world, most importantly influenced by variations in orbital parameters and ocean thermohaline circulation (Mayewski et al., 1994; Steig, 1999). By contrast, less consistency seems to exist for the Holocene centennial-scale 'short-term' changes such as the Medieval Warm Period (MWP) and the Little Ice Age (LIA). Although worldwide evidence is found for both periods (e.g. Johnson et al., 2001; Hendy, et al., 2002; Paulsen et al., 2003; Peterson and Haug, 2006; Arenada et al., 2007), it is still up for debate whether or not they were global climate events (e.g. Hughes and Diaz, 1994; Broecker, 2001; Soon et al., 2003). This is one of the reasons why driving mechanisms behind the 'short-term' climate events – orbital, solar and volcanic forcing – are still under discussion (Wanner et al., 2008). Hence, in order to understand global climate change and possible interhemispheric connections during the Holocene, it is a major challenge to obtain new paleoclimate data from widely distributed regions.

Holocene paleoclimatic surveys are comparatively rare in the Southern Hemisphere – particularly in the mid- and high-latitudes. Southern Chile is in the focus of research only since a relative short period of time although it displays a key region for paleoclimatic reconstructions (Bertrand et al., 2005). The picture of climate history is still far from being complete as can be recognized by conflicting statements of different authors. One of the main controversial issues is the temporal evolution of local precipitation changes and wind patterns, which are regulated by the position/strength of the Southern Westerly Winds and have been object of a number of proxy studies (e.g. Markgraf et al., 1992; Schäbitz, 1999; Lamy et al., 2001; Jenny, et al., 2003; Moreno, 2004; Gilli et al., 2005, Mayr et al., 2007).

Hitherto existing studies focussing on the Holocene climate evolution in Southern Chile recorded in marine sediments are found south of 40°S (Lamy et al., 2001, 2002, 2004; Kaiser et al., 2007; Mohtadi et al., 2007) and at ~33°S (Lamy et al., 1999; Kim et al. 2002). Studies of lacustrine sequences are particularly concentrated in the Chilean Lake District (e.g. Moreno, 2004; Bertrand et al., 2005, 2008) and the central Chilean Valley (e.g. Jenny et al., 2002a,b) (*Figure 4.1*). Due to the very limited number of lakes north of the Lake District, lacustrine (but also marine) surveys are so far rare between ~34-40°S. Since this area is sensitive to latitudinal changes in the Southern Westerlies due to its position close to the present-day northern extension of this wind belt, the study of new archives from this region is of high priority. Among these new archives, sediment records of the coastal lakes Lanalhue and Lleu Leu, located in the southern part of the Arauco Peninsula (38°S, 73°W, *Figure 4.1*), hold the potential of gaining significant

new knowledge of Holocene climate variability in the Southern Hemisphere mid-latitudes.
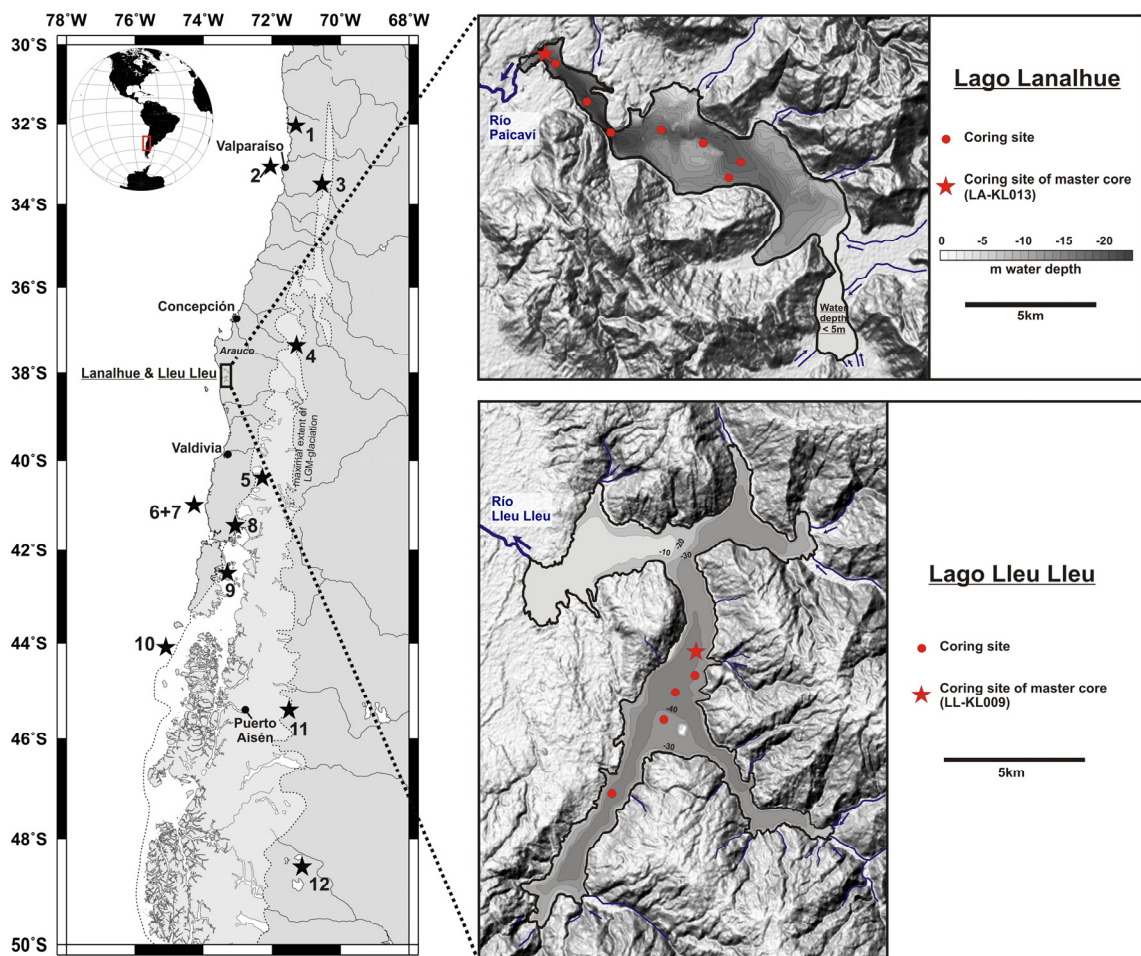
Figure 4.1: *Position of Lago Lanalhue and Lleu Lleu at the south-central Chilean margin. Left: Extended study area and locations of adjacent studies discussing Holocene paleoclimatic and –environmental changes (black stars). 1: Palo Colorado Swamp Forest (Maldonado and Villagrán, 2006), 2: marine sediment core GeoB 3302-1 (Lamy et al., 1999) 3: Laguna Aculeo (Jenny et al., 2002a and b, Villa-Martínez et al., 2003), 4: Lago Laja (Torres et al., 2008), 5: Lago Puyehue (e.g., Bertrand et al., 2005 and 2008, Sterken et al., 2008), 6+7: marine sediment core GeoB3313-1 (Lamy et al., 2001 and 2002) and ODP Site 1233 (e.g., Lamy et al., 2004), 8: Lago Condorito (Moreno, 2004), 9: Laguna Tahui and Laguna Melli (Abarzúa et al., 2004), 10: marine sediment core GeoB7186-3 (Mohtadi et al., 2007), 11 Mallín Pollux (Markgraf et al., 2007), 12: Lago Cardiel (Gilli, et al., 2005). The white shaded area markes the maximal extension of the Patagonian Ice Sheet during the Last Glacial (after Rabassa and Clapperton, 1990). Right: Shaded topography, contours, bathymetry and inflows of Lago Lanalhue and Lago Lleu Lleu (modified after Stefer et al., submitted). Isobath for Lanalhue = 1 m, isobath for Lleu Lleu = 10 m. Coring sites and locations of the respective master cores are indicated by red circles and stars, respectively.*

In this paper, we present new multi-proxy analyses of the Lanalhue and Lleu Lleu sediments, including sedimentology, mineralogy and geochemistry in combination with radiocarbon dating. Former studies of both lakes so far concentrated on the investigation of their catchment areas and drainage networks (Mardones and Reuther, 1999), their phytoplankton diversity (Parra et al., 1999), as well as on morphometrical and sedimentological aspects (Urrutia et al., 2000). However, nothing was known until now

about the sedimentary sequences of the lakes and only speculations were made about their chronological development. Based on the analysis of sediment cores, we previously demonstrated and discussed that both Lago Lanalhue and Lago Lleu Lleu were formed tectonically during the Early Holocene when they became disconnected from the ocean (Stefer et al., submitted). The aim of the present study is hence to reconstruct the variability of Holocene climate conditions in south-central Chile as recorded in the lacustrine sedimentary sequences of the lakes.

4.2   The lakes and their present environments

Lago Lanalhue and Lago Lleu Lleu are located in south-central Chile (38°S) and belong to a congeries of former coastal lagoons situated north of the maximum extent of the Patagonian Ice Field during the last glaciations. Both lakes were separated from the Pacific Ocean by tectonic uplift in the Early Holocene (Stefer et al., submitted); currently the distance from the Pacific is less than 13 km (Lago Lanalhue) and less than 7 km (Lago Lleu Lleu), respectively. The lakes are located on the southern Arauco Peninsula, which constitutes an uplifted part of the Chilean continental shelf (Kaizuka et al., 1973). The catchment areas of Lanalhue and Lleu Lleu stretch across the western slopes of the coastal cordillera (Cordillera de Nahuelbuta) and are bordered by the coastal plain in their west.

Table 4.1 *Mean characteristics of Lago Lanalhue and Lago Lleu Lleu (data compiled from Mardones and Reuther, 1999; Stefer et al., submitted; Urrutia et al., 2000)*

	Lago Lanalhue	**Lago Lleu Lleu**
Coordinates	37°55'S 73°19'W	38°09'S 73°19' W
Water level	8.0 m a.s.l.	5.0 m a.s.l.
Drainage basin	360 km^2	580 km^2
Water surface	32.05 km^2	37 km^2
Average / maximal depth	13.1 / 24 m	23.5 / >40m
Trophic conditions	eutrophic	oligotrophic
Fraction of shallow zones	100 %	60 %
Main orientation	SE-NW	NNE-SSW

*shallow zones: water depth < 30m

At present, the catchment area of Lago Lanalhue covers ~360 km^2 with a water surface area of ~32 km^2 (*Table 4.1*). The water level of the lake is at 8.0 m a.s.l. The lake basin can be subdivided into three bathymetrically different segments (*Figure 4.1*): While the southern, N-S oriented sub-basin is extremely flat and shallow (< 5 m water depth), the main basin has a SE-NW orientation and is up to 22 m deep. The greatest water depth of 24 m is reached in the western t-shaped part of the lake. Several small tributaries are discharging into the lake from the western slope of the Cordillera de Nahuelbuta. The small outlet of Lago Lanalhue – Río Paicaví – is located at the western end of the lake,

flowing into the Pacific Ocean. Regarding the present trophic conditions, Lago Lanalhue is classified as eutrophic (Mardones and Reuther, 1999; Valdovinos and Figueroa, 2000).

Lago Lleu Lleu is located 15 km south of Lago Lanalhue. Its drainage area covers ~580 km^2 with a water surface area of ~37 km^2; the lake level is presently situated at 5.0 m a.s.l. (*Table 4.1*). Lago Lleu Lleu is showing a characteristically branched shape, with its main water body extending over 17 km in NNE-SSW direction (*Figure 4.1*). In this central segment of the lake, water depth is reaching up to 40 m; on the contrary, the north-eastern part of the lake is very shallow, reaching a water depth of less than 10 m. From here, the small outlet – Río Lleu Lleu – is draining to the Pacific Ocean. The lake is presently classified as oligotrophic (Mardones and Reuther, 1999; Valdovinos and Figueroa, 2000).
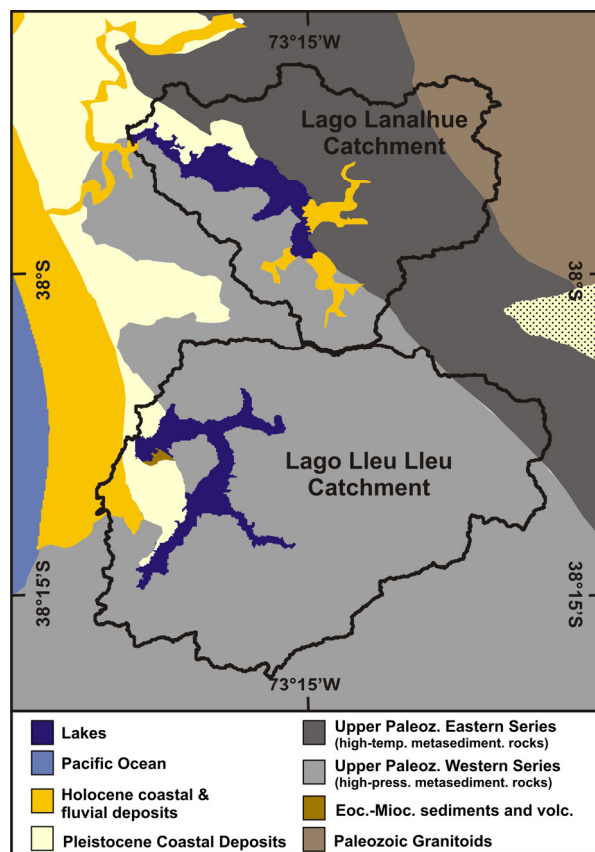
Figure 4.2: Simplified geologic map of the Lanalhue and Lleu Lleu catchment regions (catchments framed by the solid black line); modified after Melnick et al. (2009).

Adjacent to Lago Lanalhue and Lago Lleu Lleu, the Cordillera de Nahuelbuta consists of a former accretionary complex and magmatic arc (Hervé, 1988). Dominating rocks within the lake watersheds are schists, meta-greywackes, -basites, and -cherts of the accretionary complex as well as granites of the magmatic arc (Hervé, 1977) (*Figure 4.2*), which are generally forming much steeper slopes in the Lleu Lleu than in the Lanalhue catchment (*Figure 4.1*). High tectonic activity in the region is due to the subduction of the oceanic Nazca Plate beneath the South American continent. As a direct consequence several fault systems are controlling local deformation, uplift, and folding all around the Arauco Peninsula (e.g. Melnick et al., 2009). Consistently, most recent theories about the formation of Lago Lanalhue and Lago Lleu Lleu suggest a

63

tectonic lake origin caused by uplifted barriers forming natural dams (Mardones and Reuther, 1999; Stefer et al., submitted).

In the lower catchments of Lanalhue and Lleu Lleu, the vegetation is characterized by a low growing forest with the dominant species *Peumus boldus* and *Cryptocarya alba* (Mardones and Reuther, 1999). Typical for the mountainous region of the Cordillera de Nahuelbuta are two species of the southern beech-tree: *Nothofagus obliqua* and *Nothofagus procera* at lower and higher altitudes, respectively. However, nowadays the natural vegetation is in large parts displaced by pine and eucalyptus trees in the Cordillera and by ranching and farming in the coastal plain (Mardones and Reuther, 1999).

Climatically, the coastal zone of south-central Chile is characterized by an extreme north-south gradient in precipitation, since this area is lying at the transition between a summer dry Mediterranean-like climate north of ~37°S and year-round humid conditions south of ~42°S (e.g. Cerveny, 1998; Garreaud et al., 2008). These important differences are due to the latitudinal position of the southern Westerly wind system, which is in turn linked to the strength and position of the subtropical anticyclone in the south-eastern Pacific and the subantarctic low pressure belt (Markgraf, 1998). At present, the Lago Lanalhue and Lago Lleu Lleu drainage areas are influenced by a mild and humid coastal climate especially during the austral winter, but also affected by the mediterranean-like climate conditions from the north, which are dominating during the summer. Mean temperatures are 16° C in January and 10 °C in July (Cerveny, 1998). Precipitation is falling year-round with a clear maximum in the winter season (Miller, 1976). Due to orographic effects, rainfall in the drainage areas increases from west to east, reaching 2000-2500 mm/year in the headwaters of the lakes (Mardones and Reuther, 1999). Inter-annual variations in precipitation are largely affected by the El Niño Southern Oscillation (ENSO) anomaly (e.g., Markgraf, 1998). Related changes in the strength and position of the subtropical anticyclone of the south-eastern Pacific provide most of the explanation for the apparent climatic irregularities (Cerveny, 1998). During La Niña years, the pressure cell is constantly strong all-the-year, constraining cyclonic storms of the Southern Westerlies to the high latitudes (> 45°S); rainfall in the mid-latitudes is hence reduced over those periods. In contrast, during El Niño years the subtropical anticyclone is weakened, allowing the storm tracks of the Westerlies to advance further north. Cyclonic activity and precipitation in the Chilean mid-latitudes are therefore enhanced during El Niño phases.

4.3   Material and methods

4.3.1   Coring and core processing

A number of cores were retrieved from both lakes in November/December 2005, using a gravity corer as well as a 5-m-long piston corer from an anchored raft; coring sites were selected from high-resolution seismic reflection profiles (for exemplary figures of the profiles see Stefer et al., submitted). Two to three overlapping core sections were

taken with the piston-corer at each of the coring sites for guaranteeing a complete recovery of up to ~13m.

After opening, all cores were photographed and lithologically described, using the following parameters: sediment colour, grain size, structure, appearance of microfossils and the occurrence of event layers (in the uppermost part of the Lleu Lleu sediment core). The magnetic susceptibility (MS) of the sediments was measured with a Bartington MS2E-sensor at 1-mm-resolution. MS results were used to correlate the overlapping 5-m-long sections of each piston core and to correlate the records of different coring sites amongst each other. For each lake, the piston core with the best and longest recovery was defined as the 'master core', on which all analyses were carried out (Lanalhue: LA-KL013; Lleu Lleu: LL-KL009, *Figure 4.3*). The master core of Lago Lanalhue has a total length of 13.25 mcd (meter composite depth); the sequence was constructed by using part of the corresponding gravity core LA-SL012 for the topmost 1.0 m and the piston core LA-KL013 below (1.0-13.25 mcd). The Lleu Lleu master core is 12.22 mcd long; it is composed of the gravity core LL-SL008 in the uppermost 0.55 m and the corresponding piston core LL-KL009 below (0.55-12.22 mcd).
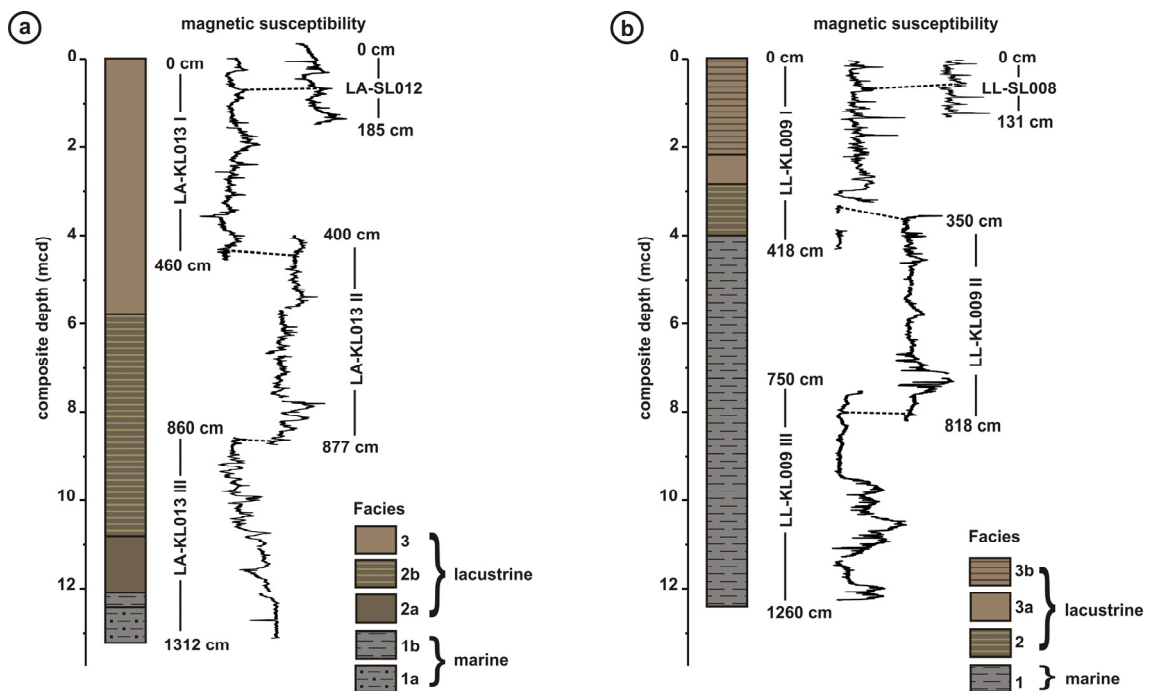
Figure 4.3: *Lithological units and splice construction based on magnetic susceptibility. (a): Lago Lanalhue master core (composed of gravity-core LA-SL012 on top and piston-core LA-KL013 below). (b): Lago Lleu Lleu master core (composed of gravity-core LL-SL008 on top and piston-core LL-KL009 below). Please note: the depth in cm given for single core sections is the depth that was used during drilling operations; the composite depth in mcd (meter composite depth) is the depth resulting from splice construction.*

4.3.2   Radiocarbon Dating

Absolute age control is based on 17 AMS (Accelerator Mass Spectrometry) radiocarbon (^{14}C) ages for core LA-KL013 and 10 AMS radiocarbon (^{14}C) dates for core LL-KL009

(*Table 4.2a+b*). Measurements were done on plant fragments, bivalve shells or foraminifera, or the bulk sediment where macrofossils were missing. Radiocarbon analyses were conducted at the Leibniz Laboratory for Radiometric Dating and Stable Isotope Research at the Christian-Albrechts-University of Kiel (Germany) and at the ETH (Swiss Federal Institute of Technology) Zürich (Switzerland).

Table 4.2a: *AMS ^{14}C ages of the Lanalhue master core (LA-KL013).*

No	Core depth (cm)	Core nr. (LA-)	Composited depth (mcd)	^{14}C AMS Age (yr)	Calibrated Age (yr cal BP)[1]	Laboratory number	Dated Material
1	0.63	SL012	0.63	210 ± 25	198	KIA31962	leaf fragm.
2	0.67	SL010	0.70	215 ± 25	204	KIA31957	leaf fragm.
3	0.84	SL010	0.87	540 ± 30	525	KIA31958	leaf fragm.*
4	0.99	SL011	1.03	370 ± 50	400	KIA31961	leaf fragm.
5	1.10	SL010	1.23	500 ± 30	513	KIA31959	leaf fragm.
6	1.33	SL010	1.71	1040 ± 30	888	KIA31960	plant fragment
7	2.15	KL013	2.44	1840 ± 30	1715	KIA29620	leaf fragm.
8	1.83	SL012	2.45	1750 ± 30	1606	KIA31963	leaf fragm.
9	2.59	KL013	2.88	3915 ± 25	4297	KIA31964	bulk sediment*
10	4.60	KL013	4.76	3555 ± 30	3779	KIA29621	plant leaf
11	5.80	KL013	5.96	3855 ± 30	4192	KIA31965	bulk sediment
12	7.27	KL013	7.43	4175 ± 30	4751	KIA29622	wood fragment
13	8.71	KL013	8.85	5860 ± 35	6593	KIA29642	leaf fragm.
14	9.39	KL013	9.53	6150 ± 35	6972	KIA31966	bulk sediments
15	10.68	KL013	10.82	7240 ± 35	7662	KIA29623	bivalve shell
16	12.19	KL013	12.33	7280 ± 35	8053	KIA29624	wood fragment
17	12.29	KL013	12.43	7790 ± 40	8186	KIA29625	bivalve shell

[1] calculated as weighted average of the obtained 2 σ ranges
*ages neglected for the age model

The radiocarbon ages were calibrated using CALIB 5.0 (Stuiver et al., 2005) with the Southern Hemisphere Calibration Curve (SHCal04) of McCormac et al. (2004) and the marine calibration curve (marine04) of Hughen et al. (2004) for the lowermost marine sections of both cores. For those datings done on marine bivalve shells and foraminifera, a regional deviation of the global reservoir effect was considered according to the embedded Marine Reservoir Correction Database (http://intcal.qub.ac.uk/marine/) ($\Delta R = 61 \pm 50$ years). Single age points were calculated as weighted average of the obtained 2 σ ranges, using the range mid-points (see, e.g. Telford et al., 2004). For the construction of the age models shown in *Figures 4.4a+b*, a linear interpolation was applied between the single dating points. The detected 'event layers' in the uppermost part of the Lleu Lleu core were subtracted from the record, in order to correct the depth for stratigraphic purposes. All ages are generally given in calibrated years before present (cal yr BP).

66

Table 4. 2b: *AMS ^{14}C ages of the Lleu Lleu master core (LL-KL009).*

No	Core depth (cm)	Core nr. (LL-)	Comp. Depth (mcd)*	^{14}C AMS Age (yr)	Calibr.Age (yr cal BP)[1]	Laboratory number	Dated Material
1	0.09	KL009	0.06	550 ± 45	533	ETH-35361	leaf fragm.
2	0.20	SL008	0.18	770 ± 25	681	KIA31982	plant leaf
3	1.08	KL009	0.86	2325 ± 45	2256	ETH-35362	leaf fragm.
4	1.29	KL009	1.06	2635 ± 45	2656	ETH-35363	leaf fragm.
5	2.57	KL009	2.20	5210 ± 55	5883	ETH-35364	leaf fragm.
6	4.30	KL009	3.62	7675 ± 40	8076	KIA29626	shell fragments
7	4.68	KL009	4.00	8075 ± 45	8481	KIA29627	shell fragments
8	9.10	KL009	8.42	9310 ± 50	10,033	KIA31979	*Ammonia tepida*
9	11.65	KL009	10.97	9230 ± 55	10,366	KIA31980	leaf fragm.
10	12.40	KL009	11.72	10,170 ± 55	11,056	KIA31981	*Ammonia tepida*

[1]calculated as weighted average of the obtained 2 σ ranges
*corrected for event layers

4.3.3   Organic and inorganic carbon detection

The total carbon (TC), total organic carbon (TOC) and organic nitrogen (N) contents of the sediments were determined using an elemental analyzer (Eurovector) at the GeoForschungsZentrum (GFZ) Potsdam (Germany). For the TC and N measurements, about 5 mg of each dried and homogenized sample were weighted in Sn-capsules. TOC was measured on decalcified samples using 3 mg of sample material that was weighted into Ag-capsules, dropped with 20% HCl, and finally heated for 3 h at 75°C. The calibration was performed using certified elemental standards and a reference sample. The reproducibility of replicate analyses is 0.2 %. For core LA-KL013, samples were taken every 5 cm; for core LL-KL009, sampling resolution was 2 cm in the uppermost part (0-3.72 mcd) and 20 cm in the lower part (3.72-12.22 mcd). The amount of total inorganic carbon (TIC) was calculated as the difference between TC and TOC (TIC = TC – TOC).

4.3.4   X-Ray fluorescence core scanning

X-Ray Fluorescence (XRF) core scanning was used to constrain changes in the chemical composition of the lake sediments. Measurements of major elements were performed on split cores with the AVAATECH XRF core scanner at the Alfred-Wegener-Institute in Bremerhaven (Germany). The sediment surface was carefully flattened and covered with thin (4μm) Ultralene film to diminish roughness and inhomogeneity, and to prevent drying during scanning. Instrumental settings for all measurements were a tube voltage of 10 kV, an X-ray current of 350 mA, and a net counting time of 30 s. Spatial resolution between the measurement points was 10 mm. The uppermost part of core LA-KL013 (0-4.78 mcd) was additionally measured in 2mm-resolution with instrumental settings of 60 s net counting time, 10 kV tube voltage and 1000 mA X-ray current. All obtained data are expressed as element intensities in

total counts (tc). Although the obtained XRF logging data are of a semi-quantitative character, relative downcore variations in the elemental composition of sediments are reliably reproduced (Richter et al., 2006).

4.3.5   X-Ray diffraction measurements & scanning electron microscope imaging

The bulk mineralogy of ten homogenized samples was detected with X-Ray powder diffraction (XRD) using a Bruker axs D-5000 diffractometer with CuKα radiation at the GFZ Potsdam (Germany). Randomly oriented powder samples were scanned between 2° and 45° 2θ. Subsequent qualitative mineral identification was done with the software DiffraCplus. A number of samples were studied with a scanning electron microscope (SEM, Zeiss NTS DSM 962) at GFZ Potsdam (Germany) in order to identify most abundant diatoms.

4.4   Results

4.4.1   Stratigraphy and sedimentation rates
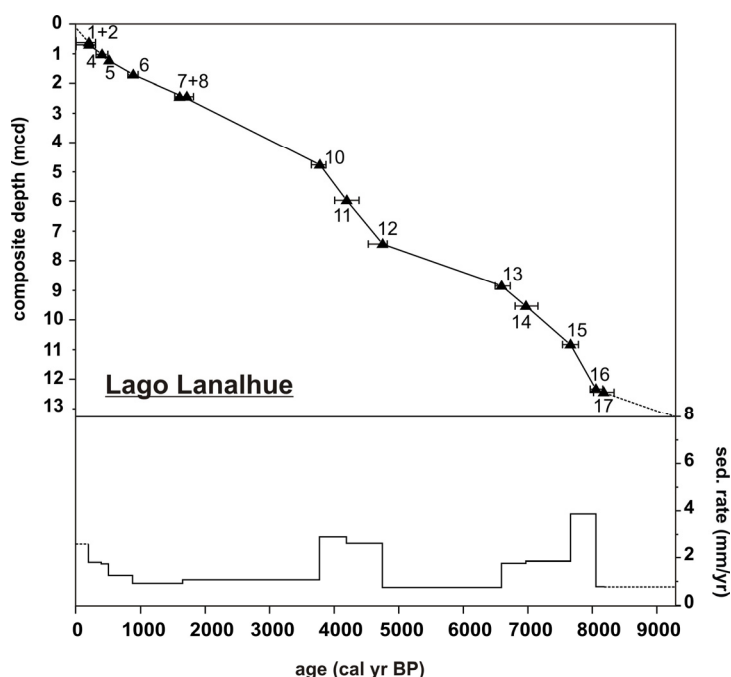
Figure 4.4a: Age-depth relationship and calculated sedimentation rates of the Lanalhue master core (LA-KL013). Numbering of single dating points refers to Table 4.2a. Grey dots are indicating non-fitting ages which were neglected for the age model. For the calculation of sedimentation rates, the mean of ages 1+2 and 7+8 was taken to avoid unnatural high sedimentation rates caused by the close sample spacing.

The age model of Lanalhue core LA-KL013 consists of 17 AMS radiocarbon ages which are, except for two outliers, in stratigraphic order (*Figure 4.4a* and *Table 4.2a*). One of the two non-fitting ages was, however, measured on the bulk sediment that may have been contaminated by reworked material; for correctness we neglected the inconsistent ages. According to the age model, the base of the core is assigned to ~9200 cal yr BP; the mean sedimentation rate for the whole sequence is hence 1.4 mm/yr. In three parts, the record is characterized by above-average sedimentation rates; these are the periods between 8050-6600 cal yr BP, 4750-3800 cal yr BP, and 900 cal yr BP to

present. The last 900 years are showing a continuous increase of the sedimentation rate. During the periods 9200-8050 cal yr BP, 6600-4750 cal yr BP, and 3800-900 cal yr BP, the sedimentation rates are contrarily below-average.

The stratigraphy of Lleu Lleu core LL-KL009 is based on 10 radiocarbon dates in stratigraphic order (*Figure 4.4b* and *Table 4.2b*). Linear interpolation between the points resulted in an age of ~11,250 cal yr BP for the base of the sedimentary sequence, which implies an overall mean sedimentation rate of 1.1 mm/yr. From the bottom of the core until ~10400 cal yr BP, the sedimentation rate is slightly below-average. By far higher rates of up to 7 mm/yr are characteristic for the period between 10400-8500 cal yr BP. Between 8500 cal yr BP and present, sedimentation rates are below-average again (*Figure 4.4b*).
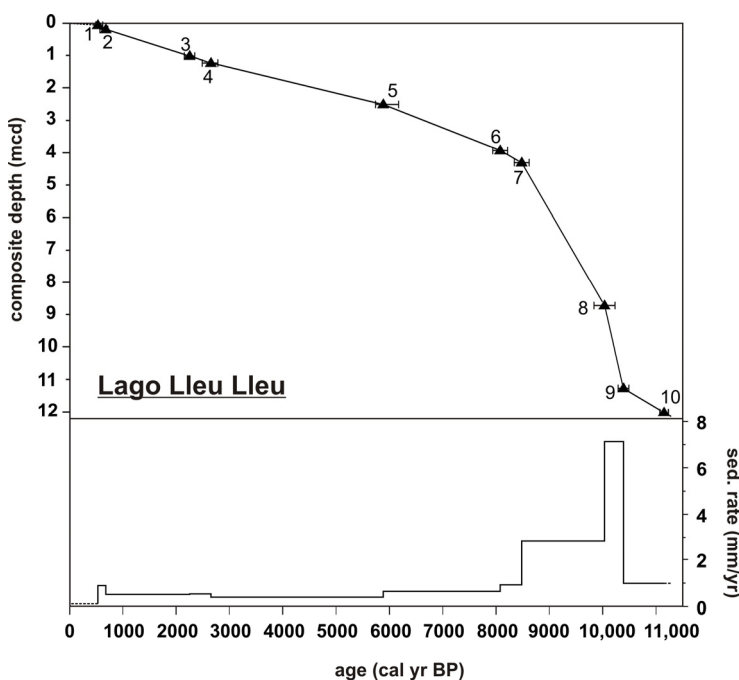
Figure 4.4b: Age-depth relationship and calculated sedimentation rates of the Lleu Lleu master core (LL-KL009). Numbering of single dating points refers to Table 4.2b. Depth is corrected for event layers.

4.4.2   Sediment lithology and composition

The following division of the Lanalhue and Lleu Lleu sequences into different sedimentary facies is based on lithological and stratigraphical qualities. In general, Facies 1 encompasses the lowermost sediments that are Early Holocene in age; Facies 2 represents Mid-Holocene and Facies 3 Late Holocene sediments. In parts, the single facies can be further subdivided; if so, the respective sub-facies are additionally labelled with lower cases.

Lago Lanalhue

The sedimentary sequence of Lago Lanalhue can be divided into five different lithological facies, including Facies 1a+b, Facies 2a+b, and Facies 3 (*Figures 4.3a* and *4.5a*):

69
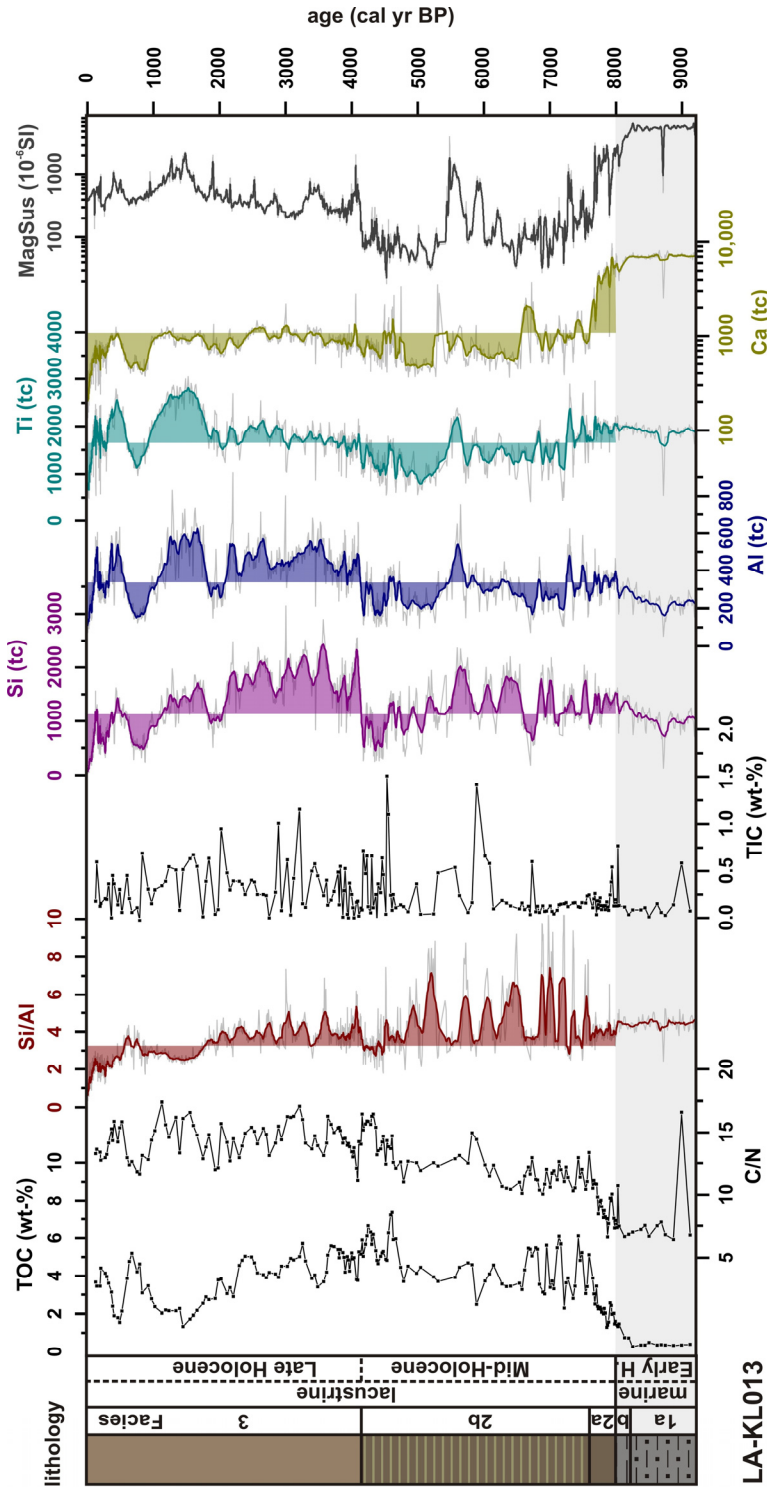
Figure 4.5a: *Overview on paleoenvironmental proxy data (versus age) measured on the Lago Lanalhue master core (LA-KL013). XRF data resolution is 10mm; thick solid lines of the XRF records display 11-point moving averages. The lowermost grey shaded part indicates the period of prevailing marine conditions. Filling of the curves displays above-/below average values only for the lacustrine part of the record. TOC = total organic carbon, TIC = total inorganic carbon.*

I) Sediments of Facies 1a at the base of the sequence (13.25-12.44 mcd, 9200-8200 cal yr BP) are dark-grey in colour and consist of clayey sand with sporadic occurrences of bivalve-shells and foraminifera of the benthic species *Ammonia tepida* (Cushman). Magnetic susceptibility values are very high, partially above 6000*10^{-6}SI. With <1 wt-% and <0.25 wt-%, total organic carbon (TOC) and total inorganic carbon (TIC), respectively, show the smallest amounts of the whole sedimentary sequence. The C/N ratio of the organic matter varies around 7. Sediments of Facies 1a are furthermore characterized by very little variations in the Al, Si, Ti, and Ca contents as well as in the

70

Si/Al ratios; the intensities of Si and Al are slightly below-, the one of Ti slightly above-average in this facies (average is 1123 tc for Si, 334 tc for Al and 1676 tc for Ti). With partly more than 8000 tc, the Ca-intensities are significantly above the whole-core average of 1462 tc. X-ray diffraction revealed that major mineralogical components are quartz, mica and feldspars (in particular: anorthite, $CaAl_2Si_2O_8$).

II) Sediments of Facies 1b (12.44-12.09 mcd, 8200-8000 cal yr BP) consist of dark-grey, homogenous silty clay, and also bear foraminifera of the species *Ammonia tepida*. Magnetic susceptibility values are slightly decreasing to values below $2000*10^{-6}SI$, while the TOC contents start to increase. The records of all other proxies are not significantly different than in Facies 1a.

III) The transition of Facies 1b to Facies 2a (12.09-10.80 mcd, 8000-7650 cal yr BP) is characterized by a sudden change in sediment lithology and composition. Facies 2a consists of very homogenous silty clay of olive-green-greyish colour; calcareous microfossils (bivalve shells as well as foraminifera) are completely absent. Magnetic susceptibility values are around $2000*10^{-6}SI$. In comparison to Facies 1a+b, the mineralogy is characterized by the additional occurrence of pyrite (FeS_2) that was detected by XRD- and SEM-analyses (*Figure 4.6*). Both TOC and TIC contents, as well as the C/N ratio are significantly higher than in Facies 1. The intensities of Si, Al, and Ti are slightly higher and more variable than in Facies 1 (*Figure 4.5a*). The Ca-intensities decrease throughout Facies 2a, while the Si/Al ratios are at a low level and very constant.

IV) Facies 2b (10.80-5.81 mcd; 7650-4150 cal yr BP) is a homogenous clay with regularly appearing diatom-rich layers. Most abundant species are *Aulacoseira granulata* (var. angustissima), *Synedra* (most likely: acus), and *Cyclotella meneghiniana* (*Figure 4.6*). Values of the magnetic susceptibility are below $500*10^{-6}SI$ in this facies. TOC values are much higher than in Facies 1a+b and Facies 2a, generally more than 3 wt-% and up to 7 wt-%. In Facies 2b, the C/N ratios further increase in two steps: from 10 to 13 between 10.80-8.45 mcd (7650-6100 cal yr BP) and up to 15 between 8.45-5.81 mcd (6100-4140 cal yr BP). The TIC contents of this sediment facies also show a twofold pattern: they are around 0.25 wt-% in the lower part of Facies 2b, while they increase conspicuously from 0.1 to 1.5 wt-% at 8.45 mcd (6100 cal yr BP) and become more variable than before. The measured intensities of Si, Al, Ti, and Ca are fluctuating around or slightly below their average values. The Si/Al ratios show a sudden increase compared to Facies 2a and are much more variable throughout entire Facies 2b.

V) The topmost Facies 3 (5.81-0 mcd, 4150 cal yr BP-present) consists of a homogenous diatom-poor silty clay. Compared to Facies 2b, the magnetic susceptibilities are higher ($1000*10^{-6}SI$). Both facies also differ in mineralogy, especially since Facies 3 is pyrite-free. TOC contents are high and range from 3 to 7 wt-%. Merely in the periods between 2260-800 cal yr BP (3.10-1.60 mcd) and 590-300 cal yr BP (1.33-0.87 mcd) the values drop below the whole-core average of 3.7 wt-% TOC. The TIC contents of Facies 3 are highly variable, ranging from 0.1 to 1.5 wt-%. The C/N ratios are above average and reach up to 17; while in the lowermost part of Facies 3 they are positively correlated to changes in the TOC contents, both records are negatively correlated in the uppermost part (2.35-0 mcd, 1850 cal yr BP to present). At

71

the transition from Facies 2b to Facies 3, the Si, Al, and Ti intensities increase significantly. Most conspicuous fluctuations of all three records occur in the upper part of Facies 3, with maxima in the periods between 1850-1050 cal yr BP (100-900 cal yr A.D.) and 600-100 cal yr BP (1350-1850 cal yr A.D.), and minima between 2150-1850 cal yr BP (200 cal yr B.C.-100 cal yr A.D.), (1050-600 cal yr BP (900-1350 cal yr A.D.), and since 100 cal yr BP (1850 cal yr A.D.) until present. The Si/Al ratios are above the average in the lower part of Facies 3, but are, however, lower than those of Facies 2b; since 1850 cal yr BP, values are below average.

Lago Lleu Lleu

The sedimentary sequence of Lago Lleu Lleu can be divided into four different lithological units, including Facies 1, Facies 2, and Facies 3a and b (*Figures 4.3b* and *4.5b*):

(I) The lowermost Facies 1 (12.22-4.01 mcd, 11,250-8150 cal yr BP) is, as in Lago Lanalhue, characterized by the regular but rare occurrence of calcareous microfossils and foraminifera of the benthic species *Ammonia tepida* (Cushman) and composed of very homogeneous silty clay. Magnetic susceptibility values are lower than in the Lanalhue sediments (generally below $700*10^{-6}$SI, in large parts below $200*10^{-6}$SI) and also show a higher variability (*Figure 4.5b*). Mineralogically, the facies is characterized by quartz, mica and feldspars (particularly anorthite). The total organic carbon contents range between 1.5-3.5 wt-% and are hence persistently below the whole-core average of 3.9 wt-%. Except for two outliers, TIC values are below 0.5 wt-% and the C/N ratio is between 10-13. The measured intensities of Al, Si, Ti, and Ca as well as the Si/Al ratio are relatively high: Si intensities vary from 3000 to 4500 tc, Al intensities from 800 to 1300 tc and Ti intensities from 3000 to 4000 tc; Ca intensities reach up to 20,000 tc.

(II) Facies 2 (4.01-2.81 mcd, 8150-6350 cal yr BP) consists of a dark, slightly laminated but homogeneous and silty clay with sporadically occurring diatoms. In contrast to Facies 1, foraminifera are absent. The magnetic susceptibility does not change at the transition from Facies 1 to Facies 2. At the same transition, the TOC amounts increase abruptly and show irregular fluctuations between 2-7 wt-%, while the TIC contents remain below 0.5 wt-%. The C/N ratios increase only slightly. The Si, Al, Ti, and Ca intensities start to decrease from the older to the younger part of this facies; the Si/Al ratios are still high, but fluctuate on a larger scale compared to Facies 1.

(III) Facies 3a (2.81-2.12 mcd, 6350-4800 cal yr BP) shows a significantly higher magnetic susceptibility (up to $600*10^{-6}$SI) compared to Facies 1 and 2. The sediment is composed of homogenous, olive-green-greyish silty clay, which does not show laminations as in the older Facies 2. While the TOC contents are only slightly lower than in Facies 2, the C/N ratios and particularly the TIC contents are significantly higher. XRD results indicate that carbonate is present as manganese-rich siderite $((Fe,Mn)CO_3)$. The records of the considered chemical elements (Si, Al, Ti, Ca) and the Si/Al ratio show pronounced minima in this part of the sequence.
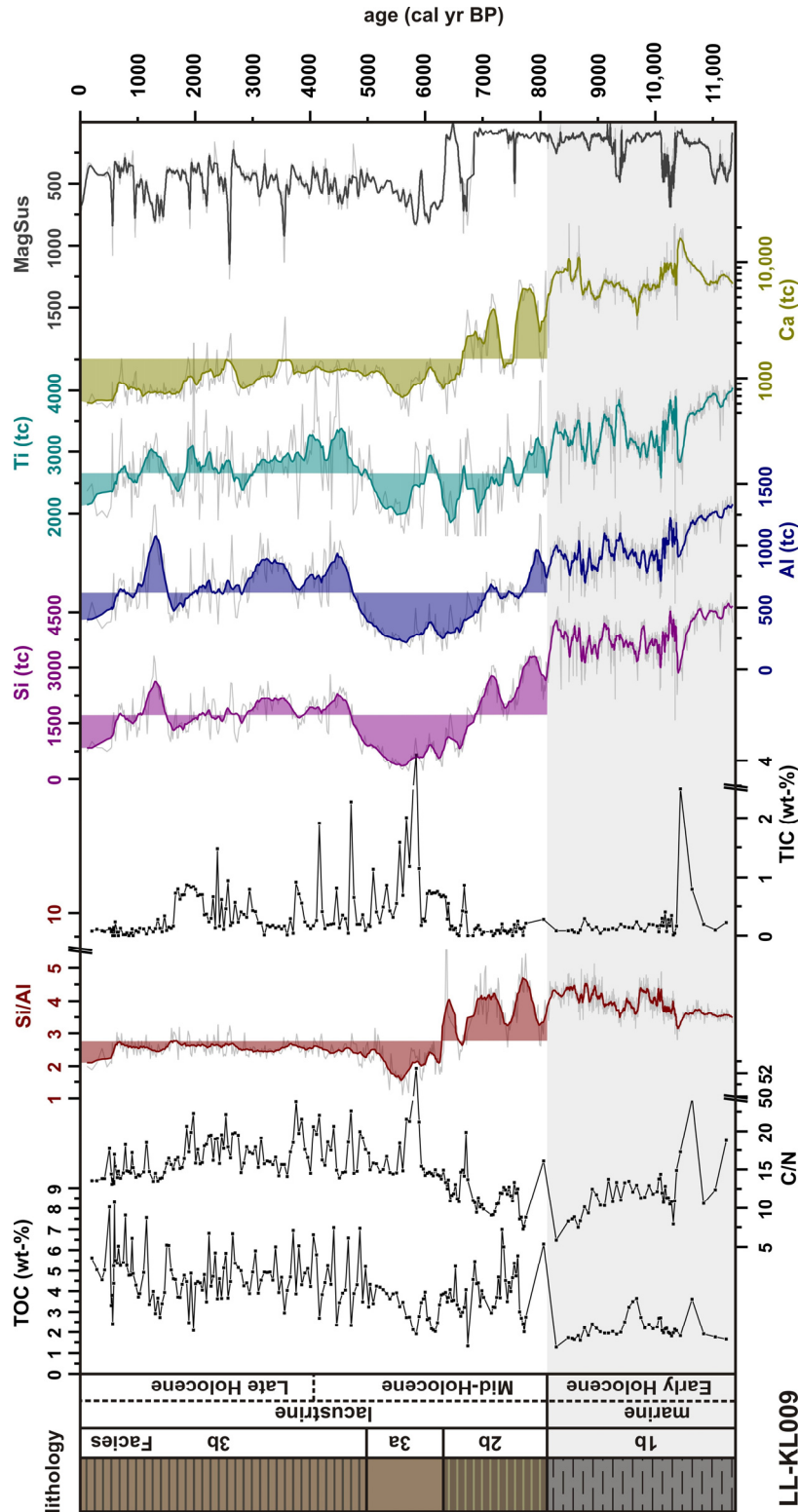
Figure 4.5b: *Overview on paleoenvironmental proxy data (versus age) measured on the Lago Lleu Lleu master core (LL-KL009). XRF data resolution is 10 mm; thick solid lines of the XRF records display 11-point moving averages. The lowermost grey shaded part indicates the period of prevailing marine conditions. Filling of the curves displays above-/below average values only for the lacustrine part of the record. TOC = total organic carbon, TIC = total inorganic carbon. Please note that the scale of magnetic susceptibility is inverted.*

(IV) The topmost Facies 3b (2.12-0 mcd, 4800 cal yr BP-present) is a homogenous olive-green-greyish, silty clay, which includes regular and frequent intercalations of 24 detrital 'event' layers. Each of the layers is mica-rich at the bottom and organic-rich on top. Maximal thickness of the layers is 3.5 cm; minimal thickness is 0.5 cm. Magnetic susceptibilities of Facies 3b are as high as in Facies 3a. XRD results indicate the additional occurrence of chlorite. TOC contents vary between ~ 2 and 8 wt-%; C/N

73

ratios are similar as in Facies 3a (15-22), only in the uppermost part (1600 cal yr BP to present) they are slightly lower (13-18). The TIC contents of the facies are relatively high (up to 1.5 wt-%) until 1600 cal yr BP and decline to values below 0.2 wt-% thereafter. From the older to the younger Facies 3b, the intensities of Al, Si, and Ti increase to values above average; the most distinct increase occurred at ~4800 cal yr BP. Contrarily, the Ca intensities as well as the Si/Al ratios are relatively low. In the Lleu Lleu record, sediments of this facies do not show such a high variability in the XRF data as in the uppermost part of the Lanalhue sequence. However, one clear maximum in the Si, Al, and Ti intensities occurs from 1500 to 1000 cal yr BP.

4.5   Interpretation and discussion

4.5.1   Considered proxies and indications for Holocene environmental changes

We used the downcore variations in aluminium and titanium intensities as indications for temporal changes in the terrigenous sediment supply to the lakes, since both elements have generally been interpreted to be exclusively associated with allochthonous components (e.g. Haug et al., 2001; Mayr et al., 2007; Moreno et al., 2007). This interpretation is supported by the high positive correlation of both elements across the entire sedimentary sequences. We suppose that erosion in the lake catchments is mainly controlled by local rainfall intensity and hence interpret the variations in detrital input to reflect temporal changes in local precipitation in the catchment.

In the upper parts (8000-0 cal yr BP) of the records, the Al- and Ti-intensities also show a high positive correlation with the detected Ca-intensities. Calcium can be, however, transported to the lake as allochthonous calcium carbonate ($CaCO_3$), incorporated in Ca-feldspars (anorthite, $CaAl_2Si_2O_8$), or precipitated as authigenic $CaCO_3$, and may hence reflect either the terrigenous input to the lake and/or the lake productivity. Since limestone is lacking in the catchments of Lanalhue and Lleu Lleu (*Figure 4.3*) and due to the positive correlation with Al and Ti, it seems reasonable to assume that most Ca in the upper part of the records is enclosed in feldspars and hence also reflecting the detrital input. In the lower parts of both sequences (>8000 cal yr BP), the correlation of Ca to Al and Ti is only weak, suggesting that Ca is mostly concentrated in calcium-carbonate shells of foraminifera.

Silicon may be of both detrital and biogenic origin. We hence consider Si normalized by Al (Si/Al) to be a proxy for biogenic silica in the sediments. The good correlation between the Si/Al-record and the occurrence of diatom-rich layers in Lago Lanalhue (*Figure 4.6*) indicates that the biogenic silica content reflects the abundance of diatoms. Its appearance can be interpreted in terms of paleoproductivity, provided that the dissolution of the siliceous skeletal relics during settling and on the lake floor is proportional to the primary biogenic production (e.g., Bertrand et al., 2008). Changes in the lake productivity can be either related to climatic variations or to higher nutrient availability (Meyers and Teranes, 2001).
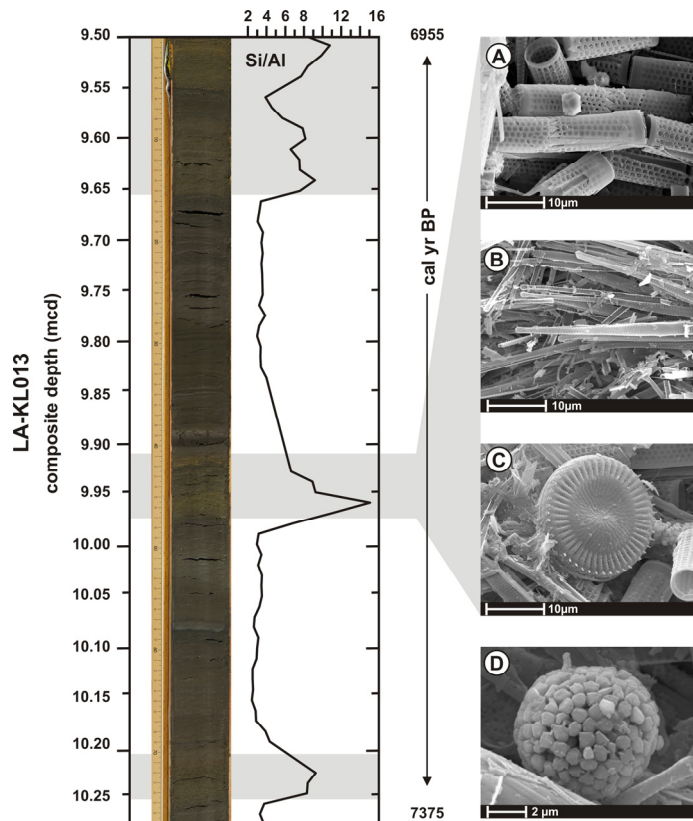
Figure 4.6: *Left: Comparison of the Si/Al ratio of the sediments and the occurrence of diatom-rich layers (highlighted in grey) in sediment core LA-KL013. Right: SEM-images of the most abundant diatoms and present framboidal pyrite.*

A*: Aulacoseira granulata*
B: *Synedra (acus?)*
C*: Cyclotella meneghiniana*
D*: framboidal pyrite.*

As a bulk value, the total organic carbon (TOC) content of the lake sediments reflects both allochthonous and autochthonous organic components that escaped remineralization during the sedimentation (Meyers, 2003). More detailed information about the bulk organic matter sources may be obtained by its C/N-ratio, which is typically ranging between 4 and 10 for algae and higher than 20 for vascular land plants (Meyers, 1994). Ratios between 13-20, as found in the Lanalhue and Lleu Lleu sediments, hence suggest a mixture of algal and vascular plant fractions (Meyers and Teranes, 2001). An increase in the C/N ratio might thus give indication for an increase in the fraction of allochthonous organic matter.

The total inorganic carbon (TIC) content reflects the carbonate components of the lake sediments. High amounts of TIC in the Mid- to Late Holocene sediments of Lago Lleu Lleu reflect the occurrence of manganese-rich siderite, as it is shown by the XRD analyses. Siderite is a common authigenic iron mineral, typically found in fine-grained sediments with a significant amount of organic matter (Postma, 1982). Its formation is generally associated with the bacterial respiration of organic matter in conjunction with an $Fe(III)$ reduction and hence indicative for a reducing environment (e.g. Pye et al., 1990).

Based on the temporal variations in the sediment composition, we classified three disparate periods/trends found in both the Lanalhue and the Lleu Lleu sequence: I) the Early Holocene period (base of the records until ~8000 cal yr BP), during which both lakes were connected to the Pacific Ocean and marine conditions prevailed, II) the Mid-Holocene period (~8000-~4200/4800 cal yr BP), which was marked by an increased aridity and a higher lake productivity, and III) the Late Holocene period (~4200/4800

cal yr BP until present), which is characterized by a higher precipitation and more variable climate conditions, most pronounced during the last 2000 years.

Early Holocene marine conditions

During the oldest period (lasting from 9200 to 8000 cal yr BP in Lago Lanalhue and from 11,250 to 8150 cal yr BP in Lago Lleu Lleu, respectively), sediments are of marine character due to the occurrence of the benthic foraminifera *Ammonia tepida*. This species is a typical indicator for a marginal marine, saline to brackish environment (e.g. Murray, 1991). Its abundance might also explain the high above-average XRF-Ca-intensities in the lower part of the records. However, for explaining the coevally low TIC values (*Figures 4.5a+b*), an alternative interpretation is required. It may be given by the occurrence of Ca-rich feldspars (anorthite) in the lowermost sediments, which are typical constituents of mafic igneous rocks and most likely originated from basaltic Andean volcanoes. The former connection with the Pacific favoured the sedimentation of material brought through the ocean; these marine sediments can be expected to contain a collective source rock signal of the continental hinterland, composed of low-grade metamorphic rocks from the Coastal Ranges and plutonic basement rocks as well as basaltic to andesitic volcanics from the low and high Andes (Zeil, 1986; Thornburg and Kulm, 1987). Low concentrations of organic matter in the marine sediments may be explained by larger grain sizes (in Facies 1 of Lago Lanalhue) and/or higher sedimentation rates in those parts of the records. Lower values of the C/N ratio, compared to the remaining sections, indicate that a higher proportion of the organic matter is derived from algal production. The end of the marine/beginning of lacustrine conditions is dated to 8000/8150 cal yr BP (*Figures 4.5a+b*).

In a parallel study, we used the transition from marine brackish sediments to lacustrine deposits to derive information about local forearc uplift rates and to reconstruct the lakes history (Stefer et al., submitted). Unlike most of the Chilean lakes, Lago Lanalhue and Lago Lleu Lleu have not been formed by glacial activity but by local tectonic deformation. The detailed way of development was for long time a matter of debate and former assumptions were reaching from the tectonic downwarping of the lake basins (Börgel, 1953) to the impounding of coastal rivers behind eastward moving dune belts (Endlicher and Mäkel, 1985). In a geomorphologically based study, Mardones and Reuther (1999) more recently pointed out that Lago Lanalhue and Lago Lleu Lleu developed in the estuary systems of pre-existing river valleys, which are nowadays separated from the ocean by uplifted barriers forming natural dams. However, this study does not provide information about the exact timing of the lakes formation. The investigation of the lake sediments allowed for the first time to reconstruct the history of the formation of Lago Lanalhue and Lago Lleu Lleu.

Long-term trend of the Mid- to Late Holocene

The Mid-Holocene period (8000– 4200 cal yr in Lanalhue and 8150-4800 cal yr BP in Lleu Lleu, respectively) is marked by slightly below-average or decreasing values of the detrital sediment input proxy data (*Figures 4.5a+b*). We hence consider this period as more arid with reduced precipitation, erosion, and ultimately terrigenous sediment

supply to the lakes. Particularly in the Lleu Lleu record, a long-term decrease in the detrital proxy records points to increasing aridity during the Mid-Holocene, culminating at around 5500 cal yr BP. Compared to the marine sediments at the base of both cores, higher amounts of organic matter and an enhanced C/N ratio are reflecting a higher fraction of vascular plant material from the lake catchments. The positive correlation between variations in the TOC contents and the C/N ratios suggest a predominant detrital input of organic matter.

At the beginning of the Mid-Holocene, the Si/Al ratios of the sediments are above-average and highly variable in both lakes. This pattern likely indicates recurrent periods of either enhanced lake productivity or diatom preservation, and may hence reflect a signal of changes in (fluvial) nutrient input or lake mixing. Although our data do not allow drawing conclusions about the ultimate reason for the Si/Al-variations, the periodic multicentennial-scale fluctuations in a range of ~300-500 years are striking, most notably in the Lanalhue record (*Figure 4.5a*). Holocene climate fluctuations on similar timescales are found, for instance, in the tree-ring based residual $\Delta^{14}C$ record of Stuiver et al. (1998); regarding this record as proxy for solar variability, we can only speculate about changes in the energy output of the Sun as supposable forcing mechanism for the detected Mid-Holocene oscillations in the lake records.

During the Late Holocene (4200/4800 cal yr BP – present), the terrigenous sediment supply to both lakes increased, as indicated by generally higher values of the respective proxies. The variability in the Si/Al ratios was less pronounced. We hence interpret the records to reflect basically enhanced precipitation and lower lake productivity compared to the Mid-Holocene.

Late Holocene variability

A peculiarity is observed in the Late Holocene sediments of Lago Lleu Lleu: they are featuring frequent 'event' layers composed of mica at the bottom and organic matter on top, which are periodically occurring during the last ~5000 years. The layers do not leave a clear signal in the magnetic susceptibility, and the resolution of the XRF, TOC and C/N records is too low for the explicit detection of single layers; this is why we detected the events only visually. Nevertheless, we corrected all measured records for the identified layers and that way considered only the undisturbed background sediments for the paleoenvironmental interpretation.

The layers are most likely representing debris flows, which preferentially originated at the exceptionally steep headwalls that are surrounding the lake basin and covered by deeply weathered material. Interestingly, none of such depositional layers are found in the record of Lago Lanalhue, most likely due to the much lower slopes of the surrounding hillsides (*Figure 4.1*). We suggest that the initiation of the debris-flows may have two causes: extreme precipitation events, which are eroding and transporting the weathered bedrock to the lake, and/or regularly occurring earthquakes that are inducing a slipping of the deeply weathered and loose material down the slopes into the lake. We identified altogether 24 mica layers and hence deduced a mean recurrence time of ~210 years. This rate is on the one hand similar to long-term recurrence times of earthquake triggered turbidites that were identified in the marine sediments at ODP Site 1232 (offshore Chile at ~40°S; Blumberg et al., 2008); it may hence support a tectonically oriented interpretation. On the other hand, the onset of the layer deposition

started synchronously with largest increases in intensity and frequency of the El Niño Southern Oscillation (ENSO; e.g. Moy et al., 2002) (*Figure 4.7*). Increased moisture loading during El Niño phases possibly increased the risk of flooding in the lake catchment. Although the depositional layers do by far not resemble the number of ENSO events during the last 5000 years (*Figure 4.7*), they might well reflect the strongest ones and hence be an indication for the increased ENSO variability during the last millennia. The resolution of our age model does not allow the exact dating of individual depositional layers; nevertheless their mean recurrence time matches a ~200-yr periodicity of flood occurrence found in a variety of archives in Meso- and South America (e.g. Schimmelmann et al., 2003). This periodicity is in accordance with the ~208-yr cycle of solar activity (Suess-cycle) and might hence also reflect general changes in the atmospheric circulation.
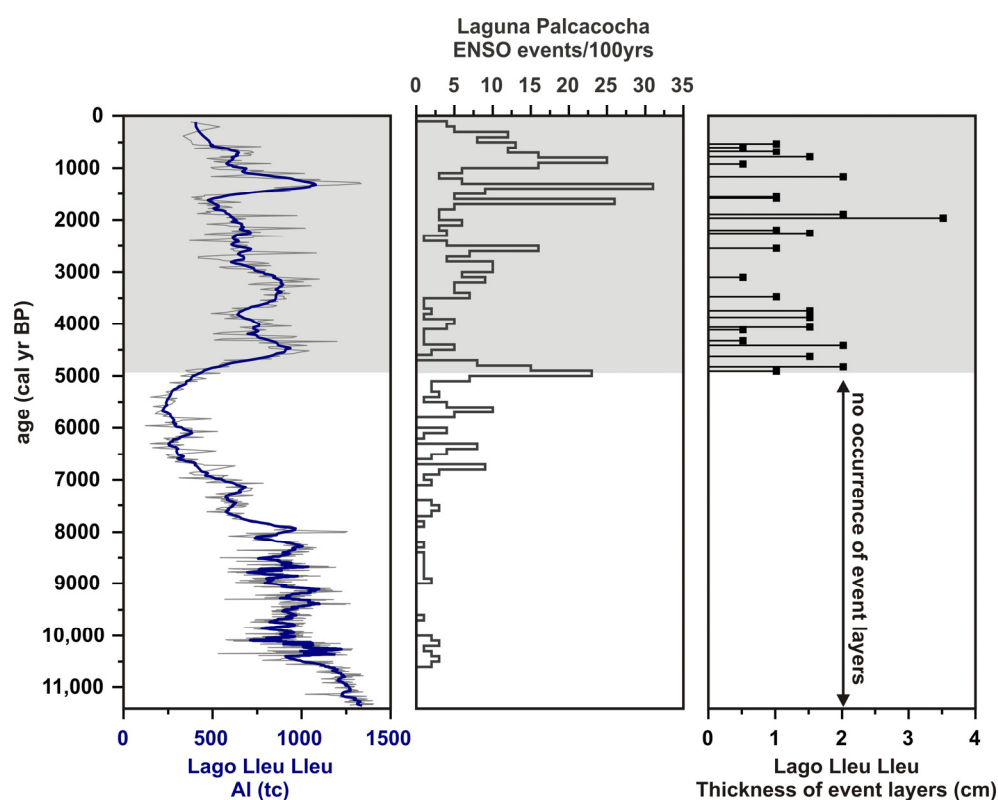
Figure 4.7: *Comparison of the aluminium intensities measured on the Lleu Lleu sediments, reflecting detrital input (left), the number of ENSO events per 100 years observed in sediments of Laguna Pallcacocha, Southern Ecuador (Moy et al., 2002) (middle), and the temporal occurrence and thickness of event layers found in the Lleu Lleu sediments (right). Thick solid line of the Al-record displays the 11-point moving average. Highlighted in grey are the last 5000 years during which ENSO events are more frequent and event layers became apparent.*

During the last 2000 years, the amplitude of variations increased for all measured proxies and a shorter-term variability becomes more apparent particularly in the sediments of Lago Lanalhue (*Figure 4.5a*). In Lago Lleu Lleu, however, the variations are less visible although we corrected the records for the occurring event layers (*Figure 4.5b*). We identified five different intervals, which we interpret to represent alternating phases of more humid and more arid climatic conditions. The periods between 2150-1800 cal yr BP (200 cal yr B.C.-150 cal yr A.D.), 1050-600 cal yr BP (900-1350 cal yr A.D.), and the time since 100 cal yr BP (1850 cal yr A.D.) are characterized by low

values of the terrigenous input indicators and high values of the productivity indicators; we hence conclude that more arid conditions prevailed. These arid phases approximately correspond to the Roman, Medieval, and Modern Warm Periods, primarily known from the North Atlantic Realm (e.g. Bianchi and McCave, 1999; McDermott et al., 2001). By contrast, during the periods between 1800-1050 cal yr BP (150-900 cal yr A.D.) and 600-100 cal yr BP (1350-1850 cal yr A.D.), proxies for the terrigenous supply are high, while those for the lake productivity are low, which suggests enhanced precipitation during these phases. Temporarily, these humid times are approximately coinciding with the Dark Ages and the Little Ice Age. Interestingly, the Little Ice Age can be split in a more humid phase at the beginning (1350-1600 cal yr A.D.) and a less humid phase thereafter (1600-1850 cal yr A.D.).

Comparison of both records

The direct comparison of the Lago Lanalhue and Lago Lleu Lleu records reveals differences in the sedimentary facies and the timing of the determined transitions. As we denoted in the discussion of the event layers in the Late Holocene Lleu Lleu sediments, we suggest differences in the nature of the lake catchments as a supposable explanation for the diverse sedimentary facies. Dissimilar characteristics of the lake systems themselves (*Table 4.1*) likely influence internal sedimentation processes in addition. Differences in the timing of the individual transitions in the two records are in all probability due to the (in-)accuracy of the established age models. 'Real' temporal differences of more than 500 years seem implausible due to the close distance between the lakes. Age control of the Mid- to Late Holocene transition in the Lanalhue record is based on three close-by dating points and, therefore, strong (*Figure 4.8*). Contrarily, age control for the transition is weak in the Lleu Lleu record, since no dating was feasible for the period between 5883 - 2656 cal yr BP. The juxtaposition of the Lanalhue and Lleu Lleu Al-curves, however, suggests that the long-term trend is strongly consistent in both sequences (*Figure 4.8*). Thus it is likely that the transition out of the Mid-Holocene took place synchronous in both lakes, in fact at the time that is detected for the Lanalhue record (4200 cal yr BP). Similar applies to the Late Holocene differences in both records: Timing during the last 2000 years is controlled by six datings in the Lanalhue record, whereas only two ages could be determined for the Lleu Lleu sediments (*Figure 4.9*). On the short term, discrepancies become even more apparent due to the disparity in sedimentation rates. General trends are nevertheless congruent in both records (e.g. in the magnetic susceptibility, *Figure 4.9*), suggesting generally synchronous changes in Lago Lanalhue and Lago Lleu Lleu.

4.5.2 *Regional context and forcings*

The analyses of temporal variations in the lacustrine sediment composition of Lago Lanalhue and Lago Lleu Lleu led to the conclusion of two superposed climatic trends: (1) a multi-millennial long term trend, differentiating between more arid climate conditions during the Mid- and more humid conditions during the Late Holocene, and (2) centennial scale variations that are most pronounced during the last 2000 years. This

pattern is overall consistent with the findings of several other studies in south-central Chile (*Figure 4.1*).

Multi-millennial long-term trend of the Mid- and Late Holocene

Less humid conditions during the Mid-Holocene are observed in the majority of continental and marine archives to the north and south of Lago Lanalhue and Lago Lleu Lleu (*Figure 4.1*). North of the study area, an increased aridity between ~8700-5700 cal yr BP and a subsequent increase in moisture since ~4200 cal yr BP is, for instance, detected in a record of pollen influx and assemblages from the Palo Colorado swamp forest (32°S, Maldonado and Villagrán, 2006). These findings are supported by geomorphic and pedologic investigations in the Norte Chico (27-33°S) that also revealed reduced precipitation from 7300 to 5000 cal yr BP (Veit, 1996). A multi-proxy analysis of lake sediments from Laguna Aculeo (34°S) shows a seasonal drying of the lake basin and hence drier conditions prior to 5700 cal yr BP; according to the authors, climatic conditions became more and more humid thereafter (Jenny et al., 2002b; Villa-Martínez et al., 2003). The same trend, with more arid and stable conditions during the Mid-Holocene compared to more humid and variable conditions during the Late Holocene, is also found in marine sediments from the continental slope at 33°S (Lamy et al., 1999). South of the study area, a sedimentological study from Lago Puyehue (40°S) points to reduced precipitation during the mid-Holocene with a culmination of the arid conditions at ~5000 cal yr BP (Sterken et al., 2008), which is in analogy to our observation for the Lleu Lleu record. At 41°S latitude, Lamy et al. (2001) suggested more arid conditions between 7700-4000 cal yr BP and a higher humidity thereafter, based on geochemical measurements and clay mineral data of marine sediments (core GeoB3313-1). The authors interpreted the iron concentration of the sediments to reflect rainfall changes in the catchment area. The record shows a large consistency with variations of the Al intensities found in the Lanalhue sediments (*Figure 4.8*), which confirms our approach of interpreting the Al changes in terms of varying rainfall intensities. Further to the south, the changeover from more arid to more humid conditions seems to occur earlier: palynological data from Laguna Tahui and Lago Melli on the Isla Grande de Chiloé (43°S) suggest that the rise in precipitation started at 7000 cal yr BP (Abarzúa et al., 2004), and a pollen study from Lago Pollux (46°S) revealed that precipitation became similar to the present at ~7500 cal yr BP (Markgraf et al., 2007).

The apparent symmetry between the listed records suggests a common driving mechanism behind the long-term trend of the Mid- and Late Holocene that also applies for the observed variations in the Lanalhue and Lleu Lleu records. Since rainfall in the Chilean mid-latitudes is almost exclusively originating from the Southern Westerlies, it is a general consensus that the transition from more arid to more humid conditions is attributed to changes in the position and/or strength of this wind belt (e.g. Lamy et al., 2001). More arid conditions during the Mid-Holocene are caused by a farther poleward position of the Westerlies, whereas more humid conditions during the Late Holocene indicate a general northward shift.
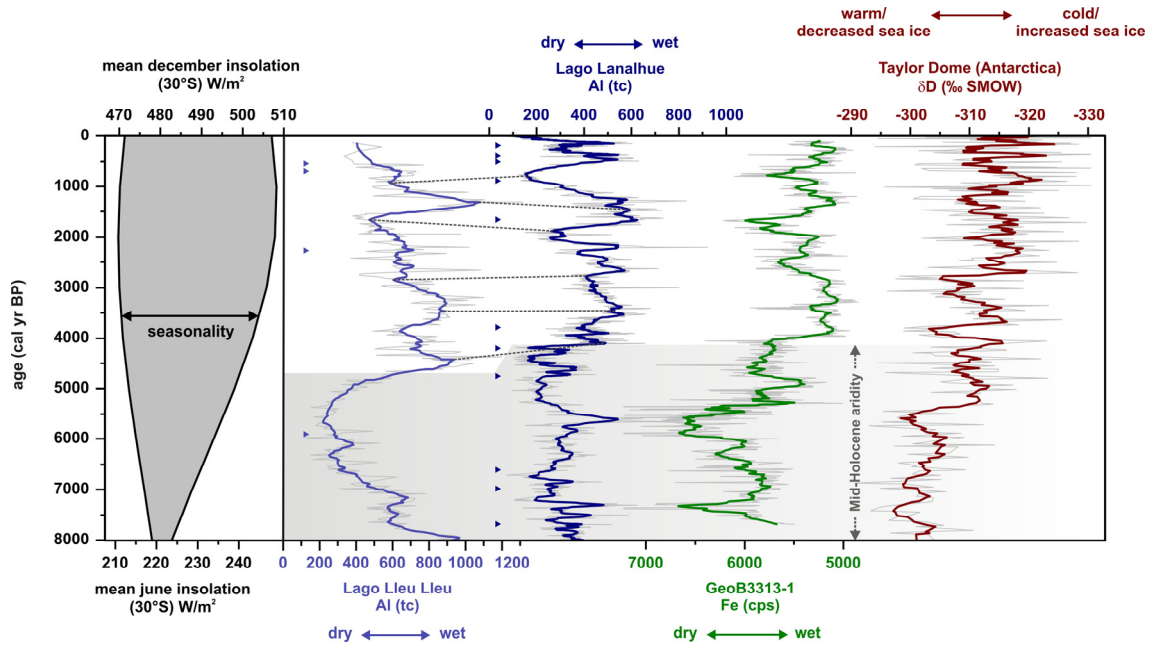
Figure 4.8: *Mid- to Late Holocene long-term trend as detected in the Al-records of the Lanalhue and Lleu Lleu sediments, the Fe-record of core GeoB3313-1 (Lamy et al., 2001), and in the isotopic composition (δD) of the Taylor Dome ice core (Antarctica) (Steig et al., 1998), compared to insolation changes at 30°S (Berger and Loutre, 1991). Thick solid lines represent the 11-point moving averages of the Lanalhue and Lleu Lleu Al-records, the 11-point moving average of the GeoB3313-1 Fe-record, and the 5-point moving average of the Taylor Dome δD-record. Filled triangles indicate dating points of the Lanalhue and Lleu Lleu sequences; dashed lines suggest correlation points between both records.*

The latitudinal position of the Southern Westerly Winds (SWW) is controlled by both, changes in the tropics and changes in the high latitudes as it primarily depends on the intensity and/or position of the Southeast Pacific anticyclone in the north and the circum-antarctic low pressure belt in the south (e.g. Aceituno et al., 1993; Markgraf, 1998). On the one hand, a southward migration of the SWW during the Mid-Holocene might thus be the result of an intensification and/or strengthening of the subtropical anticyclone. Since at present this atmospheric situation (blocking of the SWW by a strong Southeast Pacific anticyclone) is typically observed during La Niña phases (Markgraf et al., 1992), those are interpreted to be dominating the climate during the Mid-Holocene (e.g. Clement et al., 2000; Moy et al., 2002; Kaiser et al., 2008). Accordingly, the establishment of modern ENSO conditions at ~5000 cal yr (*Figure 4.7*) possibly enforced the shift to more humid conditions at the Mid- to Late Holocene transition. On the other hand, latitudinal changes of the SWW might be controlled by similar latitudinal shifts of the Antarctic Circumpolar Current (ACC) and associated sea ice expansions around Antarctica (e.g. Mayr et al., 2007). An increase in the sea ice extent during the Late Holocene, like it is interpreted from the isotopic changes of the Taylor Dome ice-core (Steig et al., 1998), most likely reflects a northward shift of the circumpolar current system. This observed trend is consistent with our data, suggesting higher precipitation due to northward displaced SWW during the Late Holocene (*Figure 4.8*).

Fundamental forcing for long-term changes in the latitudinal position of the Southern Westerlies also comes from insolation characteristics during the Mid- and Late Holocene (Markgraf et al., 1992; Markgraf, 1998). Due to changes in the precessional

cycle, the seasonality contrast on the Southern Hemisphere increased since the Early Holocene (Berger and Loutre, 1991). At around 11,000 cal yr BP, the earth-sun distance was minimal in June and maximal in December, leading to colder summers, milder winters, and hence lower seasonality than today (Martin et al., 1997). This situation reversed during the Late Holocene, resulting in relatively warmer austral summers, cooler winters, and a more pronounced seasonality. As a result, the Southern Westerlies started to move latitudinally during the Mid- and Late Holocene (Markgraf et al., 1992).

Centennial-scale short-term variations during the Late Holocene

Within the generally more humid conditions of the Late Holocene, we observed an increase in the amplitude of variations in nearly all measured parameters, most notably during the last 2000 years. We suggest higher climate variability markedly during the Late Holocene and more humid periods alternating with less humid periods for several cycles. Similar climatic variations are also discovered at other sites of the region.

Evidences for less humid/more arid conditions between 200 cal yr B.C.-200 cal yr A.D. are found by Jenny et al. (2002a) in a sedimentological, geochemical and diatom-based study on sediments from Laguna Aculeo (34°S). Relatively higher lake levels and an enhanced frequency of flood events in the period between 200-950 cal yr A.D., are pointing to subsequently enhanced precipitation (Jenny et al., 2002a). More arid conditions during the Roman Warm Period as well as more humid conditions during the Dark Ages Cold Period are also recorded in the iron-record of the marine sediment core GeoB3313-1 (Lamy et al., 2001), though they are not discussed in more detail by the authors. Additional surveys of both periods are so far lacking in the direct vicinity of Lago Lanalhue and Lago Lleu Lleu. The Laguna Pallcacocha study of Moy et al. (2002) from southern Ecuador, however, indicates that the frequency of ENSO events was low at ~2000 cal yr BP, near the peak warmth of the Roman Warm period. By contrast, the number of events increased one order of magnitude during the Dark Ages Cold Periods, possibly inducing wetter conditions (as presently observed during El Nino events) in the catchments of Lago Lanalhue and Lago Lleu Lleu.

The Medieval Warm Period (MWP) and Little Ice Age (LIA) are very prominent climatic phases of the Late Holocene, originally known for the Northern Hemisphere (e.g. Grove, 1988). In south-central Chile, records of the MWP and LIA are present although still relatively rare (Villalba, 1994; Arenada et al., 2007). To the north of Lago Lanalhue and Lago Lleu Lleu, Jenny et al. (2002b) found evidence for both events in the sedimentological record of flood events from Laguna Aculeo; they referred a period of less flooding to the MWP, followed by a period of increased moisture and frequent flooding between 1300-1700 cal yr A.D., which they ascribed to the LIA (Jenny et al., 2002a). Within this wet interval, the greatest frequency of flood events was recorded between 1400-1600 cal yr A.D., well corresponding to the more humid part of the LIA in the Lanalhue sediments. Based on pedological investigations, Veit et al. (1996) observed enhanced humidity during the LIA in the Norte Chico (27-33°S). They dated the period to persist between 1300-1800 cal yr A.D., which coincides with both our observations and the findings of Jenny et al. (2002a).

South of Lanalhue and Lleu Lleu, the Fe-record of sediment core GeoB3313-1 (41°S) gives evidence for less humid conditions during the MWP and enhanced humidity

during the LIA, corresponding to poleward and equatorward shifts of the Southern Westerly Winds, respectively (Lamy et al. 2001). Bertrand et al. (2005) found indication for a wet period between 1490-1700 cal yr A.D. in the sediments of Lago Puyehue (40°S), which they related to the LIA. Further south, in Northern Patagonia, tree ring records indicate that temperatures during the MWP (1080-1250 cal yr A.D.) were above-average (Villalba, 1994), while below-average temperatures were found for the LIA period (1490-1700 cal yr A.D.) (Lara and Villalba, 1993). Advances of Patagonian glaciers during the LIA (Grove, 1988; Villalba, 1990; Koch and Kilian, 2005) complement the large-scale climate pattern.

The observed analogy of precipitation changes detected in archives across several latitudes likely demands a common explanation for the underlying driving mechanism also on the centennial-scale. At present, solar variability is the commonly accepted explanation for the short-term climate changes during the Late Holocene, although this forcing is still a topic of debate (e.g. Wanner, et al., 2008). We hence compared our data to a record of sun spots, reconstructed on the base of dendrochronologically dated radiocarbon concentrations (Solanki et al., 2004) as well as to other more distant records from South America and Antarctica, covering the Late Holocene with an adequate resolution (*Figure 4.9*).
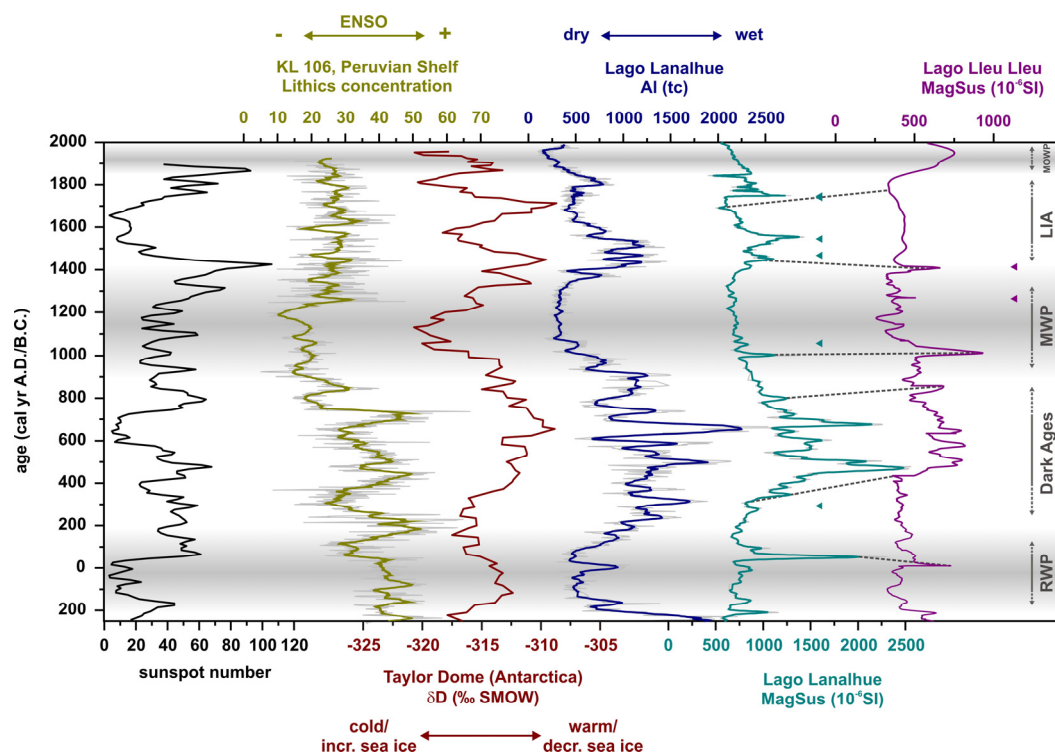
Figure 4.9: Late Holocene Climate variability as inferred from the Lanalhue and Lleu Lleu records. Displayed are from the left to the right: the magnetic susceptibility records of both lakes (9-point moving average of the Lanalhue record), the Al-record of Lago Lanalhue (measured in 2-mm-resolution, thick line = 23-point moving average), the Taylor Dome δD-record from Antarctica (Steig et al., 1998; 9-point moving average), the ENSO record of Rein et al. (2004) from the Peruvian shelf (KL106, 23-point moving average) and a record of sunspot numbers (Solanki et al., 2004). The approximate time spans of the Roman Warm Period (RWP), Medieval Warm Period (MWP), Little Ice Age (LIA) and Modern Warm Period (MOWP) are indicated; more arid periods in the lake surroundings are grey shaded. Small triangles indicate dating points of the Lanalhue and Lleu Lleu records; dashed lines suggest correlation points between both records.

The number of sunspots is clearly reduced during the LIA period as well as slightly enhanced during the MWP, highlighting the importance of solar variability in forcing short-term climate changes during the Late Holocene. It further becomes obvious that a good temporal correlation of Late Holocene climate changes is not only found for the south-central Chilean records close to each other, but also across larger distances. The long-term correlation between our data and climate changes recorded in the Antarctic Taylor Dome ice core appears to be reversed on the short-term: periods that are characterized by more humid conditions due to northward shifted Westerlies now correspond to warmer conditions and decreased sea-ice around Antarctica (*Figure 4.9*). This inversion likely requires disparate climate mechanisms acting on the different time-scales, which might be related to the previously mentioned changes in insolation and seasonality. However, the reversal might also be explained by the increase in ENSO activity during the Late Holocene, inducing a shift from a 'La Niña' to an 'El Niño' dominated system. According to Yuan and Martinson (2000, 2001) present-day warm ENSO-events account for positive (warm) temperature and negative (decreased) sea ice anomalies in the Pacific Ocean sector of Antarctica. This coherence would explain the synchronicity between cold/warm conditions at Taylor Dome and dry/wet conditions recorded in Lago Lanalhue during La Niña/El Niño dominated phases, as it is well observable during the Dark Ages and the MWP *(Figure 4.9)*. During the LIA, however, the interrelation is less clear and even inverse at its end, with warm conditions and decreased sea ice in the Antarctic corresponding to drier conditions in the Lanalhue region and vice versa. In analogy, studies of ENSO activity from the south-American low latitudes (e.g. Rein et al., 2004) suggest a minimum occurrence of ENSO during the MWP and a slight increase thereafter, but do not detect that remarkable changes in frequency/intensity within the LIA (*Figure 4.9*). It is hence quite conceivable that an external forcing becomes imposed on the tropical ENSO signal during the LIA again.

6.   *Conclusions*

The combined approach using XRF- and XRD-scanning, bulk chemistry, and SEM-imaging of radiocarbon dated sediment cores from Lago Lanalhue and Lago Lleu Lleu yields a comprehensive picture of the lakes development and local climate changes during the Holocene. We demonstrate that the lakes were formed in the Early Holocene when localized tectonic uplift constricted two ancient rivers from the Pacific Ocean. Ever since, changes in the detrital sediment input to the lakes record multi-millennial to centennial-scale precipitation changes. Our results indicate a long-term trend with less humid conditions during the Mid- and more humid conditions during the Late Holocene, which is ascribed to an equatorward shift of the Southern Westerly Winds, and which is in accordance with adjacent paleoclimate archives.

Short-term climate changes that became pronounced in the Late Holocene are recorded differently in Lago Lanalhue and Lago Lleu Lleu. The sediments of Lago Lanalhue show increased variations in the precipitation-related proxies particularly during the last 2000 years, suggesting the occurrence of a less humid Medieval Warm Period (900-1350 cal yr A.D.) and a more humid Little Ice Age (1350-1800 cal yr A.D.). By contrast, these prominent climate events are barely visible in the sediments of Lago

Lleu Lleu, since a frequent occurrence of detrital 'event layers' during the last ~5000 years interrupts the continuous lake sedimentation.

Despite the obvious differences in the sediment records of Lago Lanalhue and Lago Lleu Lleu, an overall consistent pattern of climate changes can be recognised in both nearby lakes. Precipitation changes in the catchment areas are generally related to the onset the modern ENSO and to variations in its frequency and activity. However, individual coring site positions and the specific morphology of both watersheds are likely to explain why climate impact on the sedimentation process was partly different in both lakes.

Finally, the analogy between our data-sets and other records of Holocene climate change in South America and Antarctica further supports the assumption that prominent climate events like the Medieval Warm Period and the Little Ice Age occurred on a global rather than a local scale and have not been restricted to the Northern Hemisphere.

5. CONCLUDING DISCUSSION

Each of the marine and lacustrine sediment records that were investigated within my study yielded distinct results concerning the covered time scale and the detected tectonic and climatic signals. An overview of the implemented analyses and the main outcomes for the respective archives is given in *Figure 5.1*.

Marine sediments *(ODP Site 1232 and SONNE core 50SL)*		*Lacustrine sediments* *(LA-KL013 and LL-KL009)*
Radiocarbon dating Oxygen isotope measurements Magnetic susceptibility measurements Greyscale and colour analysis	*Applied methods*	Radiocarbon dating Magnetic susceptibility measurements X-ray fluorescence (XRF) scanning X-ray diffraction Carbon content detection Scanning electron microscope (SEM) imaging
Last 140,000 years (Late Pleistocene, 10^5-10^4 yr)	*Time scale*	Last 10,000 years (Holocene, 10^3-10^2 yr)
Record of paleoseismicity	*Tectonic indication*	Forearc uplift rates
Glacial-interglacial differences of earthquake frequencies	*Climatic indication*	Short- and long-term climate changes during the Holocene

Figure 5.1: *Comparison of the used methods and main outcomes, opposing marine to lacustrine sediment records*

In order to combine my main results to an overall picture of the sedimentation processes at the active margin of south-central Chile, I modified and approved the schematic diagram of interactions between climate, tectonics and erosion that was shown in *Figure 1.1*. The updated model (*Figure 5.2*) indicates that:

·   The process of sedimentation (which broadly means the sediment supply and transport from the Andean Orogen to the deep Pacific Ocean) is directly and indirectly influenced by local climate and tectonics.

·   Regional climate affects the strength of erosion (and accordingly the amount of sediment that is transported towards the Pacific) mainly via the rate of precipitation. Temporal variations in precipitation are primarily driven by changes in the position/strength of the Southern Westerly Winds.

·   Long-term variations of the global climate on glacial/interglacial time scales additionally influence the process of sedimentation through changes of the global sea level. The latter are affecting the stability of the continental slope and that way bias the final sediment delivery to the abyssal zone.

·   Slope stability is furthermore depending on the occurrence of tectonic earthquakes, which thus also have an impact on the quantity of sediments transported to the deep ocean.

· Tectonic deformation has a twofold effect on the process of sedimentation: spaciously increased topography enhances the rate of erosion and thus the sediment transport in general. Concentrated deformation, however, creates local depressions, in which sediments are at least intermittently retained on their way from the orogen towards the abyssal zone.
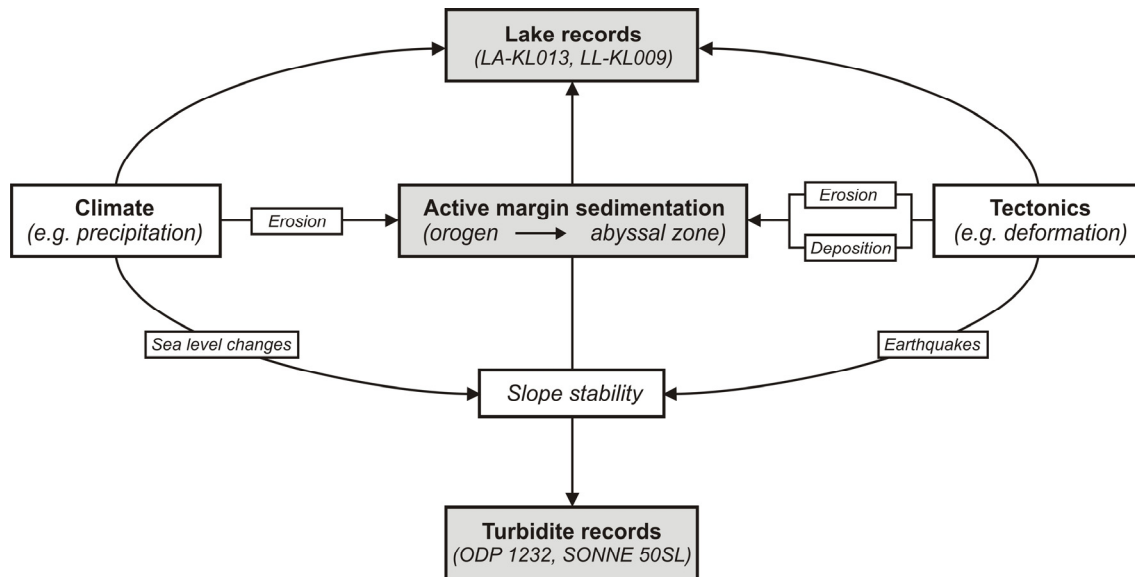
Figure 5.2: *Synoptical picture of sedimentation and its influencing factors at the active margin of south-central Chile. Climatic and tectonic processes as well as the different investigated archives are put into context.*

5.1   Thesis highlights

Reconsidering my research motivation and in relation to the current status of research, most important findings of my work are:

· The given proof for the significance of turbiditic trench deposits as paleoseismic archive. (*Chapter 2*) – On this basis, the analysis of the marine sediments from ODP Site 1232 and SONNE core 50SL allowed, for the first time, investigating the earthquake cycle of south-central Chile on a time-scale longer than the Holocene. While previous paleoseismic investigations of the region covered merely the last millennia (Cisternas et al., 2005; Bookhagen et al., 2006), the turbidite records enabled me to reconstruct the frequency of mega-earthquakes back into the Late Pleistocene. Understanding the processes that regulate the seismic cycle at convergent margins has been a major challenge during recent years, at the South American as well as at other subduction zones worldwide (e.g. Inouchi et al., 1996; Huh et al., 2004; Goldfinger, et al., 2007). My work is a relevant contribution to the ongoing discussions.

· The discovery of an additional climatic influence on the turbidite frequency, which modifies the long-term record by decreasing the recurrence rates during interglacial periods. (*Chapter 2*) – I could show that merely glacial turbidite frequencies are reliably reflecting earthquake frequencies (at least off south-central Chile). As a

consequence, attention should be paid to the fact that earthquake reconstructions based on turbiditic layer analyses may underestimate the recurrence of seismic events if they focus merely on the Holocene Epoch.

· The acquisition of new information about forearc tectonics and local deformation on the Arauco Peninsula (38°S), in particular about Holocene uplift rates. (*Chapter 3*) – Since uplift rates for the region were so far only known for time scales of 10^5-10^6 years (Melnick et al., 2009; Rehak et al., submitted), these findings constitute a step forward towards a better understanding of the South Chilean forearc evolution on different time scales. With the analyses of sediment records, I used above all an exceptional approach of deriving surface uplift rates; the latter are most commonly analyzed by the dating of emerged marine terraces (Burbank and Anderson, 2001; Keller and Pinter, 2002; Antonioli et al., 2006; Rajendran et al., 2008). My results confirm the reliability of the applied method and demonstrate the efficiency of sediment records for the reconstruction of tectonic structures.

· The temporal definition of the formation and subsequent evolution of Lago Lanalhue and Lago Lleu Lleu. (*Chapters 3 and 4*) – The date and mode of origin of both lakes was discussed for a long time (Börgel, 1953; Endlicher and Mäckel, 1985; Mardones and Reuther, 1999). In my work, I demonstrated that they developed in consequence of local tectonic deformation along a major fault zone during the Late Pleistocene/Early Holocene.

· The educated guess that recurrent depositional events observed in the sediments of Lago Lleu Lleu are in the main climatically induced. (*Chapter 4*) – Frequently occurring event deposits are found in a number of Chilean lakes and mostly interpreted to be triggered by regional earthquakes (Chapron, et al., 2006; Moernaut et al., 2007; Volland, et al., 2007; Bertrand, et al., 2008; Moernaut et al., 2009). In the sedimentary record of Lago Lleu Lleu, however, the sudden onset of the layer deposition at ~5000 cal yr BP is synchronous with largest increases of the frequency/intensity of ENSO events in Southern Ecuador (Moy et al., 2002). This concurrence – and the complete absence of the event layers before – in all likelihood suggest a climatic instead of a seismic control.

· The reconstruction of Holocene climate and environmental changes in south-central Chile (~38°S), based on the sedimentary records of Lago Lanalhue and Lago Lleu Lleu. (*Chapter 4*) – Paleoclimatic studies, particularly those carried out on lacustrine deposits, are still rare in the south-central part of Chile. Most of the existent surveys concentrate on the Chilean Lake District south of 40°S (Moreno, 2004, Bertrand et al., 2008) or the Central Chilean Valley north of 34°S (Jenny et al., 2002a; Jenny et al., 2002b), and examine either the last deglaciation (Moreno, 2004; Bertrand et al., 2008) or the Late Holocene time period (Jenny et al., 2002a; Bertrand et al., 2005). In view of this scientific gap, the new paleoclimatic data collected from the sediment records of Lago Lanalhue and Lago Lleu Lleu help to further improve the picture of past climate changes in the so far less explored region between 34-40°S. Major strengths of the data are furthermore the long-term focus on the entire Holocene and the parallel emphasis on short-term changes during the last 2000 years (as, for instance, the Medieval Warm Period and the Little Ice Age).

5.3   Conclusions and outlook on the future

The analysis of sediment records from different depositional provinces of the south-central Chilean convergent margin demonstrates an efficient approach of studying local tectonic and climatic processes working on time scales between 10^5 and 10^2 years. Depending on the nature and location of the investigated cores, these bear information about the regional paleoseismicity, local deformation and tectonic structures, about temporal changes in the intensity of erosion, and the development of regional climatic conditions through time.

In the context of studying the tectonic, erosional and climatic development of active plate margins, the investigation of sediment records has some convincing advances: *I*) It permits to study climate and tectonics in one and the same archive. This is not only timesaving, but also allows the direct comparison of both. *II*) Depending on the record(s), it offers the possibility of reconstructing climatic and tectonic changes on long and/or short time-scales. *III*) The main approach is commonly transferable to other convergent margins; this also bears the potential that the obtained data are directly comparable.

Considering the sedimentary records used for the present study, future investigations might concentrate on the following facts:

· Although the sedimentary sequence of ODP Site 1232 is merely free of drilling disturbances in the uppermost 100 mcd, it comprises a total length of more than 380 mcd. Accordingly, it most likely bears a turbidite record that is reaching back in time longer than the Late Pleistocene (possibly into the Early/Middle Pleistocene after the shipboard biostratigraphic explorations; Mix et al., 2003). Some additional effort would possibly allow extending the paleoseismic record to this longer time-scale (even though it might be discontinuous).

· Additional (well-dated) turbiditic sediment cores from the trench and slope basins of the south-central Chilean margin would facilitate the correlation of event layers over a larger area. That way, the argument for the seismic triggering of the turbidites could be further strengthened.

· Transferring the approach of using turbidites as paleoseismic indicators also to other active margins (e.g. Sunda-Java Trench, Indonesia) may help to better understand and compare earthquake cycles in different regions. Due to the fact that paleoseismic data are worldwide scarce, especially beyond the historical period, the study of earthquake history is essential for the prediction of future events and therefore of general significance.

· More precise dating of the most recent Lanalhue sediments (e.g. using the short-lived isotope ^{210}Pb) would allow investigating local environmental changes even on shorter than centennial time-scales. In combination with supplementary examinations (as for instance pollen and detailed diatom analyses), human influences may be identified, which likely interfere with the natural system of climate, tectonics and surface process interactions.

In conclusion, the interaction between tectonics, topography, climate, and surface processes represents a comprehensive and fascinating field of research that will stay an

intriguing issue also in future. Indicative of the topical relevance is, for instance, the recently established DFG-Leibniz Center for Surface Process and Climate Studies at the University of Potsdam, Germany, which aims to link studies of surface and Earth climate processes on geologic to annual time scales. It is an overriding challenge of this Center to encourage interdisciplinary research and to foster new projects in the fields of climate geology and surface-process research.

6.   BIBLIOGRAPHY

Abarzúa, A.M., Villagrán, C., Moreno, P.I. (2004) Deglacial and postglacial climate history in east-central Isla Grande de Chiloé, southern Chile (43°S). *Quaternary Research* **62**(1), 49-59

Abbott, L.D., Silver, E.A., Anderson, R.S., Smith, R., Ingles, J.C., Kling, S.A., Haig, D., Small, E. Galewsky, J., Silter, W. (1997) Measurement of tectonic surface uplift rate in a young collisional mountain belt. *Nature* **385**, 501-507

Aceituno, P., Fuenzalida, H., Rosenblüth, B. (1993) Climate along the extratropical west coast of South America. In: Mooney, H.A., Fuentes, E.R., Kronberg, B.I. (Eds.), Earth System Responses to Global Change. Academic Press, San Diego, pp. 61–69

Adams J. (1990) Paleoseismicity of the Cascadia Subduction Zone: Evidence from Turbidites off the Oregon-Washington Margin. *Tectonics* **9**, 569-583

Adams J. (1996) Great Earthquakes Recorded by Turbidites off the Oregon-Washington Coast. *USGS Professional Paper* **1560**(1), 147-158

Amante, C., Eakins, B.W. (2008) ETOPO1 1 Arc-Minute Global Relief Model: Procedures, Data Sources and Analysis, National Geophysical Data Center, NESDIS, NOAA, U.S. Department of Commerce, Boulder, CO

Amman, C., Jenny, B., Kammer, K., Messerli, B. (2001) Late Quaternary glacier response to humidity changes in the arid Andes of Chile (18-29°S). *Palaeogeography, Palaeoclimatology, Palaeoecology* **172**, 313-326

Anderson, R., Densmore, A., Ellist, M. (1999) The generation and degredation of marine terraces. *Basin Research* **11**, 7-19

Angermann D., Klotz J., Reigber C. (1999) Space-geodetic estimation of the Nazca-South America Euler vector. *Earth and Planetary Science Letters* **171**(3), 329-334

Antonioli, F., Ferranti, L., Lambeck, K., Kershaw, S., Verrubbi, V., Dai Pra, G. (2006) Late Pleistocene to Holocene record of changing uplift rates in southern Calabria and northeastern Sicily (southern Italy, Central Mediterranean Sea). *Tectonophysics* **422**, 23-40

Arenada, A., Torrejón, F., Aguayo, M., Torres, L., Cruces, F., Cisternas, M., Urrutia, R. (2007) Historical records of San Rafael glacier advances (North Patagonian Icefield): Another clue to 'Little Ice Age' timing in southern Chile? *The Holocene* **17**(7), 987-998

Arz, H.W., Gerhardt, S., Pätzold, J., Röhl, U. (2001) Millennial-scale changes of surface- and deep-water flow in the western tropical Atlantic linked to Northern Hemisphere high-latitude climate during the Holocene. *Geology* **29**, 239 - 242

Bangs N., Cande S. C. (1997) Episodic developement of a convergent margin inferred from structures and processes along the southern Chile margin. *Tectonics* **16**, 489-503

Baraza J., Lee H. J., Kayen R. E., Hampton M. A. (1990) Geotechnical characteristics and slope stability on the Ebro margin, western Mediterranean. *Marine Geology* **95**(3-4), 379-393

Bard, E., Hamelin, B., Fairbanks, R. G., Zindler, A. (1990) Calibration of the 14-C timescale over the past 30,000 years using mass spectrometric U-Th ages from Barbados corals. *Nature* **345**, 405-409

Bard E., Hamelin B., Arnold M., Montaggioni L., Cabioch G., Faure G., Rougerie, F. (1996) Deglacial sea-level record from Tahiti corals and the timing of global meltwater discharge. *Nature* **382**, 241-244

Bassett S.E., Milne G.A., Mitrovica J.X., Clark P.U. (2005) Ice Sheet and Solid Earth Influences on Far-Field Sea-Level Histories. *Science* **309**, 925-928

Beck S., Barrientos S., Kausel E., Reyes M. (1998) Source characteristics of historic earthquakes along the Central Chile subduction zone. *Journal of South American Earth Sciences* **11**, 115-129

Becek, K. (2008) Investigating error structure of shuttle radar topography mission elevation data product. *Geophysical Research Letters* **35**, doi:10.1029/2008GL034592L15403

Berger, A., Loutre, M.F. (1991) Insolation values for the climate of the last 10 million years. *Quaternary Science Reviews* **10,** 297-317

Bertrand, S., Boës,X., Castiaux, J., Charlet, F., Urrutia, R., Espinoza, C., Lepoint, G., Charlier, B., Fagel, N. (2005) Temporal evolution of sediment supply in Lago Puyehue (Southern Chile) during the last 600 yr and its climatic significance. *Quaternary Research* **64**(2), 163-175

Bertrand, S., Charlet, F., Charlier, B., Renson, V., Fagel, N. (2008) Climate variability of Southern Chile since the Last Glacial Maximum: a continuous sedimentological record from Lago Puyehue (40°S). *Journal of Paleolimnology* **39**, 179-195

Bertrand S., Charlet F., Chapron E., Fagel N., De Batist, M. (2008) Reconstruction of the Holocene seismotectonic activity of the Southern Andes from seismites recorded in Lago Icalma, Chile, 39°S. *Paleogeography, Paleoclimatology, Paleoecology* **259**, 301-322

Bianchi, G.G., McCave, I.N. (1999) Holocene periodicity in North Atlantic climate and deep-ocean flow south of Iceland. *Nature* **397**, 515-517

Bird, P. (2003) An updated digital model of plate boundaries. *Geochemistry, Geophysics, Geosystems* **4**(3), doi:10.1029/2001GC000252

Blais-Stevens A., Clague J. J. (2001) Paleoseismic signature in late Holocene sediment cores from Saanich Inlet, British Columbia. *Marine Geology* **175**(1-4), 131

Blumberg, S., Lamy, F., Arz, H.W., Echtler, H.P., Wiedicke, M., Haug, G.H., Oncken, O. (2008) Turbiditic trench deposits at the South-Chilean active margin: A Pleistocene-Holocene record of climate and tectonics. *Earth and Planetary Science Letters* **268**, 526-539

Börgel R. (1953) Geomorfología. In: *Geografía de Chile*. Instituto Geográfico Militar de Chile

Bohm, M., Lüth, S., Echtler, H., Asch, G., Bataille, K., Bruhn, C., Rietbrock, A., Wigger, P. (2002) The Southern Andes between 36° and 40°S latitude: seismicity and average velocities. *Tectonophysics* **356**, 275-289

Bohm, M. (2004) 3-D local earthquake tomography of the southern Andes between 36° and 40°S. PhD thesis, 135 pp, Free University, Berlin, Germany

Bookhagen B., Echtler H. P., Melnick D., Strecker M. R., Spencer J. Q. G. (2006) Using uplifted Holocene beach berms for paleoseismic analysis on the Santa María Island, south-central Chile. *Geophysical Research Letters* **33**, L15302

Börgel R. (1953) Geomorfología. In Geografía de Chile. Instituto Geográfico Militar de Chile

Broecker, W.S. (2001) Was the Medieval Warm Period Global? *Science* **291**, 1497-1499

Bruhn, C. (2003) Momentensensoren hochfrequenter Ereignisse in Südchile. Ph.D. thesis, 181 pp, University of Potsdam, Potsdam

Burbank, D.W., Anderson, R.S. (2001) Tectonic Geomorphology. Blackwell Science, 274 pp.

Cahill, T.A., Isacks, B.L. (1992) Seismicity and the shape of the subducted Nazca Plate. *J. Geophys. Res.* **97**, 17503-17529

Campos J., Hatzfeld D., Madariaga R., López G, Kausel E., Zollo A., Iannacone G., Fromm G., Barrientos S., Lyon-Caen H. (2002) A seismological study of the 1835 seismic gap in south-central Chile. *Physics of the Earth and Planetary Interiors* **132**, 177-195

Caputo R. (2007) Sea-level curves: Perplexities of an end-user in morphotectonic applications. *Global and Planetary Change* **57**, 417-423

Cembrano, J., Lavenu, A., Reynolds, P., Arancibia, G., López, G., Sanhueza, A. (2002) Late Cenozoic transpressional ductile deformation north of the Nazca-South America-Antarctica triple junction. *Tectonophysics*, **354**(3-4), 289-314

Cerveny, R.S. (1998) Present Climates of South America. In: Hobbs, J.E., Lindesay, J.A., Bridgman H.A. (Eds) Climates of the Southern Continents: Past, Present, and Future. Wiley, New York, pp. 107-135

Chapron, E., **Ariztegui, D., Mulsow, S., Villarosa, G., Pino, M., Outes, V., Juvignié, E., Crivelli, E.** (2006) Impact of the 1960 major subduction earthquake in Northern Patagonia (Chile, Argentina). *Quaternary International* **158**, 58-71

Chen, Y.-G., Liu, T-K. (2000) Holocene uplift and subsidence along an active tectonic margin southwestern Taiwan. *Quaternary Science Reviews* **19**, 923-930

Cifuentes I.L. (1989) The 1960 Chilean earthquake. *Journal of Geophysical Research* **94**, 665-680

Cisternas M., Atwater B. F., Torrejon F., Sawai Y., Machuca G., Lagos M., Eipert A., Youlton C., Salgado I., Kamataki T., Shishikura M., Rajendran C. P., Malik J. K., Rizal Y., and Husni M. (2005) Predecessors of the giant 1960 Chile earthquake. *Nature* **437**, 404-407

Clement, A.C., Saeger, R., Cane, M.A. (2000) Suppression of El Niño during the mid-Holocene by changes in the Earth's orbit. *Paleoceanography* **15**(6), 731-737

Clift, P., Vannucchi, P. (2004) Controls on tectonic accretion versus erosion in subduction zones: Implications for the origin and recycling of the continental crust. *Reviews of Geophysics* **42,** RG 2001

Cohen, A.S. (2003) Paleolimnology: The History and Evolution of Lake Systems. Oxford University Press, New York

Comte D., Eisenberg A., Lorca E., Pardo M., Ponce L., Saragoni R. Singh S., Suárez G. (1986) The 1985 central Chile earthquake, a repeat of previous earthquakes in the region? *Science* **233**, 449-453

Croudace, I.W., Rindby, A., Rothwell, R.G. (2006) ITRAX: description and evaluation of a new multi-function X-ray core scanner. In: Rothwell, R.G. (Ed.) New Techniques in Sediment Core Analysis. Special Publication, vol. 267. Geological Society, London, pp. 51-63

Dansgaard, W., Johnsen, S.J., Clausen, H.B., Dahl-Jensen, D., Gundestrup, N.S., Hammer, C.U., Hvidberg, C.S., Steffensen, J.P., Sveinbjörnsdottir, A.E., Jouzel, J., Bond, G. (1993) Evidence for general instability of past climate from a 250-kyr ice-core record. *Nature* **364**, 218-220

DeMenocal, P., Ortiz, J., Guilderson, T., Sarnthein, M. (2000) Coherent High- and Low-Latitude Climate Variability During the Holocene Warm Period. *Science* **288**, 2198-2202

Denton, G.H., Heusser, C.J., Lowell, T.V., Moreno, P.I., Andersen, B.G., Heusser, L.E., Schluchter, C., Marchant, D.R. (1999) Interhemsipheric linkage of Paleoclimate during the last glaciation. *Geografiska Annaler Series a – Physical Geography* **81A**, 107-153

Echtler, H.P., Glodny, J., Gräfe, K., Roseanu, M., Melnick, D., Seifert, W., Vietor, T. (2003) Active tectonics controlled by inherited structures in the long-term stationary and non-plateau south-central Andes. EGU/AGU Joint Assembly, Nice. EAE03-A-10902

Einsele G. (1996) Event deposits: the role of sediment supply and relative sea-level changes-overview. *Sedimentary Geology* **104**(1-4), 11-37

Einsele G., Chough S. K., Shiki T. (1996) Depositional events and their records--an introduction. *Sedimentary Geology* **104**(1-4), 1-9

Encinas A., Hervé F., Villa-Martinez R., Nielsen S., Finger K.L., Peterson D.E. (2006) Finding a Holocene marine layer in Algarrobo (33°22'S), central Chile. Implications for coastal uplift. *Revista Geologica de Chile*, **33**(2), 339-345

Endlicher W., Mäckel R. (1985) Natural Resources, Land Use and Degradation in the Coastal Zone of Arauco and the Nahuelbuta Range, Central Chile. *GeoJournal* **11**(1), 43-60

Fairbanks R.G. (1989) A 17,000-year glacio-eustatic sea level record: influence of glacial melting rates on the Younger Dryas event and deep-ocean circulation. *Nature* **342**, 637-642

Fleming K., Johnston P., Zwartz D., Yokoyama Y., Lambeck K., Chappell J. (1998) Refining the eustatic sea-level curve since the Last Glacial Maximum using far- and intermediate-field sites. *Earth and Planetary Science Letters* **163**(1-4), 327-342

Garcia-Castellanos D. (2006) Long-term evolution of tectonic lakes: Climatic controls on the development of internally drained basins. *Geological Society of America Special Paper* **398**, 283-294

Garreaud, **R.D., Vuille, M., Compagnucci, R., Marengo, J.** (2008) Present-day South American climate. *Palaeogeography, Palaeoclimatology, Palaeoecology,* doi: 10.1016/j.palaeo.2007.10.032

Gilli, A., Ariztegui, D., Anselmetti, F.S., McKenzie, J.A., Markgraf, V., Hajdas, I., McCulloch R.D. (2005) Mid-Holocene strengthening of the Southern Westerlies in South America: Sedimentological evidences from Lago Cardiel, Argentina (49°S). *Global and Planetary Change* **49**(1-2), 75-93

Glodny, J., Lohrmann, J., Echtler, H., Graefe, K., Seifert, W., Collao, S., Figueroa, O. (2005): Internal dynamics of a paleoaccretionary wedge: insights from combined isotope tectonochronology and sandbox modelling of the South-Central Chilean forearc, *Earth and Planetary Science Letters* **231**(1-2), 23-39

Glodny J., Echtler H., Collao S., Ardiles M., Buron P., Figueroa O. (2008) Differential Late Paleozoic active margin evolution in South-Central Chile (37°S-40°S) – The Lanalhue Fault Zone. *J. South Amer.Earth Sc.*, doi: 10.1016/j.jsames.2008.06.001

Goldfinger C., Morey A. E., Nelson C. H., Gutierrez-Pastor J., Johnson J. E., Karabanov E., Chaytor J., Eriksson A. (2007) Rupture lengths and temporal history of significant earthquakes on the offshore and north coast segments of the Northern San Andreas Fault based on turbidite stratigraphy. *Earth and Planetary Science Letters* **254**(1-2), 9-27

Goldfinger C., Nelson C. H., Johnson J. E. (2003) Holocene Earthquake Records from the Cascadia Subduction Zone and Northern San Andreas Fault Based on Precise Dating of Offshore Turbidites. *Annual Review of Earth and Planetary Sciences* **31**(1), 555-577

Gorsline D. S., De Diego T., Nava-Sanchez E. H. (2000) Seismically triggered turbidites in small margin basins: Alfonso Basin, Western Gulf of California and Santa Monica Basin, California Borderland. *Sedimentary Geology* **135**(1-4), 21

Grevemeyer I., Kaul N., Diaz-Naveas J.L., Villinger H.W., Ranero C.R., Reichert C. (2005) Heat flow and bending-related faulting at subduction trenches: case studies offshore Nicaragua and central Chile. *Earth and Planetary Science Letters* **236**(1-2), 238-248

Grove, J.M. (1988) The Little Ice Age. Methuen, London

Haberland, C., Rietbrock, A., Lange D., Bataille, K., Hofmann, S. (2006) Interaction between forearc and oceanic plate at the south-central Chilean margin as seen in local seismic data. *Geophysical Research Letters* **33**, L23302

Hackney R. I., Echtler H. P., Franz G., Götze H.-J., Lucassen F., Marchenko D., Melnick D., Meyer U., Schmidt S., Tasarova Z., Tassara A., and Wienicke S. (2006) The Segmented Overriding Plate and Coupling at the South-Central Chilean Margin (36-42°S). In *The Andes - Active Subduction Orogeny* (ed. G. C. O. Oncken, G. Franz, P. Giese, H.-J. Götze, V.A. Ramos, M.R. Strecker, P. Wigger). Springer-Verlag

Haschke, M. (2006) The Eagle III BKA system, a novel sediment core X-ray fluorescence analyzer with very high spatial resolution. In: Rothwell, R.G. (Ed.) New Techniques in Sediment Core Analysis. Special Publication, vol. 267. Geological Society, London, pp. 51-63

Haug, G.H., Hughen, K.A., Sigman, D.M., Peterson, L.C., Röhl, U. (2001) Southward migration of the Intertropical Convergence Zone through the Holocene. *Science* **293**, 1304-1308

Hebbeln D., Lamy F., Mohtadi M., Echtler H. (2007) Tracing the impact of glacial-interglacial climate variability on erosion of the southern Andes. *Geology* **35**(2), 131-134

Hendy, E.J., Gagan, M.K., Alibert, C.A., McCulloch, M.T., Lough, J.M., Isdale, P.J. (2002) Abrupt Decrease in Tropical Pacific Sea Surface Salinity at Ed of Little Ice Age. *Science* **295**, 1511-1514

Hervé, F., (1977) Petrology of the crystalline basement of the Nahuelbuta Mountains, south-central Chile. In: Ishikawa, K., Aguirre Le-Bert, L. (Eds.), Comparative studies on the geology of the circumpacific orogenic belt in Japan and Chile. Japan Society for the Promotion of Science, Tokyo, pp. 1–51

Hervé F. (1988) Late Paleozoic subduction and accretion in Southern Chile. *Episodes* **11**, 183-188

Hervé F. (1994) The Southern Andes between 39° and 44°S latitude: the geological signature of a transpressive tectonic regime related to a magmatic arc. In Tectonics of the Southern Central Andes (ed. K.-J. Reutter, E. Scheuber, and P. Wigger), pp. 243-248. Springer

Hsu, J.T. (1992) Quaternary uplift of the Peruvian coast related to the subduction of the Nazca Ridge: 13.5 to 15.6 degrees south latitude. *Quaternary International* **15** (16), 87-97

Hughen, K. A., Baillie, M. G. L., Bard, E., Bayliss, A., Beck, J. W., Blackwell, P. G., Buck, C. E., Burr, G. S., Cutler, K. B., Damon, P. E., Edwards, R. L., Fairbanks, R. G., Friedrich, M., Guilderson, T. P., Herring, C., Kromer, B., McCormac, F. G., Manning, S. W., Ramsey, C. B., Reimer, P. J., Reimer, R. W., Remmele, S., Southon, J. R., Stuiver, M., Talamo, S., Taylor, F. W., van der Plicht, J., Weyhenmeyer, C. E. (2004a). Marine04 Marine radiocarbon age calibration, 26 - 0 ka BP. *Radiocarbon* **46**, 1059-1086

Hughen K., Lehman S., Southon J., Overpeck J., Marchal O., Herring C., Turnbull J. (2004b) 14C Activity and Global Carbon Cycle Changes over the Past 50,000 Years. *Science* **303**, 202-207

Hughes, M.K., Diaz, H.F. (1994) Was there a 'medieval warm period', and if so, where and when? *Climatic Change* **26** (2-3), 109-142

Huh C.-A., Su C.-C., Liang W.-T., Ling C.-Y. (2004) Linkages between turbidites in the southern Okinawa Trough and submarine earthquakes. *Geophysical Research Letters* **31**(L12304)

Hulton, N., Sugden, D., Payne, A., Clapperton, C. (1994) Glacier modeling and the climate of Patagonia during the Last Glacial Maximum. *Quaternary Research* **42**, 1-19

Inouchi Y., Kinugasa Y., Kumon F., Nakano S., Yasumatsu S., Shiki T. (1996) Turbidites as records of intense palaeoearthquakes in Lake Biwa, Japan. *Sedimentary Geology* **104**(1-4), 117

Ito, E. (2001) Application of Stable Isotope Techniques to Inorganic and Biogenic Carbonates. In: Last, W.M., Smol, J.P. (eds.) Tracking Environmental Changes Using Lake Sediments Volume 2: Physical and Geochemical Methods. Kluwer Academic Publishers, Dordrecht

Jaccard, S.L., Haug, G.H., Sigman, D.M., Pedersen, T.F., Thierstein, H.R., Röhl, U. (2005) Glacial/interglacial changes in subarctic North Pacific stratification. *Science* **308**, 1003-1006

Jansen, J.H.F., Van der Gaast, S.J., Koster, B., Vaars, A.J., (1998) CORTEX, a shipboard XRF-scanner for element analyses in split sediment cores. *Quaternary Research* **151**, 143-153

Jenny, B., Valero-Garcés, B.L., Urrutia, R., Kelts, K., Veit, H., Appleby, P.G., Geyh, M. (2002a) Moisture changes and fluctuations of the Westerlies in Mediterranean Central Chile during the last 2000 years: The Laguna Aculeo record (33°50'S). *Quaternary International* **87**, 3-18

Jenny, B., Valero-Garcés, B.L., Villa-Martínez, R., Urrutia, R., Geyh, M., Veit, H. (2002b) Early to Mid-Holocene Aridity in Central Chile and the Southern Westerlies: The Laguna Aculeo Record (34°S). *Quaternary Research* **58**, 160-170

Johnson, T.C, Barry, S.L., Chan, Y., Wilkinson P. (2001) Decadal record of climate variability spanning the past 700 yr in the Southern Tropics of East Africa. *Geology* **29**, 83-86

Jordan, T.E., Bryan, L.I., Allmendinger, R.W., Brewer, J.A., Ramos, V.A., Ano, C.J. (1983) Andean tectonics related to geometry of subducted Nazca Plate. *Geological Society of America Bulletin* **94**, 341-361

Kaiser, J., Lamy, F., Arz, H.W., Hebbeln, D. (2007) Dynamics of the millennial scale sea surface temperature and Patagonian Ice Sheet fluctuations in southern Chile during the last 70 kyr (ODP Site 1233). *Quaternary International* **161**, 77-89

Kaiser, J., Schefuß, E., Lamy, F., Mohtadi, M., Hebbeln, D. (2008) Glacial to Holocene changes in sea surface temperature and coastal vegetation in north central Chile: high versus low latitude forcing. *Quaternary Science Reviews* **27**, 2064-2075

Kaizuka S., Matsuda T., Nogami M., Yonekura N. (1973) Quaternary Tectonic and Recent Seismic Crustal Movements in the Arauco Peninsula and its Environs, Central Chile. *Geogr. Rep. Tokyo Metrop. Univ.* **8**, 1-49

Kelleher J.A. (1972) Rupture zones of large South American earthquakes and some predictions. *Journal of Geophysical Research* **77**, 2089-2103

Keller, E.A., Pinter, N. (2002) Active Tectonics: Earthquakes, Uplift, and Landscape. Prentice Hall, Upper Saddle River, NJ

Kendrick, E., Bevis, M., Smalley, R., Brooks, B., Vargas, R.B., Lauria, E., Fortes, L.P.S. (2003) The Nazca-South America Euler vector and its rate of change. *Journal of South American Earth Sciences*, **16**(2), 125-131

Kim, J., Schneider, R.R., Hebbeln D., Müller P.J., Wefer, G. (2002) Last deglacial sea-surface temperature evolution in the southeast Pacific compared to climate changes on the South American continent. *Quaternary Science Reviews* **21**, 2085-2097

Kley, J., Monaldi, C.R., Salfity, J.A. (1999) Along-strike segmentation of the Andean foreland: causes and consequences. *Tectonophysics* **301**, 75-94

Koch, J., Kilian, R. (2005) 'Little Ice Age' glacier fluctuations, Gran Campo Nevado, southernmost Chile. *The Holocene* **15**(1), 20-28

Krawczyk C. M., SPOC-Team (2003) Amphibious seismic survey images plate interface at 1960 Chile earthquake. *EOS Transact* **84**(32/301), 304-305

Lajoie, K. (1986) Coastal tectonics. In: *Active Tectonics. Studies in Geophysics*, National Academy Press, Washington D.C., USA

Lamb S., Davis P. (2003) Cenozoic climate change as a possible cause for the rise of the Andes. *Nature* **425**, 792-797

Lamy F., Hebbeln D., Wefer G. (1999) High-Resolution Marine Record of Climatic Change in Mid-latitude Chile during the Last 28,000 Years Based on Terrigenous Sediment Parameters. *Quaternary Research* **51**(1), 83-93

Lamy F., Hebbeln D., Rohl U., Wefer G. (2001) Holocene rainfall variability in southern Chile: a marine record of latitudinal shifts of the Southern Westerlies. *Earth and Planetary Science Letters* **185**(3-4), 369-382

Lamy F., Rühlemann C., Hebbeln D., Wefer G. (2002) High- and low-latitude climate control on the position of the southern Peru-Chile Current during the Holocene. *Paleoceanography* **17,** doi:10.1029/2001PA000727

Lamy F., Kaiser J., Ninnemann U., Hebbeln D., Arz H. W., Stoner J. (2004) Antarctic Timing of Surface Water Changes off Chile and Patagonian Ice Sheet Response. *Science* **304**, 1959-1962

Lara, A., Villalba, R. (1993) A 3620-year temperature record from *Fitzroya cupressoides* tree rings in Southern South America. *Science* **260**, 1104-1106

Lee H. J., Chough S. K., Yoon S. H. (1996) Slope-stability change from late Pleistocene to Holocene in the Ulleung Basin, East Sea (Japan Sea). *Sedimentary Geology* **104**(1-4), 39-51

Lee H. J., Edwards B. D. (1986) Regional method to assess offshore slope stability. *J. Geotech. Eng.* **112**, 489-509

Liesiecki, L.E., Raymo, M.E. (2005) A Pliocene-Pleistocene stack of 57 globally distributed benthic δ^{18}O records. *Paleoceanography* **20,** doi:10.1029/2004 PA001071

Lomnitz C. (1970) Major earthquakes and tsunamis in Chile during the period 1535-1955. *Geologische Rundschau* **59**, 938-960

Lomnitz C. (2004) Major Earthquakes of Chile: A Historical Survey, 1535-1960. *Seismological Research Letters* **75**(3), 368-378

Maldonado, A., Villagrán, C. (2006) Paleoenvironmental changes in the semiarid coast of Chile (32°S) during the last 6200 years inferred from a swamp-forest pollen record. *Quaternary Research* **58**, 130-138

Mardones M., Reuther C.-D. (1999) Geomorphological aspects of the drainage pattern around Lake Lanalhue and Lake Lleulleu in the active convergent margin setting of South-Central Chile. *Mitt. Geol.-Paläont. Inst. Univ. Hamburg* **83**, 75-88

Markgraf, V. (1998) Past Climates of South America. In: Hobbs, J.E., Lindesay, J.A., Bridgman H.A. (Eds) Climates of the Southern Continents: Past, Present, and Future. Wiley, New York, pp. 249-264

Markgraf, V., Dodson, J.R., Kershaw, A.P., McGlone, M.S., Nicholls, N. (1992) Evolution of Late Pleistocene and Holocene climates in the circum-South Pacific land areas. *Climate Dynamics* **6**, 193– 211

Markgraf, V., Whitlock, C., Haberle, S. (2007) Vegetation and fire history during the last 18,000 cal yr B.P. in Southern Patagonia: Mallín Pollux, Coyhaique, Province Aisén (45°41′30″ S, 71°50′30″ W, 640 m elevation). *Palaeogeography, Palaeoclimatology, Palaeoecology* **254** (3-4), 492-507

Martin, L., Bertaux, J., Correge, T., Ledru, M.P., Mourguiart, P., Sifeddine, A., Soubies, F., Wirrmann, D., Suguio, K., Turcq, B. (1997) Astronomical forcing of contrasting rainfall changes in tropical South America between 12,400 and 8800 cal yr BP. *Quaternary Research* **47**(1), 117– 122

Mayewski, P.A. Rohling, E.E., Stager, J.C., Karlén, W., Maasch, K.A., Meeker, L.D., Meyerson, E.A., Gasse, F., Van Kreveld, S., Holmgren, K., Lee-Thorp, J., Rosqvist, G., Rack, F., Staubwasser, M., Schneider, R.R., Steig, E.J. (2004) Holocene climate variability. *Quaternary Research* **62**, 243-255

Mayr, C., Wille, M., Haberzettl, T., Fey, M., Janssen, S., Lücke, A., Ohlendorf, C., Oliva, G., Schäbitz, F., Schleser, G.H., Zolitschka, B. (2007) Holocene variability of the Southern Hemisphere westerlies in Argentinean Patagonia (52°S). *Quaternary Science Reviews* **56**, 579-584

McCaffrey, R. (2008) Global frequency of magnitude 9 earthquakes. *Geology* **36**, 263-266

McCormac, F. G., Hogg, A. G., Blackwell, P. G., Buck, C. E., Higham, T. F. G., and Reimer, P. J. (2004) SHCal04 Southern Hemisphere Calibration 0 - 1000 cal BP. *Radiocarbon* **46**,1086-1092

McCulloch, R.D., Bentley, M.J., Purves, R.S., Hulton, N.R.J., Sugden, D.E., Clapperton, C.M. (2000) Climatic inferences from glacial and palaeoecological evidence at the last glacial termination, southern South America. *Journal of Quaternary Sciences* **15**, 409-417

McDermott, F., Mattey, D.P., Hawkesworth, C. (2001) Centennial-Scale Holocene Climate Variability Revealed by a High-Resolution Speleothem $\delta^{18}O$ Record from SW Ireland. *Science* **294**, 1328-1331

Melnick D., Bookhagen B., Echtler H. P., Strecker M. R. (2006) Coastal deformation and great subduction earthquakes, Isla Santa María, Chile (37°S). *Geological Society of America Bulletin* **118**(11), 1463-1480

Melnick, D., Bookhagen, B., Strecker, M.R., Echtler, H.P. (2009) Segmentation of megathrust rupture zones from fore-arc deformation patterns over hundreds to millions of years, Arauco Peninsula, Chile. *Journal of Geophysical Research - Solid Earth*, doi10.1029/2008JB005788

Melnick D., Echtler H. P. (2006a) Inversion of forearc basins in south-central Chile caused by rapid glacial age trench fill. *Geology* **34**(9), 709-712

Melnick D., Echtler H. P. (2006b) Morphotectonic and geologic digital map compilations of the south-central Andes (36°-42°S). In: Oncken, O., Chong, G., Franz, G., Giese, P., Götze, H.-J., Ramos, V.A., Strecker, M., Wigger, P. (Editors) *The Andes - Active Subduction Orogeny*, pp. 565-568. Springer-Verlag

Meyers, P.A. (1994) Preservation of elemental and isotopic source identification of sedimentary organic matter. *Chemical Geology* **144**, 289-302

Meyers, P.A. (2003) Applications of organic geochemistry to paleolimnological reconstructions: a summary of examples from the Laurentian Great Lakes. *Organic Geochemistry* **34**, 261-289

Meyers, P.A., Ishiwatari, R. (1995) Organic Matter Accumulation Records in Lake Sediments. In: Lerman, A., Imboden, D., Gat, J. (Eds.) Physics and Chemistry of Lakes. 2nd ed., Springer, Berlin, Heidelberg

Meyers, P.A., Teranes J.L. (2001) Sediment organic matter. In: Last, M., Smol, J. (Eds.) Tracking Environmental Change Using Lake Sediments. Kluwer Academic Publishers, Dordrecht, pp. 239-269

Miller A. (1976) The Climate of Chile. In *World Survey of Climatology*, Vol. 12 (ed. W. Schwerdtfeger), pp. 113-145. Elsevier

Milne G.A., Long A.J., Bassett S.E. (2005) Modelling Holocene relative sea-level observations from the Caribbean and South America. *Quaternary Science Reviews* **24**, 1183-1202

Mix A. C., Tiedemann R., and Blum P., et al. (2003) Proc. ODP, Init. Repts., 202. In Ocean Drilling Program

Moernaut J., De Batist M., Charlet F., Heirman K., Chapron E., Pino M. Brümmer R., Urrutia R. (2007) Giant earthquakes in South-Central Chile revealed by Holocene mass-wasting events in Lake Puyehue. *Sedimentary Geology* **195**, 239-256

Moernaut, J., **De Batist, M., Heirman, K., Van Daele, M., Pino, M., Brümmer, R., Urrutia, R.** (2009) Fluidization of buried mass-wasting deposits in lake sediments and its relevance for paleoseimology: Results from a reflection seismic study of lakes Villarica and Calafquén (South-Central Chile). *Sedimentary Geology* **213**, 121-135

Mohtadi M., Hebbeln D., Marchant M. (2005) Upwelling and productivity along the Peru-Chile Current derived from faunal and isotopic compositions of planktic foraminifera in surface sediments. *Marine Geology* **216**(3), 107-126

Mohtadi, M., Romero, O.E., Kaiser, J., Hebbeln, D. (2007). Cooling of the southern high latitudes during the Medieval Period and its effect on ENSO. *Quaternary Science Reviews* **26**, 1055-1066

Montgomery, D.R., Balco, G., Willet, S.D. (2001) Climate, tectonics, and the morphology of the Andes. *Geology* **29**, 579-582

Moreno, A., Giralt, S., Valero-Garcés, B., Sáez, A., Bao, R., Prego, R., Pueyo, J.J., González-Sampériz P., Taberner, C. (2007) A 14 kyr record of the tropical Andes: The Lago Chungará sequence (18°S, northern Chilean Altiplano). *Quaternary International* **161**, 4-21

Moreno M., Klotz J., Melnick D., Grund V., Echtler H., Bataille K. (2008) Active faulting and forearc block rotation in south-central Chile from GPS-derived deformation (36-39°S), *Geochemistry, Geophysics, Geosystems* **9**, Q12024

Moreno, P.I., Jacobson, G.L. Lowell, T.V., Denton, G.H. (2001) Interhemispheric climate links revealed by late-glacial cooling episode in souther Chile. *Nature* **409**, 804-809

Moreno, P.I. (2004) Millennial-scale climate variability in northwest Patagonia over the last 15 000 yr. *Journal of Quaternary Science* **19**(1), 35-47

Moy, C.M., Seltzer, G.O., Rodbell, D.T., Anderson, D.M. (2002) Variability of El Niño/Southern Oscillation activity at millennial timescales during the Holocene epoch. *Nature* **420**, 162-165

Mpodozis, C., Ramos, V.A. (1989) The Andes of Chile and Argentina. In: Ericksen, G., Cana Pinochet, M, Reinemund, J. (Eds) Geology of the Andes and its relation to hydrocarbon and mineral resources. Volume 11: Earth Science Series - Circum-Pacific Council of Energy and Mineral Resources. Houston TX, 59-89

Muñoz J., Troncoso R., Duhart P., Crignola P., Farmer L., Stern C.R. (2000). The relation of the mid-Tertiary coastal magmatic belt in South-Central Chile to the late Oligocene increase in plate convergence rate. *Rev Geol Chile* **27**(2), 177–203

Murray J. (1991) Ecology and Palaeoecology of Benthic Foraminifera. Longman Scientific&Technical

Mutti E., Lucchi F. R., Seguret M., Zanzucchi G. (1984) Seismoturbidites: A new group of resedimented deposits. *Marine Geology* **55**(1-2), 103

Nakajima T., Kanai Y. (2000) Sedimentary features of seismoturbidites triggered by the 1983 and older historical earthquakes in the eastern margin of the Japan Sea. *Sedimentary Geology* **135**(1-4), 1-19

Nelson A. R., Manley W. F. (1992) Holocene coseismic and aseismic uplift of Isla Mocha, south-central Chile. *Quaternary International* **15-16**, 61

Nelson E., Forsythe R., Arit I. (1994) Ridge collision tectonics in terrane development. *J. South Am. Earth Sci.* **7**, 271-278

New, M, Lister, D., Hulme, M., Makin, I. (2002) A high-resolution data set of surface climate over global land areas. *Climate Research* **21**, 1-25

Oldfield, F., Dearing, J.A., Thompson, R., Garrett-Jones, S.E. (1978) Some magnetic properties of lake sediments and their possible links with erosion rates. *Polskie Archiwum Hydrobiologii* **25**, 321-331

Pahnke K., Zahn R., Elderfield H., Schulz M. (2003) 340,000-Year Centennial-Scale Marine Record of Southern Hemisphere Climate Oscillation. *Science* **301**, 948-952

Parra, O., Basualto, S., Urrutia, R., Valdovinos, C. (1999) Estudio comparativo de la diversidad fitoplanctonica de cinco lagos de diferentes niveles de eutroficacion del area litoral de la region del Bio Bio (Chile). *Gayana Botánica* **56**(2), 93-108

Paulsen, D.E., Li, H.-C., Ku, T.-L. (2003) Climate variability in central China over the last 1270 years revealed by high-resolution stalagmite records. *Quaternary Science Reviews* **22,** 691-701

Peterson, L.C. and Haug, G.H. (2006) Variability in the mean latitude of the Atlantic Intertropical Convergence Zone as recorded by riverine input of sediments to the Cariaco Basin (Venezuela). *Palaeogeography, Palaeoclimatology, Palaeoecology* **234**, 97-113

Plafker G., Savage J. C. (1970) Mechanism of the Chilean earthquakes of May 21 and 22, 1960. *Geological Society of America Bulletin* **81**(4), 1001-1030

Postma, D. (1982) Pyrite and siderite formation in brackish and freshwater swamp sediments. *American Journal of Science* **282**, 1151-1183

Pye, K., Dickson, J.A.D., Schiavon, N., Coleman M. L., Cox, M. (1990) Formation of siderite-Mg-calcite-iron sulphide concretions in intertidal marsh and sandflat sediments, north Norfolk, England. *Sedimentology* **37**, 325-343

Rabassa J., Clapperton C. (1990). Quaternary glaciations of the southern Andes. *Quaternary Science Reviews* **9**, 153-174

Radtke U. (1989) Marine Terrassen und Korallenriffe - Das Problem der quartären Meeresspiegelschwankungen erläutert an Fallstudien aus Chile, Argentinien und Barbados. Heinrich-Heine-Universität Düsseldorf

Rauch, K. (2005) Cyclicity of Peru-Chile trench sediments between 36° and 38°S: a footprint of plaeclimatic variations? *Geophysical Research Letters* **32** (8), L08302

Rajendran, K., Rajendran, C.P., Earnest, A., Ravi Prasad, G.V., Dutta, K., Ray, D.K., Anu, R. (2008) Age estimates of coastal terraces in the Andaman and Nicobar Islands and their tectonic implications. *Tectonophysics* **455**, 53-60

Rehak, K. (2008) Pliocene-Pleistocene landscape evolution in south-central Chile – Interactions between tectonic, geomorphic, and climatic processes. PhD thesis. Potsdam University, Germany

Rehak K., Strecker M. R., Echtler H. P. (2008) Morphotectonic segmentation of an active forearc, 37°-41°S, Chile. *Geomorphology* **94,** 98-116

Rehak, K., Niedermann, S., Preusser, F., Strecker M.R., Echtler, H.P. (submitted) Late Pleistocene landscape in south-central Chile constrained by luminescence and stable cosmogenic isotope dating. *GSA Bulletin*

Rein B., Sirocko F. (2001) In-situ reflectance spectroscopy – analysing techniques for high-resolution pigment logging in sediment cores. *Int. J. Earth Sci.* **91**, 950-954. doi: 10.1007 / s00531-002-0264-0

Rein, B. (2003) In-situ Reflektionsspektroskopie und digitale Bildanalyse: Gewinnung hochauflösender Paläoumweltdaten mit fernerkundlichen Methoden, habilitation thesis, 104 pp, Univ. of Mainz, Mainz, Germany

Rein, B., Lückge, A., Sirocko, F. (2004) A major Holocene ENSO anomaly during the Medieval period. *Geophysical Research Letters* **31**, doi:10.1029/2004 GL020161

Richter, T.O., Van der Gaast, S., Koster,B., Vaars, A., Gieles, R., De Stigter, H.C., De Haas, H., Van Weering, T.C.E. (2006) The Avaatech XRF Core Scanner: technical description and applications to NE Atlantic sediments. In: Rothwell, R.G. (Ed.) New Techniques in Sediment Core Analysis. *Geological Society, London, Special Publication* **267**, 39-50

Rosenau, M., Melnick, D., Echtler, H. (2006) Kinematic constraints on intra-arc shear and strain partitioning in the Southern Andes between 38°S and 42°S latitude. *Tectonics* **25(4)**, TC4013

Ruff L. J. (1989) Do Trench Sediments Affect Great Earthquake Occurrence in Subduction Zones? *PAGEOPH* **129**(1/2), 263-282

Ruff, L., Kanamori, H. (1980) Seismicity and the subduction process. *Physics of the Earth and Planetary Interiors* **23**, 240-252

Schäbitz, F. (1999) Paläoökologische Untersuchungen an geschlossenen Hohlformen in den Trockengebieten Patagoniens. *Bamberger Geographische Schriften* **17,** Bamberg

Schimmelmann, A., Lange, C.B., Meggers, B.J. (2003) Palaeoclimatic and archaeological evidence for a ~200-yr recurrence of floods and droughts linking California, Mesoamerica and South America over the past 2000 years. *The Holocene* **13**(5), 763-778

Schweller W.J., Kulm L.D., Prince R.A. (1981) Tectonics, structure and sedimentary framework of the Peru-Chile-Trench. In: *Nazca Plate: Crustal Formation and Andean Convergence*, Vol. 154 (ed. L. D. Kulm, et al.), pp. 323-350. Geol. Soc. America Mem.

Schwerdtfeger, W. (1976) Climates of Central and South America. Elsevier.

Shiki T., Kumon F., Inouchi Y., Kontani Y., Sakamoto T., Tateishi M., Matsubara H., Fukuyama K. (2000) Sedimentary features of the seismo-turbidites, Lake Biwa, Japan. *Sedimentary Geology* **135**(1-4), 37-50

Solanki, S.K., Usoskin, I.G., Kromer, B., Schüssler, M., Beer, J. (2004) Unusual activity of the Sun during recent decades compared to the previous 11,000 years. *Nature* **431**, 1084 - 1087

Soon, W., Baliunas, S., Idso, C., Idso, S., Legates, D. (2003) Reconstructing climatic and environmental changes of the past 1000 years: a reappraisal. *Energy&Environment* **14** (2-3), 233-299

Stefer S., Arz H.W., Lamy, F., Haug G.H. (submitted) Holocene climate changes in South-Central Chile (38°S) as documented in sediments of the two coastal lakes Lanalhue and Lleu Lleu. *Palaeogeography, Palaeoclimatology, Palaeoecology*

Stefer, S., Moernaut, J., Melnick, D., Echtler., H.P., Arz, H.W., Lamy, F., De Batist M., Haug, G.H. (in Review) Forearc uplift rates deduced from sediment cores of two coastal lakes in south-central Chile. *Tectonophysics*

Steig, E.J. (1999) Mid-Holocene Climate Change. *Science* **286**, 1485-1487

Steig, E.J., Brook, E.J., White, J.W.C., Sucher, C.M., Bender, M.L., Lehman, S.J., Morse, D.L., Waddington, E.D., Clow, G.D. (1998) Synchronous climate changes in Antarctica and the North Atlantic. *Science* **282**, 92-95

Sterken, M., Verleyen, E., Sabbe, K., Terryn, G., Charlet, F., Bertrand, S., Boës, X., Fagel, N., De Batist, M., Vyverman, W. (2008). Late Quaternary climatic changes in Southern Chile, as recorded in a diatom sequence of Lago Puyehue (40° 40′ S). *Journal of Paleolimnology* **39**, 219-235

Stern, C.R. (2004). Active Andean volcanism: its geologic and tectonic setting. *Revista Geológica de Chile* **31**(2), 161-206

Stern, R.J. (2001) Subduction Zones. *Review of Geophysics* **40**, doi:10.1029/ 2001RG000108

Strub P. T., Mesias J. M., Montecino V., Rutllant J., and Salinas S. (1998) Coastal ocean circulation off western South America. In: The Global Coastal Ocean - Regional Studies and Synthesis (ed. A. R. Robinson, Brink, K.H.), pp. 273-313. Wiley

Stuiver M., Reimer P. J., Bard E., Beck J. W., Burr G. S., Hughen K. A., Kromer B., McCormac G., Van der Pflicht J., Spurk M. (1998) INTCAL98 radiocarbon age calibration, 24,000-0 cal BP. *Radiocarbon* **40**, 1041-1083

Stuiver, M., Reimer, P. J., Reimer, R. W. (2005) CALIB 5.0. [WWW program and documentation]

Stuut J.-B. W., Kasten S., Lamy F., Hebbeln D. (2007) Sources and modes of terrigenous sediment input to the Chilean continental slope. *Quaternary International* **161**(1), 67-76

Tassara, A. (2005). Structure of the Andean continental margin and causes of its segmentation. PhD thesis, FU Berlin, 165 p.

Tebbens S.F., Cande S.C. (1997) Southeast Pacific tectonic evolution from early Oligocene to Present. *Journal of Geophysical Research - Solid Earth* **102**(B6), 12061-12084

Telford R.J., Heegaard E., Birks H.J.B. (2004) The intercept is a poor estimate of calibrated radiocarbon age. *The Holocene* **14**, 2, 296-298

Thornburg T. M., Kulm L. D. (1987) Sedimentation in the Chile Trench: Petrofacies and Provenance. *Journal of Sedimentary Petrology* **57**(1), 55-74

Thornburg T. M., Kulm, L.D., Hussong, D.M. (1990) Submarine-fan developement in the southern Chile Trench: A dynamic interplay of tectonics and sedimentation. *Geological Society of America Bulletin* **102**, 1658-1680

Torres, L., Parra, O., Araneda, A., Urrutia, R., Cruces, F., Chrinos, L. (2008) Vegetational and climatic history during the Late Holocene in Lake Laja basin (central Chile) inferred from sedimentary pollen record. *Review of Palaeobotany and Palynology* **149**, 18-28

Trenbert, K.E. (1991) Storm Tracks in the Southern Hemisphere. *Journal of the Atmospheric Sciences* **48**, 2159-2178

Urrutia, R., Cisternas, M., Araneda, A., Retamal, O., Parra, O. (2000) Caracterización morfométrica y sedimentológica de cinco lagos costeros de la VIII Región, Chile. Rev. *Geográfica de Chile Terra Australis* **45**, 7-24

Valdovinos, C., Figueroa, R. (2000) Benthic community metabolism and trophic conditions of four South American lakes. *Hydrobiologia* **429**, 151-156

Vargas G., Ortlieb L., Chapron E., Valdes J., Marquardt C. (2005) Paleoseismic inferences from a high-resolution marine sedimentary record in northern Chile (23°S). *Tectonophysics* **399**(1-4), 381

Veit H. (1996) Southern Westerlies during the Holocene deduced from geomorphological and pedological studies in the Norte Chico, Northern Chile (27-33°S). *Palaeogeography, Palaeoclimatology, Palaeoecology* **123**(1-4), 107

Villa-Martínez, R., Villagrán, C., Jenny, B. (2003) The last 7500 cal yr B.P. of westerly rainfall in Central Chile inferred from a high-resolution pollen record from Laguna Aculeo (34°S). *Quaternary Research* **60**, 284-293

Villalba, R. (1990) Climatic fluctuations in Northern Patagonia during the last 1000 years as inferred from tree-ring records. *Quaternary Research* **34**, 346-360

Villalba, R. (1994) Tree-ring and glacial evidence for the Medieval Warm Epoch and the Little Ice Age in southern South America. *Climatic Change* **26**, 183-197

Völker D., Wiedicke M., Ladage S., Gaedicke C., Reichert C., Rauch K., Kramer W., Heubeck C. (2006) Latitudinal variations in sedimentary processes in the Peru-Chile trench off Central Chile. In: The Andes - Active Subduction Orogeny (ed. G. C. O. Oncken, G. Franz, P. Giese, H.-J. Götze, V.A. Ramos, M.R. Strecker, P. Wigger), pp.193-216. Springer-Verlag

Volland, S., Sturm, M., Lukas, S., Pino, M., Müller, J. (2007) Geomorphological and sedimentological evolution of a lake basin under strong volcano-tectonic influence: the seismic record of Lago Calafquén (south-central Chile). *Quaternary International* **161**, 32-45

von Huene, R., Scholl, D.W. (1991) Concerning sediment subduction, subduction erosion, and the groth of continental crust. *Reviews of Geophysics* **29**, 279-316

Waelbroeck C., Labeyrie L., Michel E., Duplessy J. C., McManus J. F., Lambeck K., Balbon E., Labracherie M. (2002) Sea-level and deep water temperature changes derived from benthic foraminifera isotopic records. *Quaternary Science Reviews* **21**(1-3), 295-305

Walker, M. (2005) Quaternary Dating Methods. Willey, Chichester

Wanner, H., Beer, J., Bütikofer, J., Crowley, T.J., Cubasch, U., Flückinger, J., Goosse, H., Grosjean, M., Joos, F., Kapna, J.O., Küttel, M., Müller, S.A., Prentice, I.O., Solomina, O., Stocker, T.F., Tarasov, P., Wagern, M., Widmann, M. (2008) Mid- to Late Holocene climate change: an overview. *Quaternary Science Reviews*. doi:10.1016/j.quascirev.2008.06.013

Weltje, G.J., Tjallingii, R. (2008). Calibration of XRF core scanners for quantitative geochemical logging of soft sediment cores: theory and application. *Earth and Planetary Science Letters*. doi:10.1016/j.epsl.2008.07.054

Wiedicke-Hombach M., Andruleit H., Balmaceda G., Bruns A., Contardo X., Cramer B., Delisle G., Diaz-Naveas J. L., Erbacher J., Fenner J., Goergens R., Gomez C., Harazim B., Heubeck C., Kloep F., Kramer W., Kus J., Lückge A., Mohtadi M., Mühr P., Panten D., Reinhardt L., Steinmann D., Stummeyer J., Zeibig M. (2002) SO161 – 5 SPOC (Subduction Processes off Chile) Geologie – Geochemie - Wärmestrom. BGR

Wien K., Holz C., Kolling M., Schulz H. D. (2006) Age models for pelagites and turbidites from the Cap Timiris Canyon off Mauritania. *Marine and Petroleum Geology* **23**(3), 337-352

Willet, S., Hovius, N., Brandon, M.T., Fisher, D.M. (2006) (Eds.) Tectonics, Climate and Landscape Evolution. The Geological Society of America, Special Paper 398

Yáñez, G., Cembrano, J. (2004). Role of viscous plate coupling in the late Tertiary Andean tectonics. *Journal of Geophysical Research* **109**, B02407, doi:10.1029/ 2003JB002494

Yuan, X., Martinson, D.G. (2000) Antarctic sea ice extent variability and its global connectivity. *Journal of Climate* **13**, 1697-1717

Yuan, X., Martinson D.G. (2001) The Antarctic dipole and its predictability. *Geophysical Research Letters* **28**, 3609-3612

Zapata R. A. (2001) Estudio batimétrico del margen Chileno. Universidad de Chile

Zeil, W. (1986) Südamerika, Enke, Stuttgart

Ziegler, A.M., Barrett, S.F., Scotese, C.R. (1981) Paleoclimate, sedimentation and continental accretion. *Philos. Trans. R. Soc. London* **A 301**, 253-264

APPENDIX

I   Oxygen isotope data of the sediments at ODP Site 1232

Leg	Site	Hole	Core	Section	Top of the sample (cm)	Corrected depth (m)	Age (kyr BP)	δ18O (‰VPDB)
202	1232	C	1	1	60	0.35	12.47	0.7
202	1232	C	1	1	80	0.48	18.04	1.7
202	1232	C	1	1	105	0.67	18.23	2.3
202	1232	C	1	1	140	0.95	18.51	2.7
202	1232	C	1	2	15	1.21	18.77	2.5
202	1232	C	1	2	90	1.8	19.35	2.4
202	1232	C	1	3	30	2.4	19.94	2.7
202	1232	C	1	3	45	2.55	20.09	2.4
202	1232	C	1	4	10	2.83	20.37	2.5
202	1232	C	1	4	30	2.99	20.53	2.5
202	1232	B	1	2	20	3.19	20.81	2.6
202	1232	B	1	2	60	3.55	21.31	2.6
202	1232	B	1	2	75	3.7	21.52	2.9
202	1232	B	1	2	95	3.84	21.73	2.6
202	1232	B	1	3	10	4.26	22.33	2.6
202	1232	B	1	3	45	4.54	22.72	2.4
202	1232	B	1	3	75	4.76	23.03	2.6
202	1232	B	1	3	105	5.02	23.24	2.3
202	1232	B	1	3	140	5.27	23.46	2.6
202	1232	B	1	4	25	5.6	23.73	3
202	1232	B	1	4	135	6.67	24.63	2.9
202	1232	B	1	5	5	6.87	24.8	2.3
202	1232	B	1	5	110	7.78	25.56	2.4
202	1232	C	2	3	40	8.58	26.23	2.5
202	1232	C	2	3	60	8.71	26.34	2.6
202	1232	C	2	3	90	8.9	26.5	3
202	1232	C	2	4	40	9.68	27.15	1.8
202	1232	C	2	5	60	10.8	28.1	2.1
202	1232	B	2	2	67.5	11.3	28.51	2.4
202	1232	B	2	2	95	11.57	28.74	2.2
202	1232	B	2	2	115	11.66	28.82	2.9
202	1232	B	2	3	115	12.53	29.64	2.4
202	1232	B	2	5	5	13.73	30.76	2.7
202	1232	B	2	5	105	14.39	31.38	2.5
202	1232	C	3	2	35	14.97	31.92	2.9
202	1232	C	3	3	65	16.01	32.9	2
202	1232	C	3	3	133	16.4	33.26	1.9
202	1232	B	3	2	10	17.35	34.15	1.9
202	1232	B	3	2	30	17.45	34.25	2
202	1232	B	3	2	45	17.55	34.34	2.2
202	1232	B	3	2	75	17.71	34.62	3.1
202	1232	B	3	4	105	19.4	37.59	2.5
202	1232	B	3	4	125	19.54	37.83	2.6
202	1232	B	3	4	145	19.68	38.08	2.5
202	1232	B	3	5	55	20.16	38.92	2.9
202	1232	B	3	6	75	20.94	40.3	3.6
202	1232	B	3	6	90	21.03	40.45	2.8
202	1232	C	4	1	100	21.14	40.64	2.1
202	1232	C	4	1	120	21.27	40.88	2.5
202	1232	C	4	3	30	21.63	41.52	3
202	1232	C	4	3	70	21.86	41.91	2.5
202	1232	C	4	3	65	22.57	43.16	2.3
202	1232	C	4	3	95	22.73	43.44	2.7
202	1232	C	4	3	130	22.89	43.72	2.3
202	1232	C	4	4	20	23.19	44.24	2.2
202	1232	C	4	4	55	23.38	44.71	1.6
202	1232	C	4	4	70	23.46	44.91	2
202	1232	B	4	2	85	23.95	46.13	2.3
202	1232	B	4	2	142.5	24.29	46.96	2.4
202	1232	B	4	3	15	24.42	47.28	2.5
202	1232	B	4	3	30	24.47	47.41	2.2
202	1232	B	4	3	65	24.68	47.92	2.1
202	1232	B	4	3	95	24.82	48.26	2
202	1232	B	4	3	105	24.88	48.41	2.1
202	1232	B	4	3	135	25.02	48.76	1.9
202	1232	B	4	4	15	25.26	49.34	2.1
202	1232	B	4	4	40	25.49	49.91	2
202	1232	B	4	4	90	25.8	50.68	1.9
202	1232	B	4	4	115	25.98	51.11	2.3

202	1232	B	4	4	145	26.14	51.51	2.3
202	1232	B	4	5	30	26.34	52.01	2
202	1232	B	4	5	50	26.43	52.23	2.2
202	1232	B	4	5	75	26.57	52.56	2.7
202	1232	B	4	5	115	26.8	53.14	2.3
202	1232	B	4	5	142.5	26.98	53.56	2.3
202	1232	B	4	6	15	27.09	53.85	2.5
202	1232	B	4	6	70	27.52	54.91	2.9
202	1232	B	4	6	125	27.89	55.82	2.5
202	1232	B	4	6	145	27.99	56.06	2.1
202	1232	B	4	7	10	28.06	56.24	1.5
202	1232	B	4	7	35	28.29	56.79	1.4
202	1232	B	5	1	5	28.45	57.19	2
202	1232	B	5	1	45	28.61	57.58	2.2
202	1232	B	5	1	80	28.83	58.11	1.5
202	1232	B	5	1	110	29.07	58.72	1.5
202	1232	B	5	1	135	29.28	59.24	1.7
202	1232	B	5	2	35	29.58	59.98	2
202	1232	B	5	3	30	30.67	62.65	2.4
202	1232	B	5	3	80	31.01	63.49	2.5
202	1232	B	5	3	110	31.15	63.83	2.5
202	1232	B	5	3	130	31.25	64.07	2.6
202	1232	B	5	4	15	31.53	64.76	2.5
202	1232	B	5	4	35	31.59	64.92	2.3
202	1232	B	5	4	70	31.75	65.32	1.6
202	1232	B	5	4	90	31.9	65.68	1.4
202	1232	B	5	4	115	32.07	66.09	1.4
202	1232	B	5	4	140	32.28	66.54	1.6
202	1232	B	5	5	25	32.59	67.22	1.8
202	1232	B	5	6	10	33.64	69.49	2.6
202	1232	B	6	3	50	37.78	78.46	2.1
202	1232	B	6	3	135	38.39	79.79	2.4
202	1232	B	7	5	20	45.53	95.27	1.8
202	1232	B	7	6	65	46.88	98.19	2.3
202	1232	B	8	1	45	48.48	101.65	1.9
202	1232	B	8	3	30	50.39	105.79	1.4
202	1232	B	8	3	70	50.5	106.04	1.6
202	1232	B	8	3	100	50.62	106.29	2
202	1232	B	9	1	75	53.54	112.62	1.7
202	1232	B	9	2	98	53.98	113.58	1.7
202	1232	B	9	2	110	54	113.6	1.7
202	1232	B	9	3	20	54.36	113.99	1.3
202	1232	B	9	3	65	54.5	114.13	0.8
202	1232	B	9	3	90	54.94	114.31	1.5
202	1232	B	9	3	130	54.9	114.56	1.7
202	1232	B	9	4	20	55.15	114.82	1.8
202	1232	B	9	4	35	55.24	114.92	2.1
202	1232	B	9	4	100	55.61	115.31	1.8
202	1232	B	9	4	135	55.77	115.48	0.7
202	1232	B	9	5	15	55.97	115.69	1.5
202	1232	B	9	5	110	56.7	116.47	1.7
202	1232	B	9	6	5	56.99	116.77	1
202	1232	B	10	1	15	58.34	118.2	1.5
202	1232	B	10	1	45	58.54	118.42	1.6
202	1232	B	10	1	85	58.74	118.63	1
202	1232	B	10	2	25	59.32	119.24	0.7
202	1232	B	10	2	75	59.67	119.62	1.7
202	1232	B	10	2	100	59.83	119.79	1.3
202	1232	B	10	2	140	60.23	120.21	0.6
202	1232	B	10	3	50	60.63	128.18	2.1
202	1232	B	10	3	60	60.69	129.25	2.2
202	1232	B	10	3	75	60.79	129.5	2.2
202	1232	B	10	3	105	61.05	130.15	2.2
202	1232	B	10	4	20	61.7	131.79	2.5
202	1232	B	10	4	40	61.86	132.17	2.4
202	1232	B	10	4	75	62.19	132.99	2.4
202	1232	B	10	4	115	62.59	133.98	2.4
202	1232	B	10	5	10	63.01	135.03	2.2
202	1232	B	10	5	40	63.25	135.65	2.1
202	1232	B	10	5	85	63.7	136.77	2.6
202	1232	B	10	5	115	63.92	137.32	2.5
202	1232	B	10	5	145	64.09	137.73	2.1
202	1232	B	10	6	20	64.26	138.16	2.8
202	1232	B	10	6	65	64.56	138.91	2.5
202	1232	B	10	6	115	64.88	139.71	2.7
202	1232	B	10	6	135	65.04	140.1	2
202	1232	B	10	7	30	65.36	140.9	2.1
202	1232	B	10	7	60	65.5	141.24	2.2

II

II   Turbiditic layers recorded in the sediments at ODP Site 1232

Leg	Site	Hole	Core	Section	Turbidite top (cm)	Original depth turbidite top (mcd)	Turbidite thickness (cm)	Corrected depth (mccd)	Age (kyr BP)	Turbidite recurrence time (yr)
202	1232	C	1	1	11.4	0.114	2.15	0.114	1.7	1699
202	1232	C	1	1	16.6	0.166	3.01	0.145	3.07	1373
202	1232	C	1	1	24.1	0.241	4.14	0.189	5.09	2017
202	1232	C	1	1	28.8	0.288	1.05	0.195	5.32	230
202	1232	C	1	1	35.5	0.355	1.28	0.252	7.9	2576
202	1232	C	1	1	37.9	0.379	1.82	0.263	8.39	491
202	1232	C	1	1	41.5	0.415	3.1	0.280	9.17	788
202	1232	C	1	1	46.4	0.464	1.53	0.299	10.02	842
202	1232	C	1	1	48.5	0.485	2.31	0.304	10.26	248
202	1232	C	1	1	51.9	0.519	0.94	0.315	10.76	495
202	1232	C	1	1	55.0	0.550	2.06	0.337	11.73	973
202	1232	C	1	1	58.7	0.587	1.99	0.353	12.47	738
202	1232	C	1	1	64.0	0.640	1.04	0.386	13.94	1468
202	1232	C	1	1	65.6	0.656	1.57	0.392	14.22	284
202	1232	C	1	1	67.8	0.678	0.84	0.398	14.49	270
202	1232	C	1	1	71.6	0.716	1.93	0.428	15.84	1346
202	1232	C	1	1	76.9	0.769	1.54	0.461	17.32	1486
202	1232	C	1	1	83.0	0.830	1.48	0.507	18.07	746
202	1232	C	1	1	87.4	0.874	1.22	0.536	18.1	28
202	1232	C	1	1	89.9	0.899	1.36	0.549	18.11	13
202	1232	C	1	1	93.2	0.932	1.64	0.568	18.13	19
202	1232	C	1	1	122.8	1.228	2.8	0.848	18.41	277
202	1232	C	1	1	130.3	1.303	3.84	0.895	18.45	46
202	1232	C	1	2	19.7	1.707	7.93	1.260	18.82	362
202	1232	C	1	2	67.7	2.187	8.38	1.661	19.21	397
202	1232	C	1	3	23.0	2.950	0.41	2.340	19.88	672
202	1232	C	1	3	24.5	2.965	0.88	2.351	19.89	11
202	1232	C	1	3	45.4	3.174	0.82	2.552	20.09	198
202	1232	C	1	4	2.8	3.418	3.1	2.787	20.33	233
202	1232	C	1	4	14.8	3.538	3.49	2.877	20.41	89
202	1232	B	1	2	5.5	3.795	3.38	3.099	20.68	265
202	1232	B	1	2	11.9	3.859	1.65	3.129	20.72	43
202	1232	B	1	2	52.8	4.268	4.81	3.521	21.28	554
202	1232	B	1	2	78.1	4.521	3.36	3.726	21.57	290
202	1232	B	1	2	87.3	4.613	1.84	3.785	21.65	84
202	1232	B	1	2	101.2	4.752	3.57	3.905	21.82	170
202	1232	B	1	2	118.1	4.921	4.79	4.038	22.01	188
202	1232	B	1	2	140.8	5.148	15.55	4.217	22.26	253
202	1232	B	1	3	27.6	5.526	7.49	4.440	22.58	316
202	1232	B	1	3	66.6	5.916	7.91	4.755	23.02	445
202	1232	B	1	3	97.3	6.223	4.48	4.983	23.22	195
202	1232	B	1	3	129.0	6.540	9.1	5.256	23.45	228
202	1232	B	1	4	3.9	6.789	2.51	5.413	23.58	132
202	1232	B	1	4	100.0	7.750	3.14	6.349	24.36	786
202	1232	B	1	5	52.4	8.774	5.77	7.342	25.2	833
202	1232	B	1	5	81.6	9.066	3.76	7.576	25.39	196
202	1232	B	1	5	94.3	9.193	1.47	7.666	25.47	75
202	1232	B	1	5	105.7	9.307	2.88	7.765	25.55	83
202	1232	B	1	5	129.6	9.546	7.43	7.975	25.73	177
202	1232	B	1	5	143.6	9.686	3.5	8.040	25.78	55
202	1232	C	2	3	43.2	10.292	4.18	8.611	26.26	479
202	1232	C	2	3	48.7	10.347	3.2	8.625	26.27	12
202	1232	C	2	3	64.8	10.508	7.27	8.754	26.38	108
202	1232	C	2	3	82.2	10.682	3.62	8.855	26.47	84
202	1232	C	2	3	103.5	10.895	9.5	9.032	26.61	149
202	1232	C	2	3	118.0	11.040	2.27	9.082	26.66	42
202	1232	C	2	4	2.6	11.386	7.42	9.406	26.93	272
202	1232	C	2	4	28.3	11.643	3	9.588	27.08	153
202	1232	C	2	4	59.0	11.950	5.2	9.865	27.31	232
202	1232	C	2	4	66.0	12.020	7.97	9.883	27.33	15
202	1232	C	2	4	122.6	12.586	15.43	10.370	27.74	409
202	1232	C	2	5	2.6	12.886	2.4	10.515	27.86	122
202	1232	C	2	5	8.6	12.946	3.98	10.551	27.89	30
202	1232	C	2	5	13.0	12.990	3.04	10.555	27.89	4
202	1232	C	2	5	28.0	13.140	8.66	10.675	27.94	43
202	1232	C	2	5	29.8	13.158	7.48	10.606	27.96	21
202	1232	C	2	5	39.8	13.258	0.72	10.632	27.99	36
202	1232	C	2	5	45.0	13.310	2.13	10.676	27.99	1
202	1232	C	2	5	70.7	13.567	2.98	10.912	28.19	198

continuation of table II

202	1232	C	2	5	75.0	13.610	6.13	10.925	28.2	11
202	1232	B	2	2	29.9	13.789	3.83	11.043	28.3	99
202	1232	B	2	2	49.1	13.981	7.13	11.197	28.43	129
202	1232	B	2	2	65.7	14.147	1.41	11.291	28.51	79
202	1232	B	2	2	96.5	14.455	8.71	11.585	28.76	247
202	1232	B	2	2	110.9	14.599	2.25	11.642	28.8	48
202	1232	B	2	2	124.1	14.731	4.11	11.752	28.91	101
202	1232	B	2	2	139.3	14.883	7.27	11.862	29.01	104
202	1232	B	2	3	1.1	14.991	1.32	11.898	29.04	34
202	1232	B	2	3	15.6	15.136	10.29	12.030	29.17	123
202	1232	B	2	3	33.4	15.314	7.86	12.105	29.24	70
202	1232	B	2	3	54.1	15.521	7.39	12.233	29.36	120
202	1232	B	2	3	71.4	15.694	11.79	12.332	29.45	93
202	1232	B	2	3	91.2	15.892	1.56	12.412	29.52	75
202	1232	B	2	3	97.0	15.950	5.9	12.455	29.56	40
202	1232	B	2	3	106.3	16.043	4.37	12.488	29.6	32
202	1232	B	2	3	115.7	16.137	2.02	12.539	29.64	48
202	1232	B	2	3	132.1	16.301	2.06	12.682	29.78	134
202	1232	B	2	4	4.9	16.519	10.78	12.880	29.96	185
202	1232	B	2	4	18.8	16.658	3.48	12.911	29.99	29
202	1232	B	2	4	36.4	16.834	20.05	13.052	30.12	132
202	1232	B	2	4	73.0	17.200	10.81	13.218	30.28	156
202	1232	B	2	4	90.2	17.372	1.37	13.281	30.34	59
202	1232	B	2	4	99.1	17.461	2.8	13.357	30.41	71
202	1232	B	2	4	107.7	17.547	2.2	13.415	30.46	55
202	1232	B	2	4	118.5	17.655	4.44	13.501	30.54	81
202	1232	B	2	4	144.2	17.912	9.16	13.714	30.74	199
202	1232	B	2	5	14.9	18.119	0.79	13.829	30.85	109
202	1232	B	2	5	18.8	18.158	8.45	13.860	30.88	29
202	1232	B	2	5	31.7	18.287	4.88	13.905	30.92	42
202	1232	B	2	5	44.0	18.410	5.17	13.979	30.99	69
202	1232	B	2	5	59.2	18.562	6.11	14.079	31.09	94
202	1232	B	2	5	91.2	18.882	8.72	14.339	31.33	243
202	1232	B	2	5	112.6	19.096	5.85	14.465	31.45	119
202	1232	B	2	5	130.6	19.276	3.81	14.587	31.56	114
202	1232	B	2	6	0.7	19.477	3.52	14.750	31.71	153
202	1232	C	3	2	18.4	19.674	10.48	14.911	31.87	151
202	1232	C	3	2	55.5	20.045	20.65	15.177	32.11	249
202	1232	C	3	2	77.8	20.268	4.23	15.193	32.13	15
202	1232	C	3	2	97.7	20.467	1.33	15.351	32.28	147
202	1232	C	3	2	111.7	20.607	9	15.477	32.4	118
202	1232	C	3	2	133.5	20.825	22.24	15.606	32.52	120
202	1232	C	3	3	14.4	21.134	2.56	15.692	32.6	81
202	1232	C	3	3	19.2	21.182	3.96	15.715	32.62	21
202	1232	C	3	3	34.5	21.335	1.6	15.827	32.72	106
202	1232	C	3	3	51.3	21.503	10.7	15.980	32.87	143
202	1232	C	3	3	82.1	21.811	18.7	16.181	33.06	189
202	1232	C	3	3	111.1	22.101	7.97	16.284	33.15	96
202	1232	C	3	3	127.4	22.264	3.15	16.367	33.23	78
202	1232	C	3	3	133.6	22.326	3.17	16.397	33.26	28
202	1232	C	3	3	140.7	22.397	3.1	16.437	33.3	37
202	1232	B	3	2	4.8	23.338	4.48	17.347	34.15	852
202	1232	B	3	2	14.4	23.434	4.33	17.398	34.2	48
202	1232	B	3	2	23.0	23.520	5.82	17.441	34.24	40
202	1232	B	3	2	38.1	23.671	5.1	17.534	34.32	87
202	1232	B	3	2	50.1	23.791	9.22	17.602	34.43	106
202	1232	B	3	2	67.5	23.965	4.78	17.685	34.57	145
202	1232	B	3	2	80.4	24.094	1.62	17.766	34.72	143
202	1232	B	3	2	90.1	24.191	8.28	17.846	34.86	141
202	1232	B	3	2	99.7	24.287	2.83	17.859	34.88	22
202	1232	B	3	2	104.4	24.334	3.16	17.878	34.91	34
202	1232	B	3	2	113.7	24.427	4.13	17.939	35.02	107
202	1232	B	3	2	125.7	24.547	3.69	18.018	35.16	138
202	1232	B	3	2	144.0	24.730	9.28	18.164	35.42	257
202	1232	B	3	3	9.7	24.897	1.02	18.238	35.55	131
202	1232	B	3	3	16.6	24.966	6.45	18.297	35.65	103
202	1232	B	3	3	29.2	25.092	19.02	18.358	35.76	108
202	1232	B	3	3	51.9	25.319	2.43	18.396	35.82	66
202	1232	B	3	3	62.2	25.422	20.96	18.474	35.96	138
202	1232	B	3	3	88.3	25.683	3.39	18.526	36.05	90
202	1232	B	3	3	102.3	25.823	15.8	18.632	36.24	187
202	1232	B	3	3	134.8	26.148	30.91	18.799	36.53	294
202	1232	B	3	4	33.4	26.644	5.27	18.986	36.86	328
202	1232	B	3	4	51.3	26.823	6.94	19.112	37.08	221
202	1232	B	3	4	61.0	26.920	3.17	19.139	37.13	49
202	1232	B	3	4	69.5	27.005	3.95	19.193	37.22	94
202	1232	B	3	4	80.3	27.113	8.06	19.261	37.34	120
202	1232	B	3	4	89.3	27.203	2.8	19.270	37.36	16

IV

continuation of table II

202	1232	B	3	4	118.6	27.496	6.02	19.536	37.83	467
202	1232	B	3	4	136.9	27.679	5.84	19.659	38.04	216
202	1232	B	3	5	20.8	28.028	4.83	19.949	38.55	511
202	1232	B	3	5	28.7	28.107	3.14	19.980	38.61	54
202	1232	B	3	5	36.5	28.185	1.53	20.027	38.69	82
202	1232	B	3	5	48.7	28.307	3.94	20.133	38.88	187
202	1232	B	3	5	72.0	28.540	11.65	20.326	39.22	340
202	1232	B	3	5	90.6	28.726	18.86	20.396	39.34	123
202	1232	B	3	5	113.7	28.957	2.26	20.438	39.41	74
202	1232	B	3	5	120.6	29.026	6.45	20.485	39.5	82
202	1232	B	3	5	127.4	29.094	1.76	20.489	39.5	7
202	1232	B	3	5	132.9	29.149	4.39	20.526	39.57	65
202	1232	B	3	5	141.1	29.231	3.77	20.564	39.63	67
202	1232	B	3	6	0.5	29.335	2.85	20.631	39.75	118
202	1232	B	3	6	12.1	29.451	19.65	20.718	39.9	153
202	1232	B	3	6	45.2	29.782	6.7	20.853	40.14	237
202	1232	B	3	6	58.4	29.914	10.52	20.917	40.26	114
202	1232	B	3	6	71.3	30.043	3.78	20.941	40.3	42
202	1232	B	3	6	78.6	30.116	6.26	20.977	40.36	63
202	1232	B	3	6	101.1	30.341	7.94	21.138	40.64	284
202	1232	C	4	1	110.6	30.526	6.69	21.244	40.83	186
202	1232	C	4	1	126.5	30.685	3.3	21.336	40.99	162
202	1232	C	4	1	131.9	30.739	10	21.358	41.03	37
202	1232	C	4	2	0.9	30.929	1.8	21.448	41.19	158
202	1232	C	4	2	7.4	30.994	2.28	21.494	41.27	82
202	1232	C	4	2	20.7	31.127	6.36	21.605	41.46	194
202	1232	C	4	2	34.1	31.261	5.46	21.675	41.59	123
202	1232	C	4	2	42.4	31.344	4.54	21.703	41.64	50
202	1232	C	4	2	54.5	31.465	4.15	21.780	41.77	134
202	1232	C	4	2	63.9	31.559	3.12	21.832	41.86	91
202	1232	C	4	2	76.3	31.683	1.1	21.924	42.02	163
202	1232	C	4	2	83.1	31.751	6.83	21.981	42.13	100
202	1232	C	4	2	90.4	31.824	10.51	21.986	42.13	9
202	1232	C	4	2	104.5	31.965	3.99	22.022	42.2	63
202	1232	C	4	2	110.0	32.020	4.21	22.037	42.22	26
202	1232	C	4	2	119.5	32.115	5.11	22.091	42.32	94
202	1232	C	4	2	136.6	32.286	11.08	22.210	42.53	211
202	1232	C	4	2	150.0	32.420	2.6	22.233	42.57	40
202	1232	C	4	3	9.7	32.527	10.13	22.314	42.71	142
202	1232	C	4	3	30.2	32.732	6.8	22.417	42.89	182
202	1232	C	4	3	37.9	32.809	0.77	22.426	42.91	16
202	1232	C	4	3	39.4	32.824	1.85	22.434	42.92	13
202	1232	C	4	3	50.7	32.937	7.44	22.528	43.09	166
202	1232	C	4	3	60.5	33.035	2.85	22.553	43.13	43
202	1232	C	4	3	74.0	33.170	7.19	22.659	43.32	186
202	1232	C	4	3	82.9	33.259	1.22	22.676	43.35	31
202	1232	C	4	3	87.7	33.307	5.26	22.711	43.41	62
202	1232	C	4	3	95.9	33.389	1.47	22.741	43.46	51
202	1232	C	4	3	100.4	33.434	1.65	22.771	43.51	54
202	1232	C	4	3	109.6	33.526	3.96	22.847	43.65	133
202	1232	C	4	3	114.2	33.572	1.84	22.854	43.66	12
202	1232	C	4	3	117.3	33.603	8.01	22.866	43.68	22
202	1232	C	4	3	127.2	33.702	2.22	22.884	43.71	32
202	1232	C	4	3	142.4	33.854	6.22	23.015	43.94	230
202	1232	C	4	4	12.6	34.066	5.28	23.165	44.21	263
202	1232	C	4	4	23.2	34.172	2.63	23.218	44.32	117
202	1232	C	4	4	28.2	34.222	0.71	23.241	44.38	57
202	1232	C	4	4	30.8	34.248	0.94	23.261	44.43	48
202	1232	C	4	4	35.6	34.296	5.42	23.298	44.52	93
202	1232	C	4	4	46.9	34.409	6.29	23.357	44.66	145
202	1232	C	4	4	60.6	34.546	6.91	23.431	44.85	182
202	1232	C	4	4	71.2	34.652	2.33	23.469	44.94	91
202	1232	C	4	4	75.3	34.693	1.64	23.486	44.98	43
202	1232	C	4	4	81.0	34.750	3.25	23.527	45.08	100
202	1232	C	4	4	89.2	34.832	3.55	23.576	45.2	121
202	1232	C	4	4	96.4	34.904	2.78	23.613	45.29	91
202	1232	C	4	4	102.8	34.968	2.19	23.650	45.38	90
202	1232	C	4	4	106.4	35.004	1.1	23.663	45.42	32
202	1232	C	4	4	120.6	35.146	8.78	23.794	45.74	323
202	1232	C	4	4	133.3	35.273	3.99	23.834	45.84	97
202	1232	C	4	4	140.7	35.347	2.57	23.868	45.92	84
202	1232	B	4	2	73.5	35.405	2.14	23.899	46	78
202	1232	B	4	2	80.0	35.470	3.91	23.944	46.11	109
202	1232	B	4	2	86.2	35.532	2.83	23.966	46.16	56
202	1232	B	4	2	91.8	35.588	3.46	23.994	46.23	69
202	1232	B	4	2	97.9	35.649	4.1	24.021	46.3	64
202	1232	B	4	2	104.5	35.715	2.55	24.045	46.36	60
202	1232	B	4	2	130.5	35.975	10.87	24.280	46.93	578

continuation of table II

202	1232	B	4	2	144.4	36.114	2.15	24.310	47.01	75
202	1232	B	4	3	1.4	36.194	1.69	24.369	47.15	143
202	1232	B	4	3	4.6	36.226	2.81	24.384	47.19	37
202	1232	B	4	3	9.3	36.273	3.82	24.402	47.24	46
202	1232	B	4	3	16.9	36.349	6.16	24.440	47.33	93
202	1232	B	4	3	23.9	36.419	3.78	24.449	47.35	21
202	1232	B	4	3	49.5	36.675	14.1	24.667	47.89	537
202	1232	B	4	3	67.1	36.851	4.06	24.702	47.97	85
202	1232	B	4	3	72.3	36.903	3.25	24.714	48	29
202	1232	B	4	3	77.3	36.953	4.11	24.731	48.04	42
202	1232	B	4	3	85.9	37.039	4.64	24.776	48.15	111
202	1232	B	4	3	96.5	37.145	4.23	24.836	48.3	147
202	1232	B	4	3	112.0	37.300	6.21	24.948	48.58	276
202	1232	B	4	3	123.7	37.417	9.68	25.003	48.71	136
202	1232	B	4	3	135.1	37.531	2.31	25.021	48.76	43
202	1232	B	4	4	10.0	37.780	3.8	25.247	49.31	556
202	1232	B	4	4	30.0	37.980	1.71	25.408	49.71	396
202	1232	B	4	4	53.1	38.211	1.47	25.623	50.24	528
202	1232	B	4	4	55.4	38.234	0.88	25.630	50.25	18
202	1232	B	4	4	65.6	38.336	7.05	25.723	50.48	230
202	1232	B	4	4	77.3	38.453	7.46	25.770	50.6	115
202	1232	B	4	4	84.9	38.529	2	25.772	50.6	4
202	1232	B	4	4	103.4	38.714	7.45	25.936	51.01	405
202	1232	B	4	4	118.6	38.866	4.24	26.014	51.2	192
202	1232	B	4	4	132.0	39.000	9.43	26.106	51.42	226
202	1232	B	4	4	147.6	39.156	6	26.167	51.57	150
202	1232	B	4	5	4.6	39.236	3.08	26.187	51.62	49
202	1232	B	4	5	11.3	39.303	1.63	26.223	51.71	88
202	1232	B	4	5	20.9	39.399	5.09	26.303	51.91	197
202	1232	B	4	5	34.4	39.534	4.68	26.387	52.12	206
202	1232	B	4	5	41.4	39.604	1.64	26.411	52.17	59
202	1232	B	4	5	44.4	39.634	4.55	26.424	52.21	32
202	1232	B	4	5	58.6	39.776	5.3	26.521	52.44	238
202	1232	B	4	5	68.6	39.876	6.46	26.568	52.56	116
202	1232	B	4	5	84.6	40.036	3.58	26.663	52.79	234
202	1232	B	4	5	97.2	40.162	1.86	26.754	53.02	223
202	1232	B	4	5	102.9	40.219	10.79	26.791	53.11	93
202	1232	B	4	5	121.9	40.409	5.88	26.874	53.31	204
202	1232	B	4	5	135.1	40.541	4.57	26.947	53.49	180
202	1232	B	4	5	145.2	40.642	10.77	27.002	53.63	136
202	1232	B	4	6	50.4	41.194	5.7	27.446	54.72	1092
202	1232	B	4	6	57.2	41.262	4.96	27.457	54.75	27
202	1232	B	4	6	64.5	41.335	1.43	27.481	54.81	59
202	1232	B	4	6	97.9	41.669	2.86	27.801	55.59	786
202	1232	B	4	6	102.5	41.715	5.28	27.818	55.64	44
202	1232	B	4	6	110.0	41.790	9.8	27.840	55.69	53
202	1232	B	4	6	132.3	42.013	10.16	27.965	56	308
202	1232	B	4	6	147.5	42.165	5.74	28.015	56.12	123
202	1232	B	4	7	4.0	42.240	3.14	28.034	56.17	45
202	1232	B	5	1	0.3	42.673	3.13	28.435	57.15	987
202	1232	B	5	1	6.6	42.736	4.99	28.467	57.23	78
202	1232	B	5	1	12.6	42.796	4.23	28.477	57.25	24
202	1232	B	5	1	23.0	42.900	2.24	28.539	57.41	153
202	1232	B	5	1	30.2	42.972	7.47	28.588	57.53	121
202	1232	B	5	1	38.6	43.056	5.16	28.597	57.55	23
202	1232	B	5	1	58.3	43.253	5.03	28.743	57.91	357
202	1232	B	5	1	65.6	43.326	6.21	28.766	57.97	57
202	1232	B	5	1	75.7	43.427	2.18	28.805	58.06	96
202	1232	B	5	1	85.9	43.529	3.87	28.884	58.26	196
202	1232	B	5	1	90.2	43.572	1.6	28.889	58.27	13
202	1232	B	5	1	127.1	43.941	3.69	29.241	59.14	866
202	1232	B	5	1	136.2	44.032	2.43	29.296	59.27	134
202	1232	B	5	1	141.4	44.084	1.33	29.324	59.34	68
202	1232	B	5	2	1.0	44.190	6.26	29.417	59.57	229
202	1232	B	5	2	8.3	44.263	3.4	29.427	59.59	25
202	1232	B	5	2	20.4	44.384	2.8	29.514	59.81	213
202	1232	B	5	2	29.8	44.478	3.17	29.579	59.97	162
202	1232	B	5	2	33.5	44.515	1.94	29.584	59.98	12
202	1232	B	5	2	75.8	44.938	5.35	29.988	60.97	993
202	1232	B	5	2	85.0	45.030	9.11	30.027	61.07	96
202	1232	B	5	2	131.5	45.495	9.8	30.401	61.99	919
202	1232	B	5	3	8.3	45.773	10.07	30.581	62.43	443
202	1232	B	5	3	22.3	45.913	2.86	30.620	62.53	97
202	1232	B	5	3	59.6	46.286	15.7	30.964	63.37	846
202	1232	B	5	3	85.0	46.540	12.2	31.062	63.61	240
202	1232	B	5	3	103.2	46.722	3.99	31.122	63.76	148
202	1232	B	5	3	117.8	46.868	10.42	31.228	64.02	261
202	1232	B	5	4	2.5	47.235	8.94	31.490	64.67	644

VI

continuation of table II

202	1232	B	5	4	18.1	47.391	7.49	31.557	64.83	165
202	1232	B	5	4	29.0	47.500	5.71	31.591	64.91	84
202	1232	B	5	4	40.2	47.612	11.26	31.646	65.05	135
202	1232	B	5	4	56.0	47.770	4.45	31.692	65.16	112
202	1232	B	5	4	62.9	47.839	3.32	31.716	65.22	59
202	1232	B	5	4	79.9	48.009	5.16	31.853	65.56	338
202	1232	B	5	4	95.3	48.163	1.75	31.955	65.81	251
202	1232	B	5	4	104.2	48.252	4.37	32.026	65.99	176
202	1232	B	5	4	112.1	48.331	2.16	32.062	66.07	88
202	1232	B	5	4	130.3	48.513	2.93	32.223	66.42	350
202	1232	B	5	4	136.5	48.575	1.45	32.256	66.49	71
202	1232	B	5	5	19.9	48.919	4.45	32.585	67.21	713
202	1232	B	5	5	54.5	49.265	4.77	32.886	67.86	652
202	1232	B	5	5	76.6	49.486	6.45	33.060	68.24	377
202	1232	B	5	5	85.0	49.570	2.21	33.079	68.28	41
202	1232	B	5	5	123.4	49.954	4.1	33.440	69.06	784
202	1232	B	5	5	133.1	50.051	8.66	33.497	69.19	123
202	1232	B	5	5	147.4	50.194	5.3	33.553	69.31	121
202	1232	B	5	6	19.2	50.422	5.65	33.728	69.69	381
202	1232	B	5	6	39.2	50.622	6.13	33.872	70	311
202	1232	B	5	6	47.8	50.708	2.96	33.896	70.05	53
202	1232	B	5	6	57.9	50.809	3.71	33.968	70.21	154
202	1232	B	5	6	66.6	50.896	3.9	34.018	70.31	110
202	1232	B	5	6	85.3	51.083	10.7	34.166	70.63	320
202	1232	B	5	6	101.7	51.247	3.5	34.222	70.76	122
202	1232	B	5	6	114.4	51.374	4.57	34.315	70.96	200
202	1232	B	5	6	121.2	51.442	3.1	34.337	71.01	49
202	1232	B	5	6	147.8	51.708	8.89	34.572	71.52	509
202	1232	B	5	7	32.4	52.064	2.23	34.839	72.09	579
202	1232	B	5	7	48.3	52.223	2.65	34.976	72.39	296
202	1232	B	6	1	12.4	52.344	4.41	35.070	72.59	204
202	1232	B	6	1	19.4	52.414	1.83	35.097	72.65	58
202	1232	B	6	1	27.4	52.494	4.65	35.158	72.78	132
202	1232	B	6	1	64.7	52.867	2.38	35.484	73.49	708
202	1232	B	6	1	130.8	53.528	2.76	36.122	74.87	1382
202	1232	B	6	2	33.8	54.068	8.13	36.634	75.98	1110
202	1232	B	6	2	42.5	54.155	2.6	36.640	76	13
202	1232	B	6	2	50.0	54.230	1.95	36.689	76.1	106
202	1232	B	6	2	88.2	54.612	8.59	37.052	76.89	786
202	1232	B	6	2	136.1	55.091	17.69	37.444	77.74	850
202	1232	B	6	3	7.6	55.316	3.49	37.492	77.84	105
202	1232	B	6	3	21.1	55.451	4.27	37.593	78.06	218
202	1232	B	6	3	29.6	55.536	2.5	37.635	78.15	91
202	1232	B	6	3	37.0	55.610	1.19	37.684	78.26	105
202	1232	B	6	3	41.0	55.650	2.58	37.712	78.32	62
202	1232	B	6	3	70.6	55.946	8.21	37.982	78.91	585
202	1232	B	6	3	85.2	56.092	4.26	38.046	79.04	138
202	1232	B	6	3	111.2	56.352	1.33	38.264	79.52	472
202	1232	B	6	3	113.2	56.372	4.3	38.270	79.53	14
202	1232	B	6	3	122.7	56.467	4.44	38.322	79.64	112
202	1232	B	6	3	131.0	56.550	0.99	38.360	79.73	83
202	1232	B	6	4	13.0	56.880	5.05	38.681	80.42	695
202	1232	B	6	4	30.6	57.056	6.2	38.807	80.69	272
202	1232	B	6	4	71.6	57.466	12.66	39.154	81.45	754
202	1232	B	6	4	102.0	57.770	17.16	39.331	81.83	384
202	1232	B	6	4	122.9	57.979	3.4	39.369	81.91	81
202	1232	B	6	4	131.3	58.063	4.51	39.419	82.02	108
202	1232	B	6	5	1.4	58.274	5.92	39.585	82.38	360
202	1232	B	6	5	9.8	58.358	8.26	39.610	82.43	54
202	1232	B	6	5	31.6	58.576	10.97	39.745	82.73	294
202	1232	B	6	5	74.5	59.005	5.57	40.065	83.42	692
202	1232	B	6	5	97.5	59.235	7.76	40.239	83.8	377
202	1232	B	6	5	119.7	59.457	3.6	40.383	84.11	314
202	1232	B	6	5	129.1	59.551	3.78	40.441	84.24	126
202	1232	B	6	5	148.2	59.742	4.15	40.594	84.57	332
202	1232	B	6	6	8.1	59.851	10.53	40.662	84.71	147
202	1232	B	6	6	22.8	59.998	3.5	40.704	84.8	91
202	1232	B	6	6	28.1	60.051	1.78	40.722	84.84	38
202	1232	B	6	6	30.4	60.074	2.99	40.726	84.85	10
202	1232	B	6	6	36.3	60.133	2.87	40.756	84.92	65
202	1232	B	6	6	48.2	60.252	0.95	40.846	85.11	194
202	1232	B	6	6	50.2	60.272	1.65	40.857	85.14	24
202	1232	B	6	6	52.4	60.294	4.91	40.862	85.15	11
202	1232	B	6	6	62.9	60.399	4.18	40.918	85.27	121
202	1232	B	6	6	81.3	60.583	12.46	41.060	85.58	309
202	1232	B	6	6	103.9	60.809	4.69	41.162	85.8	220
202	1232	B	6	6	124.8	61.018	3.35	41.324	86.15	351
202	1232	B	6	6	129.3	61.063	10.22	41.335	86.17	25

continuation of table II

202	1232	B	6	6	145.3	61.223	3.43	41.393	86.3	126
202	1232	B	6	7	17.9	61.459	16.19	41.595	86.74	437
202	1232	B	6	7	37.5	61.655	2.87	41.629	86.81	74
202	1232	B	6	7	48.6	61.766	1.31	41.711	86.99	178
202	1232	B	6	7	52.9	61.809	1.05	41.741	87.05	65
202	1232	B	7	1	4.2	61.902	2.61	41.823	87.23	178
202	1232	B	7	1	8.3	61.943	9.23	41.838	87.26	33
202	1232	B	7	1	24.3	62.103	6.69	41.906	87.41	147
202	1232	B	7	1	44.7	62.307	5.73	42.043	87.71	297
202	1232	B	7	1	53.6	62.396	2.49	42.075	87.78	70
202	1232	B	7	1	68.6	62.546	1.91	42.200	88.05	270
202	1232	B	7	1	89.9	62.759	14.14	42.394	88.47	420
202	1232	B	7	1	110.1	62.961	6.3	42.455	88.6	132
202	1232	B	7	1	125.6	63.116	6.02	42.546	88.8	199
202	1232	B	7	1	136.4	63.224	3.3	42.595	88.9	105
202	1232	B	7	2	0.0	63.380	14.59	42.717	89.17	266
202	1232	B	7	2	23.0	63.610	2.64	42.801	89.35	182
202	1232	B	7	2	31.3	63.693	3.11	42.858	89.47	123
202	1232	B	7	2	35.1	63.731	3.23	42.865	89.49	15
202	1232	B	7	2	43.0	63.810	4.23	42.912	89.59	101
202	1232	B	7	2	57.0	63.950	12.92	43.010	89.8	212
202	1232	B	7	2	89.8	64.278	7.65	43.208	90.23	431
202	1232	B	7	2	103.6	64.416	3.83	43.270	90.37	134
202	1232	B	7	2	123.9	64.619	2.08	43.435	90.72	357
202	1232	B	7	2	128.7	64.667	9.56	43.462	90.78	58
202	1232	B	7	3	1.9	64.909	3.76	43.608	91.1	318
202	1232	B	7	3	11.0	65.000	1.24	43.661	91.21	114
202	1232	B	7	3	16.9	65.059	17.28	43.708	91.31	101
202	1232	B	7	3	39.4	65.284	6.45	43.760	91.43	113
202	1232	B	7	3	48.2	65.372	1.74	43.784	91.48	52
202	1232	B	7	3	57.7	65.467	7.45	43.861	91.65	168
202	1232	B	7	3	79.3	65.683	6.76	44.003	91.95	308
202	1232	B	7	3	102.9	65.919	9.97	44.172	92.32	365
202	1232	B	7	3	117.9	66.069	1.29	44.222	92.43	109
202	1232	B	7	3	129.7	66.187	10.38	44.327	92.66	227
202	1232	B	7	4	2.7	66.427	2.63	44.463	92.95	296
202	1232	B	7	4	18.2	66.582	9.85	44.592	93.23	279
202	1232	B	7	4	38.2	66.782	8.06	44.693	93.45	219
202	1232	B	7	4	57.3	66.973	11.99	44.803	93.69	238
202	1232	B	7	4	75.1	67.151	2.77	44.862	93.82	127
202	1232	B	7	4	92.1	67.321	8.48	45.004	94.12	308
202	1232	B	7	4	112.1	67.521	5.91	45.119	94.37	249
202	1232	B	7	4	130.8	67.708	7.75	45.247	94.65	279
202	1232	B	7	5	5.7	67.967	4.02	45.428	95.04	393
202	1232	B	7	5	24.0	68.150	17.17	45.571	95.35	309
202	1232	B	7	5	56.8	68.478	3.86	45.728	95.69	339
202	1232	B	7	5	75.5	68.665	6.62	45.876	96.01	322
202	1232	B	7	5	97.0	68.880	8.85	46.025	96.34	321
202	1232	B	7	5	121.6	69.126	11.16	46.183	96.68	342
202	1232	B	7	6	0.4	69.414	3.75	46.359	97.06	382
202	1232	B	7	6	17.4	69.584	1.91	46.491	97.35	287
202	1232	B	7	6	56.4	69.974	6.61	46.862	98.15	804
202	1232	B	7	6	76.8	70.178	5.36	47.000	98.45	299
202	1232	B	7	6	99.4	70.404	21.76	47.172	98.82	372
202	1232	B	7	7	54.9	71.479	3.21	48.030	100.68	1859
202	1232	B	8	1	84.7	72.357	13.08	48.875	102.51	1833
202	1232	B	8	1	108.6	72.596	8.34	48.983	102.75	235
202	1232	B	8	1	124.2	72.752	1.71	49.056	102.91	157
202	1232	B	8	2	34.1	73.371	26.11	49.678	104.25	1348
202	1232	B	8	2	61.3	73.643	1.78	49.689	104.28	23
202	1232	B	8	2	77.5	73.805	3.83	49.833	104.59	313
202	1232	B	8	2	91.6	73.946	8.7	49.936	104.81	223
202	1232	B	8	2	132.1	74.351	8.23	50.254	105.5	689
202	1232	B	8	2	141.4	74.444	2.8	50.264	105.52	22
202	1232	B	8	2	149.3	74.523	7.08	50.316	105.64	112
202	1232	B	8	3	9.3	74.643	11.64	50.345	105.7	64
202	1232	B	8	3	22.6	74.776	5.03	50.362	105.74	36
202	1232	B	8	3	33.9	74.889	14.37	50.424	105.87	134
202	1232	B	8	3	54.1	75.091	12.94	50.482	106	126
202	1232	B	8	3	68.9	75.239	2.91	50.502	106.04	42
202	1232	B	8	3	74.7	75.297	5.28	50.531	106.1	63
202	1232	B	8	3	84.9	75.399	6.78	50.579	106.21	105
202	1232	B	8	3	93.8	75.488	4.53	50.600	106.25	46
202	1232	B	8	3	101.9	75.569	4.24	50.636	106.33	78
202	1232	B	8	3	108.9	75.639	4.63	50.664	106.39	59
202	1232	B	8	3	116.4	75.714	6.96	50.692	106.45	62
202	1232	B	8	3	125.4	75.804	1.71	50.713	106.5	45
202	1232	B	8	3	129.3	75.843	3.21	50.735	106.54	47

VIII

continuation of table II

202	1232	B	8	3	134.0	75.890	2.28	50.750	106.58	33
202	1232	B	8	4	6.8	76.138	2.5	50.975	107.06	487
202	1232	B	8	4	15.8	76.228	4.87	51.040	107.21	141
202	1232	B	8	4	31.7	76.387	2.04	51.150	107.44	239
202	1232	B	8	4	65.6	76.726	1.15	51.469	108.14	691
202	1232	B	8	4	72.9	76.799	5.35	51.531	108.27	134
202	1232	B	8	4	85.0	76.920	4.76	51.598	108.41	145
202	1232	B	8	4	98.8	77.058	1.22	51.688	108.61	195
202	1232	B	8	4	102.4	77.094	4.29	51.712	108.66	52
202	1232	B	8	4	109.9	77.169	3.93	51.745	108.73	70
202	1232	B	8	4	146.8	77.538	2.33	52.074	109.45	713
202	1232	B	8	5	7.7	77.667	6.59	52.179	109.67	229
202	1232	B	8	5	39.5	77.985	10.05	52.432	110.22	547
202	1232	B	8	5	54.3	78.133	5.73	52.479	110.33	104
202	1232	B	8	5	61.4	78.204	2.64	52.492	110.35	28
202	1232	B	8	5	69.2	78.282	2.91	52.544	110.47	112
202	1232	B	8	5	75.0	78.340	6.13	52.573	110.53	63
202	1232	B	8	5	82.9	78.419	5.45	52.591	110.57	38
202	1232	B	8	5	89.9	78.489	1.61	52.607	110.6	35
202	1232	B	8	5	96.4	78.554	3.49	52.655	110.71	104
202	1232	B	8	5	105.4	78.644	1.69	52.710	110.83	120
202	1232	B	8	5	112.6	78.716	4.08	52.766	110.95	121
202	1232	B	8	5	118.7	78.777	3.01	52.786	110.99	43
202	1232	B	8	6	4.6	78.836	7.87	52.815	111.05	63
202	1232	B	8	6	21.5	79.005	3.68	52.905	111.25	194
202	1232	B	8	6	34.9	79.139	1.43	53.002	111.46	212
202	1232	B	9	1	45.0	79.620	19.74	53.469	112.47	1010
202	1232	B	9	1	65.8	79.828	3.56	53.479	112.49	23
202	1232	B	9	1	79.2	79.962	5.17	53.578	112.71	214
202	1232	B	9	1	94.1	80.111	1.39	53.675	112.92	212
202	1232	B	9	2	101.1	81.691	6.71	53.991	113.59	102
202	1232	B	9	2	108.9	81.769	3.45	54.002	113.6	12
202	1232	B	9	2	120.3	81.883	10.03	54.082	113.69	85
202	1232	B	9	2	134.2	82.022	4.16	54.120	113.73	40
202	1232	B	9	2	139.0	82.070	2.6	54.127	113.73	7
202	1232	B	9	2	142.3	82.103	1.64	54.134	113.74	7
202	1232	B	9	2	149.4	82.174	4.09	54.189	113.8	58
202	1232	B	9	3	28.4	82.474	18.44	54.448	114.07	275
202	1232	B	9	3	48.3	82.673	8.34	54.462	114.09	15
20	1232	B	9	3	58.5	82.775	4.41	54.482	114.11	20
202	1232	B	9	3	72.7	82.917	2.72	54.579	114.21	103
202	1232	B	9	3	83.3	83.023	5.27	54.658	114.3	84
202	1232	B	9	3	93.9	83.129	5.06	54.711	114.35	56
202	1232	B	9	3	109.0	83.280	1.57	54.812	114.46	107
202	1232	B	9	3	113.1	83.321	5.62	54.837	114.49	27
202	1232	B	9	3	122.3	83.413	4.62	54.872	114.52	37
202	1232	B	9	3	140.3	83.593	5.83	55.006	114.67	142
202	1232	B	9	4	1.3	83.723	1.16	55.078	114.74	76
202	1232	B	9	4	5.9	83.769	5.81	55.113	114.78	37
202	1232	B	9	4	14.1	83.851	4.42	55.136	114.8	25
202	1232	B	9	4	26.4	83.974	5.96	55.215	114.89	83
202	1232	B	9	4	39.2	84.102	2.42	55.284	114.96	73
202	1232	B	9	4	42.8	84.138	3.25	55.295	114.97	12
202	1232	B	9	4	58.1	84.291	7.72	55.416	115.1	128
202	1232	B	9	4	69.6	84.406	4.8	55.454	115.14	40
202	1232	B	9	4	80.0	84.510	4.12	55.510	115.2	59
202	1232	B	9	4	90.3	84.613	5.42	55.571	115.27	65
202	1232	B	9	4	102.4	84.734	4.29	55.638	115.34	71
202	1232	B	9	4	111.6	84.826	9.18	55.688	115.39	53
202	1232	B	9	4	124.2	84.952	6.51	55.721	115.43	36
202	1232	B	9	4	135.6	85.066	2.28	55.770	115.48	52
202	1232	B	9	5	0.1	85.241	10.12	55.923	115.64	162
202	1232	B	9	5	55.2	85.792	10.4	56.373	116.12	477
202	1232	B	9	5	78.9	86.029	3.22	56.505	116.26	141
202	1232	B	9	5	83.2	86.072	1.91	56.516	116.27	12
202	1232	B	9	5	86.9	86.109	4.39	56.534	116.29	19
202	1232	B	9	5	102.1	86.261	1.77	56.643	116.4	115
202	1232	B	9	5	115.9	86.399	2.66	56.763	116.53	127
202	1232	B	9	5	123.8	86.478	3.28	56.815	116.58	55
202	1232	B	9	5	133.7	86.577	3.98	56.881	116.65	70
202	1232	B	9	5	138.8	86.628	1.08	56.892	116.67	12
202	1232	B	9	5	145.8	86.698	2.54	56.951	116.73	63
202	1232	B	9	5	148.9	86.729	1.67	56.957	116.74	6
202	1232	B	9	6	1.4	86.764	2.49	56.976	116.76	20
202	1232	B	9	6	12.0	86.870	4.71	57.056	116.84	85
202	1232	B	9	6	19.9	86.949	7.25	57.089	116.87	34
202	1232	B	9	6	30.4	87.054	8.77	57.121	116.91	34
202	1232	B	9	6	42.9	87.179	5.77	57.159	116.95	40

continuation of table II

202	1232	B	9	6	53.9	87.289	1.41	57.211	117	55
202	1232	B	9	6	56.6	87.316	3.62	57.223	117.02	13
202	1232	B	9	6	62.3	87.373	5.89	57.244	117.04	22
202	1232	B	9	6	74.2	87.492	5.15	57.304	117.1	63
202	1232	B	9	6	82.3	87.573	7.31	57.334	117.13	32
202	1232	B	9	6	91.3	87.663	3.81	57.351	117.15	18
202	1232	B	9	6	96.1	87.711	1.64	57.361	117.16	11
202	1232	B	9	6	101.6	87.766	5.4	57.400	117.2	41
202	1232	B	9	6	140.3	88.153	4.61	57.732	117.56	352
202	1232	B	9	6	146.9	88.219	1.98	57.752	117.58	21
202	1232	B	9	7	14.9	88.399	8.45	57.913	117.75	170
202	1232	B	9	7	27.0	88.520	2.86	57.949	117.79	39
202	1232	B	9	7	31.2	88.562	4.65	57.963	117.8	14
202	1232	B	9	7	42.7	88.677	4.23	58.031	117.87	72
202	1232	B	9	7	63.2	88.882	6.29	58.193	118.05	172
202	1232	B	10	1	6.2	89.072	7.24	58.321	118.18	135
202	1232	B	10	1	17.8	89.188	2.73	58.364	118.23	46
202	1232	B	10	1	23.5	89.245	1.19	58.393	118.26	31
202	1232	B	10	1	29.8	89.308	3.15	58.445	118.31	55
202	1232	B	10	1	40.3	89.413	2.4	58.518	118.39	77
202	1232	B	10	1	46.7	89.477	10.74	58.559	118.43	43
202	1232	B	10	1	58.0	89.590	1.16	58.564	118.44	6
202	1232	B	10	1	63.3	89.643	3.17	58.606	118.48	44
202	1232	B	10	1	69.1	89.701	3.27	58.631	118.51	27
202	1232	B	10	1	82.0	89.830	1.86	58.729	118.61	103
202	1232	B	10	1	88.1	89.891	2.44	58.771	118.66	45
202	1232	B	10	1	92.2	89.932	4.61	58.787	118.68	18
202	1232	B	10	1	97.2	89.982	1.31	58.791	118.68	4
202	1232	B	10	1	101.0	90.020	1.99	58.816	118.71	27
202	1232	B	10	1	105.9	90.069	2.51	58.845	118.74	31
202	1232	B	10	1	111.0	90.120	3.01	58.871	118.76	28
202	1232	B	10	1	126.2	90.272	0.73	58.993	118.89	129
202	1232	B	10	1	127.7	90.287	1.43	59.001	118.9	8
202	1232	B	10	1	130.4	90.314	2.64	59.013	118.92	13
202	1232	B	10	2	2.8	90.558	3.35	59.231	119.15	231
202	1232	B	10	2	9.1	90.621	6.88	59.261	119.18	31
202	1232	B	10	2	17.1	90.701	3.54	59.272	119.19	12
202	1232	B	10	2	30.9	90.839	6.11	59.374	119.3	108
202	1232	B	10	2	38.9	90.919	3.67	59.393	119.32	21
202	1232	B	10	2	52.6	91.056	4.44	59.493	119.42	106
202	1232	B	10	2	78.5	91.315	5.27	59.708	119.65	228
202	1232	B	10	2	90.0	91.430	3.65	59.770	119.72	65
202	1232	B	10	3	4.7	92.087	2.13	60.391	123.36	3638
202	1232	B	10	3	8.9	92.129	6.75	60.411	123.76	407
202	1232	B	10	3	30.7	92.347	12.3	60.562	126.79	3026
202	1232	B	10	3	51.8	92.558	4.67	60.650	128.54	1752
202	1232	B	10	3	68.9	92.729	5.02	60.774	129.47	932
202	1232	B	10	3	97.3	93.013	3.86	61.008	130.05	582
202	1232	B	10	4	8.5	93.655	2.38	61.611	131.56	1503
202	1232	B	10	4	35.3	93.923	4.41	61.855	132.17	608
202	1232	B	10	4	69.4	94.264	2.33	62.153	132.91	740
202	1232	B	10	4	139.0	94.960	1.35	62.825	134.58	1675
202	1232	B	10	5	5.1	95.131	2.6	62.983	134.97	393
202	1232	B	10	5	33.5	95.415	5.25	63.241	135.62	643
202	1232	B	10	5	92.3	96.003	3.33	63.776	136.95	1333
202	1232	B	10	5	108.1	96.161	4.55	63.901	137.26	311
202	1232	B	10	5	125.4	96.334	8.99	64.028	137.58	316
202	1232	B	10	5	137.9	96.459	4.45	64.063	137.67	88
202	1232	B	10	6	5.4	96.654	7.17	64.214	138.04	375
202	1232	B	10	6	16.2	96.762	2.59	64.250	138.13	90
202	1232	B	10	6	32.7	96.927	9.8	64.389	138.48	347
202	1232	B	10	6	59.4	97.194	5.22	64.558	138.9	421
202	1232	B	10	6	77.3	97.373	12.03	64.685	139.21	316
202	1232	B	10	6	107.5	97.675	5.79	64.867	139.67	452
202	1232	B	10	6	124.2	97.842	4.12	64.976	139.94	273
202	1232	B	10	7	0.8	98.108	6.46	65.201	140.5	560
202	1232	B	10	7	17.3	98.273	0.72	65.301	140.75	248
202	1232	B	10	7	18.8	98.288	5.96	65.309	140.77	21
202	1232	B	10	7	39.2	98.492	16.37	65.453	141.13	359
202	1232	B	10	7	63.6	98.736	3.84	65.534	141.33	200

X

III   Oxygen isotope data of the sediments of SONNE Core SL50

Corrected core depth (m)	Age (kyr BP)	δ18O (‰VPDB)
0.05	0.35	0.79
0.15	1.84	0.65
0.82	15.24	2.57
0.91	16.44	2.59
1.01	17.54	2.45
1.19	17.89	3.09
1.27	18.03	3.49
1.35	18.09	3.72
1.4	18.15	3.34
1.44	18.22	2.64
1.54	18.32	2.62
1.64	18.41	3.47
1.75	18.51	3.2
1.87	18.62	2.35
1.97	18.7	3.54
2.05	18.77	3.24
2.15	18.85	3.49
2.25	18.92	3.57
2.36	19	3.79
2.42	19.09	3.36
2.6	19.23	3.51
2.68	19.29	3.12
2.76	19.4	3.31
2.84	19.52	3.51
2.94	19.69	3.14
3.0	19.75	2.79
3.1	19.87	3.35
3.2	19.97	3.62
3.27	20.07	3.58
3.31	20.18	3.12
3.43	20.33	3.62
3.52	20.42	3.53
3.61	20.6	3.45
3.68	20.7	3.76
3.79	20.84	2.75
3.91	21.01	3.37
3.99	21.11	3.06
4.05	21.2	2.93
4.08	21.23	2.92
4.11	21.32	3.57
4.17	21.51	3.32
4.24	21.59	3.56
4.26	21.66	3.35
4.33	21.81	3.21
4.42	22.03	3.35
4.53	22.15	2.9
4.66	22.32	2.77
4.78	22.47	2.91
4.88	22.58	3.23
4.98	22.68	3.09
5.06	22.77	3.08
5.36	22.9	3.12
5.42	23.25	3.34

IV   Turbiditic layers recorded in the sediments of SONNE Core SL50

Orig. depth top of turbidite (mcd)	Turbidite thickness (cm)	Corr. turbidite depth (mccd)	Age (kyr BP)	Turbidite recurrence time (yr)
0.33	6	0.33	5.34	5341
0.43	3	0.37	6.15	808
0.51	7	0.42	7.16	1010
0.64	3	0.48	8.37	1212
0.73	1	0.54	9.58	1212
0.88	2	0.68	12.41	2828
0.92	1	0.7	12.82	404
1.07	2	0.84	15.48	2666
1.42	2	1.17	17.84	2358
1.54	2	1.27	18.02	175
1.68	4	1.39	18.14	121
1.76	5	1.43	18.18	40
1.85	2	1.47	18.22	40
1.91	2	1.51	18.26	40
2.02	1	1.6	18.35	91
2.13	3	1.7	18.45	101
2.29	3	1.83	18.58	131
2.5	2	2.01	18.76	182
2.92	6	2.41	19.17	404
3.33	7	2.76	19.52	354
3.44	8	2.8	19.56	40
3.62	11	2.9	19.66	101
3.76	2	2.93	19.69	30
3.83	3	2.98	19.74	51
3.93	2	3.05	19.81	71
3.99	4	3.09	19.85	40
4.21	3	3.27	20.12	268
4.28	6	3.31	20.19	66
4.43	2	3.4	20.34	148
4.61	8	3.56	20.6	263
4.79	3	3.66	20.76	165
4.91	2	3.75	20.91	148
5.02	2	3.84	21.06	148
5.07	2	3.87	21.11	49
5.18	2	3.96	21.26	148
5.26	2	4.02	21.36	99
5.37	7	4.11	21.5	148
5.5	11	4.17	21.6	99
5.7	6	4.26	21.75	148
5.83	7	4.33	21.87	115
5.95	11	4.38	21.95	82
6.1	1	4.42	22.01	66
6.32	3	4.63	22.29	273
6.5	2	4.78	22.47	183
6.9	3	5.16	22.93	463
7.13	1	5.36	23.18	244
7.2	6	5.42	23.25	73

XII